

EXPERIMENTAL AND NUMERICAL STUDY
OF OPEN-AIR ACTIVE COOLING

BY
SALMAN AMSARI AL-FIFI

MAY 2010

**EXPERIMENTAL AND NUMERICAL STUDY OF
OPEN-AIR ACTIVE COOLING**

BY

SALMAN AMSARI AL-FIFI

A Thesis Presented to the
DEANSHIP OF GRADUATE STUDIES

KING FAHD UNIVERSITY OF PETROLEUM & MINERALS

DHAHRAN, SAUDI ARABIA

In Partial Fulfillment of the
Requirements for the Degree of

MASTER OF SCIENCE

In

AEROSPACE ENGINEERING

May 2010

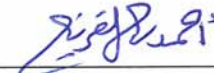
KING FAHD UNIVERSITY OF PETROLEUM & MINERALS

DHAHRAN 31261, SAUDI ARABIA

DEANSHIP OF GRADUATE STUDIES

This thesis, written by SALMAN AMSARI AL-FIFI under the direction of his thesis advisor and approved by his thesis committee, has been presented to and accepted by Dean of Graduate Studies, in partial fulfillment of the requirements for the degree of MASTER OF SCIENCE IN **AEROSPACE ENGINEERING**.

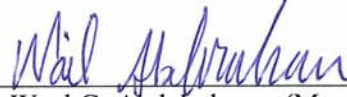
Thesis Committee



Dr. Ahmed Z. AL-Garni (Advisor)



Dr. Ayman Kassem (Co-Advisor)



Dr. Wael G. Abdelrahman (Member)



Dr. Syed A. M. Said (Member)



Dr. Syed M. Zubair (Member)



Dr. Ahmed Z. AL-Garni
(Chairman, Department of Aerospace Engineering)



Dr. Salam A. Zummo
(Dean of Graduate Studies)

Date

21/6/10



*Dedicated to
My beloved
parents, wife, brother, sisters and my kids*

Acknowledgements

"In the name of Allah (God), Most Gracious, Most Merciful. Read, In the name of thy lord and Cherisher, Who created man from a [leech - like] clot. Read, and thy Lord Is Most Bountiful, He Who taught [the use of] the pen. Taught man that which he know not. Nay, but man doth Transgress all bounds. In that he looketh upon himself as self- sufficient. Verily, to thy Lord is the return [of all]. " (The Holy QURAN, Surah No. 96).

All praise and thanks are due to Almighty Allah, Most Gracious Most Merciful, for his immense beneficences and blessings. He gave me the extra-ordinary patience to bear the hardships and carry out the work which has resulted in the accomplishment of this research. May peace and blessings be upon Prophet Muhammad (PBUH), his family and his companions.

Acknowledgement is due to King Fahd University of Petroleum and Minerals for the support extended towards my research.

First and foremost I offer my sincerest gratitude to my advisor, Dr. Ahmed Z. AL-Garni, who has supported me throughout my thesis with his help, generous support, valuable suggestions and timely advice. I attribute the level of my Masters degree to his encouragement and constant guidance and motivation, in spite of his busy time schedule. He was always kind, understanding and sympathetic to me. One simply could not wish for a better or friendlier advisor.

I am heartily thankful to my co-advisor, Dr. Ayman Kassem, whose encouragement, guidance and support from the initial to the final level enabled me to develop an understanding of the subject, especially in the computational part.

Many thanks and appreciation to my committee members, Dr. Wael G. Abdelrahman, Dr. Syed A. M. Said and Dr. Syed M. Zubair, for their valuable help and advice.

My sincere and heartfelt appreciations are dedicated to my parents, my wife, my brother, sisters and all my relatives. My deep gratitude is towards my parents, for their incessant prayers, moral support, guidance encouragement and patience during the course of my studies. They are the source of power, inspiration and confidence in me.

Lastly, I offer my regards and blessings to my sincere friend Mubarak for his help, and to all of those who supported me in any respect during the completion of this work.

TABLE OF CONTENTS

ACKNOWLEDGMENTS.....	iv
List of Tables.....	xi
List of Figures.....	xiv
Abstract (English).....	xxvi
Abstract (Arabic).....	xxviii
NOMENCLATURE.....	xxxii
CHAPTER 1.....	1
INTRODUCTION.....	1
1.1 Overview.....	1
1.2 Objective of the Study.....	2
CHAPTER 2.....	3
LITERATURE REVIEW.....	3
2.1 Climatic Characteristics and Features of Regions in Saudi Arabia.....	3
2.2 Passive Cooling.....	9
2.3 Evaporative Active Cooling.....	10
CHAPTER 3.....	15
METHODOLOGY AND EXPERIMENTAL SET-UP.....	15
3.1 First Stage (Without Mist).....	15
3.1.1 Angle Effect (Without Mist).....	17
3.2 Second Stage (With Mist).....	19
3.2.1 Angle Effect (With Mist).....	21
3.3 Computational Study.....	22
3.4 Outline of the Present Work.....	23
CHAPTER 4.....	24
BACKGROUND INFORMATION.....	24
4.1 Passive Cooling.....	24
4.1.1 Passive Cooling Strategies.....	24
4.1.1.1 Natural Ventilation.....	24
4.1.1.2 High Thermal Mass.....	25
4.1.1.3 High Thermal Mass with Night Ventilation.....	25

4.1.1.4	Evaporative Cooling.....	25
4.1.2	Which Passive Cooling Strategy is Right to Use?.....	26
4.2	Active Cooling.....	29
4.2.1	Active Cooling Methods.....	29
4.3	Comparisons to Air-conditioning.....	34
CHAPTER 5.....		38
FAN AIRSPEED MEASUREMENT.....		38
CHAPTER 6.....		44
EXPERIMENTAL SETUP AND TECHNIQUES.....		44
6.1	First Stage (Without Mist).....	44
6.1.1	20-inch Fan.....	45
6.1.1.1	1-Diameter in Height.....	45
6.1.1.2	2-Diameter in Height.....	48
6.1.1.3	3-Diameter in Height.....	50
6.1.1.4	4-Diameter in Height.....	52
6.1.1.5	5-Diameter in Height.....	54
6.1.1.6	Angle Effect of 20-inch Fan.....	57
6.1.1.7	Side-wise Investigation of 20-inch Fan.....	61
6.1.2	24-inch Fan.....	63
6.1.2.1	1-Diameter in Height.....	63
6.1.2.2	2-Diameter in Height.....	65
6.1.2.3	3-Diameter in Height.....	67
6.1.2.4	4-Diameter in Height.....	69
6.1.2.5	5-Diameter in Height.....	71
6.1.2.6	Angle Effect of 24-inch Fan.....	74
6.1.2.7	Side-wise Investigation of 24-inch Fan.....	76
6.1.3	30-inch Fan.....	77
6.1.3.1	1-Diameter in Height.....	77
6.1.3.2	2-Diameter in Height.....	79
6.1.3.3	3-Diameter in Height.....	81
6.1.3.4	4-Diameter in Height.....	83
6.1.3.5	5-Diameter in Height.....	85
6.1.3.6	Angle Effect of 24-inch Fan.....	88
6.1.3.7	Side-wise Investigation of 30-inch Fan.....	90

6.2 Second Stage (With Mist).....	91
6.2.1 Experimental Setup and Equipments.....	91
6.2.2 20-inch Fan (with mist).....	96
6.2.2.1 1-Diameter in Height.....	96
6.2.2.2 2-Diameter in Height.....	99
6.2.2.3 3-Diameter in Height.....	101
6.2.2.4 4-Diameter in Height.....	103
6.2.2.5 5-Diameter in Height.....	105
6.2.2.6 Angle Effect of 20-inch Fan.....	108
6.2.2.7 Side-wise Investigation of 20-inch Fan.....	111
6.2.3 24-inch Fan (with mist).....	113
6.2.3.1 1-Diameter in Height.....	113
6.2.3.2 2-Diameter in Height.....	115
6.2.3.3 3-Diameter in Height.....	117
6.2.3.4 4-Diameter in Height.....	119
6.2.3.5 5-Diameter in Height.....	121
6.2.3.6 Angle Effect of 24-inch Fan.....	124
6.2.3.7 Side-wise Investigation of 24-inch Fan.....	126
6.2.4 30-inch Fan (with mist).....	127
6.2.4.1 1-Diameter in Height.....	127
6.2.4.2 2-Diameter in Height.....	129
6.2.4.3 3-Diameter in Height.....	131
6.2.4.4 4-Diameter in Height.....	133
6.2.4.5 5-Diameter in Height.....	135
6.2.4.6 Angle Effect of 30-inch Fan.....	138
6.2.4.7 Side-wise Investigation of 30-inch Fan.....	140
CHAPTER 7.....	141
NUMERICAL SOLUTION.....	141
7.1 Thermodynamic Model for an Evaporating Water Droplet.....	141
7.1.1 Evaporation Model.....	142
7.2 Computational Procedure.....	144
7.2.1 Molecular Mass of Air.....	149
7.2.2 Calculation Sequence.....	153
7.2.3 Computational Procedure Flow Chart.....	155

7.3 20-inch Fan.....	156
7.3.1 Angle Effect of 20-inch Fan (computational).....	163
7.3.1.1 $\theta_1 = 26.56^\circ$	164
7.3.1.2 $\theta_2 = 45^\circ$	169
7.3.2 Side-wise Investigation of 20-inch Fan (computational).....	176
7.4 24-inch Fan.....	179
7.4.1 Angle Effect of 24-inch Fan (computational).....	186
7.4.1.1 $\theta_1 = 26.56^\circ$	187
7.4.1.2 $\theta_2 = 45^\circ$	192
7.4.2 Side-wise Investigation of 24-inch Fan (computational).....	199
7.5 30-inch Fan.....	202
7.5.1 Angle Effect of 30-inch Fan (computational).....	209
7.5.1.1 $\theta_1 = 26.56^\circ$	210
7.5.1.2 $\theta_2 = 45^\circ$	215
7.5.2 Side-wise Investigation of 30-inch Fan (computational).....	222
CHAPTER 8.....	225
RESULTS AND DISCUSSION.....	225
8.1 Results of 20-inch Fan.....	225
8.2 Results of 24-inch Fan.....	231
8.3 Results of 30-inch Fan.....	236
8.4 Relationships and Concluded Remarks of the Three Fans.....	241
8.5 Heat Absorbed by Water Droplets.....	255
8.5.1 Heat Absorbed by Water Droplets of 20-inch Fan.....	258
8.5.2 Heat Absorbed by Water Droplets of 24-inch Fan.....	260
8.5.3 Heat Absorbed by Water Droplets of 30-inch Fan.....	262
8.6 Effect of Operating Parameters of Evaporation Rate and Drying Time performance.....	264
8.6.1 Effect of Air Humidity.....	265
8.6.2 Effect of Operating Pressure.....	267
8.6.3 Effect of Air Velocity.....	269
8.6.4 Effect of Air Temperature.....	271

CHAPTER 9.....	273
CONCLUSIONS AND RECOMMENDATIONS.....	273
9.1 Conclusions.....	273
9.2 Summery.....	275
9.3 Recommendations for Future Research Work.....	278
APPENDIX A: ERROR ANALYSIS ON UNCERTAINTY CALCULATIONS	
.....	279
REFERENCES.....	284
VITAE.....	289

List of Tables

Table 5.1 Experimental data of airspeed versus voltage.....	39
Table 5.2 Airspeed of the three fans.....	43
Table 6.1 Airspeed measurements of 20-inch fan (D_S) for 1-diameter in height ($h=1$).....	46
Table 6.2 Airspeed measurements of 20-inch fan (D_S) for 2-diameter in height ($h=2$).....	48
Table 6.3 Airspeed measurements of 20-inch fan (D_S) for 3-diameter in height ($h=3$).....	50
Table 6.4 Airspeed measurements of 20-inch fan (D_S) for 4-diameter in height ($h=4$).....	52
Table 6.5 Airspeed measurements of 20-inch fan (D_S) for 5-diameter in height ($h=5$).....	54
Table 6.6 Airspeed measurements of 20-inch fan (D_S) for angle case.....	59
Table 6.7 Airspeed measurements in the side-wise of 20-inch Fan.....	62
Table 6.8 Airspeed measurements of 24-inch fan (D_m) for 1-diameter in height ($h=1$).....	63
Table 6.9 Airspeed measurements of 24-inch fan (D_m) for 2-diameter in height ($h=2$).....	65
Table 6.10 Airspeed measurements of 24-inch fan (D_m) for 3-diameter in height ($h=3$).....	67
Table 6.11 Airspeed measurements of 24-inch fan (D_m) for 4-diameter in height ($h=4$).....	69
Table 6.12 Airspeed measurements of 24-inch fan (D_m) for 5-diameter in height ($h=5$).....	71
Table 6.13 Airspeed measurements of 24-inch fan (D_m) for angle case.....	74
Table 6.14 Airspeed measurements in the side-wise of 24-inch Fan.....	76
Table 6.15 Airspeed measurements of 30-inch fan (D_L) for 1-diameter in height ($h=1$).....	77

Table 6.16 Airspeed measurements of 30-inch fan (D_L) for 2-diameter in height ($h=2$).....	79
Table 6.17 Airspeed measurements of 30-inch fan (D_L) for 3-diameter in height ($h=3$).....	81
Table 6.18 Airspeed measurements of 30-inch fan (D_L) for 4-diameter in height ($h=4$).....	83
Table 6.19 Airspeed measurements of 30-inch fan (D_L) for 5-diameter in height ($h=5$).....	85
Table 6.20 Airspeed measurements of 30-inch fan (D_L) for angle case.....	88
Table 6.21 Airspeed measurements in the side-wise of 30-inch Fan.....	90
Table 6.22 Temperature measurements of 20-inch fan (D_S) for 1-diameter in height ($h=1D$) (with mist).....	97
Table 6.23 Temperature measurements of 20-inch fan (D_S) for 2-diameter in height ($h=2D$) (with mist).....	99
Table 6.24 Temperature measurements of 20-inch fan (D_S) for 3-diameter in height ($h=3D$) (with mist).....	101
Table 6.25 Temperature measurements of 20-inch fan (D_S) for 4-diameter in height ($h=4D$) (with mist).....	103
Table 6.26 Temperature measurements of 20-inch fan (D_S) for 5-diameter in height ($h=5D$) (with mist).....	105
Table 6.27 Temperature measurements of 20-inch fan (D_S) for angle case (with mist).....	109
Table 6.28 Temperature measurements in the side-wise of 20-inch Fan (D_S) (with mist).....	112
Table 6.29 Temperature measurements of 24-inch fan (D_m) for 1-diameter in height ($h=1D$) (with mist).....	113
Table 6.30 Temperature measurements of 24-inch fan (D_m) for 2-diameter in height ($h=2D$) (with mist).....	115
Table 6.31 Temperature measurements of 24-inch fan (D_m) for 3-diameter in height ($h=3D$) (with mist).....	117

Table 6.32 Temperature measurements of 24-inch fan (D_m) for 4-diameter in height ($h = 4D$) (with mist).....	119
Table 6.33 Temperature measurements of 24-inch fan (D_m) for 5-diameter in height ($h = 5D$) (with mist).....	121
Table 6.34 Temperature measurements of 24-inch fan (D_m) for angle case (with mist).....	124
Table 6.35 Temperature measurements in the side-wise of 24-inch Fan (D_m) (with mist).....	126
Table 6.36 Temperature measurements of 30-inch fan (D_L) for 1-diameter in height ($h = 1D$) (with mist).....	127
Table 6.37 Temperature measurements of 30-inch fan (D_L) for 2-diameter in height ($h = 2D$) (with mist).....	129
Table 6.38 Temperature measurements of 30-inch fan (D_L) for 3-diameter in height ($h = 3D$) (with mist).....	131
Table 6.39 Temperature measurements of 30-inch fan (D_L) for 4-diameter in height ($h = 4D$) (with mist).....	133
Table 6.40 Temperature measurements of 30-inch fan (D_L) for 5-diameter in height ($h = 5D$) (with mist).....	135
Table 6.41 Temperature measurements of 30-inch fan (D_L) for angle case (with mist).....	138
Table 6.42 Temperature measurements in the side-wise of 30-inch Fan (D_L) (with mist).....	140
Table 7.1 Molecular weight of air.....	149
Table 7.2 Fixed parameters values in the computational solution.....	154
Table 8.1 Fan maximum range with respect to airspeed of the three fans.....	242
Table 8.2 Fan maximum range with respect to temperature of the three fans.....	242
Table 8.3 Fan maximum side-wise range with respect to airspeed of the three fans.....	249
Table 8.4 Fan maximum side-wise range with respect to temperature of the three fans.....	251

List of Figures

Figure 2.1 Map of the Climatic Zones of Saudi Arabia.....	4
Figure 2.2 Profiles of Monthly Mean Dry Bulb and Wet Bulb Temperatures.....	6
Figure 3.1 Fans (20 inch, 24 inch and 30 inch) used in experiments.....	15
Figure 3.2 Temperature domain for first fan diameter in height.....	16
Figure 3.3 Different fan heights.....	17
Figure 3.4 Configuration of angle effect case study.....	18
Figure 3.5 Fan with mist nozzles.....	19
Figure 3.6 Temperature domain for first fan diameter in height with mist.....	20
Figure 3.7 Different fan heights with mist.....	20
Figure 3.8 Configuration of angle effect case study with mist.....	21
Figure 4.1 Bioclimatic chart.....	26
Figure 4.2 Swamp cooler – drier.....	30
Figure 4.3 Comfort chart.....	36
Figure 5.1 Small fan and Voltmeter used.....	38
Figure 5.2 Relation of airspeed and voltage of airspeed measuring device.....	40
Figure 5.3 Reading locations taken across the fan.....	41
Figure 5.4 Variation in airspeed coming off fan tips versus near fan hub.....	42
Figure 6.1. Reading locations taken across the 20-inch fan.....	45
Figure 6.2 20-inch fan (D_s) for the first 1-diameter in height ($h = 1D$).....	45
Figure 6.3 Airspeed measurements of 20-inch fan (D_s) for 1-diameter in height ($h=1$)..	47
Figure 6.4 Airspeed measurements of 20-inch fan (D_s) for 2-diameter in height ($h =2$)..	49

Figure 6.5 Airspeed measurements of 20-inch fan (D_S) for 3-diameter in height ($h=3$).	51
Figure 6.6 Airspeed measurements of 20-inch fan (D_S) for 4-diameter in height ($h=4$).	53
Figure 6.7 Airspeed measurements of 20-inch fan (D_S) for 5-diameter in height ($h=5$).	55
Figure 6.8 Airspeed measurements of 20-inch fan (D_S) for all heights.....	56
Figure 6.9 Configuration of angle effect case study of 20-inch fan (D_S).....	58
Figure 6.10 Airspeed measurements of 20-inch fan (D_S) for angle case.....	60
Figure 6.11 Airspeed measurements in the side-wise of 20-inch Fan.....	61
Figure 6.12 Airspeed measurements in the side-wise of 20-inch Fan.....	62
Figure 6.13 Airspeed measurements of 24-inch fan (D_m) for 1-diameter in height ($h=1$).....	64
Figure 6.14 Airspeed measurements of 24-inch fan (D_m) for 2-diameter in height ($h=2$).....	66
Figure 6.15 Airspeed measurements of 24-inch fan (D_m) for 3-diameter in height ($h=3$).....	68
Figure 6.16 Airspeed measurements of 24-inch fan (D_m) for 4-diameter in height ($h=4$).....	70
Figure 6.17 Airspeed measurements of 24-inch fan (D_m) for 5-diameter in height ($h=5$).....	72
Figure 6.18 Airspeed measurements of 24-inch fan (D_m) for all heights.....	73
Figure 6.19 Airspeed measurements of 24-inch fan (D_m) for angle case.....	75
Figure 6.20 Airspeed measurements in the side-wise of 24-inch Fan.....	76
Figure 6.21 Airspeed measurements of 30-inch fan (D_L) for 1-diameter in height ($h=1$).....	78

Figure 6.22 Airspeed measurements of 30-inch fan (D_L) for 2-diameter in height ($h=2$).....	80
Figure 6.23 Airspeed measurements of 30-inch fan (D_L) for 3-diameter in height ($h=3$).....	82
Figure 6.24 Airspeed measurements of 30-inch fan (D_L) for 4-diameter in height ($h=4$).....	84
Figure 6.25 Airspeed measurements of 30-inch fan (D_L) for 5-diameter in height ($h=5$).....	86
Figure 6.26 Airspeed measurements of 30-inch fan (D_L) for all heights.....	87
Figure 6.27 Airspeed measurements of 30-inch fan (D_L) for angle case.....	89
Figure 6.28 Airspeed measurements in the side-wise of 30-inch Fan.....	90
Figure 6.29 Fan with mist nozzles.....	91
Figure 6.30 Location of the mist experiments.....	92
Figure 6.31 Reservoir used in the mist experiment.....	92
Figure 6.32 Water pump used in the mist experiment.....	93
Figure 6.33 The pressure gage of the water pump.....	93
Figure 6.34 Conducting experiments with my advisor Dr. Ahmed AL-Garni.....	94
Figure 6.35 A very sensitive thermometer used in the experiments.....	94
Figure 6.36 A very sensitive remote-laser thermometer used in the experiments.....	95
Figure 6.37 An instrument used to measure temperature and relative humidity.....	95
Figure 6.38 An instrument used to measure the relative humidity.....	95
Figure 6.39 20-inch fan (D_S) for the first 1-diameter in height ($h = 1D$) (with mist).....	96
Figure 6.40 Temperature measurements of 20-inch fan (D_S) for 1-diameter in height ($h=1D$) (with mist).....	98

Figure 6.41 Temperature measurements of 20-inch fan (D_S) for 2-diameter in height ($h=2D$) (with mist).....	100
Figure 6.42 Temperature measurements of 20-inch fan (D_S) for 3-diameter in height ($h=3D$) (with mist).....	102
Figure 6.43 Temperature measurements of 20-inch fan (D_S) for 4-diameter in height ($h=4D$) (with mist).....	104
Figure 6.44 Temperature measurements of 20-inch fan (D_S) for 5-diameter in height ($h=5D$) (with mist).....	106
Figure 6.45 Temperature measurements of 20-inch fan (D_S) for all heights (with mist).....	107
Figure 6.46 Configuration of angle effect case study of 20-inch fan (D_S) with mist....	108
Figure 6.47 Temperature measurements of 20-inch fan (D_S) for angle case (with mist).....	110
Figure 6.48 Temperature measurements in the side-wise of 20-inch Fan.....	111
Figure 6.49 Temperature measurements in the side-wise of 20-inch Fan (D_S) (with mist).....	112
Figure 6.50 Temperature measurements of 24-inch fan (D_m) for 1-diameter in height ($h=1D$) (with mist).....	114
Figure 6.51 Temperature measurements of 24-inch fan (D_m) for 2-diameter in height ($h=2D$) (with mist).....	116
Figure 6.52 Temperature measurements of 24-inch fan (D_m) for 3-diameter in height ($h=3D$) (with mist).....	118
Figure 6.53 Temperature measurements of 24-inch fan (D_m) for 4-diameter in height ($h=4D$) (with mist).....	120

Figure 6.54 Temperature measurements of 24-inch fan (D_m) for 5-diameter in height ($h=5D$) (with mist).....	122
Figure 6.55 Temperature measurements of 24-inch fan (D_m) for all heights (with mist).....	123
Figure 6.56 Temperature measurements of 24-inch fan (D_m) for angle case (with mist).....	125
Figure 6.57 Temperature measurements in the side-wise of 24-inch Fan (D_m) (with mist).....	126
Figure 6.58 Temperature measurements of 30-inch fan (D_L) for 1-diameter in height ($h=1D$) (with mist).....	128
Figure 6.59 Temperature measurements of 30-inch fan (D_L) for 2-diameter in height ($h=2D$) (with mist).....	130
Figure 6.60 Temperature measurements of 30-inch fan (D_L) for 3-diameter in height ($h=3D$) (with mist).....	132
Figure 6.61 Temperature measurements of 30-inch fan (D_L) for 4-diameter in height ($h=4D$) (with mist).....	134
Figure 6.62 Temperature measurements of 30-inch fan (D_L) for 5-diameter in height ($h=5D$) (with mist).....	136
Figure 6.63 Temperature measurements of 30-inch fan (D_L) for all heights (with mist).....	137
Figure 6.64 Temperature measurements of 30-inch fan (D_L) for angle case (with mist).....	139
Figure 6.65 Temperature measurements in the side-wise of 30-inch Fan (D_L) (with mist).....	140

Figure 7.1 Schematic representation of a bubble of water during the evaporation process.....	143
Figure 7.2 Psychrometric chart.....	147
Figure 7.3 Computational Procedure Flow Chart.....	155
Figure 7.4 The rate of evaporation of droplet mass for 20-inch fan (D_S) for 4-diameter in height ($h=4D_S$).....	156
Figure 7.5 Droplet temperature versus time for 20-inch fan (D_S) for 4-diameter in height ($h = 4D_S$).....	157
Figure 7.6 Air temperature versus time for 20-inch fan (D_S) for 4-diameter in height ($h=4D_S$).....	158
Figure 7.7 Droplet injection height versus the horizontal range for 20-inch fan (D_S) for 4-diameter in height ($h = 4D_S$).....	159
Figure 7.8 Droplet injection height in diameter versus the horizontal range in diameter for 20-inch fan (D_S) for 4-diameter in height ($h = 4D_S$).....	160
Figure 7.9 Droplet and air temperatures versus the horizontal range for 20-inch fan (D_S) for 4-diameter in height ($h = 4D_S$).....	161
Figure 7.10 Droplet and air temperatures versus the horizontal range in diameter for 20-inch fan (D_S) for 4-diameter in height ($h = 4D_S$).....	162
Figure 7.11 Configuration of angle effect case study (computational).....	163
Figure 7.12 Droplet and air temperatures versus time of angle case ($\theta_1 = 26.56^\circ$) for 20-inch fan (D_S).....	164
Figure 7.13 Droplet injection height versus the horizontal range of angle case ($\theta_1 = 26.56^\circ$) for 20-inch fan (D_S).....	165
Figure 7.14 Droplet injection height in diameter versus the horizontal range in diameter of angle case ($\theta_1 = 26.56^\circ$) for 20-inch fan (D_S).....	166

Figure 7.15 Droplet and air temperatures versus the horizontal range of angle case ($\theta_1 = 26.56^\circ$) for 20-inch fan (D_S).....	167
Figure 7.16 Droplet and air temperatures versus the horizontal range in diameter of angle case ($\theta_1 = 26.56^\circ$) for 20-inch fan (D_S).....	168
Figure 7.17 Droplet and air temperatures versus time of angle case ($\theta_2 = 45^\circ$) for 20-inch fan (D_S).....	169
Figure 7.18 Droplet injection height versus the horizontal range of angle case ($\theta_2 = 45^\circ$) for 20-inch fan (D_S).....	170
Figure 7.19 Droplet injection height in diameter versus the horizontal range in diameter of angle case ($\theta_2 = 45^\circ$) for 20-inch fan (D_S).....	171
Figure 7.20 Droplet and air temperatures versus the horizontal range of angle case ($\theta_2 = 45^\circ$) for 20-inch fan (D_S).....	172
Figure 7.21 Droplet and air temperatures versus the horizontal range in diameter of angle case ($\theta_2 = 45^\circ$) for 20-inch fan (D_S).....	173
Figure 7.22 Droplet trajectories for different angles of 20-inch fan (D_S).....	174
Figure 7.23 Droplet trajectories for different angles of 20-inch fan (D_S) in terms of fan diameter.....	175
Figure 7.24 Side-wise Investigation of 20-inch Fan (computational).....	176
Figure 7.25 Droplet maximum side-wise range for 20-inch fan (D_S) for 4-diameter in height ($h = 4D_S$).....	177
Figure 7.26 Droplet maximum side-wise range in diameter for 20-inch fan (D_S) for 4-diameter in height ($h = 4D_S$).....	178
Figure 7.27 The rate of evaporation of droplet mass for 24-inch fan (D_m) for 4-diameter in height ($h = 4D_m$).....	179

Figure 7.28 Droplet temperature versus time for 24-inch fan (D_m) for 4-diameter in height ($h = 4D_m$).....	180
Figure 7.29 Air temperature versus time for 24-inch fan (D_m) for 4-diameter in height ($h = 4D_m$).....	181
Figure 7.30 Droplet injection height versus the horizontal range for 24-inch fan (D_m) for 4-diameter in height ($h = 4D_m$).....	182
Figure 7.31 Droplet injection height in diameter versus the horizontal range in diameter for 24-inch fan (D_m) for 4-diameter in height ($h = 4D_m$).....	183
Figure 7.32 Droplet and air temperatures versus the horizontal range for 24-inch fan (D_m) for 4-diameter in height ($h = 4D_m$).....	184
Figure 7.33 Droplet and air temperatures versus the horizontal range in diameter for 24-inch fan (D_m) for 4-diameter in height ($h = 4D_m$).....	185
Figure 7.34 Droplet and air temperatures versus time of angle case ($\theta_1 = 26.56^\circ$) for 24-inch fan (D_m).....	187
Figure 7.35 Droplet injection height versus the horizontal range of angle case ($\theta_1 = 26.56^\circ$) for 24-inch fan (D_m).....	188
Figure 7.36 Droplet injection height in diameter versus the horizontal range in diameter of angle case ($\theta_1 = 26.56^\circ$) for 24-inch fan (D_m).....	189
Figure 7.37 Droplet and air temperatures versus the horizontal range of angle case ($\theta_1 = 26.56^\circ$) for 24-inch fan (D_m).....	190
Figure 7.38 Droplet and air temperatures versus the horizontal range in diameter of angle case ($\theta_1 = 26.56^\circ$) for 24-inch fan (D_m).....	191
Figure 7.39 Droplet and air temperatures versus time of angle case ($\theta_2 = 45^\circ$) for 24-inch fan (D_m).....	192

Figure 7.40 Droplet injection height versus the horizontal range of angle case ($\theta_2 = 45^\circ$) for 24-inch fan (D_m).....	193
Figure 7.41 Droplet injection height in diameter versus the horizontal range in diameter of angle case ($\theta_2 = 45^\circ$) for 24-inch fan (D_m).....	194
Figure 7.42 Droplet and air temperatures versus the horizontal range of angle case ($\theta_2 = 45^\circ$) for 24-inch fan (D_m).....	195
Figure 7.43 Droplet and air temperatures versus the horizontal range in diameter of angle case ($\theta_2 = 45^\circ$) for 24-inch fan (D_m).....	196
Figure 7.44 Droplet trajectories for different angles of 24-inch fan (D_m).....	197
Figure 7.45 Droplet trajectories for different angles of 24-inch fan (D_m) in terms of fan diameter.....	198
Figure 7.46 Droplet maximum side-wise range for 24-inch fan (D_m) for 4-diameter in height ($h = 4D_m$).....	200
Figure 7.47 Droplet maximum side-wise range in diameter for 24-inch fan (D_m) for 4-diameter in height ($h = 4D_m$).....	201
Figure 7.48 The rate of evaporation of droplet mass for 30-inch fan (D_L) for 4-diameter in height ($h = 4D_L$).....	202
Figure 7.49 Droplet temperature versus time for 30-inch fan (D_L) for 4-diameter in height ($h = 4D_L$).....	203
Figure 7.50 Air temperature versus time for 30-inch fan (D_L) for 4-diameter in height ($h = 4D_L$).....	204
Figure 7.51 Droplet injection height versus the horizontal range for 30-inch fan (D_L) for 4-diameter in height ($h = 4D_L$).....	205

Figure 7.52 Droplet injection height in diameter versus the horizontal range in diameter for 30-inch fan (D_L) for 4-diameter in height ($h = 4D_L$).....	206
Figure 7.53 Droplet and air temperatures versus the horizontal range for 30-inch fan (D_L) for 4-diameter in height ($h = 4D_L$).....	207
Figure 7.54 Droplet and air temperatures versus the horizontal range in diameter for 30-inch fan (D_L) for 4-diameter in height ($h = 4D_L$).....	208
Figure 7.55 Droplet and air temperatures versus time of angle case ($\theta_1 = 26.56^\circ$) for 30-inch fan (D_L).....	210
Figure 7.56 Droplet injection height versus the horizontal range of angle case ($\theta_1 = 26.56^\circ$) for 30-inch fan (D_L).....	211
Figure 7.57 Droplet injection height in diameter versus the horizontal range in diameter of angle case ($\theta_1 = 26.56^\circ$) for 30-inch fan (D_L).....	212
Figure 7.58 Droplet and air temperatures versus the horizontal range of angle case ($\theta_1 = 26.56^\circ$) for 30-inch fan (D_L).....	213
Figure 7.59 Droplet and air temperatures versus the horizontal range in diameter of angle case ($\theta_1 = 26.56^\circ$) for 30-inch fan (D_L).....	214
Figure 7.60 Droplet and air temperatures versus time of angle case ($\theta_2 = 45^\circ$) for 30-inch fan (D_L).....	215
Figure 7.61 Droplet injection height versus the horizontal range of angle case ($\theta_2 = 45^\circ$) for 30-inch fan (D_L).....	216
Figure 7.62 Droplet injection height in diameter versus the horizontal range in diameter of angle case ($\theta_2 = 45^\circ$) for 30-inch fan (D_L).....	217
Figure 7.63 Droplet and air temperatures versus the horizontal range of angle case ($\theta_2 = 45^\circ$) for 30-inch fan (D_L).....	218

Figure 7.64 Droplet and air temperatures versus the horizontal range in diameter of angle case ($\theta_2 = 45^\circ$) for 30-inch fan (D_L).....	219
Figure 7.65 Droplet trajectories for different angles of 30-inch fan (D_L).....	220
Figure 7.66 Droplet trajectories for different angles of 30-inch fan (D_L) in terms of fan diameter.....	221
Figure 7.67 Droplet maximum side-wise range for 30-inch fan (D_L) for 4-diameter in height ($h = 4D_L$).....	223
Figure 7.68 Droplet maximum side-wise range in diameter for 30-inch fan (D_L) for 4-diameter in height ($h = 4D_L$).....	224
Figure 8.1 Temperature ($^\circ\text{C}$) VS distance in diameter (D_S), for the small fan (D_S), for 4-diameter in height ($h = 4D_S$).....	227
Figure 8.2 Temperature ($^\circ\text{C}$) VS distance in diameter (D_m), for the medium fan (D_m), for 4-diameter in height ($h = 4D_m$).....	232
Figure 8.3 Temperature ($^\circ\text{C}$) VS distance in diameter (D_L), for the big fan (D_L), for 4-diameter in height ($h = 4D_L$).....	237
Figure 8.4 Fan maximum range with respect to fan airspeed (for fan airspeed $v \neq 0$) as a function of fan diameter.....	243
Figure 8.5 Fan maximum range with respect to temperature (for $\Delta T \neq 0$) as a function of fan diameter.....	244
Figure 8.6 Fan maximum range with respect to fan airspeed (for fan airspeed $v \neq 0$) in inches.....	245
Figure 8.7 Fan maximum range with respect to temperature (for $\Delta T \neq 0$) in inches.....	246
Figure 8.8 Mean airspeed profile of a fan range area.....	247
Figure 8.9 Mean temperature profile of a mist fan range area.....	248

Figure 8.11 Fan maximum side-wise range with respect to fan airspeed (for fan airspeed $v \neq 0$) as a function of fan diameter.....	250
Figure 8.12 Fan maximum side-wise range with respect to temperature (for $\Delta T \neq 0$) as a function of fan diameter.....	252
Figure 8.13 Fan maximum side-wise range with respect to fan airspeed (for fan airspeed $v \neq 0$) in inches.....	253
Figure 8.14 Fan maximum side-wise range with respect to temperature (for $\Delta T \neq 0$) in inches.....	254
Figure 8.15 A control volume of conserved mass and energy.....	255
Figure 8.16 Volume of cooled air in fan covered range area of 20-inch fan (D_S).....	259
Figure 8.17 Volume of cooled air in fan covered range area of 24-inch fan (D_m).....	261
Figure 8.18 Volume of cooled air in fan covered range area of 30-inch fan (D_L).....	263
Figure 8.19 Effect of relative humidity on evaporation performance.....	265
Figure 8.20 Effect of relative humidity on drying performance.....	266
Figure 8.21 Effect of operating pressure on evaporation performance.....	267
Figure 8.22 Effect of operating pressure on drying performance.....	268
Figure 8.23 Effect of air velocity on evaporation performance.....	269
Figure 8.24 Effect of air velocity on drying performance.....	270
Figure 8.25 Effect of air temperature on evaporation performance.....	271
Figure 8.26 Effect of air temperature on drying performance.....	272

Abstract (English)

Name: SALMAN AMSARI AL-FIFI
Title: Experimental and Numerical Study of Open Air Active Cooling
Degree: Master of Science
Field: Aerospace Engineering (Aerodynamics, Gas Dynamics & Propulsion)
Date of Degree: May 2010

The topic of my thesis is Experimental and Numerical Study of Open Air Active Cooling. The present research is intended to investigate experimentally and Numerically the effectiveness of cooling large open areas like stadiums, shopping malls, national gardens, amusement parks, zoos, transportation facilities and government facilities or even in buildings outdoor gardens and patios. Our cooling systems are simple cooling fans with different diameters and a mist system. This type of cooling systems has been chosen among the others to guarantee less energy consumption, which will make it the most favorable and applicable for cooling such places mentioned above. In the experiments, the main focus is to study the temperature domain as a function of different fan diameters aerodynamically similar in different heights till we come up with an empirical relationship that can determine the temperature domain for different fan diameters and for different heights of these fans. The experimental part has two stages. The first stage is devoted to investigate the maximum range of airspeed and profile for three different fan diameters and for different heights without mist, while the second stage is devoted to investigate the maximum range of temperature and profile for the three different diameter fans and for different heights with mist. The computational study is devoted to built an experimentally verified mathematical model to be used in the design and optimization

of water mist cooling systems, and to compare the mathematical results to the experimental results and to get an insight of how to apply such evaporative mist cooling for different places for different conditions. In this study, numerical solution is presented based on experimental conditions, such dry bulb temperature, wet bulb temperature, relative humidity, operating pressure and fan airspeed. In the computational study, all experimental conditions are kept the same for the three fans except the fan airspeed which varies according to different fan diameter. Then, a detailed discussion is presented to study and compare the effects of operating parameters playing role in evaporation rate process and drying performance like, parameters are air humidity, operating pressure, airspeed and air temperature.

Master of Science Degree
King Fahd University of Petroleum and Minerals
Dhahran, Saudi Arabia
May 2010
Jumada'I 1431 H

Abstract (Arabic)

ملخص الرسالة

اسم:	سلمان بن امساري حسين العمري الفيبي
عنوان الرسالة:	دراسة تجريبية وحسابية في تبريد الأماكن المفتوحة
الدرجة:	ماجستير في العلوم الهندسية
حقل التخصص:	هندسة الطيران والفضاء (الحركة الهوائية والغازية والدفع)
تاريخ الدرجة:	مايو ٢٠١٠

موضوع الرسالة البحثي دراسة تجريبية وحسابية عددية في تبريد الأماكن المفتوحة. يهدف البحث الحالي إلى دراسة فاعلية تبريد هذه الأماكن المفتوحة بالطرق التجريبية مدعمة بالطرق الحسابية، مثل الملاعب، المجمعات التجارية، الحدائق العامة، ساحات المعارض، حدائق الحيوان، مرافق المواصلات، المرافق العامة أو حتى في ساحات المنازل الخاصة. نظام التبريد المستخدم في الدراسة يعتبر نظام تبريد بسيط، يتكون من مجموعة من المراوح بأطوال ريش مختلفة ونظام رذاذ ضبابي. تم اختيار هذا النظام التبريدي المبسط لنضمن درجة أقل من استهلاك الطاقة مقارنة مع أنظمة التبريد الأخرى خاصة وهي الأنسب لتبريد أماكن واسعة كالتالي ذكرت في الأعلى. النقطة الرئيسية في هذا العمل هي دراسة المجال الحراري لمراوح تبريد مزودة بنظام الرذاذ الضبابي، كل هذه المراوح تتصف بنفس مواصفات التصميم الهوائي ما عدا الاختلاف في أطوال القطر لكل مروحة، لتكون الدراسة متمحورة حول تأثير اختلاف طول القطر في المجال الحراري لكل مروحة، مع الربط بتأثير ارتفاع المروحة لارتفاعات مختلفة، والخلاص بعلاقات رياضية تصف هذا التأثير.

الدراسة التجريبية تشتمل على مرحلتين. المرحلة الأولى مكرسة لدراسة مجال التأثير الهوائي المتمثلة في سرعة الهواء لكل المراوح المستخدمة باختلاف أطوال أقطارها وبارتفاعات مختلفة، والخلاص بعلاقات رياضية تصف هذا التأثير. المرحلة الثانية مكرسة لدراسة مجال التأثير الحراري لكل المراوح المستخدمة باختلاف أطوال أقطارها وبارتفاعات مختلفة باستخدام نظام الرذاذ الضبابي، والخلاص بعلاقات رياضية تصف هذا التأثير.

الدراسة الحسابية العددية مكرسة لبناء خوارزمية حسابية لتحقيق النتائج المتحصل عليها من التجارب ومقارنتها، ولاستخدامها لاحقاً في تصميم النظام الضبابي المناسب في حالة اختلاف المكان والظروف الجوية المحيطة. في هذه الدراسة يوجد حل رياضي يعتمد في مدخلاته على الشروط والعوامل التجريبية مثل درجة الحرارة المحيطة، درجة الحرارة للثرموميتر المبلل، الرطوبة النسبية، الضغط الجوي وسرعة الهواء للمروحة. في الدراسة الحسابية كل الشروط والظروف الجوية كانت ثابتة وغير متغيرة، ما عدا سرعة الهواء لكل مروحة ذات العلاقة المباشرة بطول قطر كل مروحة، والذي يتمحور حول تأثيره هذا البحث. ويتم كذلك دراسة تأثير هذه

العوامل حسابياً في فعالية وأداء نظام التبريد المستخدم في عملية التبخر، والوقت الذي تستغرقه مثل الرطوبة، الضغط الجوي، سرعة الهواء الخارجة من المروحة ودرجة الحرارة.

درجة الماجستير في العلوم الهندسية
جامعة الملك فهد للبترول والمعادن
الظهران، المملكة العربية السعودية
جمادى الأولى ١٤٣١ هـ - (مايو ٢٠١٠ م)

NOMENCLATURE

A_p	surface area of water droplet (m^2)
B	barometric pressure in (Pa)
b	radius of water bubble (m)
C_b	concentration of bubble (kg/m^3)
C_g	vapor concentration in the bulk gas (kg/m^3)
C_s	vapor concentration at the droplet surface (kg/m^3)
C_{pa}	specific heat of air (J/kg K)
C_{pe}	specific heat of water (J/kg K)
D_g	diffusion coefficient (m^2/s)
D_p	diameter of water droplet (m)
D_L	fan diameter of 30-inch Fan (m)
D_m	fan diameter of 24-inch Fan (m)
D_S	fan diameter of 20-inch Fan (m)
h	enthalpy (J/kg)
hc	heat transfer coefficient ($W/m^2.K$)
k_c	mass transfer coefficient (m/s)
L_{vap}	latent heat of water (J/kg)
m_a	mass of air (kg)
m_e	mass of water (kg)
m_l	liquid mass of water (kg)
m_{evap}	evaporated mass of water droplet (kg)
M_p	Molecular weight of H_2O in (g / mole)
N	number of droplets
N_c	evaporation rate in (kg/s)
Nu	Nussle number
Pr	Prandtle number
P_v	partial vapor pressure (Pa)
$P_{sat,d}$	saturated vapor pressure at dry bulb temperature (Pa)
$P_{sat}(T_p)$	saturated pressure at water droplet temperature (Pa)
Q_p	heat absorbed by water droplet
Q_{total}	total heat absorbed by water droplets

R	universal gas constant in ($\text{m}^3 \cdot \text{Pa} / \text{K} \cdot \text{mol}$)
Re	Reynolds number
RH	relative humidity
R_p	radius of water droplet (m)
Sc	Schmidt number
Sh	Sherwood number
T	temperature ($^{\circ}\text{C}$)
T_b	temperature of bubble
t	drying time (s)
T_d	dry bulb temperature ($^{\circ}\text{C}$)
T_a	air temperature ($^{\circ}\text{C}$)
T_p	droplet temperature ($^{\circ}\text{C}$)
T_{p0}	initial value of water droplet temperature ($^{\circ}\text{C}$)
V_a	air volume (m^3)
X_i	mole fraction
X	distance in x-direction (m)
Y	distance in y-direction (m)
μ_a	dynamic viscosity of air (Pa.s)
ρ_a	density of air (kg/m^3)
ρ_w	density of water (kg/m^3)
v	droplet speed (m/s)
λ_a	thermal conductivity in [$\text{W}/\text{m} \cdot \text{k}$]
θ_0	zero angle deflection (default case, $\theta_0=0^{\circ}$)
θ_1	first angle deflection ($\theta_1=26.56^{\circ}$)
θ_2	second angle deflection ($\theta_2=45^{\circ}$)

CHAPTER 1

INTRODUCTION:

1.1 Overview

During the last three decades, Saudi Arabia has witnessed significant economic, industrial, and technological developments. One important aspect of these developments is the implementation of modern cooling techniques. Air conditioning or providing thermal comfort always has been of primary concern and for this purpose, cooling systems were introduced. To our knowledge, most buildings in hot regions in Saudi Arabia have been provided with electric air conditioning systems, which has led to a large increase in electric energy consumption. The volume of these systems is expected to increase of about four times by the year 2010 [1]. Cooling large open areas is really a need for the population nowadays and for this, in turn, it will lead to a huge electricity supply demand, which is a great challenge in the country with the increase in the cost of energy production. Therefore, cooling large open areas with possible economic solutions or energy alternatives will be the main subject of this study by finding a way for possible aerodynamic cooling system, which consumes less amount of energy to be able to cover and provide thermal comfort to large open areas. Such as, stadiums, shopping malls, national gardens, amusement parks, zoos, open transportation facilities and open government facilities or even in buildings outdoor gardens and patios.

1.2 Objective of the Study

The objective of this thesis is to understand and investigate the relationships and parameters governing the evaporative cooling process such as, the relationship

between the temperature domain and cooling fan diameters from one aspect and the relationship between the temperature domain and cooling fan heights from the other aspect with and without mist. Evaporative cooling by using mist is an aim of this thesis to guarantee less energy consumption, which allows the use of solar energy as the energy source of this cooling system. In this manner, it is highly possible to provide thermal comfort to so many active and livable places all over the kingdom of Saudi Arabia without putting any pressure on the government for providing energy.

CHAPTER 2

LITERATURE REVIEW:

The purpose of this chapter is to provide a general understanding of the relationship between the relevant literature and the present work. This chapter consists of three main sections. The first section describes the climatic characteristics and features of regions in Saudi Arabia. The second describes some applications of passive cooling systems. The third reviews the research conducted on evaporative cooling.

2.1 Climatic Characteristics and Features of Regions in Saudi Arabia

Hot climatic regions prevail on the western sides of land masses between 15 and 30 degrees north and south of the equator in central and western Asia, Africa, Australia, the Middle East and North and South America. Those regions are characterized by their aridity, which is caused by the dry Trade Winds which blow southwest and northwest towards the equator [2].

Saudi Arabia is located within the hot-dry climatic zones of the world, but it may be further divided into five climatic zones by geographic characteristics [2]: (1) the hot-humid zone, which includes the Red Sea coastal plain in the west; (2) the upland from 1200 to 1800 meters in the west; (3) the upland over 1800 meters in the west; (4) the hot-dry zone, which includes the central plateau, ringed by Nafud, Dahna, and Rub Al-Khali deserts; and (5) the composite zone, which includes the coastal plain of the Arabian Gulf in the eastern area (Figure 2.1). Only the hot zones are included in the present study where we can decrease the temperature and provide more thermal comfort.

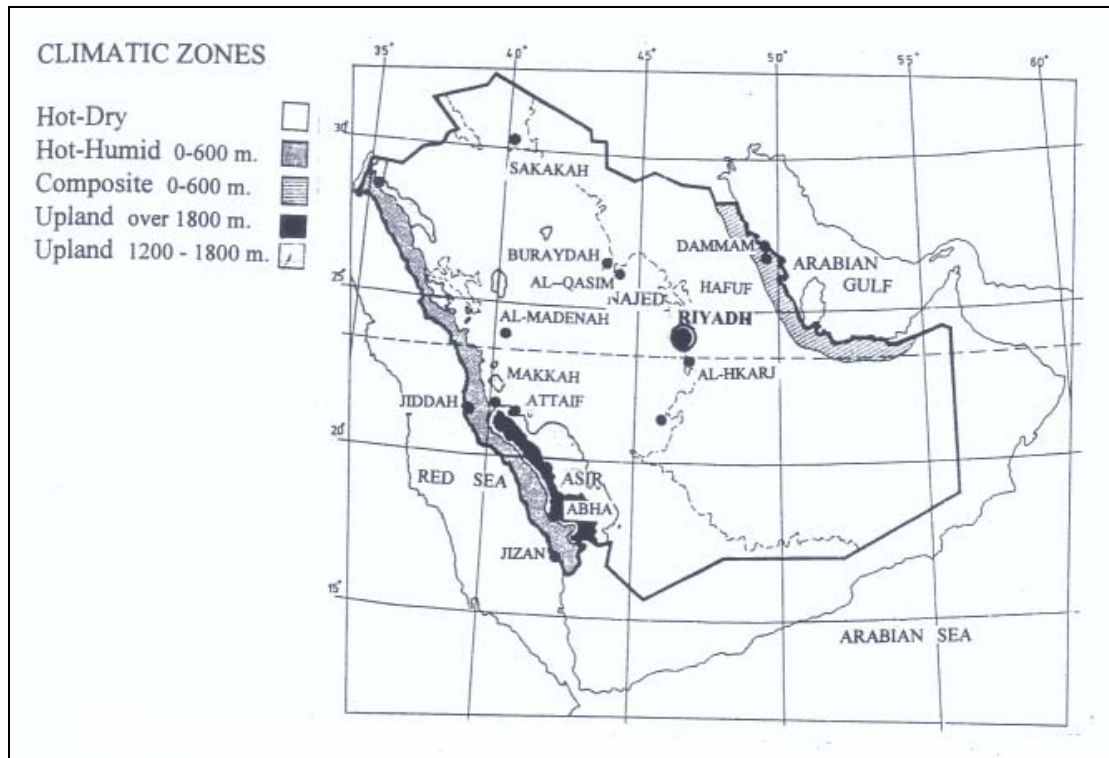


Figure 2.1 Map of the Climatic Zones of Saudi Arabia

The hot climatic regions of Saudi Arabia are characterized by six factors [4]. The first factor is high summer daytime temperature, ranging from 32° C to 36° C with the hotter regions going well above 40° C and up to 50° C. the second is high solar radiation ranging between 800 to 1100 Watts/m² on horizontal surface. In addition, reflected solar radiation from high-colored terrain greatly increase the direct radiation. The third is frequent afternoon dust storms and haze, which are caused by conventional air currents which, in turn, are induced by heating of air mass near the ground. The fourth, depending on location and season, is the vapor

pressure, which varies from 5 to 15 mm Hg and causes wide fluctuation in temperature and relative humidity from summer to winter. The fifth is low wind speed in the morning hours, reaching a peak in the afternoon. These afternoon high speeds are often accompanied by sand and dust storms. The sixth is low annual rainfall, as low as 140 mm, but the rain may come in sporadic heavy showers and thunderstorm during the winter months from December to February.

Temperatures are subject to considerable diurnal and seasonal fluctuations. Winters (December to February) are cool to warm. Summers (June to September) tend to be very hot with temperatures above 40° C widespread and common and may approach 50° C. Humidity is generally low, except along the coasts where it may be quite high.

Average August temperature in western region is 32° C but may reach 49° C, winter temperature average 24° C, and relative humidity varies seasonally between 55% and 65%.

Summer months in the central region are intensely hot with a daily maximum about 45° C. Winters are cooler, with a maximum temperature of 22° C declining to 10° C or lower. Relative humidity also varies with seasons with typical summer humidity of between 15 to 20 %.

The Gulf coast is warm and humid in summer with average maximum of 42° C and winter maximum average of 22° C. Humidity varies seasonally greatly from 40% in summer to about 70% in winter [4].

Figure 2.2 shows the monthly mean dry bulb temperature profile, where July is the hottest month, representing the center-line of symmetry between months of

April, May, and June versus August, September, and October. In figure 5, the profile of the monthly wet bulb temperature shows that, during the summer period, the dry bulb temperature can be lowered close to the wet bulb temperature by using evaporative cooling techniques.

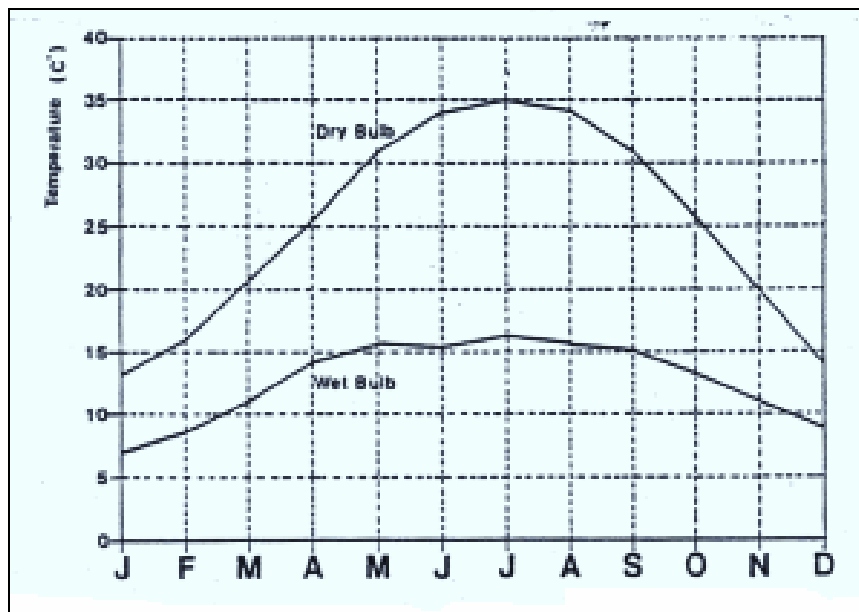


Figure 2.2 Profiles of Monthly Mean Dry Bulb and Wet Bulb Temperatures

The Saudi Presidency of Metrology and Environment (PME) [6] summaries the climatic characteristics of summer in Saudi Arabia and states that During the month of June of each year fall sunlight perpendicular to the Tropic of Cancer (23.5 degrees to the equator) marked the beginning of summer climate in the northern hemisphere where this line that exists on the amount of mid Kingdom solar radiation Fallen lead to higher temperatures for most areas Which leads to lower air pressure and a low heat on the Arabian peninsula related sprawl Low seasonal India, which Limited north

and west until it reaches to the eastern Mediterranean, is among the characteristics that this low-temperature air mass of very hot and dry and reflected the temperature in this Chapter reach Britain, where between 44 to 47 degrees Celsius up to 50 degrees Celsius especially at the east of the Kingdom can rank the first part of this period is, until July half the dry summer period where there is this period northern winds and dry warm and active periods leading The polluting peaking amid the day interaction with the air along the high-centered in the north west of Saudi Arabia, which arise with differences in the values of temperature, pressure, and the eastern and central regions of the Kingdom. The areas west of Saudi Arabia affected by the winds East (poisons) that blow from time to time and be very hot and dry and loaded with dust.

The remainder of the period in question until the end of the summer period could be classified on the coasts wet summer (July and last until the end of September) and is characterized by a rise in temperature and humidity, which runs frequently.

When the East wind prevails and light to moderate at times eastern region and are loaded with water vapor and because of the high temperatures, they are demanding significantly.

Yet this does not chapter in Gulf of nice to make the heights of Asir, Baha and Taif resort destination nationals of the Kingdom and Gulf countries, so if we gazed rate temperatures about 16 degrees smaller percentage may fall to 10 degrees as previously recorded Abha in 1994.

If we add to this mountain terrain and the presence of subtropical Front, which is characterized by large amounts of water vapor in the South and moved north to reach the fullest extent of the district of Medina, cause these things together in rainfall

may be heavy in some years as previously And registered the highest amount of precipitation in this chapter of Khamis Mushait (146 mm), Abha (112 mm), Taif (143 mm) and in 1992 had been accompanied by activity in surface winds depressed by wind where it arrived in Jizan (110 knots in 1991).

It should be noted that at a time when the rain stopped on the eastern Mediterranean influence extends well front subtropical zone until Medina since the torrential rains of 6 mm and 9 mm Riyadh, both in July 1978 either Mecca reports had registered the highest amount of precipitation presidency with the 1992 and 1998 Approximately (40 mm) and during the month of July.

2.2 Passive Cooling

The term "passive" means not "active". The term "passive" refers to the method of cooling a building with the use of natural renewable sources without sophisticated mechanical equipment [7]. A passive cooling system may include simple devices such as a water pump or a fan when its application might enhance the system's performance [8]. The natural cooling mechanisms which are employed most are cooling by ambient cool air, long-wave radiation to the night sky, water evaporation and earth . These natural sources act as a heat sink to store heat from building that will

be cooled. Each of these cooling sources can be manipulated in different ways to result in various cooling systems.

Passive cooling systems are classified based on the different natural recourses. The natural sources useful in cooling and the systems derived are: (1) ambient cool air, from which the comfort ventilation and nocturnal convective cooling systems are derived; (2) night sky, on which the direct radiant cooling and indirect radiant cooling systems are based; (3) water evaporation, which can be utilized in direct and indirect passive evaporative cooling, and (4) earth, which can be used in direct earth-coupling cooling and indirect earth cooling.

Passive cooling techniques have been developed to achieve three major objectives: (1) to cool buildings with the use of renewable inexpensive natural energy sources, (2) to lower the cost of cooling, (3) to provide a solution to the "green house" effect. Mechanical air conditioning is considered expensive compared to passive cooling in terms of the initial cost, maintenance, and repairs. Moreover, mechanical cooling intensifies the use of electricity in peak demand hours during summer days. Thus, applying passive cooling systems reduces peak demand and flattens electricity use profiles. Even, if there is a need to use an expensive source such as electricity to operate passive coolers, the amount of energy will be lower than the energy needed for mechanical air conditioning because the coefficient of performance (COP) (the ratio of the cooling obtained (Watt) to the power input (Watt) of the passive system) is about five times higher than the mechanical air conditioning [9].

The technology harnessing natural phenomena to achieve cooler temperatures inside dwellings, particularly in hot dry regions, has been known since early times [10]. Traditional methods of designing and integrating passive cooling systems within

residential units such as storing night coolness in thick walls, underground rooms, and creating fountains and ponds and wind towers or so called " Baud Geer" in iran, were quite rudimentary and their efficiency was relatively low [11]. The wind towers have been used for centuries in the hot dry and hot humid climates in Afghanistan, the Arabian Gulf states, Egypt, Iraq, Iran and Pakistan.

2.3 Evaporative Active Cooling

Active cooling is the method of supplying cooling with the help of mechanical cooling systems like fans, air conditioners and cooling towers.

The active cooling can be generated by air blowing devices like fans or can be generated by water as in cooling towers or it can generated by both air and water together known as evaporative active cooling.

An evaporating droplet is a complex phenomenon, and much effort, both experimental and theoretical has been performed in an attempt to elucidate and describe the mechanisms. From the experimental point of view, compromises have been made, and in order to develop the theory, simplifications have been necessary.

Most of the theoretical studies have been based on constant sphere diameter and negligible convective flux due to diffusion. The case in which the sphere diameter is changing was investigated by Brain and Hales [12], and to simplify the problem, the fluid properties were assumed constant. However, significant differences between constant and variable property results have been reported [13]. In general, because of the complexity of calculation involved in the describing equations, many simplifications have been necessary. For example, droplets were assumed to have

spherical shapes, heat conducted through the droplet was assumed negligible, constant properties were assumed [14].

Gilbert D. Kinzer and Ross Gunn [15] in 1950 made a theoretical and experimental study of the physical behavior of freely falling water drops, including the influence of ventilation and environment upon the evaporation and equilibrium temperature formulated in a quantitative terms. The theoretical approach emphasized the vapor and heat transferred to packets of environmental air that make transient contact with the liquid sphere. The basic psychrometric equation was derived for a freely falling spherical drop. Measurements of evaporation, equilibrium temperature and time to reach equilibrium were carried out for single drops and compared with theory. And new methods and apparatus especially devised to study freely falling drops were described.

S. E. Woo and A. E. Hamielec in 1971 [16] investigated a numerical solution of the Navier-Stokes equations of motion and the equation of mass transfer have been obtained for the steady-state transfer of chemically inert substance from the surface of a single rigid sphere moving at its terminal velocity in an unbounded fluid. Local Sherwood numbers were calculated for spheres with Reynolds numbers in the range of 0.05 -300 and for a fluid with Schmidt number of 0.71. the objective of this study was to model the effect of ventilation on the rate of evaporation of cloud drops falling at terminal velocity in air sub-saturated with respect to water.

M. Pasandideh-Fard, S. D. Aziz, S. Chandra and J. Mostaghimi in 2001 [17] studied using both experiments and a numerical model, the impact of water droplets on a hot stainless steel surface. Initial substrate temperatures were varied from 50°C to 120°C (low enough to prevent boiling in the drop) and impact velocities from 0.5 to 4

m/s. fluid mechanics and heat transfer during droplet impact were modeled using a "Volume-of-Fluid" (VOF) code. Numerical calculations of droplet shape and substrate temperature during impact agreed well with experimental results. Both simulations and experiments show that increasing impact velocity enhances heat flux from the substrate by only a small amount. The principal effect of rising droplet velocity is that it makes the droplet spread more during impact, increasing the wetted area across which heat transfer takes place. They also developed a simple model of heat transfer into the droplet by one-dimensional conduction across a thin boundary layer which gives estimates of droplet cooling effectiveness that agree well with results from the numerical model.

José Rui Camargo, Carlos Daniel Ebinuma and José Luz Silveira in 2005 [18] studied the Basic principles of the evaporative cooling process for human thermal comfort, the principals of operation for the direct evaporative cooling systems and the mathematical development of the equations of thermal exchanges, allowing the determination of the effectiveness of saturation. They also presented the results of experimental tests in a direct evaporative cooler that take place in the Air Conditioning Laboratory at the University of Taubate Mechanical Engineering Department, and the experimental results used to determine the convective heat transfer coefficient to compare with mathematical model.

Jiří Smolík, Lucie Džumbová, Jaroslav Schwarz and Markku Kulmala in 2000 [19] investigated the heat and mass transfer from evaporating water droplets using wind tunnel technique. The results were compared with results of other authors and correlated by an empirical fit proposed by Clift, Grace, and Weber [20]. It was found that the fit gave reasonably accurate predictions for Reynolds numbers ranging from 0

to 400. the accuracy of the obtained expression was tested comparing measured and calculated droplet temperatures. The results agree always within 5% and usually even within 1%. This represents an experimental validation for mass and heat flux expressions commonly used in condensation and evaporation studies.

Much experimental work has been published. Studies have been carried out under many different conditions, including forced and free convection, laminar or turbulent flow, varying temperature [21] and pressure [22, 23] and so on. In each case, the droplet was either supported on a fiber or on a thermocouple, or falling freely. Other factors influencing the evaporation rate from droplets, such as vibration, rotation [24, 25] and the effect of the deviation of the shape of the droplet from that of a true sphere [26] have also been the subject of several studies. In order to simplify the complex system, some of the studies have been carried out with constant droplet diameter. This was achieved by matching the feed rate to the droplet through a micro burette, which also carried the droplet, to the rate of evaporation.

Y. F. Li, and W. K. Chow in 2007 [27] studied the evaporation of water droplets while traveling in hot layer. The air-droplet system was analyzed by solving the mass, momentum and energy conservation equations for each phase. The droplet phase was described by the Lagrangian Approach. The Runge-Kutta algorithm was used to solve the ordinary differential equation group for the droplet motion with heat transfer. Droplet positions, velocities, temperatures and diameters were calculated while traveling in the hot air reservoir.

CHAPTER 3

METHODOLOGY AND EXPERIMENTAL SET-UP

Experimental part has been basically done in two stages. The first stage has been conducted without mist and the second stage has been done with mist.

3.1 First Stage (Without Mist)

The first stage was devoted to find empirical relationship that relates the fan coverage area with fan diameter from one aspect and the fan coverage area with fan heights from the other aspect. For this stage of experiment, three fans have been selected with the following diameters (20 inch, 24 inch and 30 inch) as shown in figure 3.1. These fans were selected specifically to have exactly aerodynamic similarities except the length of diameter where we have three different lengths of diameters as stated above.



Figure 3.1 Fans (20 inch, 24 inch and 30 inch) used in experiments

As shown in figure 3.2, the fans were leveled to their first diameter in height and then operated to take the airspeed measurements for each diameter of the three fans in front of each one, where we called it the coverage area domain. The airspeed and temperature were measured by placing sensors in the domain.

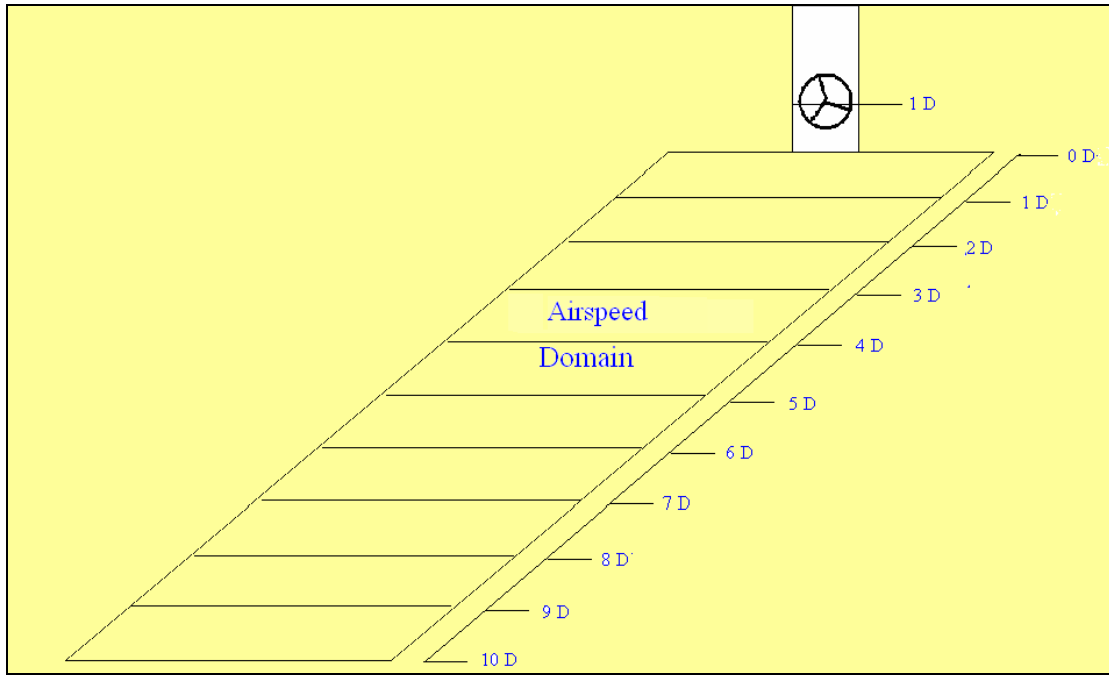


Figure 3.2 Temperature domain for first fan diameter in height

Then the fans were leveled to their second, third, fourth, and fifth diameter in height in which the airspeed and temperature were measured in the same manner as stated in the previous paragraph. For different fan heights, see figure 3.3.

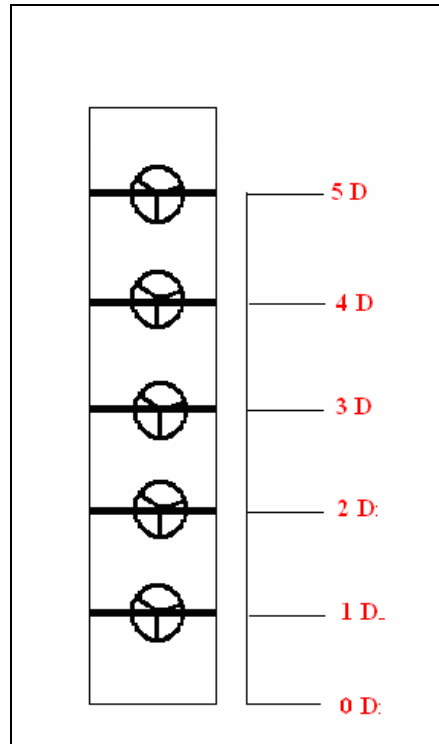


Figure 3.3 Different fan heights

3.1.1 Angle Effect (Without Mist)

Also one aspect that was included in the experiments was the angle effect of the fans. For zero angle as explained in default case, the airspeed and temperature effect could reach maximum range but for higher levels of fans like in the 4th Diameter and in the 5th Diameter, the area that is directly below the fan was not affected much and the airspeed and temperature decrease in that area were lesser than we wish to achieve thermal comfort, so because of that, the fans were angled down to 20 Diameter and 10 Diameter angles as expressed in equations (3.1), (3.2) and (3.3); and the airspeed and temperature were measured as shown in figure 3.4.

3.2 Second Stage (With Mist)

The second stage was devoted to investigate the temperature domain for the same three different fan diameters (20 inch fan diameter, 24 inch fan diameter and 30 inch fan diameter) as shown in figure 3.1; and for different heights with mist; to find empirical relationship that relates temperature with fan diameter from one aspect and temperature with fan heights from the other aspect.

Mist system was attached to each fan consists of six nozzles each nozzle was of about 200 micrometer diameter with an operating pressure of about 50 bar as shown in figure 3.5.

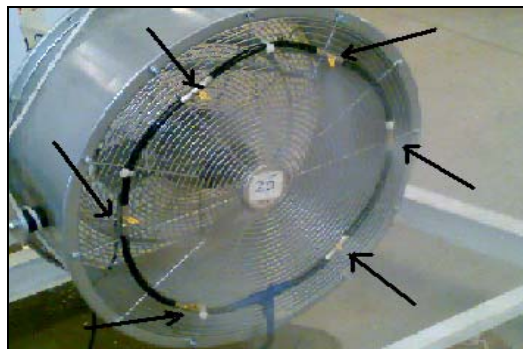


Figure 3.5 Fan with mist nozzles

As shown in figure 3.6, the fans were leveled to their first diameter in height and then operated with mist system to take the airspeed and temperature measurements in each diameter of this fan in front of it where we called it the temperature domain. The temperature was measured by placing sensitive thermometers at each diameter range till the maximum range of diameters is reached in which we reach the atmospheric air temperature and there was no more drop in temperature values.

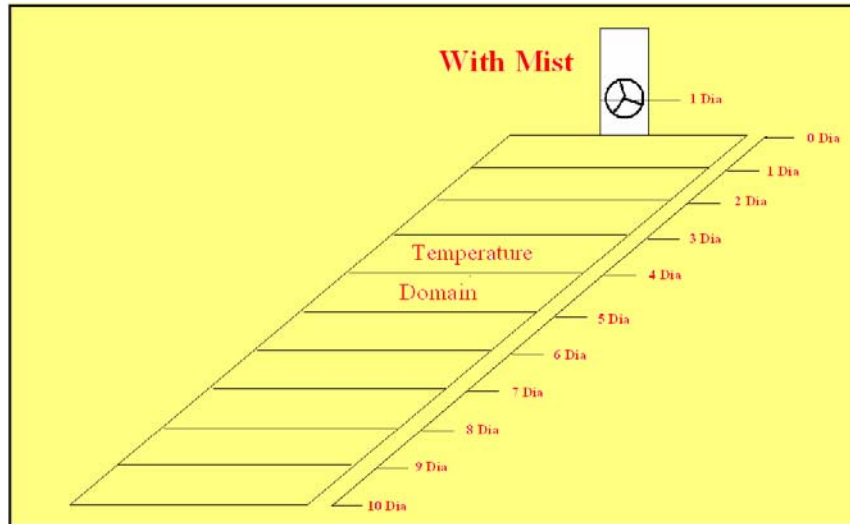


Figure 3.6 Temperature domain for first fan diameter in height with mist

Then the fans were leveled to their second, third, fourth, and fifth diameter in height, in which the airspeed and temperature were measured in the same manner as stated in the previous paragraph. For different fan highest, see figure 3.7.

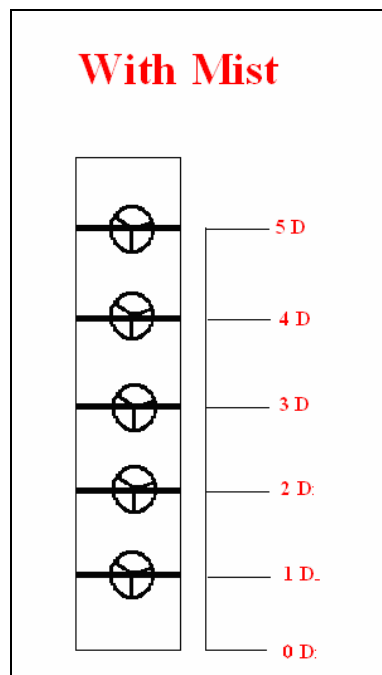


Figure 3.7 Different fan heights with mist

3.3 Computational Study

The aim of the computational study is to built an experimentally verified mathematical model to be used in the design and optimization of water mist cooling systems and to compare the mathematical results to the experimental results and to get an insight of how to apply such evaporative mist cooling for different places for different conditions. In this study, mathematical solution is presented based on experimental conditions, such dry bulb temperature, wet bulb temperature, relative humidity, operating pressure and fan airspeed.

All experimental conditions were kept the same for the three fans except the fan airspeed which varies according to different fan diameter. The mathematical study was conducted based on mass transfer diffusion equation to calculate the evaporation rate as a first step and based on energy balance equation to calculate the temperature for each fan as a second step.

In the thermodynamic modeling of an evaporating liquid-water droplet, use may be made of the transient form of the First Law of Thermodynamics applied to control volume with a moving boundary. There are some assumptions made for the model as follows:

- The surface of the control volume coincides with the surface of the droplet.
- The droplet is assumed to be in a spherical shape.
- The heat transfer at the surface is due to convection.
- The mass transfer occurs as evaporation takes place at the interface between the droplet and air.

- The temperature in the droplet is assumed to be uniform during the evaporation process..

3.4 Outline of the Present Work

Following this brief introduction is chapter 2, which is a review of the literature on climatic characteristics and features of regions of Saudi Arabia and the research on evaporative cooling systems, including some of their application. In chapter 3, a demonstration of methodology and experimental set-up is introduced with declaring special case studies. In chapter 4, an introduction is given as background of cooling methods and strategies generally of passive cooling, active cooling and comparison between evaporative coolers and electric coolers. In chapter 5, there is a detailed explanation of the method used to determine the fan airspeed experimentally. Chapter 6 describes in detail the experimental set-up and methodology including the instrumentation and finally the experimental results. Chapter 7 contains a detailed discussion of the computational solution and results. In chapter 8, there is a detailed discussion of the results both the experimental and the computational and analyzing the data coming up with relations that the research was devoted for. This includes a detailed discussion of factors that affect the evaporation process in the evaporative cooling like air humidity, operating pressure, airspeed and air temperature. Chapter 9 contains a detailed discussion and conclusion with recommendations for future research work.

CHAPTER 4

BACKGROUND INFORMATION:

4.1 Passive Cooling

Before refrigeration technology first appeared, people kept cool using natural methods: breezes flowing through windows, water evaporating from springs and fountains as well as large amounts of stone and earth absorbing daytime heat. These ideas were developed over thousands of years as integral parts of building design. Today they are called "passive cooling." Ironically, passive cooling is considered an "alternative" to mechanical cooling that requires complicated refrigeration systems. By employing passive cooling techniques into modern buildings, we can eliminate mechanical cooling or at least reduce the size and cost of the equipment.

4.1.1 Passive Cooling Strategies

4.1.1.1 Natural Ventilation [28]

It depends solely on air movement to cool occupants. Window openings on opposite sides of the building enhance cross ventilation driven by breezes. Since natural breezes can't be scheduled, designers often choose to enhance natural ventilation using tall spaces within buildings called stacks. With openings near the top of the stack, warm air can escape, while cooler air enters the building from openings near the ground. Ventilation requires the building to be open during the day to allow airflow.

4.1.1.2 High Thermal Mass [29]

It depends on the ability of materials in the building to absorb heat during the day. Each night the mass releases heat, making it ready to absorb heat again the next day. To be effective, thermal mass must be exposed to the living spaces. Residential buildings are considered to have average mass when the exposed mass area is equal to the floor area. So, for every square foot of floor area there is one square foot of exposed thermal mass. A slab floor would be an easy way to accomplish this in a design. High mass buildings would have up to three square feet of exposed mass for each square foot of floor area. Large masonry fireplaces and interior brick walls are two ways to incorporate high mass

4.1.1.3 High Thermal Mass with Night Ventilation

It relies on the daily heat storage of thermal mass combined with night ventilation that cools the mass. The building must be closed during the day and opened at night to flush the heat away.

4.1.1.4 Evaporative Cooling

It lowers the indoor air temperature by evaporating water. In dry climates, this is commonly done directly in the space. But indirect methods, such as roof ponds, allow evaporative cooling to be used in more temperate climates too.

Ventilation and evaporative cooling are often supplemented with mechanical means, such as fans. Even so, they use substantially less energy to maintain comfort compared to refrigeration systems. It is also possible to use these strategies in completely passive systems that require no additional machinery or energy to operate.

4.1.2 Which Passive Cooling Strategy is Right to Use?

Passive cooling is based on the interaction of the building and its surroundings. Before adopting a passive cooling strategy, we must be sure that it matches our local climate.

In the book *Sun, Wind and Light* [30], G.Z. Brown identifies the four passive cooling strategies discussed above: natural ventilation, evaporative cooling, high thermal mass and high thermal mass with night ventilation. All these passive cooling strategies rely on daily changes in temperature and relative humidity. We can identify the passive cooling strategies that are appropriate for our building site by using a bioclimatic chart.

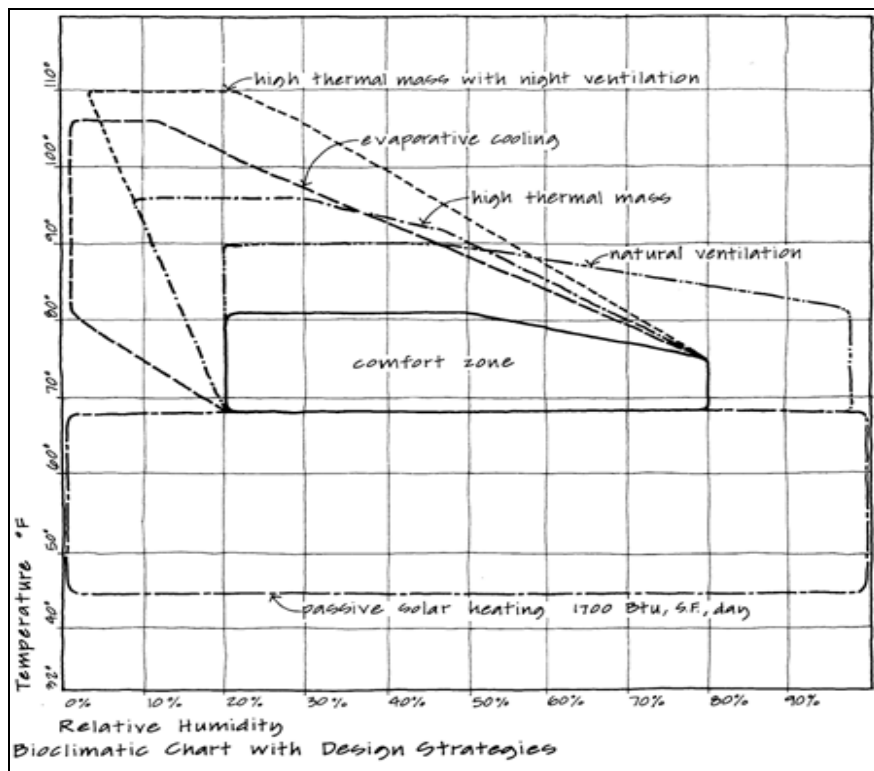


Figure 4.1 Bioclimatic chart

This bioclimatic chart defines the four passive cooling strategies based on temperature and relative humidity. This chart can be used to determine which passive cooling strategies are appropriate for the climate at the building site.

First, we find the following local weather information for each of the months of the year:

- average maximum temperature
- average minimum temperature
- average maximum relative humidity
- average minimum relative humidity

This information can be found in weather records kept by most local airports. An extensive list of climate data can be seen on the World Wide Web at www.ugems.psu.edu/~owens/climate.html.

On the bioclimatic chart, we plot two points for each month. The first point is the minimum temperature and the maximum relative humidity (RH). The second point is the maximum temperature and the minimum RH. (Note that the highest temperature is paired with the lowest RH and vice versa.) We connect these points with a line we plot a similar line for each month. Each line represents the change in temperature and RH over an average day.

Passive cooling strategies are shown on this version of the bioclimatic chart as overlapping zones. When our lines cross zones, it indicates that this strategy may work for our climate. Some months may lend themselves to several different strategies. To reduce cost, we would probably choose one or two strategies that are compatible with each other and the building design.

These passive cooling concepts address getting rid of heat that accumulates in buildings. Of course, we also want to reduce heat gains in the first place with high insulation levels, heat blocking windows, proper solar orientation and good shading from building elements and vegetation.

Passive solar heating can also be assessed using the bioclimatic chart. Passive solar heating is usually an appropriate strategy when the plotted lines fall anywhere below the comfort zone.

4.2 Active Cooling

Active cooling is the method of supplying cooling with the help of mechanical cooling systems like fans, air conditioners and cooling towers.

The active cooling can be generated by air blowing devices like fans or can be generated by water as in cooling towers or it can be generated by both air and water together known as evaporative active cooling.

We have all noticed how cool it feels near a waterfall on a hot summer day. That's evaporative cooling: the reduction in air temperature that occurs when water evaporates. Evaporative coolers, commonly called "swamp coolers," use this effect to cool homes. Evaporative coolers have a low first cost, use a lot less electricity than conventional air conditioners, and do not use refrigerants, such as chlorofluorocarbons (CFCs) and hydro-chlorofluorocarbons (HCFCs), which can harm the ozone layer.

There are two types of evaporative coolers: direct and indirect.

- In a direct evaporative cooler, a blower forces air through a permeable, water-soaked pad (fan-pad) or fog/mist system. As the air passes through the pad, it is filtered, cooled, and humidified.
- An indirect evaporative cooler has a secondary heat exchanger which prevents humidity from being added to the air stream which enters the home.

4.2.1 Evaporative Cooling Methods

When water evaporates, it absorbs a large amount of heat from its surroundings (about 1000 BTU per pound of water evaporated) [31]. The most familiar example of this is the cooling effect of evaporating perspiration on the human skin. In arid, hot

climates, body temperature is partially controlled by the rapid evaporation of perspiration from the surface of the skin. In hot climates with high atmospheric moisture, the cooling effect is less because the high moisture content of the surrounding air. In both situations, however, the evaporation rate is raised as air movement is increased. Both of these facts can be applied to natural cooling of structures.

Evaporative methods can be used to enhance the cooling rates in convective cooling systems. One way of doing this is to bring the outdoor air into the house through a moist filter or pad as shown in Figure 4.2. The familiar evaporative cooler, precursor to the air conditioner, is a mechanical system which uses these principles with a motor to force air movement and distribution. Passive cooling strategies with earth tubes and/or cool towers use the same principles but utilize natural systems for air drivers and distribution.

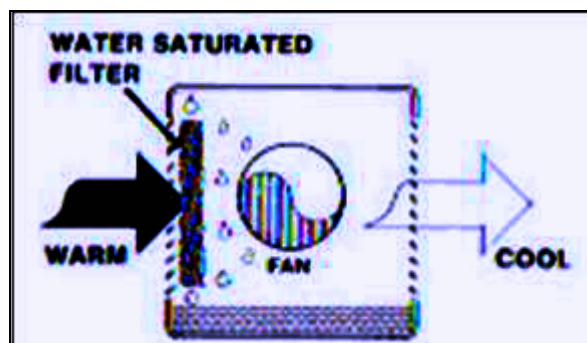


Figure 4.2 Swamp cooler - drier

Cool towers utilize wet cooling pads, and the force of gravity. Heavier, cooled air "falls", via gravity, into the building and its momentum floods the habitable area. This cool tower action can be enhanced and distribution extended, by the placement of thermal chimney "drivers" which can pull the cooled air through the building with an increase in both air quantity and velocity. In either case, the cooler air now has a higher relative humidity, but this is not usually a problem and can even be a benefit in arid climates.

In some areas, there may be a time of higher humidity (desert monsoon season). While sensible heat continues to be mitigated by passive cooling techniques, the latent heat contained in the humid air is more difficult to dissipate, which renders evaporative cooling less effective. The integration of air dehumidification system easily corrects this short term problematic condition.

With all evaporative cooling methods, it is important to maximize airflow across the exposed water. Fresh air must be continually available to replace the humid air being built up near or over the water. Failing this, air will be quickly saturated with water vapor, and the evaporation and cooling rates will decline abruptly. Lips, edges and other structures or buildings that could block or deflect prevailing winds away from the water surfaces should be studiously avoided. Sometimes, a small fan to disturb the air over a pond will greatly aid the evaporation rate on a hot, sultry day or night.

Even with direct, active evaporative cooler systems, provision of interior thermal mass combined with direct evaporative cooling is a combination that works effectively. During the day, the structure can utilize the stored coolness in the walls and floors, and maintain an improved level of comfort while reducing power

requirements of direct evaporative cooler system. In many areas which are considered hot, arid zones, periods of higher humidity renders mechanical evaporative cooling unsatisfactory even when optimized techniques are used. A solution to this is the two-stage evaporative cooling system, which has been shown to be an effective alternative to direct evaporative cooling or refrigerated air-conditioning.

While not a passive system, two-stage evaporative cooling is an important element to be considered as part of passive cooling strategies. Cooling is accomplished by pre-cooling ambient air without humidification before further cooling by evaporation. The cool air entering the structure is then exhausted, typically through areas of heat gain such as windows or the attic. The pre-cooling may be accomplished by a combined cooling tower, heat exchanger unit, or by nocturnally cooled rock bed through which air is drawn. The second stage, evaporative cooling, is accomplished by a standard commercial evaporative cooling device, or by passive cooling elements of earth tubes or cool towers. Rock bed mechanical cooling has been used extensively in Australia with high degrees of effectiveness.

Two-stage evaporative system can also be combined with active and hybrid solar heating systems using the same storage (rock bed) system for both seasons. This type of system is necessarily suited for new construction because of the requirement for the rock bed, which is most effectively located beneath the structure. It works well during hot, humid periods using only slightly more power than direct evaporative cooling and the comfort attained is similar to that of refrigerated air-conditioning.

Recuperative and regenerative evaporative cooling options are other methods to produce greater comfort using evaporative cooling. These techniques use the relatively cool air exhausted from the structure to improve the performance of the evaporative cooling device. Evaporatively cooled water reduces in temperature the ambient air in the heat exchanger without humidification as it enters the structure. The cool, dry air warms a few degrees as it passes through the structure and exits through the evaporative cooling device or a cooling structure. Since the exiting air is cool and dry, the wet bulb temperature is lower and the water produced by the evaporative cooling device is cooler than if ambient air were used. The rock bed heat exchanger and the evaporative cooling device could be combined into a single unit. If the rock bed is used to store heat in the winter, the cost effectiveness of the system is improved.

Because of the large volumes of air that are moved in an effective evaporative system, the ducts must be large and appropriately sized. Typically, evaporative cooler ducts are at least three times the cross-section area of ducts refrigeration; ducts should be laid out using the shortest route possible and a minimum of turns. Evaporative cooling has been shown to be an effective alternative to refrigerated air-conditioning throughout the desert regions of the southwest of US. The selection of the particular evaporative cooling techniques must be made carefully through analyzing the local climatic conditions. These cooling systems should be integrated into the design of the home and where possible, with the design of the solar heating system. By integrating these systems at the design stage, greater efficiencies and more attractive economics can be obtained.

4.3 Comparisons to Air Conditioning

Comparison of evaporative cooling to electric [air conditioning](#) according to reference [32]:

Less expensive to install

- Estimated cost for installation is 1/8 to 1/2 that of refrigerated air conditioning

Less expensive to operate

- Estimated cost of operation is 1/4 that of refrigerated air.
- Power consumption is limited to the fan and water pump vs. compressors, pumps, and blowers in case of refrigerated air.

Ease of Maintenance

- The only two mechanical parts in most basic evaporative coolers are the fan motor and the water pump, both of which can be repaired for very little cost and often by a mechanically able homeowner.

Ventilation air

- The constant and high volumetric flow rate of air through the building reduces the age-of-air in the building dramatically.
- Evaporative cooling increases humidity, which, in dry climates, may improve the breath ability of the air.
- The pad itself acts as a rather effective air filter when properly maintained; it is capable of removing a variety of contaminants in air, including urban ozone

caused by pollution, regardless of very dry weather. Refrigeration-based cooling systems lose this ability whenever there is not enough humidity in the air to keep the evaporator wet while providing a constant trickle of condensate that washes out dissolved impurities removed from the air.

- Carbon Dioxide emissions are many times lower than refrigerated [33].
- Evaporative cooling systems produce thermal comfort for people especially in the dry weather; but it may cause them thermal discomfort in the humid regions when the humidity registers high values. Basically, the feeling of comfort or discomfort depends on many factors such as air temperature, temperature of adjacent surfaces, air humidity, air movements, and individual's health and perception. When the climatic conditions are such that the rate of exchange of heat between the body and the environment are in balance then this range of environmental temperature is called the comfort zone. In the comfort zone, the heat balance is maintained primarily by regulating the flow of blood in the body. For a clothed and resting person this zone lies between 20 and 23 degrees centigrade. When the surrounding temperature is slightly above the comfort zone, the body uses the additional mechanism of perspiration to maintain the body temperature. The range of temperature where this happens is called the zone of evaporative control. The maximum temperature that the body can deal with in this way is called the limit of tolerance. Rise in temperature beyond this level can cause heat stroke and event death. At temperature below zone of comfort the body maintains its temperature by body generating more heat internally, which results in loss of heat from the body. This is called the zone of cooling. In this zone the the temperature of the peripheral parts of the body reduces, which the body is able

to withstand, however continued reduction causes reduction in core body temperature leading to death by freezing. The comfort chart (figure 4.3) relates [effective temperature](#), dry-bulb temperature, relative humidity, wet-bulb temperature, and air movement to human comfort. This chart indicates comfort zones of people for different weather conditions [34].

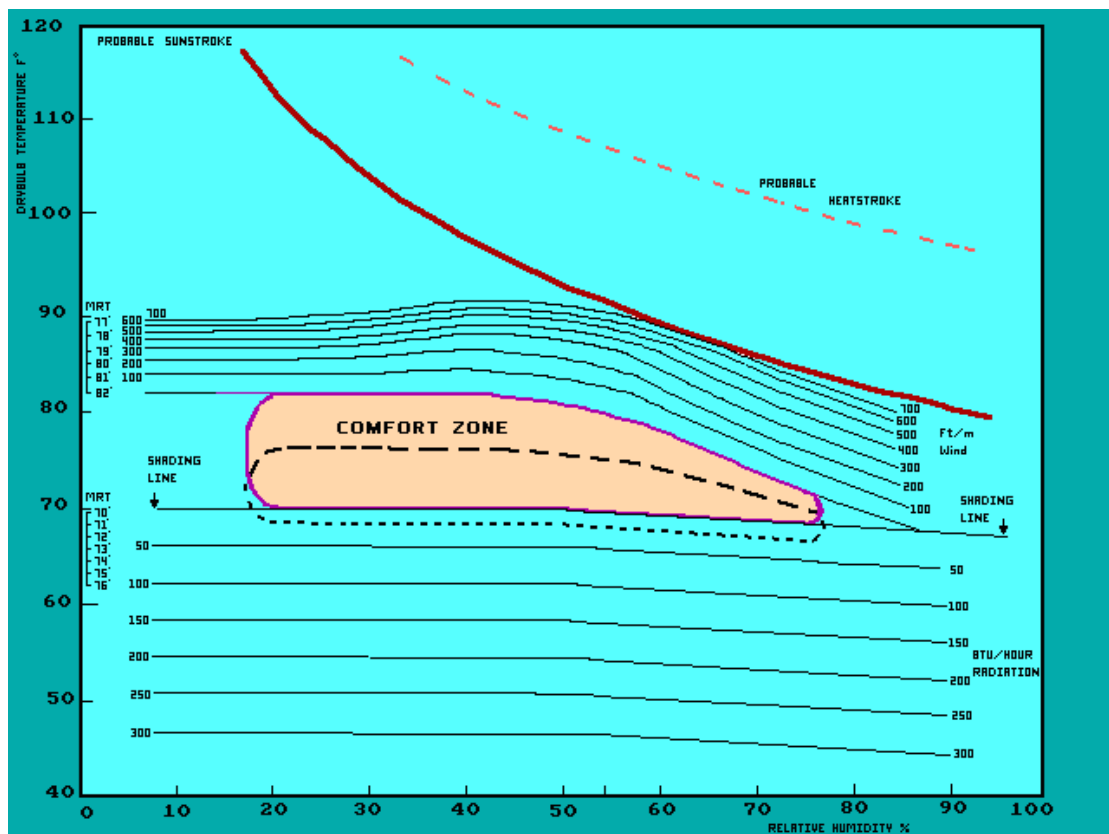


Figure 4.3 Comfort chart

In this chart, the air temperature is plotted on the vertical axis and relative humidity on the horizontal axis. The shaded solid line area near the center of the graph shows the combination of temperature and humidity which most humans would find comfortable during the summer if they are sitting in the shade. The dotted area shows the comfort zone for the winter. It is

interesting to see that the human body can actually adjust somewhat to different seasons.

The climatic elements around the comfort zone are shown by means of curves, which indicate the nature of corrective measures necessary to restore the feeling of comfort at any point outside the comfort zone. For any point of known dry-bulb temperature and relative humidity, which falls within the boundaries of the comfort zone, no corrective measures are needed.

CHAPTER 5

FAN AIRSPEED MEASUREMENT

The determination of fan airspeed is important since it plays the biggest role in evaporation process and in determination of the area covered for each fan.

For the lack of information of fan airspeed for the three fans used in the experiment, it was necessary to think about some way to measure the fan airspeed for each fan.

The measurement of fan airspeed was done in two stages. The first stage was to find a relationship for calculating the fan airspeed by using a small fan connected to a voltmeter in the following manner. By using a car moving in different speeds while the small fan was fixed outside the car and taking the readings of the voltmeter for each car speed as shown in figure 5.1. A relationship that relates airspeed and voltage is now available and could be used later to calculate each fan airspeed as stated in the second stage.



Figure 5.1 Small fan and Voltmeter used

The experimental data is shown in table 5.1.

Table 5.1 Experimental data of airspeed versus voltage

Car Airspeed (m/s)	Volt (v)
5.55555556	0.85
8.33333333	2.1
11.11111111	3.3
13.88888889	3.9
16.66666667	4.4
19.44444444	5.5
22.22222222	6
25	6.9
27.77777778	7.7
30.55555556	8.8
33.33333333	9.4
36.11111111	10.4
38.88888889	11.1
41.66666667	12.1
44.44444444	12.6

The relation of Voltmeter versus airspeed is shown in figure 5.2.

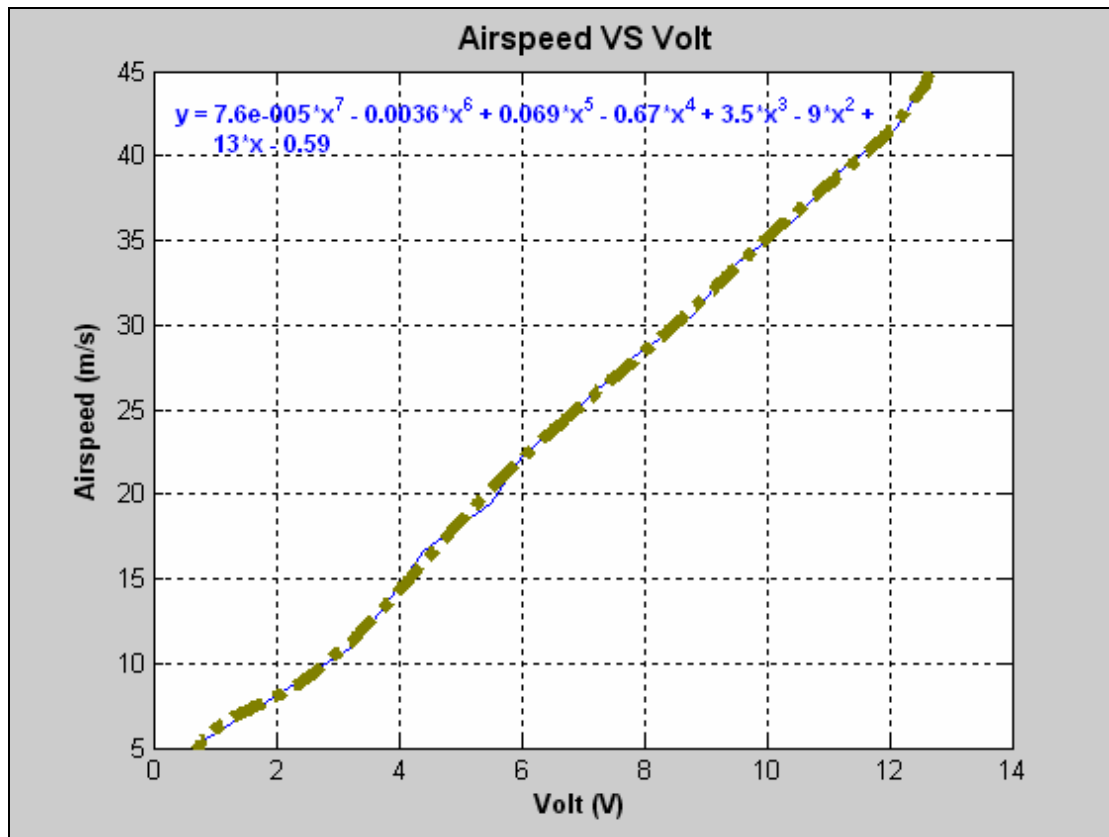


Figure 5.2 Relation of airspeed and voltage of airspeed measuring device

Equation (5.1) relates the fan airspeed and voltage.

Fan airspeed =

$$7.6 \times 10^{-5} \text{ Volt}^7 - 0.0036 \text{ Volt}^6 + 0.069 \text{ Volt}^5 - 0.67 \text{ Volt}^4 + 3.5 \text{ Volt}^3 - 9 \text{ Volt}^2 + 13 \text{ Volt} - 0.59 \dots\dots\dots(5.1)$$

In the second stage, the airspeed is measured for each fan with the small fan and with the voltmeter at the discharge side or intake into a fan. Airspeeds are more accurately determined on the discharge side of the fan than on the inlet side according to reference [35]. Many readings should be taken across the face of the fan to get an average airspeed. Because this is a rather crude field measurement, including as many readings as possible, using the nine readings shown in the fan figure as a minimum as shown in figure 5.3. Each measurement represents only a very small area of airflow over the fan face. Airspeed varies greatly across the face of a fan, with highest velocities coming off the blade tips and minimal velocity near the drive shaft. Velocities are determined near the blade tip, at the blade midpoint, and at the center of the fan as shown in figure 5.4.

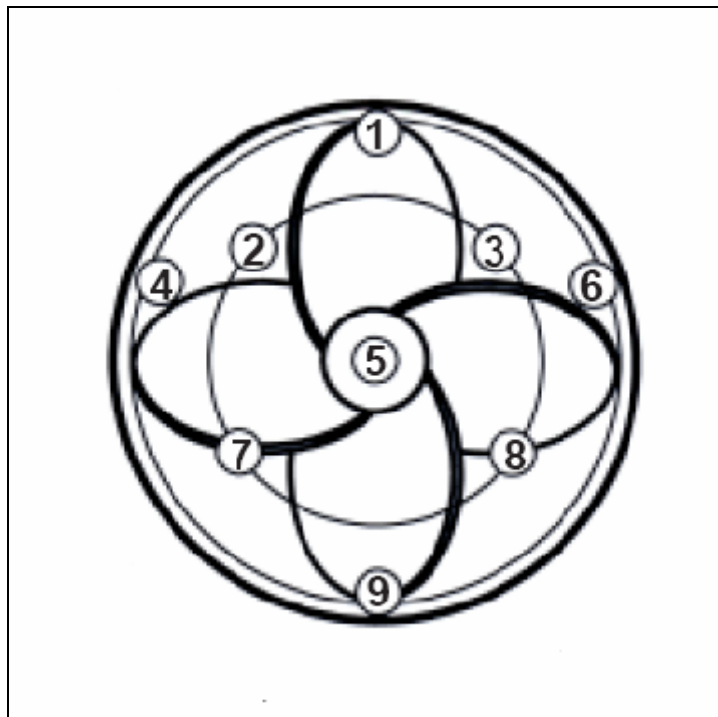


Figure 5.3 Reading locations taken across the fan

While measuring, it is preferred to step back out of the airflow, to the side of the fan when possible to minimize the amount of airflow that the body blocks. A long cable attaching the small fan and the voltmeter offers an advantage here.

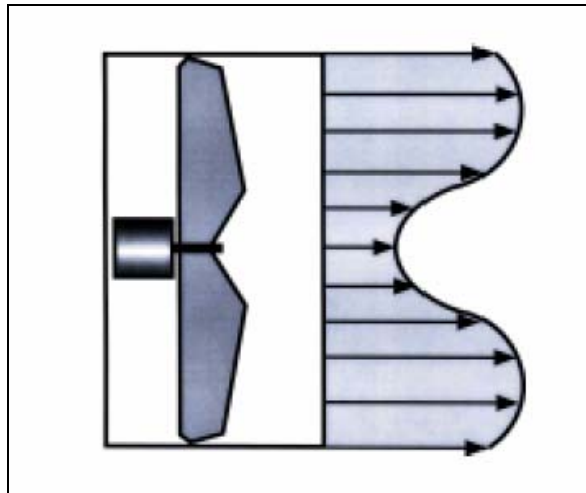


Figure 5.4 Variation in airspeed coming off fan tips versus near fan hub

Instead of using this method in measuring fan airspeed, there are several instruments which are appropriate for measuring the fast airspeed exiting a fan, listed in preferential order: vane anemometer, hot-wire anemometer, velocity manometer, or airspeed streamer.

The 20-inch fan:

- Maximum voltage reading is 0.65
- Maximum airspeed corresponds to voltage reading is 4.74 m/s

The 24-inch fan:

- Maximum voltage reading is 1.12 V
- Maximum airspeed corresponds to voltage reading is 6.36 m/s

The 30-inch fan:

- Maximum voltage reading is 1.95 V
- Maximum airspeed corresponds to voltage reading is 7.99 m/s

Table 5.2 Airspeed of the three fans

Fan Type	20-inch Fan	24-inch Fan	30-inch Fan
Diameter (m)	0.5	0.6	0.75
Max. Airspeed (m/s)	4.74	6.36	7.99

CHAPTER 6

EXPERIMENTAL SET-UP AND TEQUNIQUES

In this chapter, experimental procedure and results are presented for the first stage (without mist) and for the second stage with (mist).

6.1 First Stage (Without Mist)

The first stage is devoted to find empirical relationship that relates the fan coverage area with fan diameter from one aspect and the fan coverage area with fan heights from the other aspect. For this stage of experiment, three fans are selected with the following diameters (20 inch, 24 inch and 30 inch). These fans are selected specifically to have exactly aerodynamic similarities except the length of diameter where we have three different lengths of diameters as stated above.

It was proposed to measure the temperature for each diameter in the coverage area of each fan but that it was difficult because of the minor differences of temperature reading and it was impossible to be able to note these little differences with the used thermometers.

6.1.1 20-inch Fan

The airspeed of the 20-inch fan was measured as discussed in detail in chapter 5.

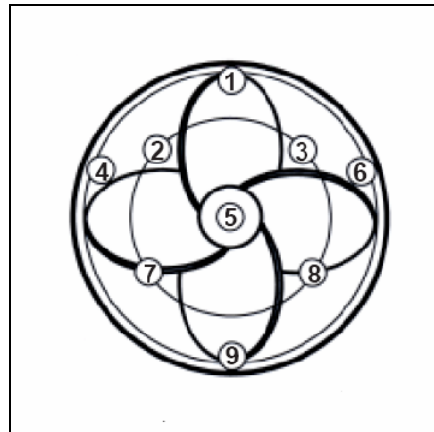


Figure 6.1. Reading locations taken across the 20-inch fan

6.1.1.1 1-Diameter in Height

The 20-inch fan is leveled for its first diameter in height as shown in figure 6.2.

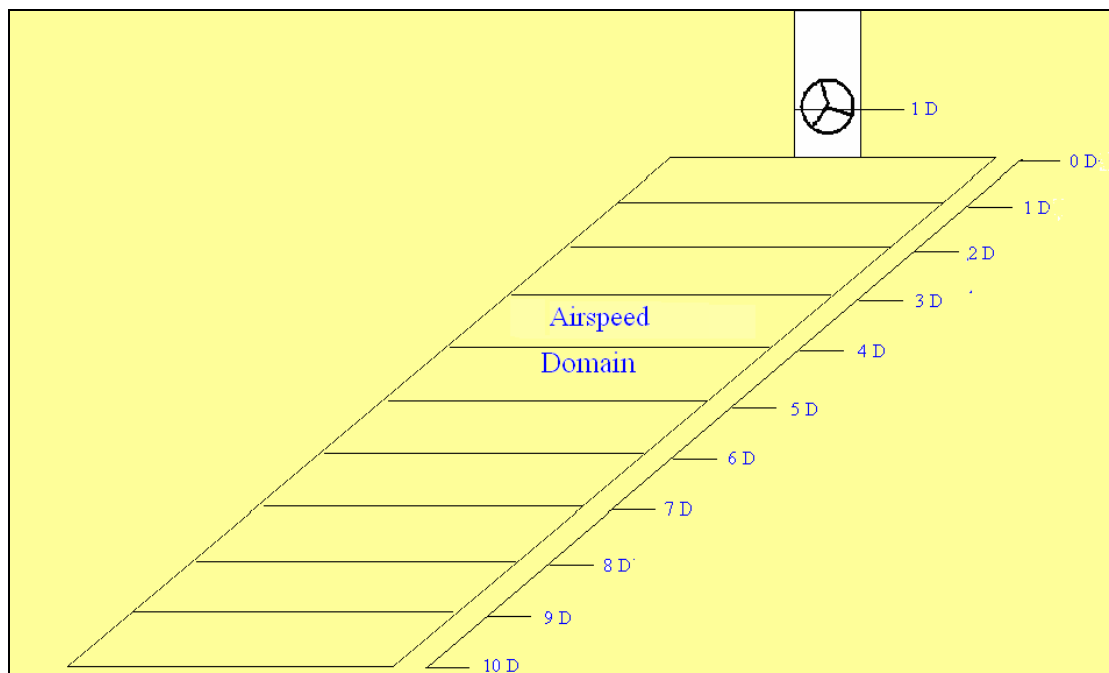


Figure 6.2 20-inch fan (D_s) for the first 1-diameter in height ($h = 1D$)

The airspeed is measured for each diameter converge area for the first diameter in height and tabulated in table 6.1

Table 6.1 Airspeed measurements of 20-inch fan (D_s) for 1-diameter in height ($h = 1$)

Distance in diameter	Airspeed (m/s)
1	0.9
2	1.5
3	2
4	2.6
5	3.5
6	2.5
7	1.7
8	1.0
9	0.55
10	0

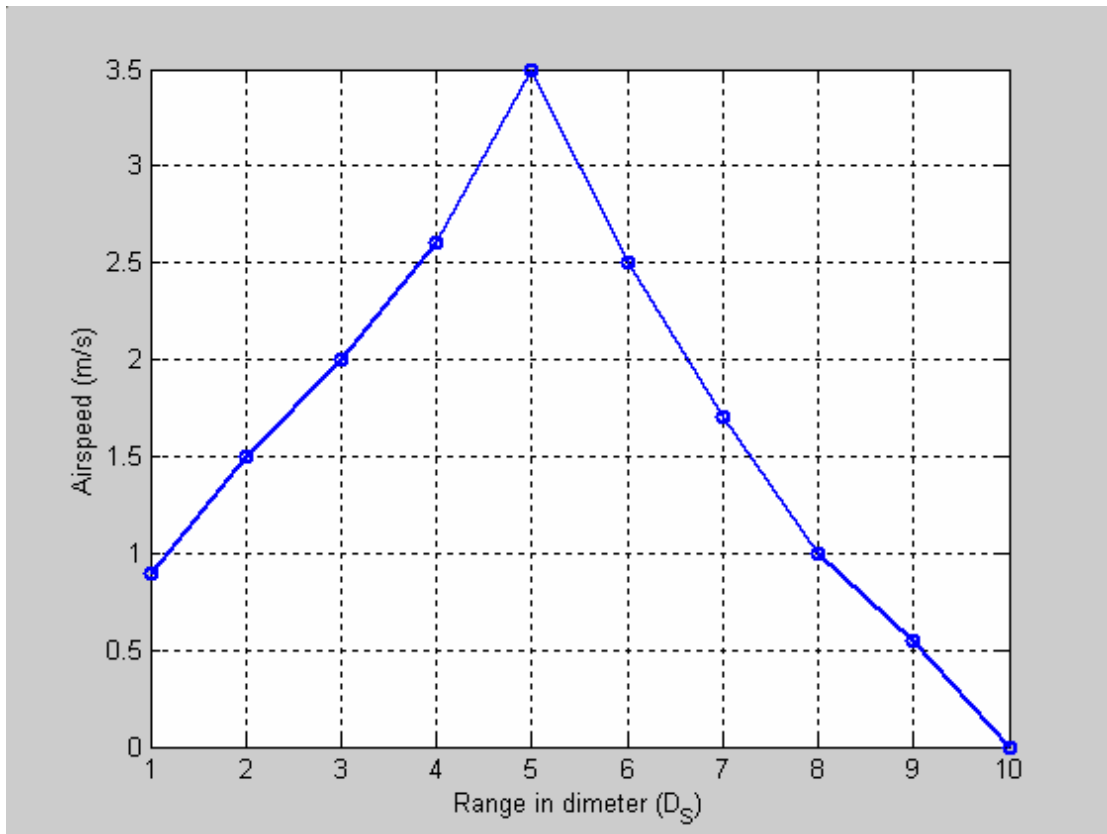


Figure 6.3 Airspeed measurements of 20-inch fan (D_S) for 1-diameter in height ($h = 1$)

6.1.1.2 2-Diameter in Height

The 20-inch fan is leveled for its second diameter in height. The airspeed is measured for each diameter converge area and tabulated in table 6.2

Table 6.2 Airspeed measurements of 20-inch fan (D_S) for 2-diameter in height ($h = 2$)

Range in diameter (D_S)	Airspeed (m/s)
1	0.03
2	0.31
3	0.81
4	1.4
5	2.12
6	2.85
7	2
8	1.4
9	1
10	0.6
11	0.3
12	0

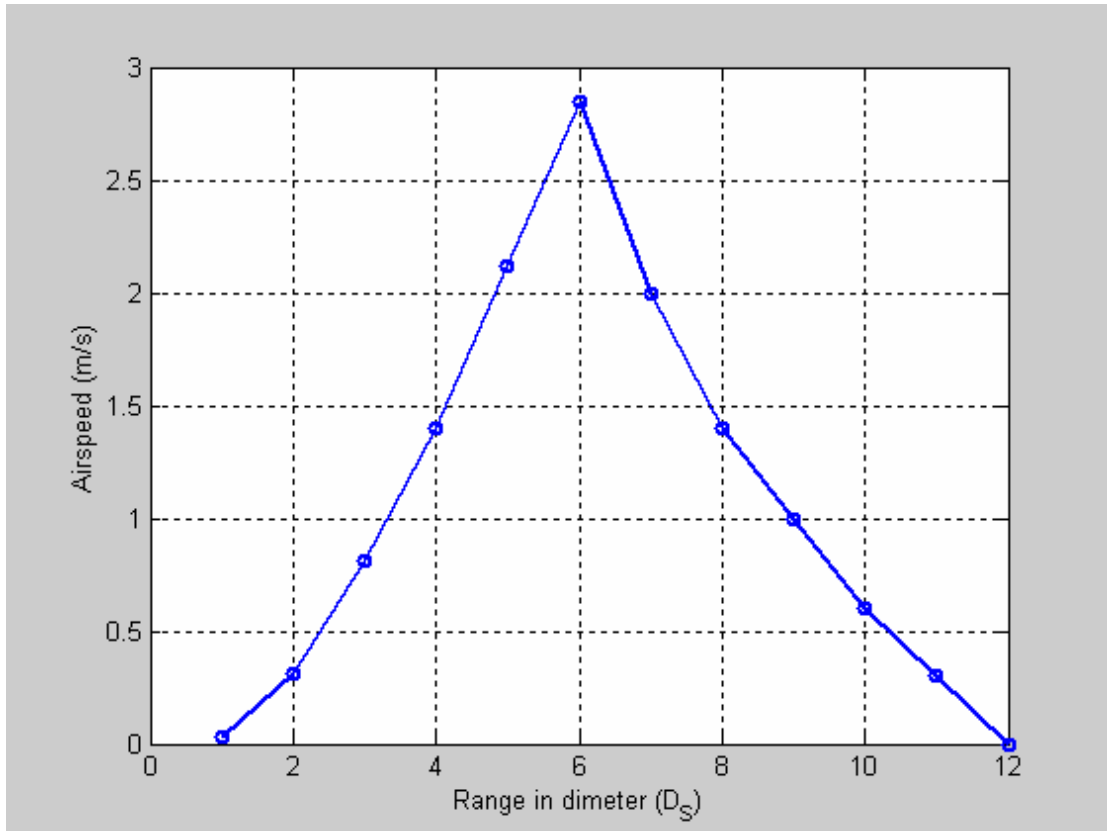


Figure 6.4 Airspeed measurements of 20-inch fan (D_S) for 2-diameter in height ($h=2$)

6.1.1.3 3-Diameter in Height

The 20-inch fan is leveled for its third diameter in height. The airspeed is measured for each diameter converge area and tabulated in table 6.3

Table 6.3 Airspeed measurements of 20-inch fan (D_s) for 3-diameter in height ($h = 3$)

Range in diameter (D_s)	Airspeed (m/s)
1	0.01
2	0.07
3	0.22
4	0.43
5	0.7
6	1.01
7	2.58
8	1.7
9	1.2
10	0.8
11	0.5
12	0.3
13	0.1
14	0

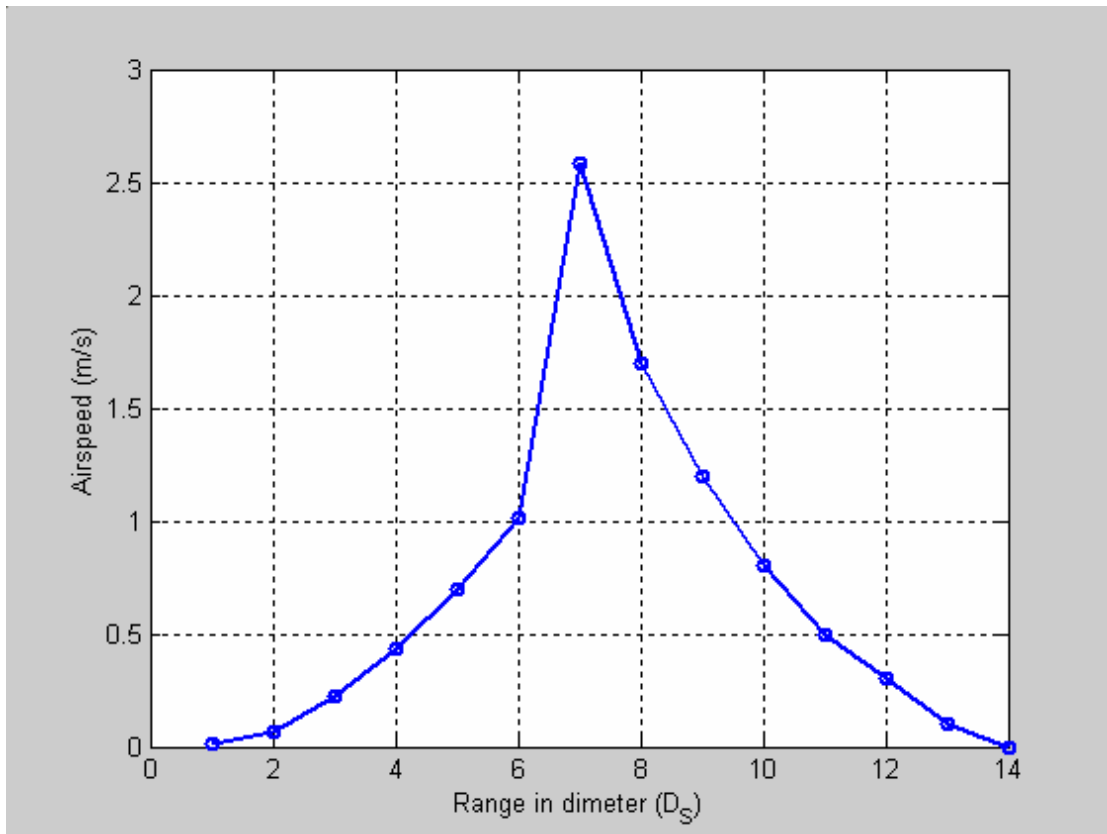


Figure 6.5 Airspeed measurements of 20-inch fan (D_S) for 3-diameter in height ($h=3$)

6.1.1.4 4-Diameter in Height

The 20-inch fan is leveled for its fourth diameter in height. The airspeed is measured for each diameter converge area and tabulated in table 6.4.

Table 6.4 Airspeed measurements of 20-inch fan (D_s) for 4-diameter in height ($h = 4$)

Range in diameter (D_s)	Airspeed (m/s)
1	0
2	0.02
3	0.05
4	0.13
5	0.23
6	0.5
7	0.8
8	2.0
9	1
10	0.7
11	0.5
12	0.4
13	0.3
14	0.2
15	0.1
16	0

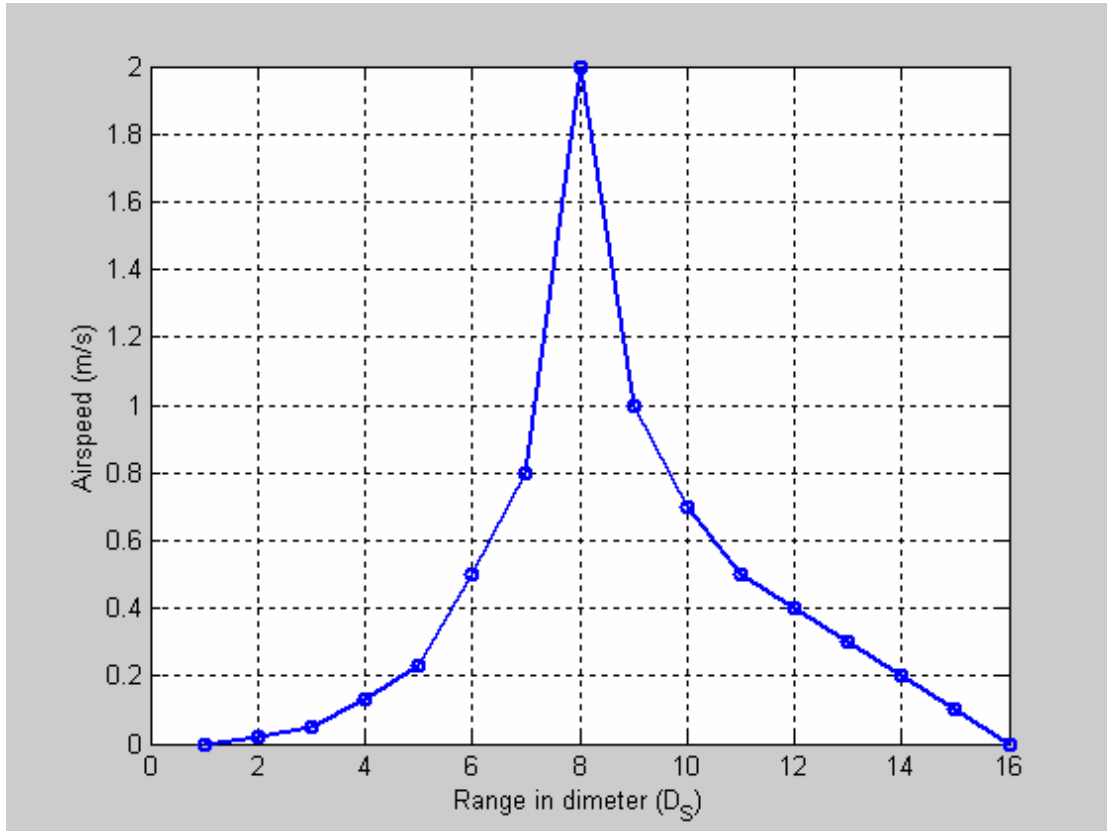


Figure 6.6 Airspeed measurements of 20-inch fan (D_S) for 4-diameter in height ($h=4$)

6.1.1.5 5-Diameter in Height

The 20-inch fan is leveled for its fifth diameter in height. The airspeed is measured for each diameter converge area and tabulated in table 6.5

Table 6.5 Airspeed measurements of 20-inch fan (D_s) for 5-diameter in height ($h = 5$)

Range in diameter (D_s)	Airspeed (m/s)
1	0
2	0
3	0
4	0.01
5	0.03
6	0.08
7	0.14
8	0.27
9	1.5
10	1
11	0.55
12	0.1
13	0.05
14	0

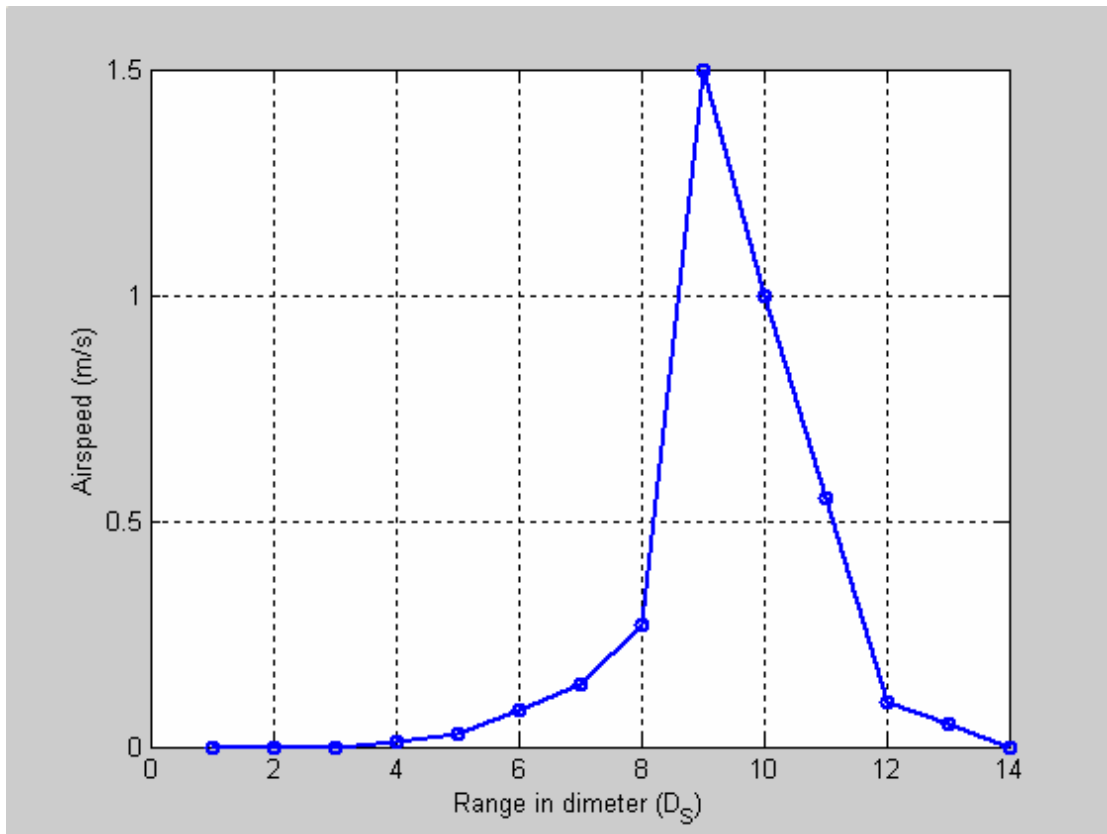


Figure 6.7 Airspeed measurements of 20-inch fan (D_s) for 5-diameter in height ($h=5$)

The airspeed measurements of 20-inch fan for all heights are plotted in figure 6.8 showing fan maximum airspeed range occurs at the 4th diameter height.

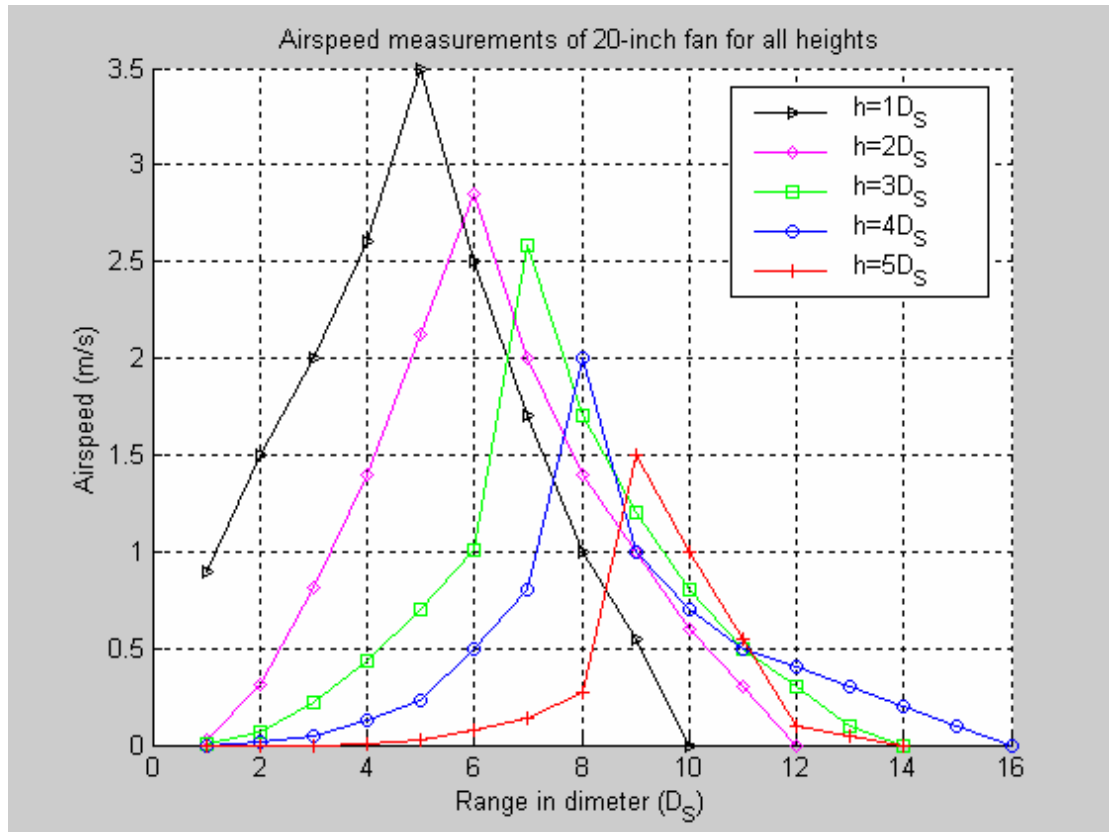


Figure 6.8 Airspeed measurements of 20-inch fan (D_S) for all heights

6.1.1.6 Angle Effect of 20-inch Fan

The angle effect of the fans is included in the experiments. For zero angle (θ_0) as explained in default case, the airspeed and temperature effect could reach maximum range but for higher levels of fans like in the 4th Diameter and in the 5th Diameter, the area that is directly below the fan is affected and the airspeed and temperature decrease in that area could be lesser than we wish to achieve thermal comfort, so because of that, the fans are configured to different angles as expressed in equations (6.1), (6.3) and (6.2); and the airspeed is measured as shown in figure 6.9.

$$\tan \theta_0 = \frac{5D}{\infty} = 0 \quad \rightarrow \quad \theta_0 = 0 \quad (\text{default case}) \quad (6.1)$$

$$\tan \theta_1 = \frac{5D}{10D} = \frac{1}{2} \quad \rightarrow \quad \theta_1 = 26.56^\circ \quad (6.2)$$

$$\tan \theta_2 = \frac{5D}{5D} = 1 \quad \rightarrow \quad \theta_2 = 45^\circ \quad (6.3)$$

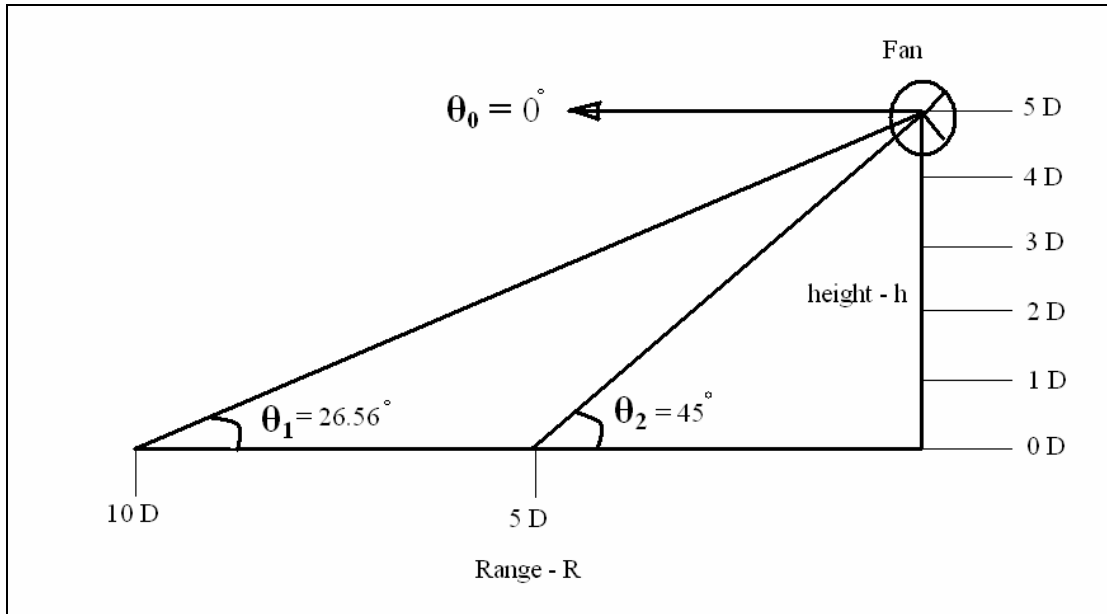


Figure 6.9 Configuration of angle effect case study of 20-inch fan (D_s)

Table 6.6 Airspeed measurements of 20-inch fan (D_s) for angle case

20-inch Fan (angle case)			
Range in diameter (D_s)	Airspeed (m/s)		
	θ_0	θ_1	θ_2
1	0	0	0.01
2	0	0.01	0.02
3	0	0.03	0.05
4	0.01	0.06	0.11
5	0.03	0.11	0.19
6	0.08	0.19	0.29
7	0.14	0.28	1.25
8	0.27	1.4	0.9
9	1.5	1.1	0.55
10	1	0.65	0
11	0.55	0.25	0
12	0.1	0	0
13	0.05	0	0
14	0	0	0

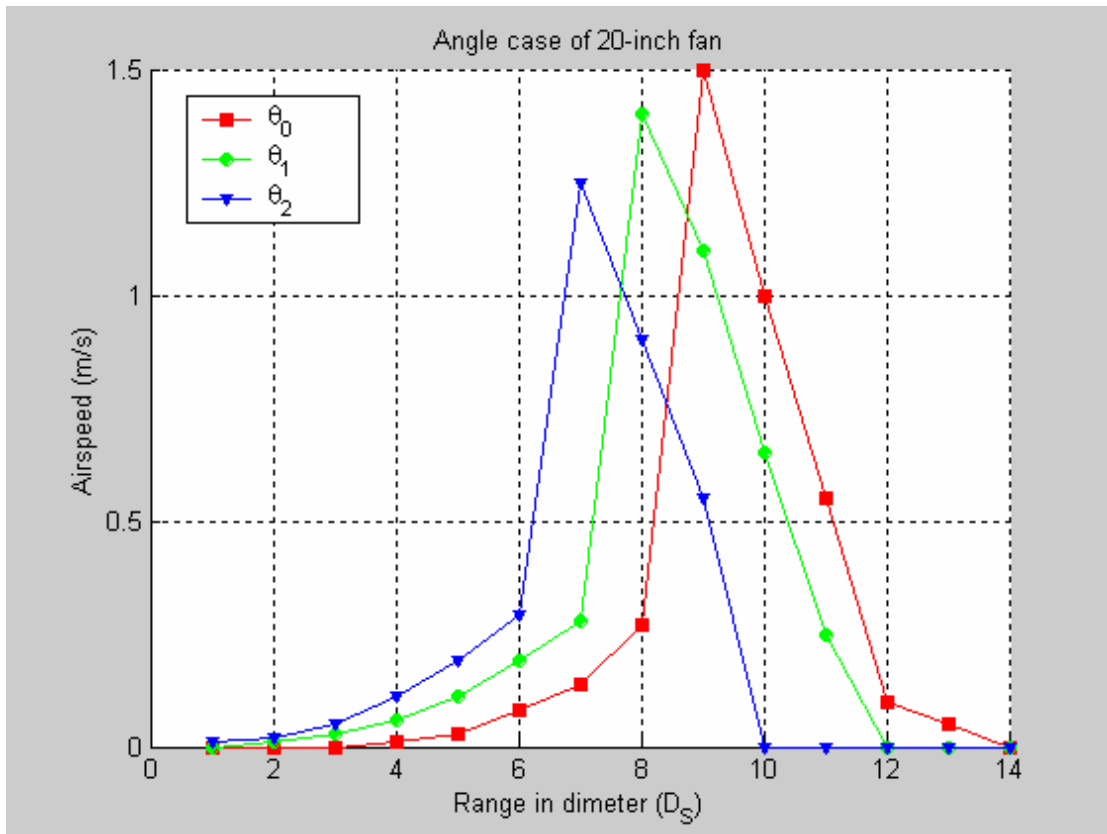


Figure 6.10 Airspeed measurements of 20-inch fan (D_S) for angle case

6.1.1.7 Side-wise Investigation of 20-inch Fan

As shown in figure 6.8, the maximum covered area range of the 20-inch fan is 16 diameters front-wise ($16D_s$) in the fourth diameter in height. The side-wise maximum range is investigated as shown in figure 6.11.

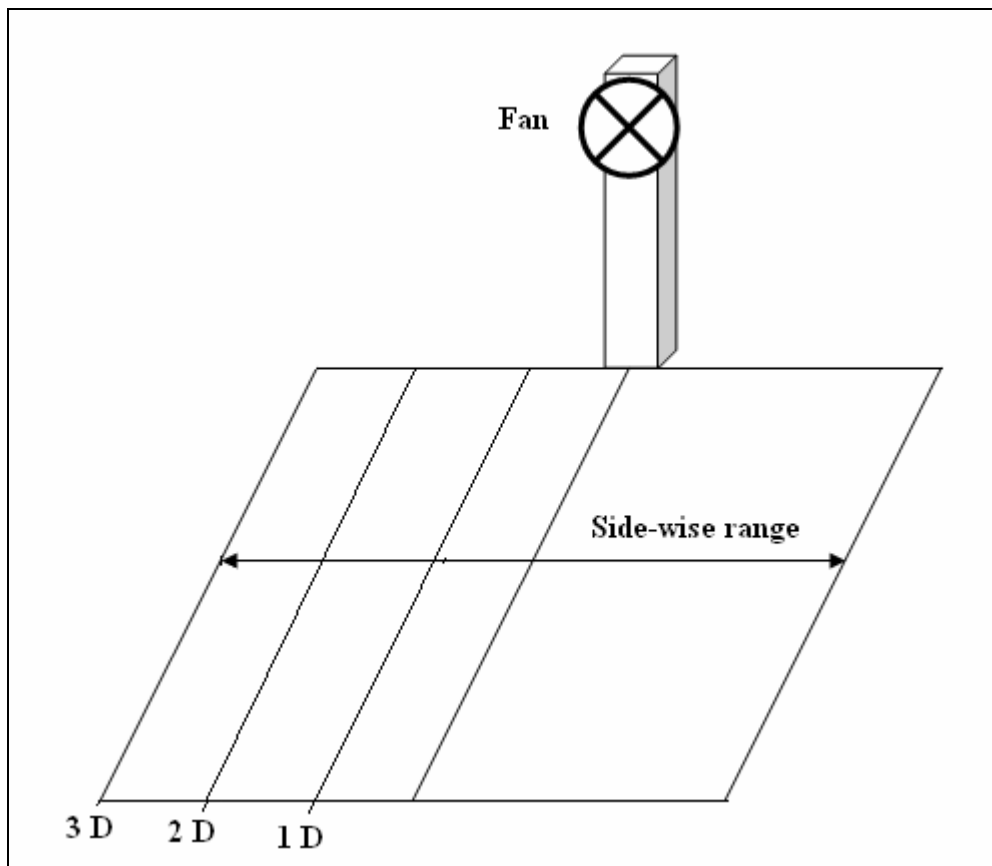


Figure 6.11 Airspeed measurements in the side-wise of 20-inch Fan

The airspeeds were measured along the 8th diameter ($8D_S$) front wise location where the maximum airspeed value was registered before.

Table 6.7 Airspeed measurements in the side-wise of 20-inch Fan

20-inch Fan (side-wise)			
Distance in diameter (D_S)	Airspeed (m/s)		
	1-D side-wise	2-D side-wise	3-D side-wise
8	2.0	0.8	0

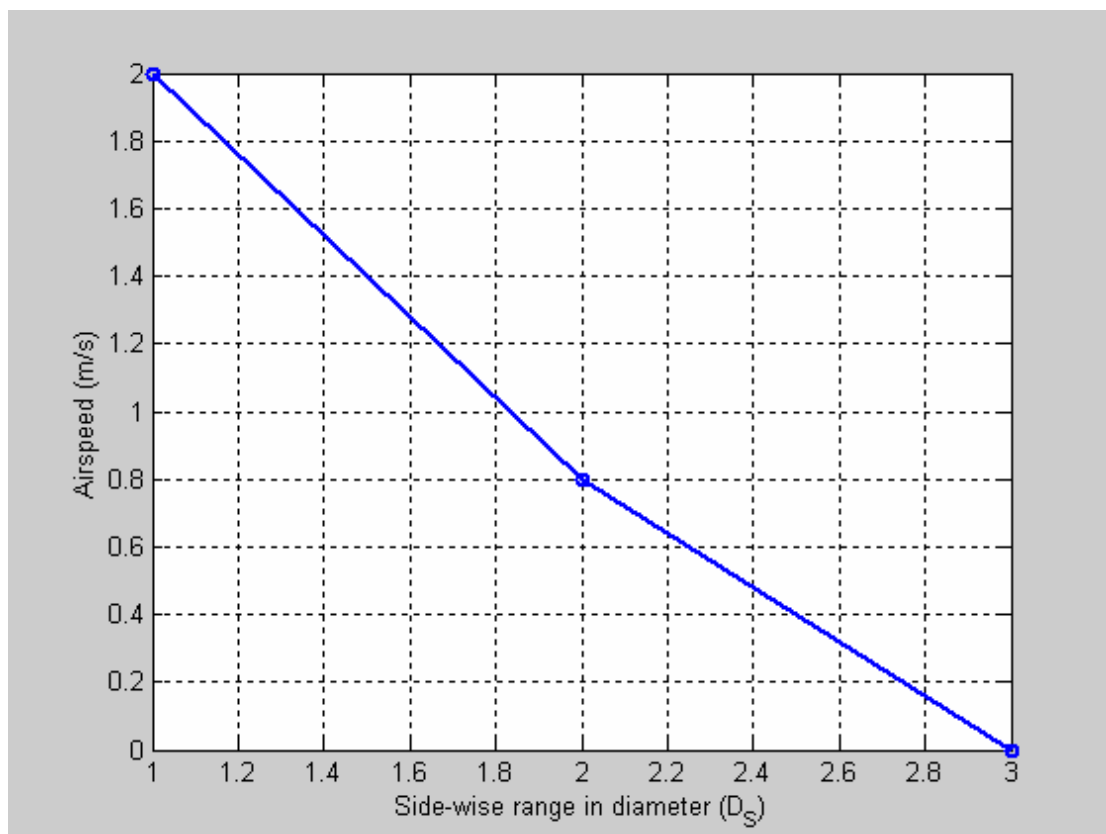


Figure 6.12 Airspeed measurements in the side-wise of 20-inch Fan

6.1.2 24-inch Fan

The airspeed of the 24-inch fan was measured as discussed in detail in chapter 5.

6.1.2.1 1-Diameter in Height

The 24-inch fan is leveled for its first to fifth diameters consequently as the same as it has been done for the 20-inch fan shown in figure 6.2.

The airspeed is measured for each diameter converge area for the first diameter in height and tabulated in table 6.8

Table 6.8 Airspeed measurements of 24-inch fan (D_m) for 1-diameter in height ($h=1$)

Range in diameter (D_m)	Airspeed (m/s)
1	2.2
2	3.1
3	4
4	5.63
5	4
6	2.6
7	1.05
8	0

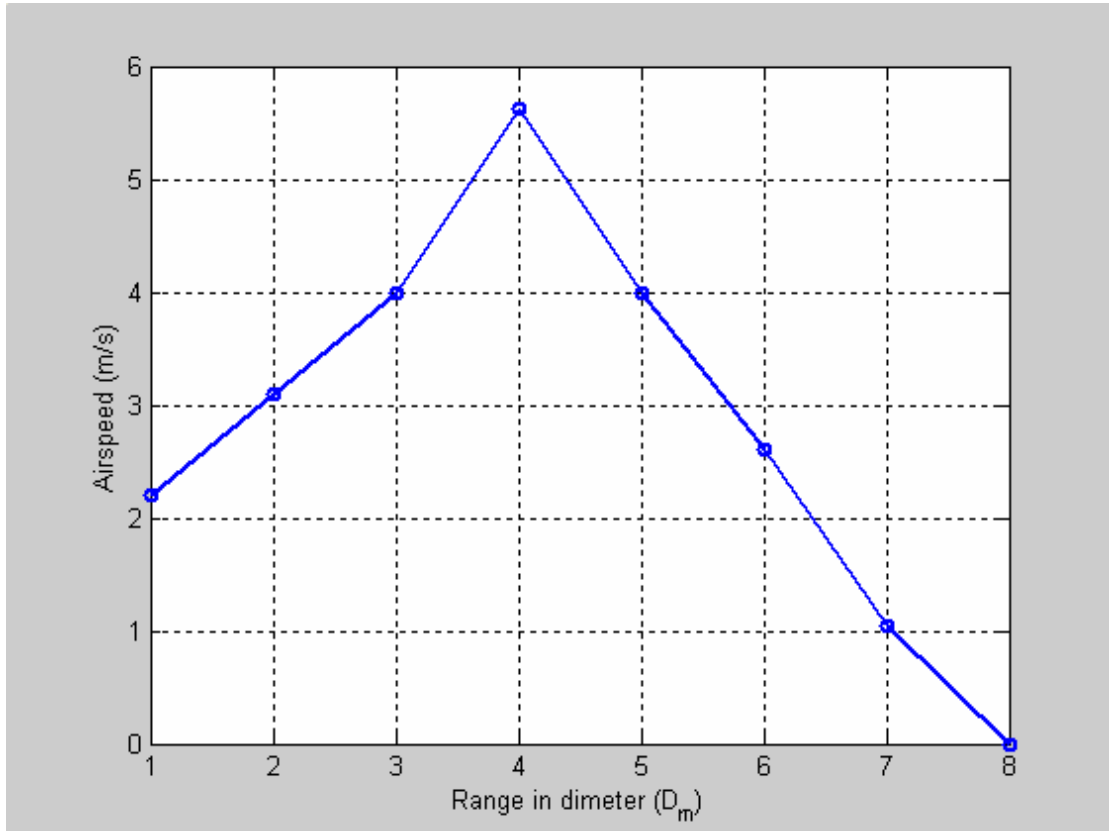


Figure 6.13 Airspeed measurements of 24-inch fan (D_m) for 1-diameter in height ($h=1$)

6.1.2.2 2-Diameter in Height

The 24-inch fan is leveled for its second diameter in height. The airspeed is measured for each diameter converge area and tabulated in table 6.9

Table 6.9 Airspeed measurements of 24-inch fan (D_m) for 2-diameter in height ($h = 2$)

Range in diameter (D_m)	Airspeed (m/s)
1	0.05
2	0.52
3	1.36
4	2.39
5	4.52
6	3
7	2
8	1.2
9	0.5
10	0

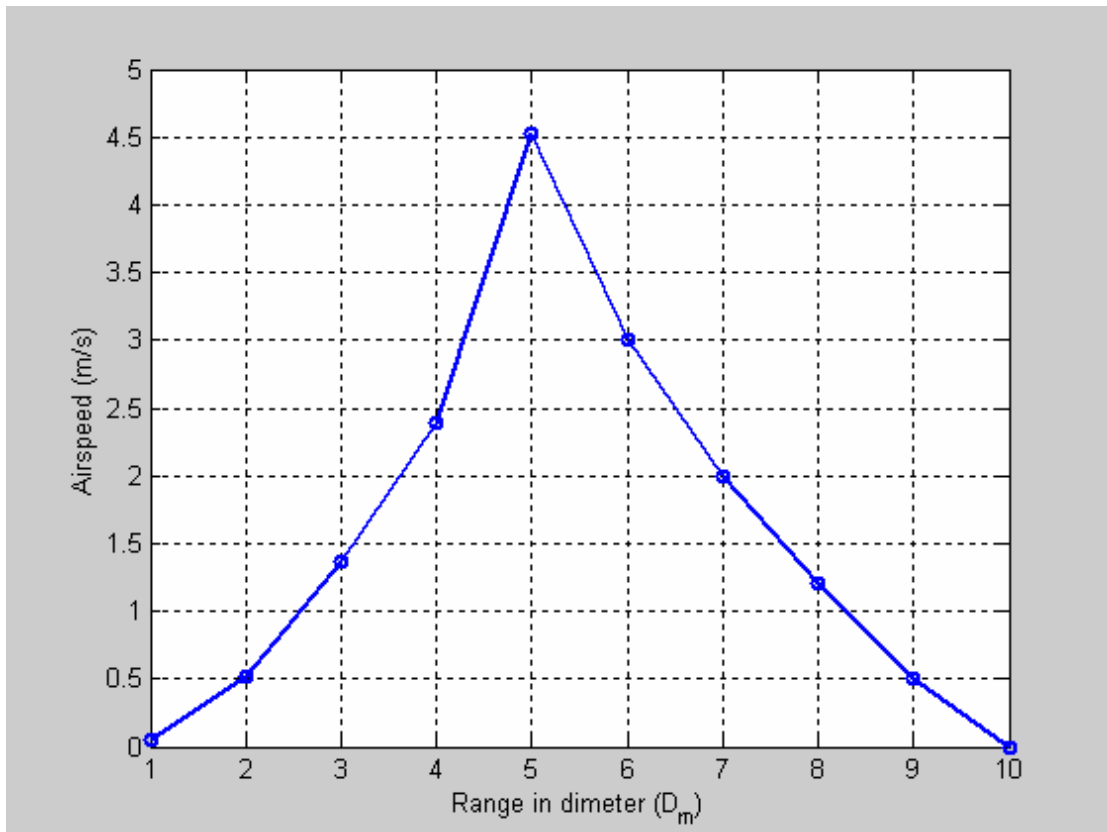


Figure 6.14 Airspeed measurements of 24-inch fan (D_m) for 2-diameter in height ($h=2$)

6.1.2.3 3-Diameter in Height

The 24-inch fan is leveled for its third diameter in height. The airspeed is measured for each diameter converge area and tabulated in table 6.10

Table 6.10 Airspeed measurements of 24-inch fan (D_m) for 3-diameter in height ($h=3$)

Range in diameter (D_m)	Airspeed (m/s)
1	0.02
2	0.16
3	0.47
4	0.91
5	1.44
6	3.67
7	2.4
8	1.4
9	1
10	0.6
11	0.3
12	0

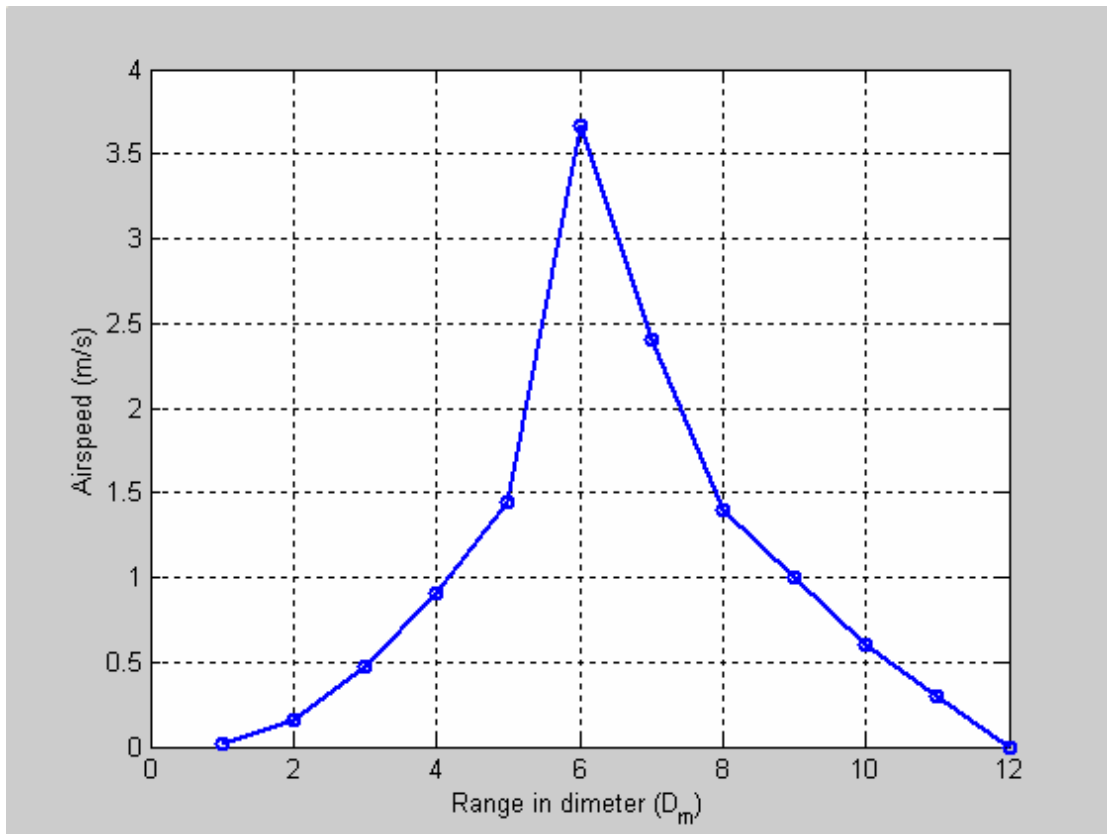


Figure 6.15 Airspeed measurements of 24-inch fan (D_m) for 3-diameter in height ($h=3$)

6.1.2.4 4-Diameter in Height

The 24-inch fan is leveled for its fourth diameter in height. The airspeed is measured for each diameter converge area and tabulated in table 6.11

Table 6.11 Airspeed measurements of 24-inch fan (D_m) for 4-diameter in height ($h=4$)

Range in diameter (D_m)	Airspeed (m/s)
1	0
2	0.05
3	0.18
4	0.39
5	0.67
6	1.1
7	2.87
8	2
9	1.4
10	0.8
11	0.5
12	0.3
13	0.1
14	0

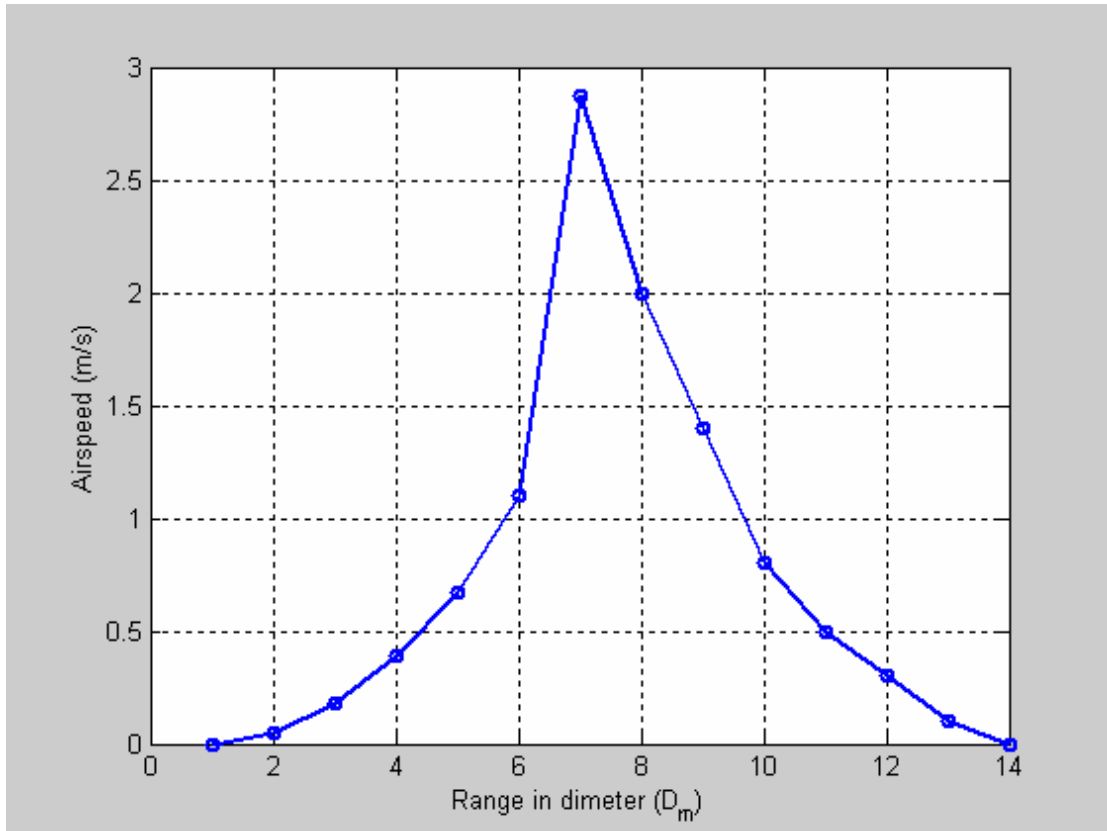


Figure 6.16 Airspeed measurements of 24-inch fan (D_m) for 4-diameter in height ($h=4$)

6.1.2.5 5-Diameter in Height

The 24-inch fan is leveled for its fifth diameter in height. The airspeed is measured for each diameter converge area and tabulated in table 6.12

Table 6.12 Airspeed measurements of 24-inch fan (D_m) for 5-diameter in height ($h=5$)

Range in diameter (D_m)	Airspeed (m/s)
1	0
2	0
3	0
4	0.03
5	0.11
6	0.25
7	0.49
8	1.47
9	0.95
10	0.5
11	0.2
12	0

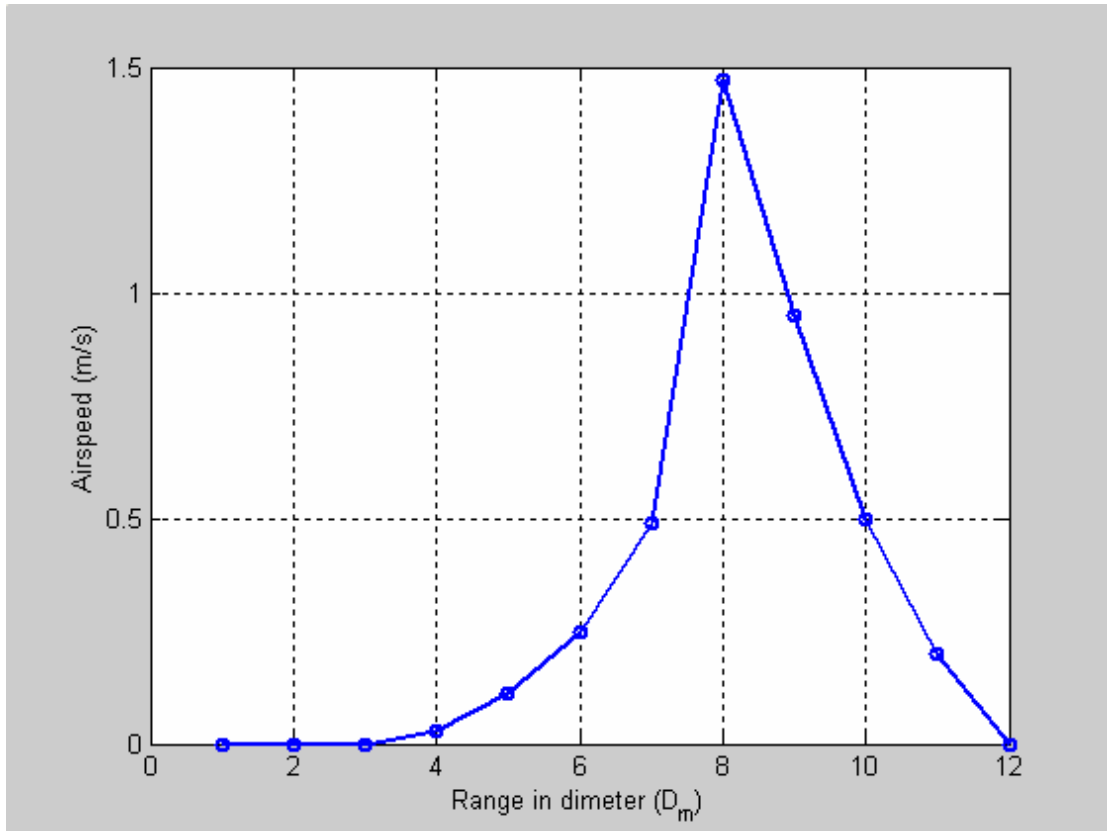


Figure 6.17 Airspeed measurements of 24-inch fan (D_m) for 5-diameter in height ($h=5$)

The airspeed measurements of 24-inch fan for all heights are plotted in figure 6.18 showing fan maximum airspeed range occurs at the 4th diameter height.

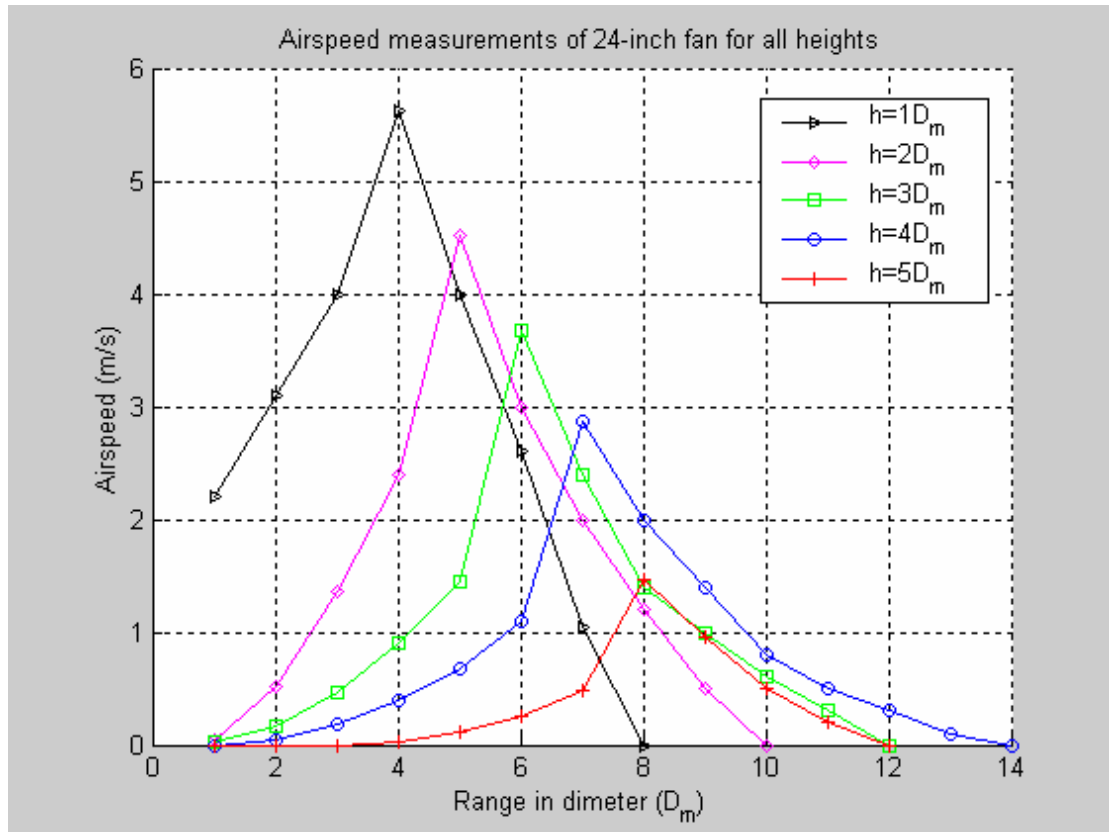


Figure 6.18 Airspeed measurements of 24-inch fan (D_m) for all heights

6.1.2.6 Angle Effect of 24-inch Fan

The angle effect of the 24-inch fan is included in the experiments. For zero angle (θ_0) as explained in default case, the airspeed and temperature effect could reach maximum range but for higher levels of fans like in the 4th Diameter and in the 5th Diameter, the area that is directly below the fan is affected and the airspeed and temperature decrease in that area could be lesser than we wish to achieve thermal comfort, so because of that, the fans are configured to different angles as expressed in equations (6.1), (6.3) and (6.2); and the airspeed is measured as shown in figure 6.9.

Table 6.13 Airspeed measurements of 24-inch fan (D_m) for angle case

24-inch Fan (angle case)			
Range in diameter (D_m)	Airspeed (m/s)		
	θ_0	θ_1	θ_2
1	0	0	0.06
2	0	0.03	0.16
3	0	0.1	0.25
4	0.03	0.2	0.4
5	0.11	0.3	0.6
6	0.25	0.5	1.39
7	0.49	1.44	1.15
8	1.47	1.14	0.8
9	0.95	0.7	0
10	0.5	0.2	0
11	0.2	0	0
12	0	0	0

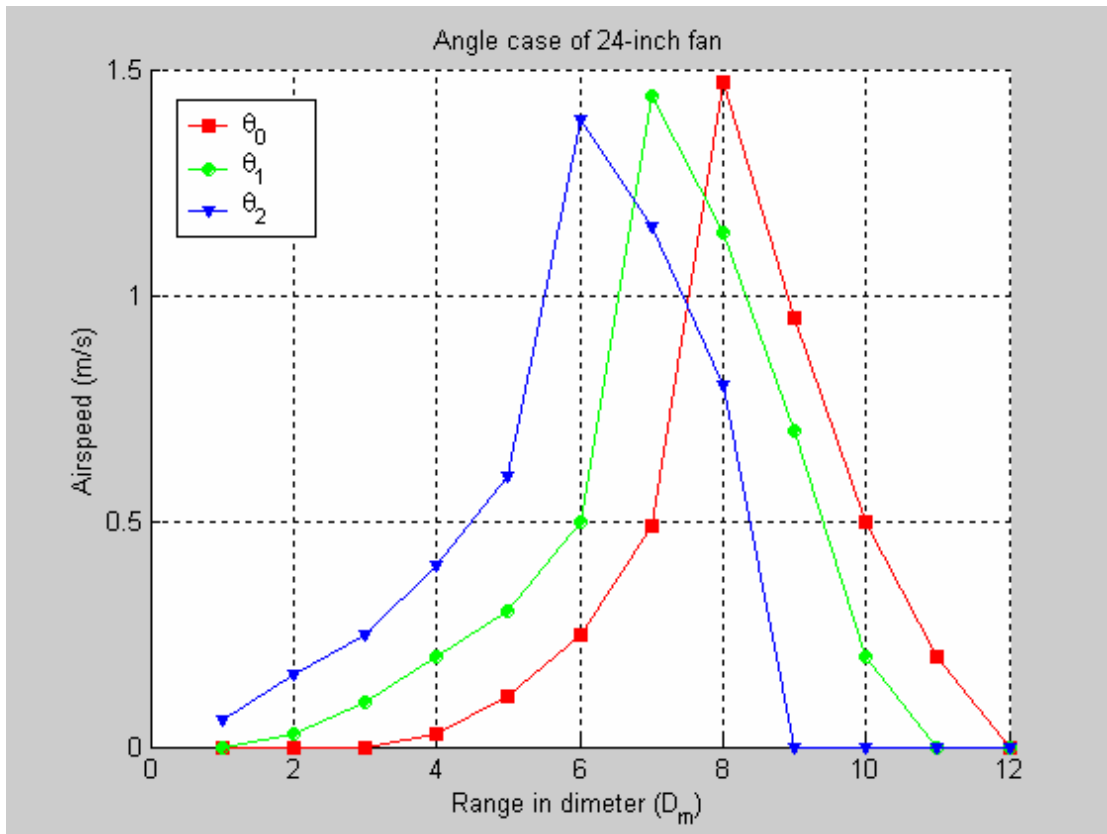


Figure 6.19 Airspeed measurements of 24-inch fan (D_m) for angle case

6.1.2.7 Side-wise Investigation of 24-inch Fan

As shown in figure 6.18, the maximum covered range of the 24-inch fan is 14 diameters front-wise ($14D_m$) in the fourth diameter in height. The side-wise maximum range is investigated as shown in figure 6.11.

The airspeeds were measured along the 7th diameter ($7D_m$) front wise location where the maximum airspeed value was registered before.

Table 6.14 Airspeed measurements in the side-wise of 24-inch Fan

24-inch Fan (side-wise)			
Distance in diameter (D_m)	Airspeed (m/s)		
	1-D side-wise	2-D side-wise	3-D side-wise
7	2.87	1.2	0

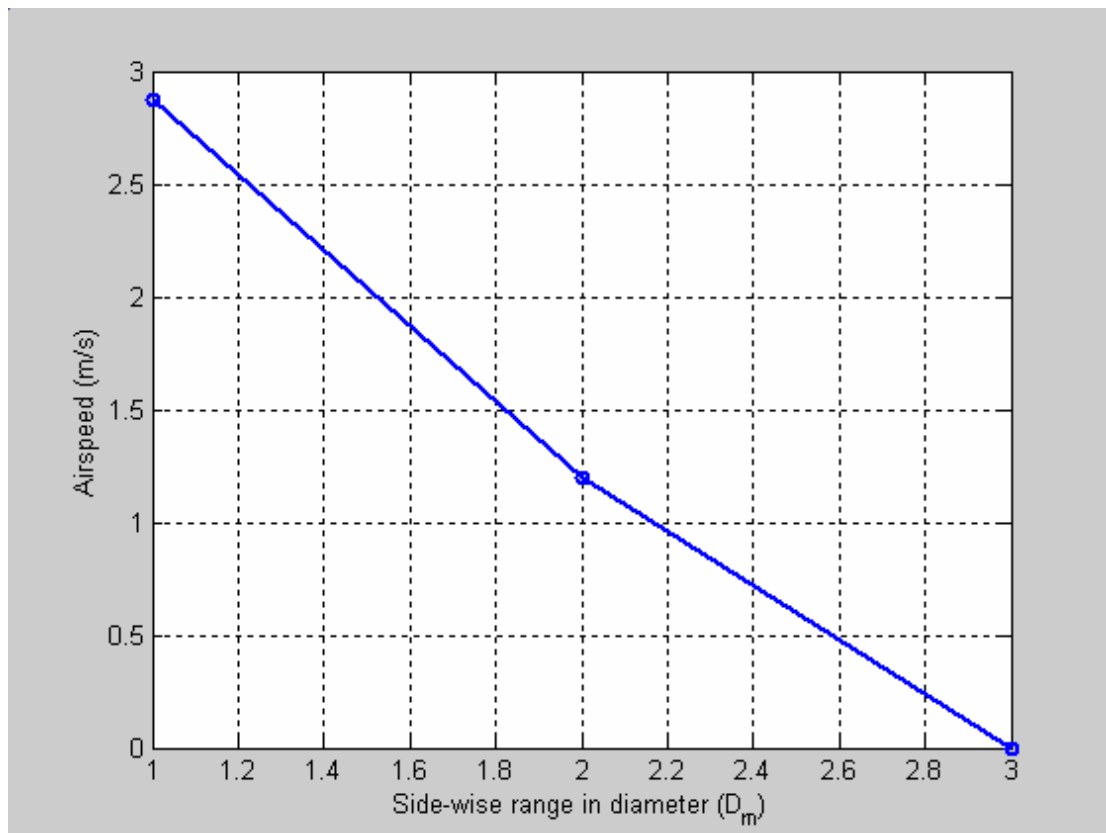


Figure 6.20 Airspeed measurements in the side-wise of 24-inch Fan

6.1.3 30-inch Fan

The airspeed of the 30-inch fan was measured as discussed in detail in chapter 5.

6.1.3.1 1-Diameter in Height

The 30-inch fan is leveled for its first to fifth diameters consequently as the same as it has been done for the 20-inch fan and 24-inch fan shown in figure 6.2.

The airspeed is measured for each diameter converge area for the first diameter in height and tabulated in table 6.15.

Table 6.15 Airspeed measurements of 30-inch fan (D_L) for 1-diameter in height ($h=1$)

Range in diameter (D_L)	Airspeed (m/s)
1	2.63
2	4.1
3	6.4
4	4.7
5	2.8
6	0

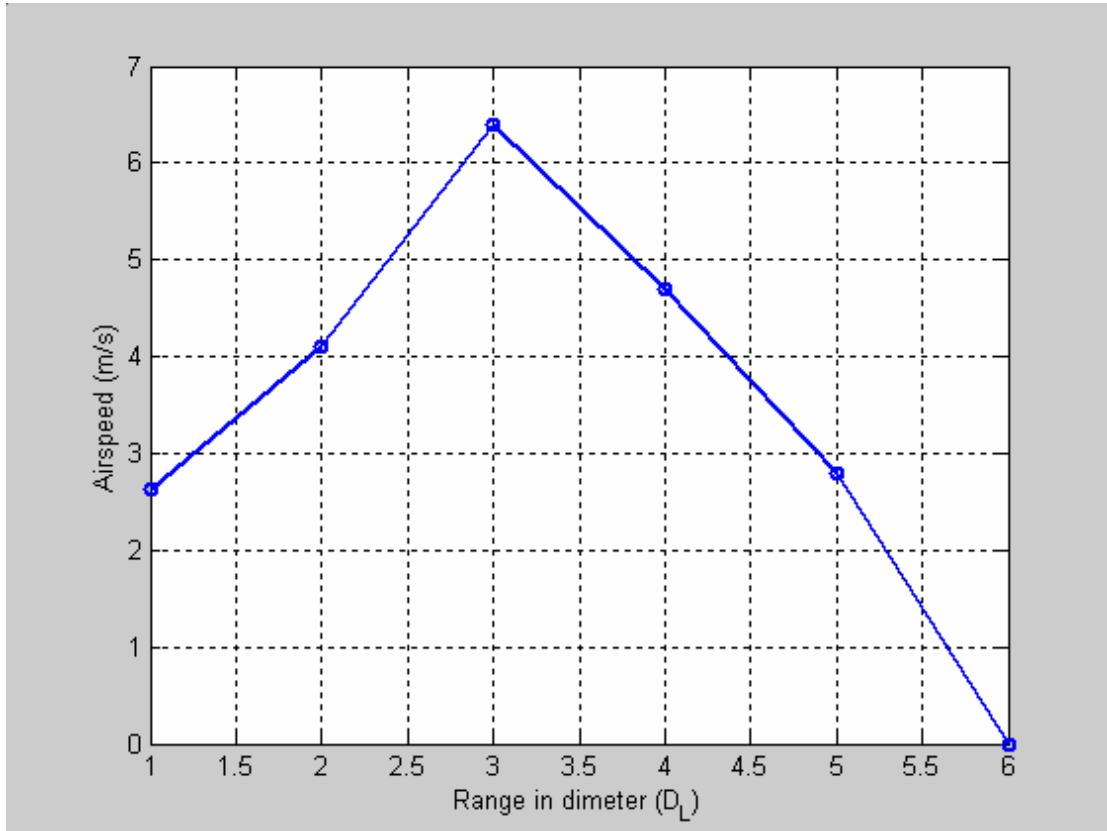


Figure 6.21 Airspeed measurements of 30-inch fan (D_L) for 1-diameter in height ($h=1$)

6.1.3.2 2-Diameter in Height

The 30-inch fan is leveled for its second diameter in height. The airspeed is measured for each diameter converge area and tabulated in table 6.16

Table 6.16 Airspeed measurements of 30-inch fan (D_L) for 2-diameter in height ($h=2$)

Range in diameter (D_L)	Airspeed (m/s)
1	0.49
2	1.8
3	3.0
4	5.3
5	3.9
6	2.5
7	1.4
8	0

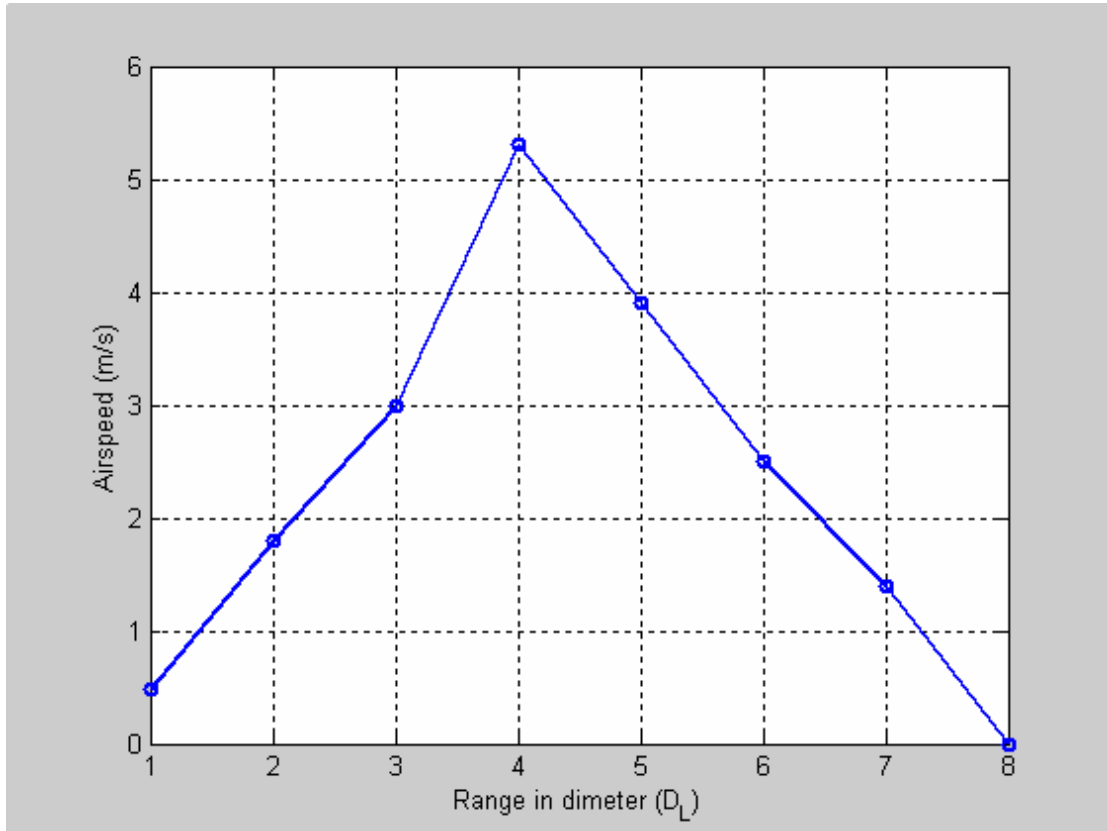


Figure 6.22 Airspeed measurements of 30-inch fan (D_L) for 2-diameter in height ($h=2$)

6.1.3.3 3-Diameter in Height

The 30-inch fan is leveled for its third diameter in height. The airspeed is measured for each diameter converge area and tabulated in table 6.17

Table 6.17 Airspeed measurements of 30-inch fan (D_L) for 3-diameter in height ($h=3$)

Range in diameter (D_L)	Airspeed (m/s)
1	0.07
2	0.47
3	1.12
4	1.92
5	4.46
6	3
7	2
8	1.3
9	0.6
10	0

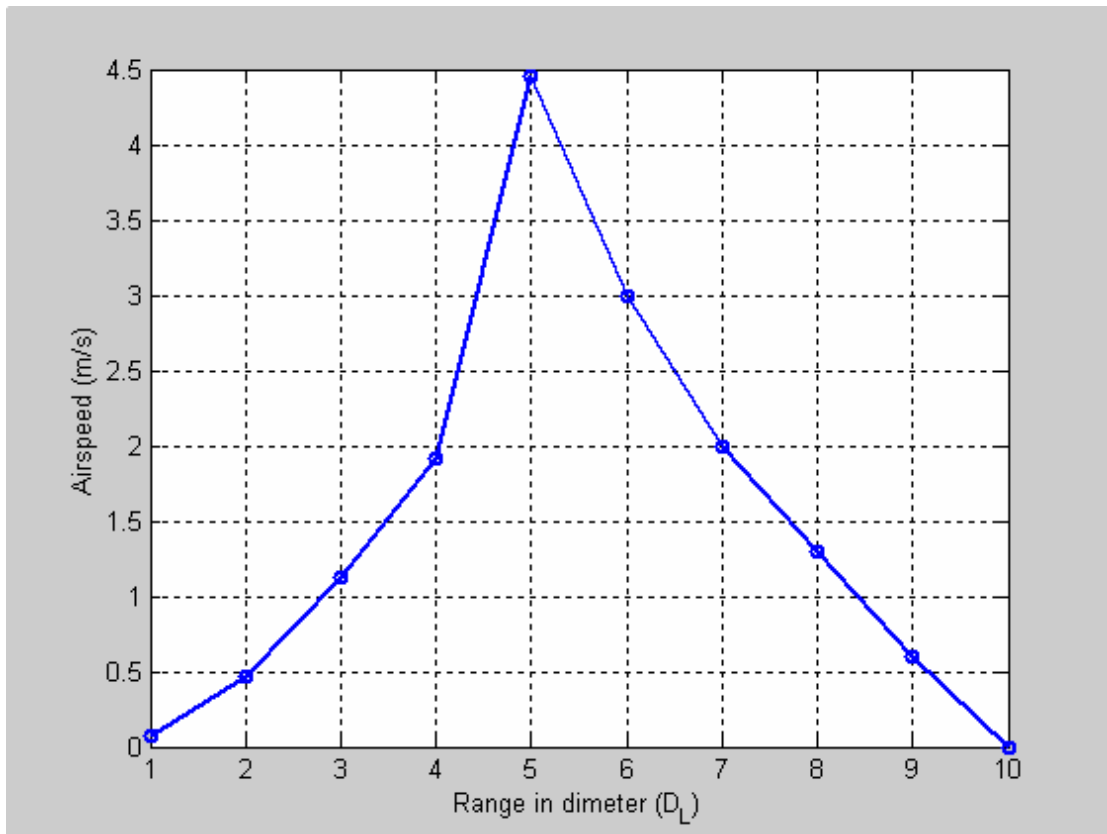


Figure 6.23 Airspeed measurements of 30-inch fan (D_L) for 3-diameter in height ($h=3$)

6.1.3.4 4-Diameter in Height

The 30-inch fan is leveled for its fourth diameter in height. The airspeed is measured for each diameter converge area and tabulated in table 6.18.

Table 6.18 Airspeed measurements of 30-inch fan (D_L) for 4-diameter in height ($h=4$)

Range in diameter (D_L)	Airspeed (m/s)
1	0
2	0.13
3	0.53
4	0.98
5	1.68
6	3.68
7	2.7
8	1.8
9	1.3
10	0.8
11	0.4
12	0

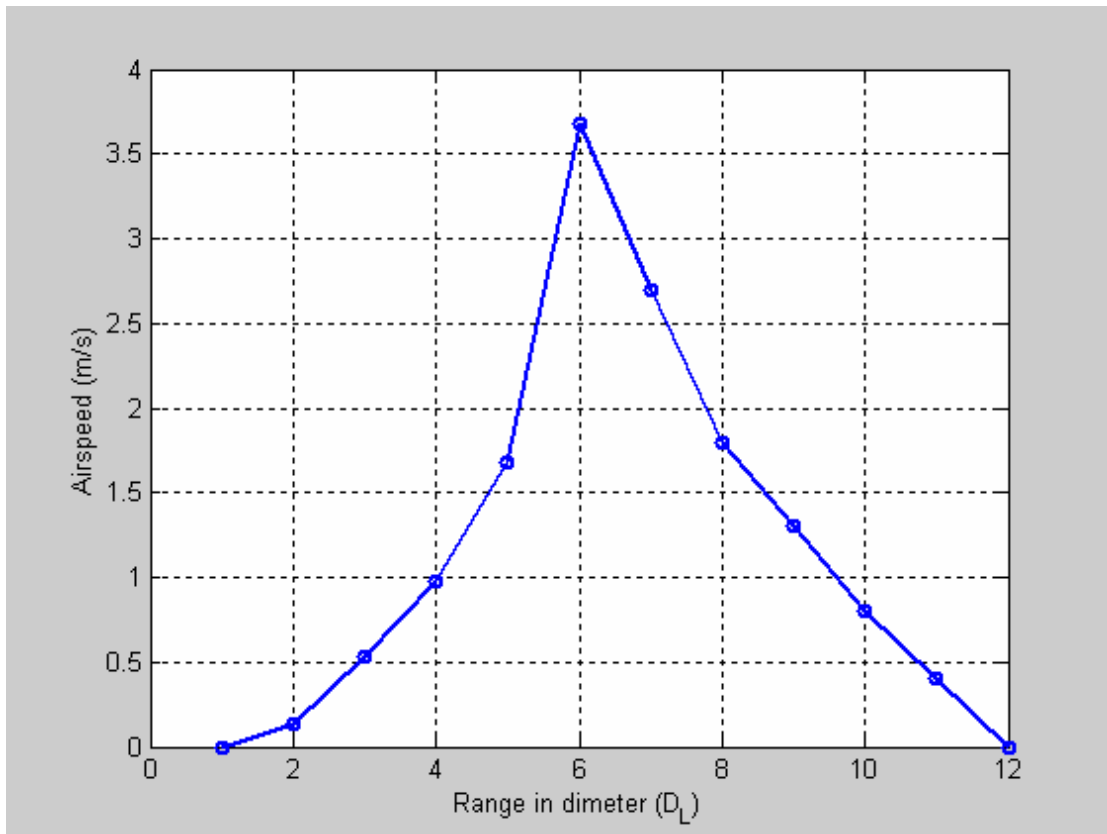


Figure 6.24 Airspeed measurements of 30-inch fan (D_L) for 4-diameter in height ($h=4$)

6.1.3.5 5-Diameter in Height

The 30-inch fan is leveled for its fifth diameter in height. The airspeed is measured for each diameter converge area and tabulated in table 6.19

Table 6.19 Airspeed measurements of 30-inch fan (D_L) for 5-diameter in height ($h=5$)

Distance in diameter	Airspeed (m/s)
1	0
2	0
3	0
4	0.16
5	0.53
6	1.03
7	1.91
8	1.1
9	0.5
10	0

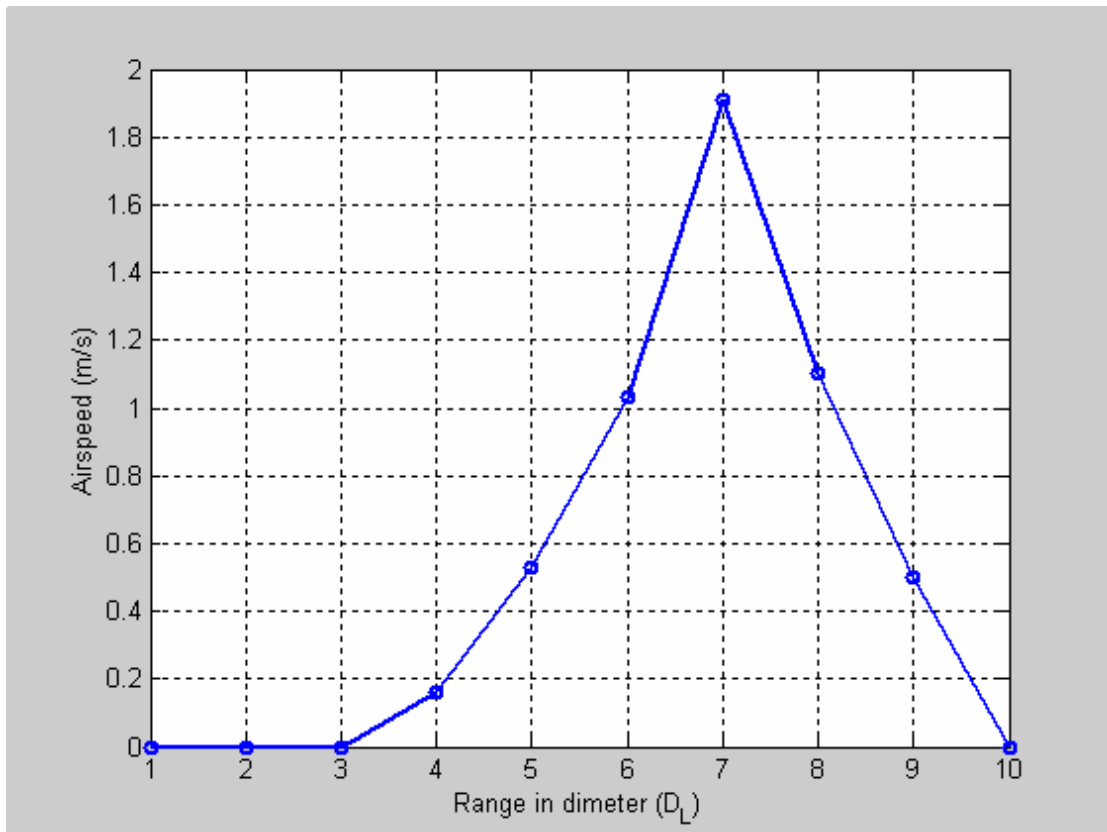


Figure 6.25 Airspeed measurements of 30-inch fan (D_L) for 5-diameter in height ($h=5$)

The airspeed measurements of 30-inch fan for all heights are plotted in figure 6.26 showing fan maximum airspeed range occurs at the 4th diameter height.

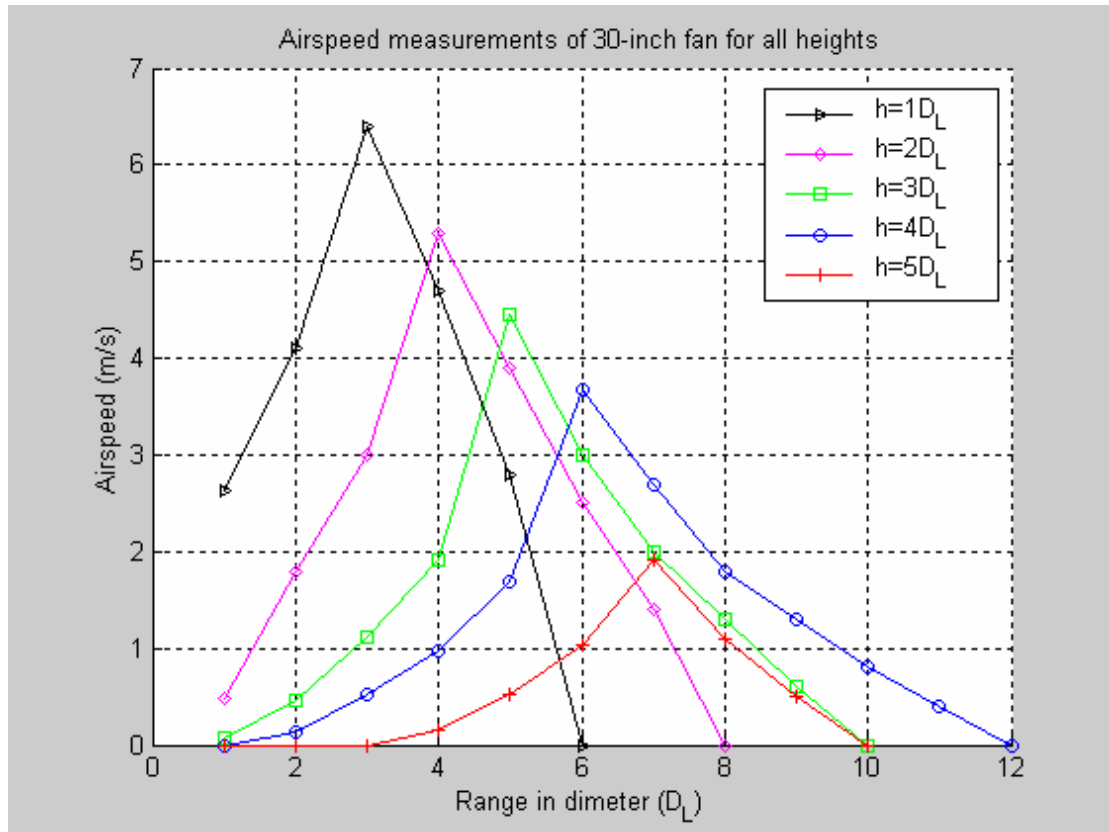


Figure 6.26 Airspeed measurements of 30-inch fan (D_L) for all heights

6.1.3.6 Angle Effect of 30-inch Fan

The angle effect of the 30-inch fan is included in the experiments. For zero angle (θ_0) as explained in default case, the airspeed and temperature effect could reach maximum range but for higher levels of fans like in the 4th Diameter and in the 5th Diameter, the area that is directly below the fan is affected and the airspeed and temperature decrease in that area could be lesser than we wish to achieve thermal comfort, so because of that, the fans are configured to different angles as expressed in equations (6.1), (6.3) and (6.2); and the airspeed is measured as shown in figure 6.9.

Table 6.20 Airspeed measurements of 30-inch fan (D_L) for angle case

30-inch Fan (angle case)			
Range in diameter (D_L)	Airspeed (m/s)		
	θ_0	θ_1	θ_2
1	0	0	0.2
2	0	0.13	0.35
3	0	0.25	0.6
4	0.16	0.6	0.9
5	0.53	1	1.7
6	1.03	1.8	1.19
7	1.91	1.3	0.75
8	1.1	0.75	0
9	0.5	0	0
10	0	0	0

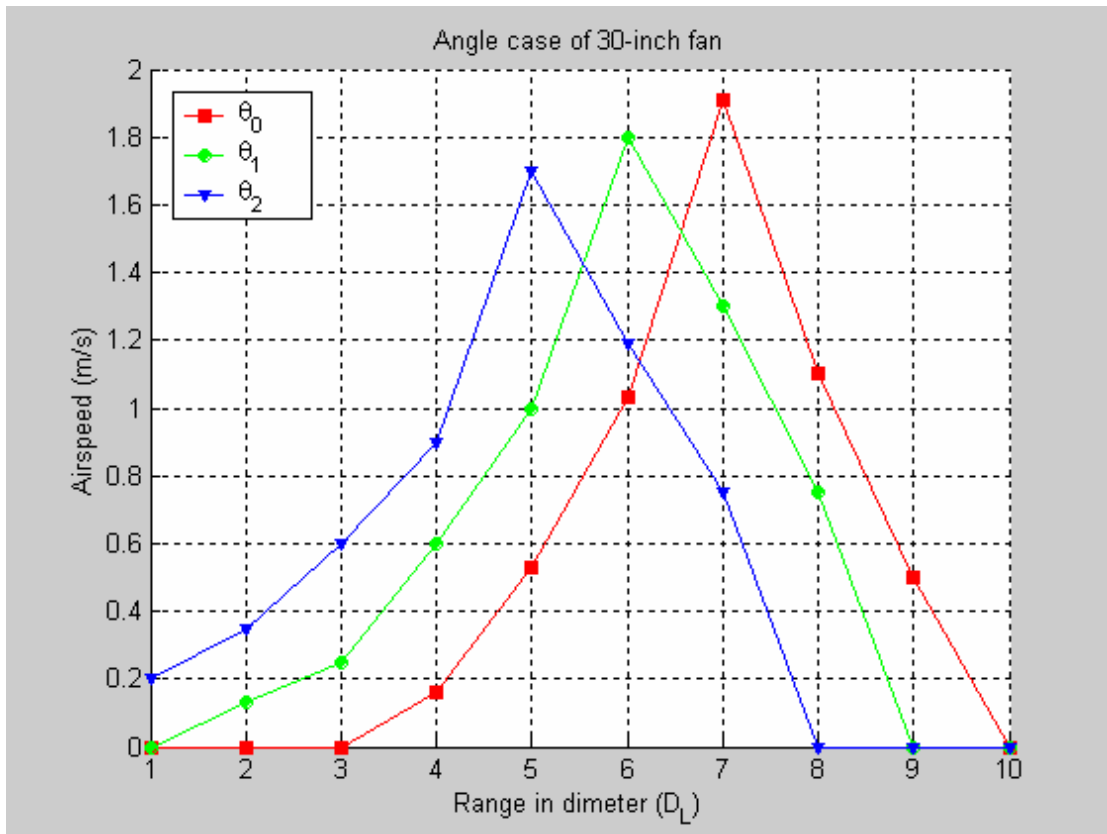


Figure 6.27 Airspeed measurements of 30-inch fan (D_L) for angle case

6.1.3.7 Side-wise Investigation of 30-inch Fan

As shown in figure 6.26, the maximum covered range of the 30-inch fan is 12 diameters front-wise ($12D_L$) in the fourth diameter in height. The side-wise maximum range is investigated as shown in figure 6.11.

The airspeeds were measured along the 6th diameter ($6D_L$) front wise location where the maximum airspeed value was registered before.

Table 6.21 Airspeed measurements in the side-wise of 30-inch Fan

30-inch Fan (side-wise)			
Distance in diameter (D_L)	Airspeed (m/s)		
	1-D side-wise	2-D side-wise	3-D side-wise
6	3.68	1.5	0

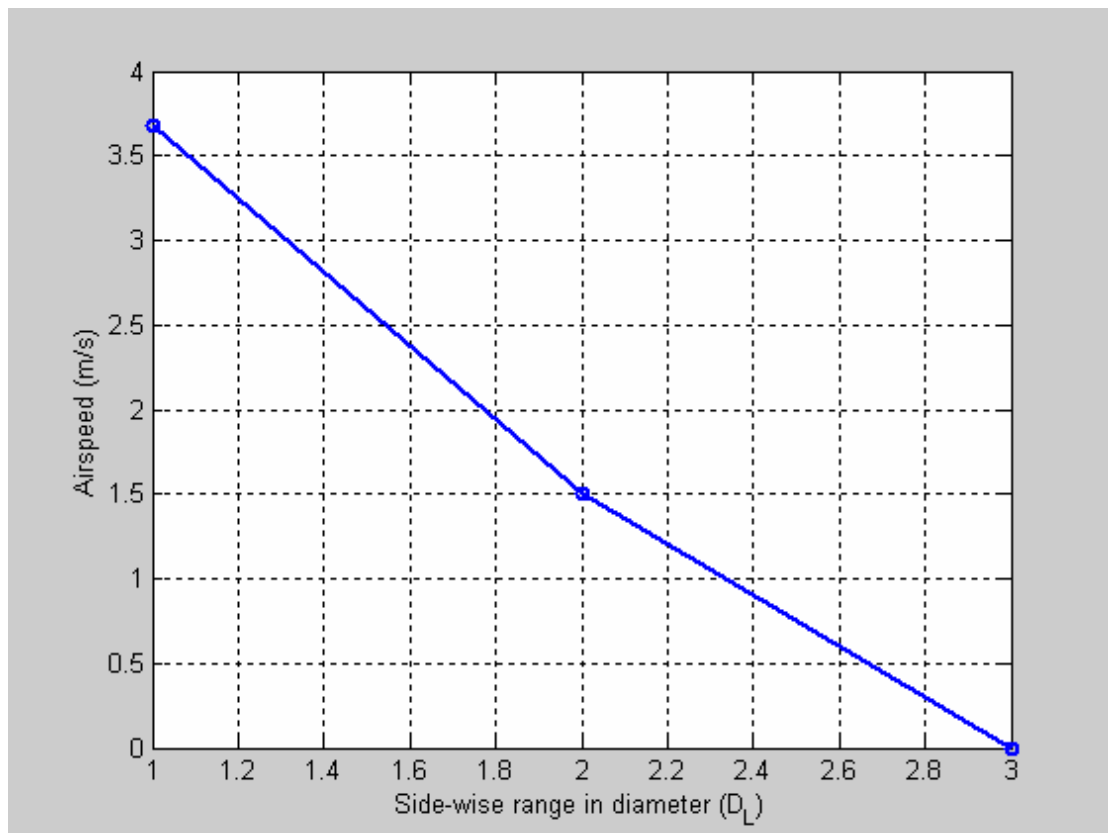


Figure 6.28 Airspeed measurements in the side-wise of 30-inch Fan

6.2 Second Stage (With Mist)

6.2.1 Experimental Setup and Equipments

The second stage is devoted to investigate the temperature domain for the same three different fan diameters (20 inch fan diameter, 24 inch fan diameter and 30 inch fan diameter) used in the first stage as shown in figure 3.1; and for different heights with mist; to find empirical relationship that relates temperature with fan diameter from one aspect and temperature with fan heights from the other aspect.

Mist system was attached to each fan consists of six nozzles, each nozzle was of about 200 micrometer diameter with an operating pressure of about 50 bar as shown in figure 6.29.

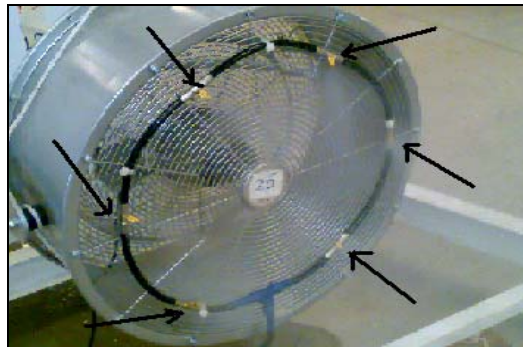


Figure 6.29 Fan with mist nozzles

To generate mist, an air small pump is used to pump the water from a reservoir to a water pump which pumps the water with a pressure of about 50 bar to the nozzles attached to each fan as shown in figures 6.30 to 6.34.



Figure 6.30 Location of the mist experiments



Figure 6.31 Reservoir used in the mist experiment



Figure 6.32 Water pump used in the mist experiment



Figure 6.33 The pressure gage of the water pump



Figure 6.34 Conducting experiments with my advisor Dr. Ahmed AL-Garni

There were some instruments used in the experiments to measure the airspeed as discussed in detail in chapter 4, also there were thermometers used to measure the temperature and humidity as shown in the following figures.



Figure 6.35 A very sensitive thermometer used in the experiments



Figure 6.36 A very sensitive remote-laser thermometer used in the experiments



Figure 6.37 An instrument used to measure temperature and relative humidity



Figure 6.38 An instrument used to measure the relative humidity

In the second stage, the experimental procedure is exactly repeated the same way of the first stage but adding the effect of the mist, keeping in mind the air temperature is about 40 °C and the relative humidity is about 50%.

6.2.2 20-inch Fan (with mist)

6.2.2.1 1-Diameter in Height

The 20-inch fan is leveled for its first diameter in height as shown in figure 6.39.

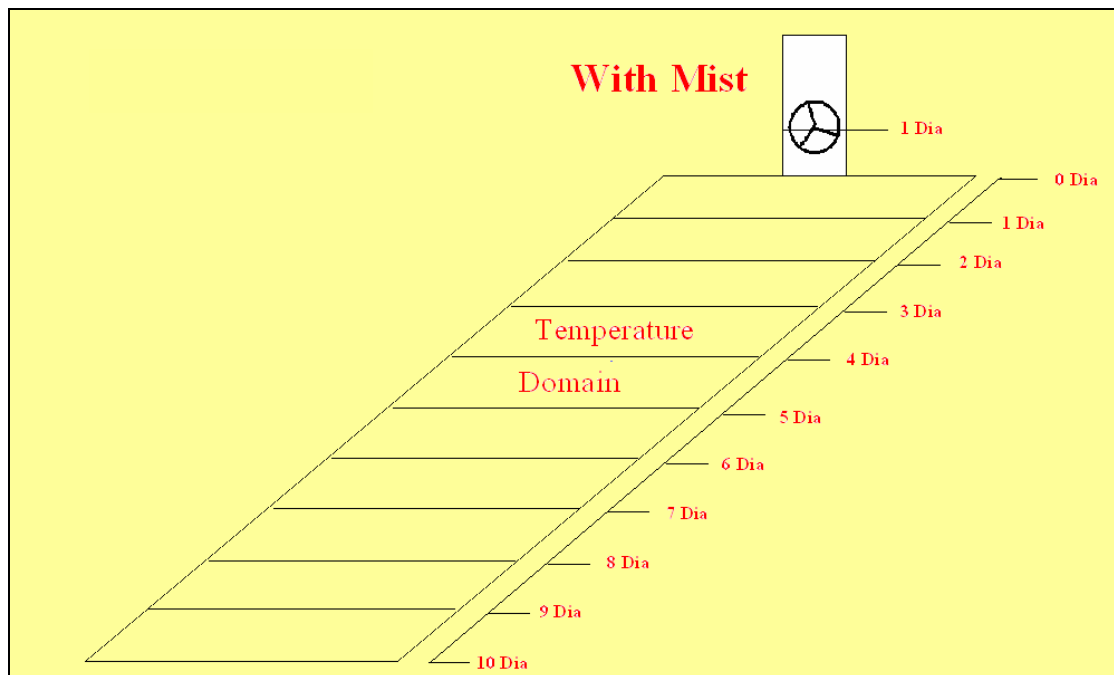


Figure 6.39 20-inch fan (D_s) for the first 1-diameter in height ($h = 1D$) (with mist)

The temperature is measured for each diameter converge area for the first diameter in height and tabulated in table 6.22

Table 6.22 Temperature measurements of 20-inch fan (D_s) for 1-diameter in height

($h = 1D$) (with mist)

Range in diameter (D_s)	Temperature ($^{\circ}C$)
1	36.5
2	35.8
3	35
4	34.6
5	33.9
6	33.6
7	32.9
8	32.4
9	32.8
10	34.8
11	37.4
12	40

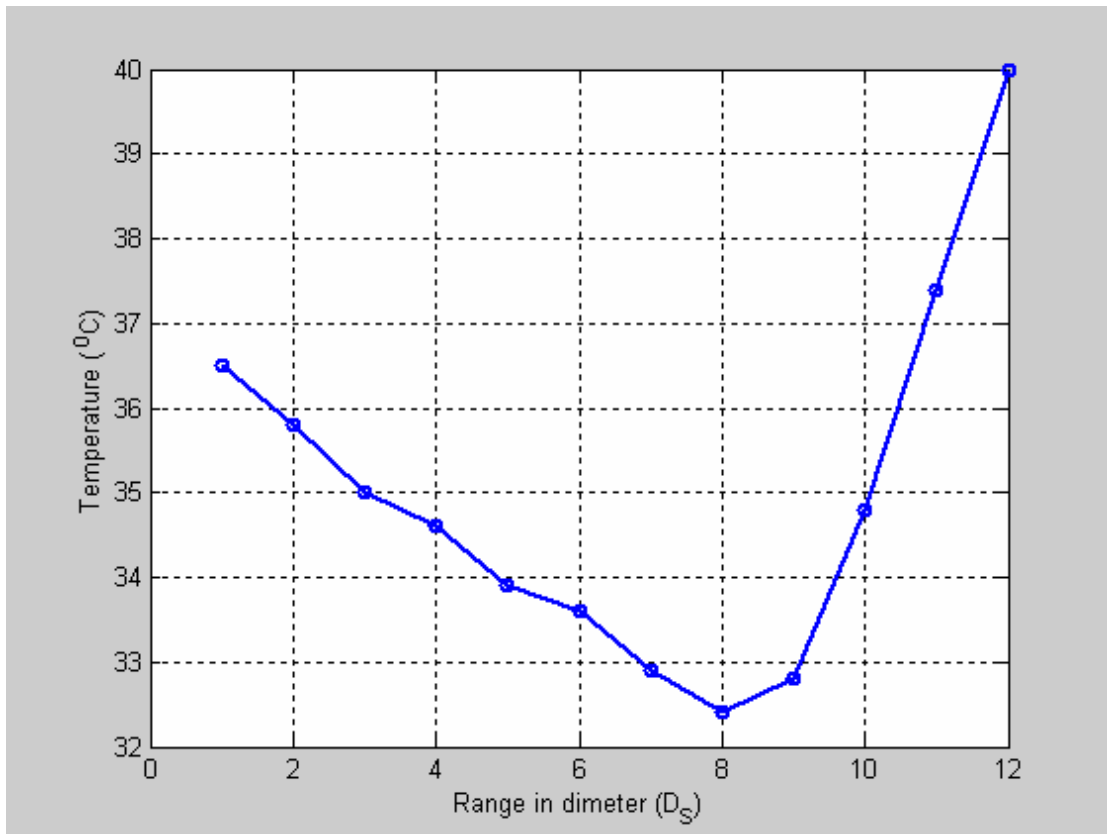


Figure 6.40 Temperature measurements of 20-inch fan (D_S) for 1-diameter in height (h = 1D) (with mist)

6.2.2.2 2-Diameter in Height

The 20-inch fan is leveled for its second diameter in height. The temperature is measured for each diameter converge area and tabulated in table 6.23

Table 6.23 Temperature measurements of 20-inch fan (D_s) for 2-diameter in height ($h = 2D$) (with mist)

Range in diameter (D_s)	Temperature ($^{\circ}\text{C}$)
1	37
2	36.2
3	35.5
4	35.1
5	34.4
6	34.0
7	33.5
8	33.0
9	32.3
10	32.6
11	33.8
12	35.4
13	37.8
14	40

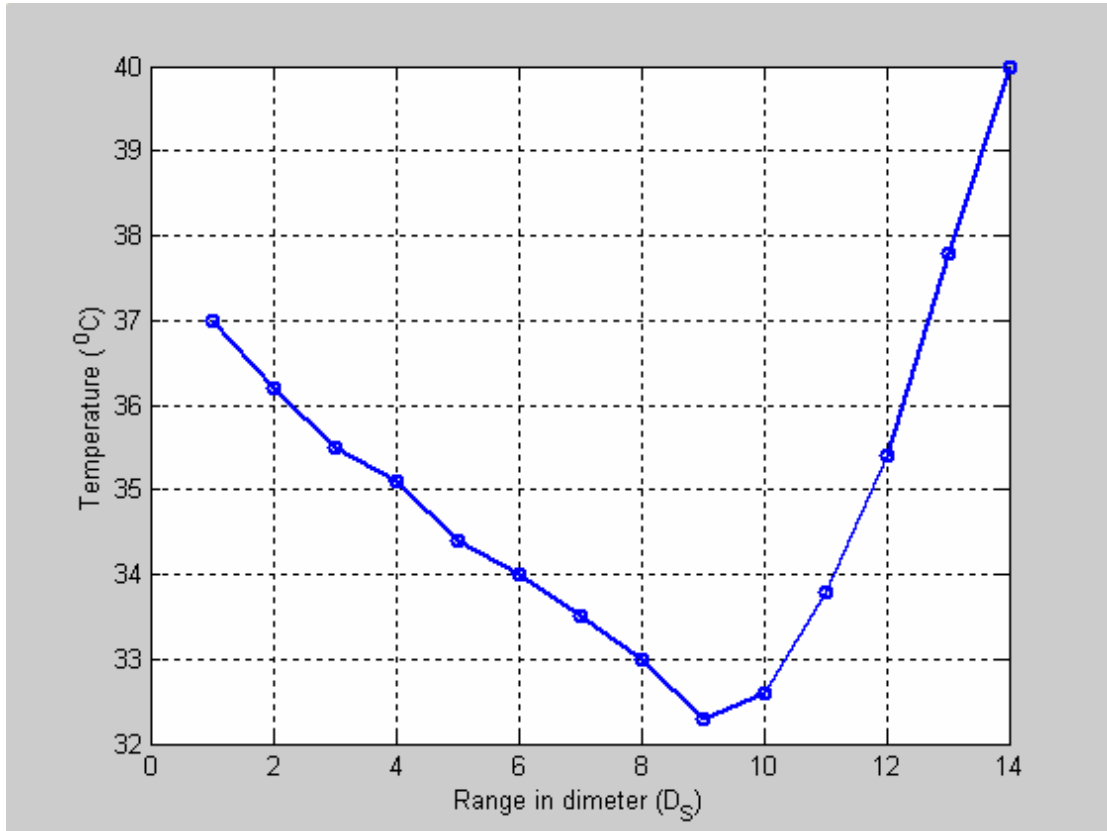


Figure 6.41 Temperature measurements of 20-inch fan (D_S) for 2-diameter in height ($h = 2D$) (with mist)

6.2.2.3 3-Diameter in Height

The 20-inch fan is leveled for its third diameter in height. The temperature is measured for each diameter converge area and tabulated in table 6.24

Table 6.24 Temperature measurements of 20-inch fan (D_s) for 3-diameter in height
($h = 3D$) (with mist)

Range in diameter (D_s)	Temperature ($^{\circ}C$)
1	38
2	36.8
3	36.4
4	35.5
5	34.7
6	34.4
7	33.9
8	33.5
9	33.2
10	32.5
11	32.6
12	33.4
13	34.5
14	36.2
15	38.4
16	40

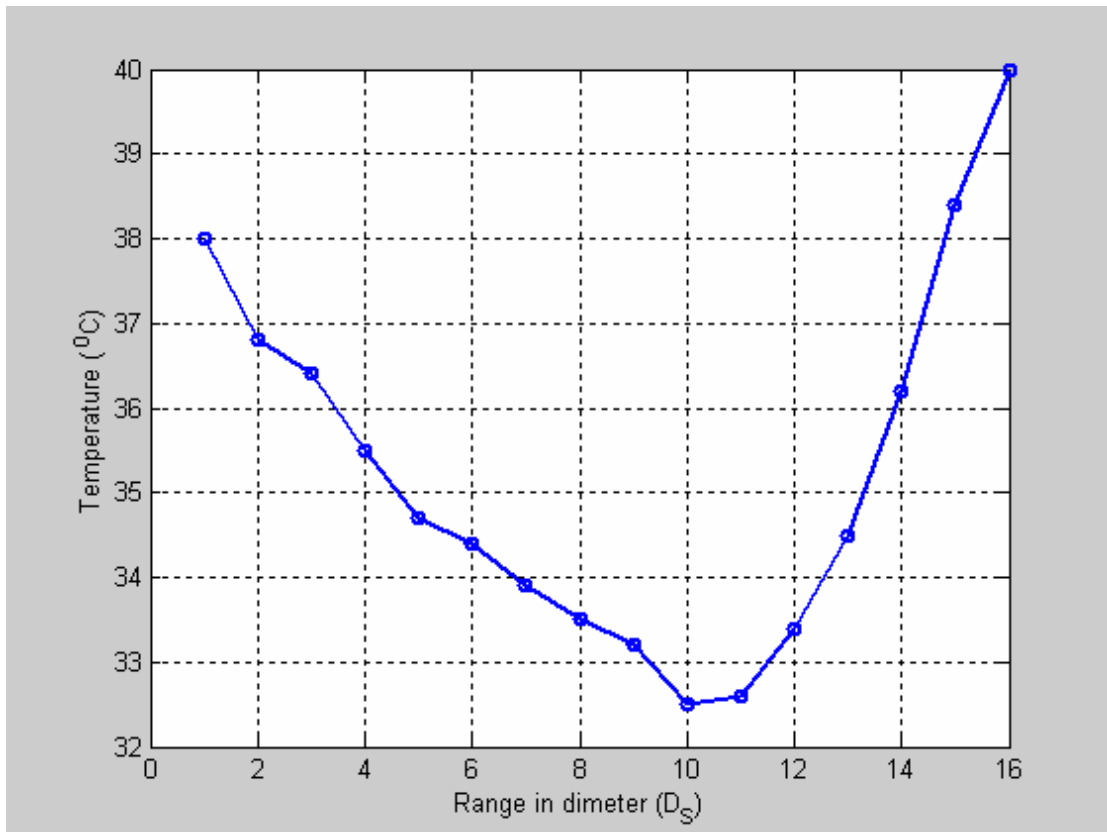


Figure 6.42 Temperature measurements of 20-inch fan (D_S) for 3-diameter in height (h = 3D) (with mist)

6.2.2.4 4-Diameter in Height

The 20-inch fan is leveled for its fourth diameter in height. The temperature is measured for each diameter converge area and tabulated in table 6.25

Table 6.25 Temperature measurements of 20-inch fan (D_s) for 4-diameter in height ($h = 4D$) (with mist)

Range in diameter (D_s)	Temperature ($^{\circ}\text{C}$)
1	38.9
2	37.5
3	36.7
4	36
5	35.2
6	34.8
7	34.5
8	34
9	33.7
10	33.2
11	32.5
12	32.8
13	33.2
14	34
15	35.5
16	37
17	38.4
18	40

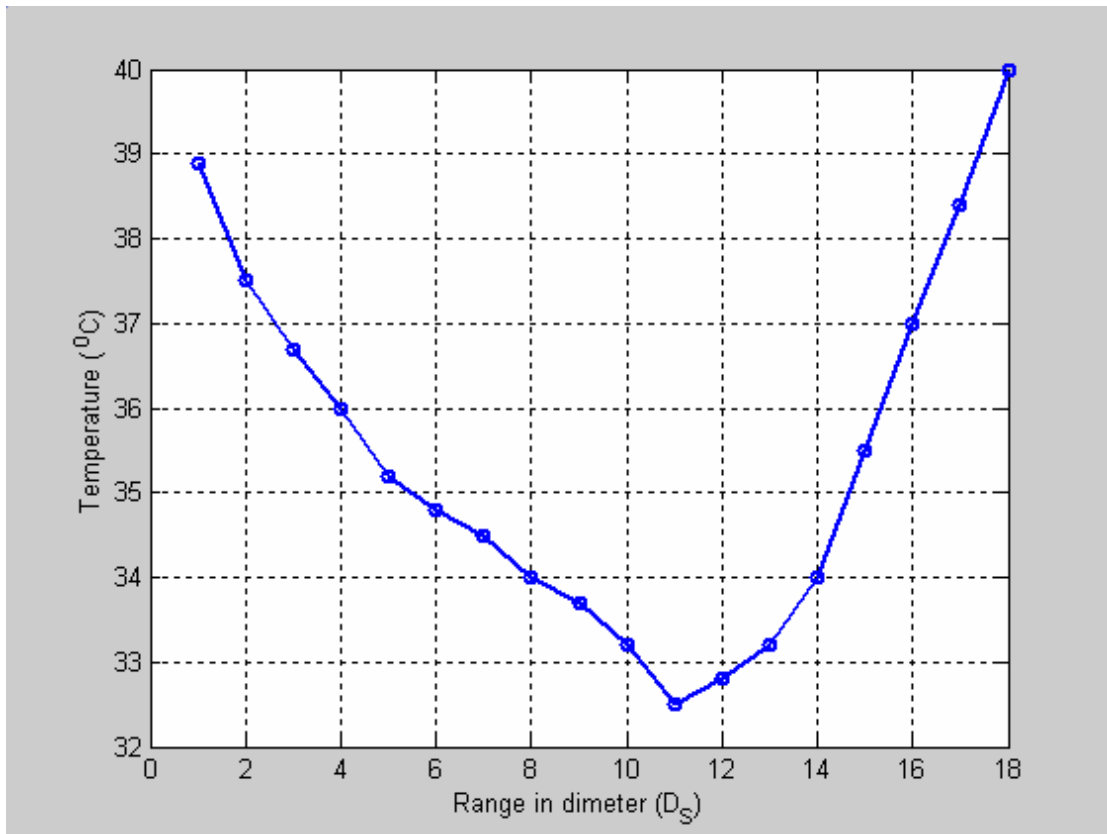


Figure 6.43 Temperature measurements of 20-inch fan (D_S) for 4-diameter in height ($h = 4D$) (with mist)

6.2.2.5 5-Diameter in Height

The 20-inch fan is leveled for its fifth diameter in height. The temperature is measured for each diameter converge area and tabulated in table 6.26

Table 6.26 Temperature measurements of 20-inch fan (D_s) for 5-diameter in height ($h = 5D$) (with mist)

Range in diameter (D_s)	Temperature ($^{\circ}\text{C}$)
1	39.9
2	38.4
3	37.3
4	36.5
5	35.7
6	35.1
7	34.7
8	34.4
9	33.7
10	32.6
11	32.9
12	33.7
13	34.8
14	36.5
15	38.9
16	40

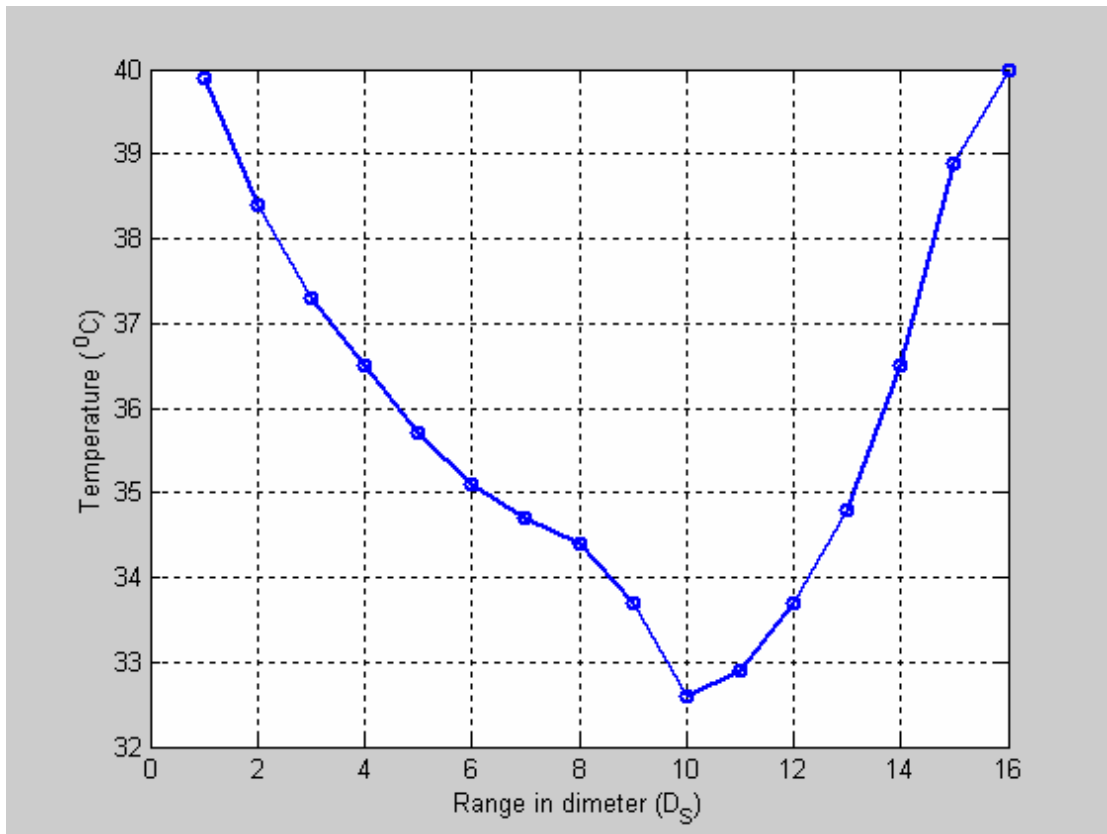


Figure 6.44 Temperature measurements of 20-inch fan (D_S) for 5-diameter in height ($h = 5D$) (with mist)

The temperature measurements of 20-inch fan for all heights are plotted in figure 6.45 showing fan maximum temperature range occurs at the 4th diameter height.

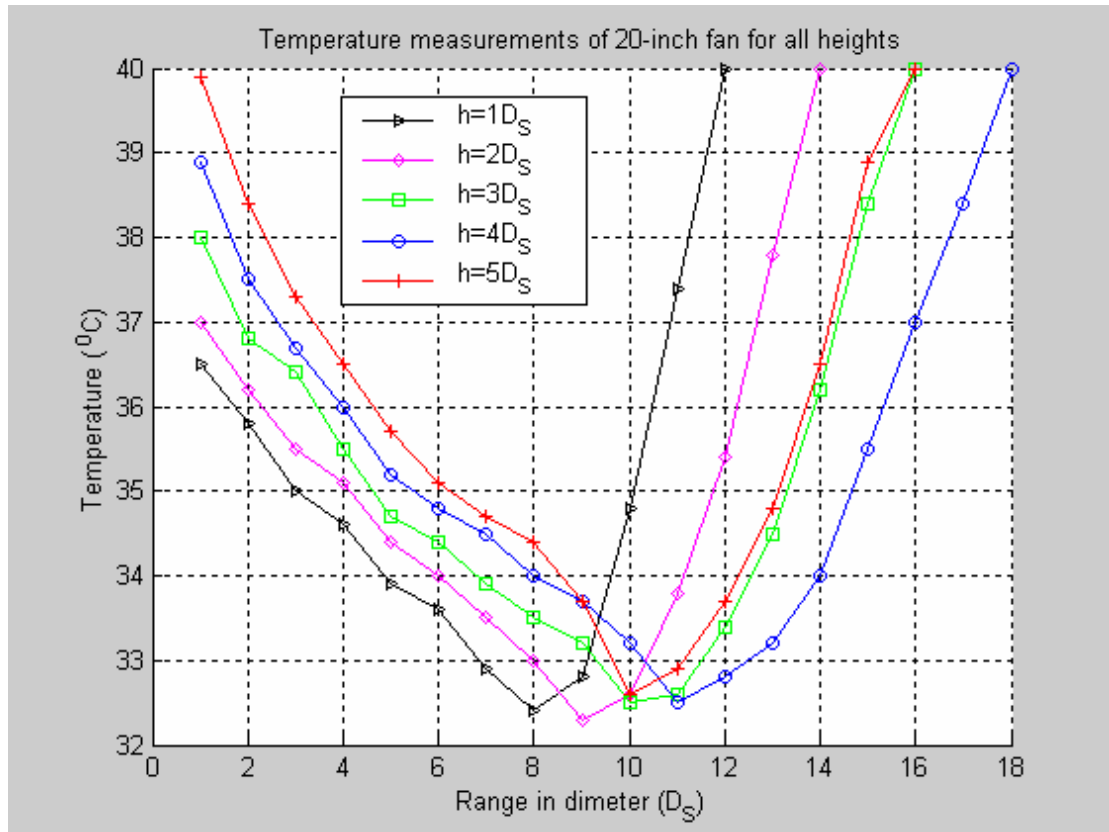


Figure 6.45 Temperature measurements of 20-inch fan (D_S) for all heights (with mist)

6.2.2.6 Angle Effect of 20-inch Fan (with mist)

As done in the first stage, the angle effect of the three fans is also investigated in the second stage with mist; Starting with the 20-inch fan by using equations (6.4), (6.5) and (6.6); measuring the temperature as shown in figure 6.44.

$$\tan \theta_0 = \frac{5D}{\infty} = 0 \quad \rightarrow \quad \theta_0 = 0 \quad (\text{default case}) \quad (6.4)$$

$$\tan \theta_1 = \frac{5D}{10D} = \frac{1}{2} \quad \rightarrow \quad \theta_1 = 26.56^\circ \quad (6.5)$$

$$\tan \theta_2 = \frac{5D}{5D} = 1 \quad \rightarrow \quad \theta_2 = 45^\circ \quad (6.6)$$

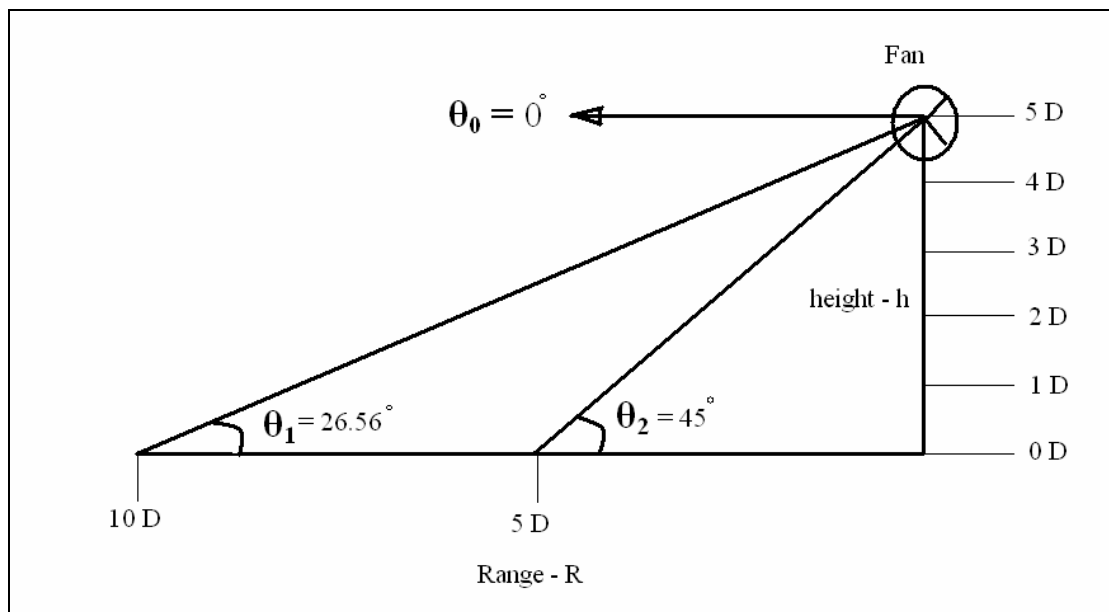


Figure 6.46 Configuration of angle effect case study of 20-inch fan (D_s) with mist

Table 6.27 Temperature measurements of 20-inch fan (D_s) for angle case (with mist)

20-inch Fan (angle case)			
Range in diameter (D_s)	Temperature ($^{\circ}\text{C}$)		
	θ_0	θ_1	θ_2
1	39.9	38.9	37.9
2	38.4	37.4	36.4
3	37.3	36.3	35.3
4	36.5	35.5	34.5
5	35.7	34.7	33.7
6	35.1	34.1	33.4
7	34.7	33.7	33
8	34.4	33.4	32.7
9	33.7	32.7	33.2
10	32.6	33.4	34.9
11	32.9	34.4	36.7
12	33.7	36	40
13	34.8	37.7	
14	36.5	40	
15	38.9		
16	40		

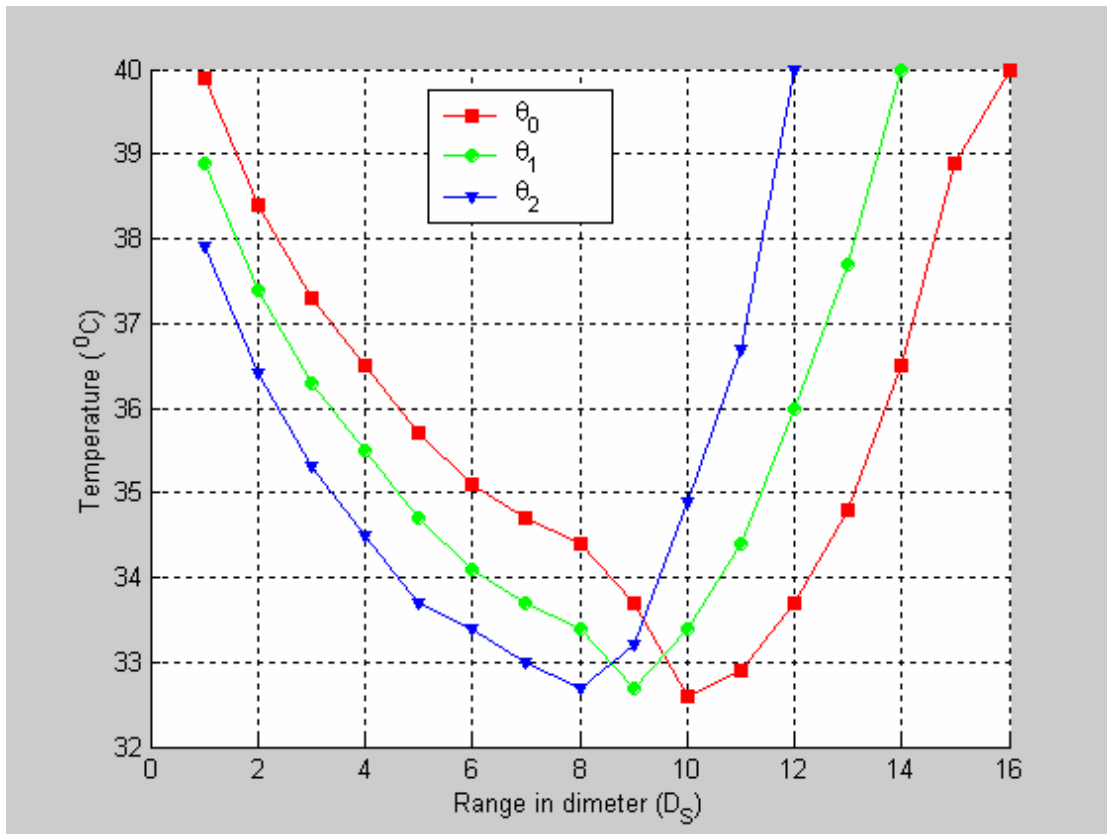


Figure 6.47 Temperature measurements of 20-inch fan (D_S) for angle case (with mist)

6.2.2.7 Side-wise Investigation of 20-inch Fan (with mist)

As shown in figure 6.45, the maximum covered range of the 20-inch fan is 18 diameters front-wise ($18D_s$) in the fourth diameter in height. The side-wise maximum range is investigated as shown in figure 6.48.

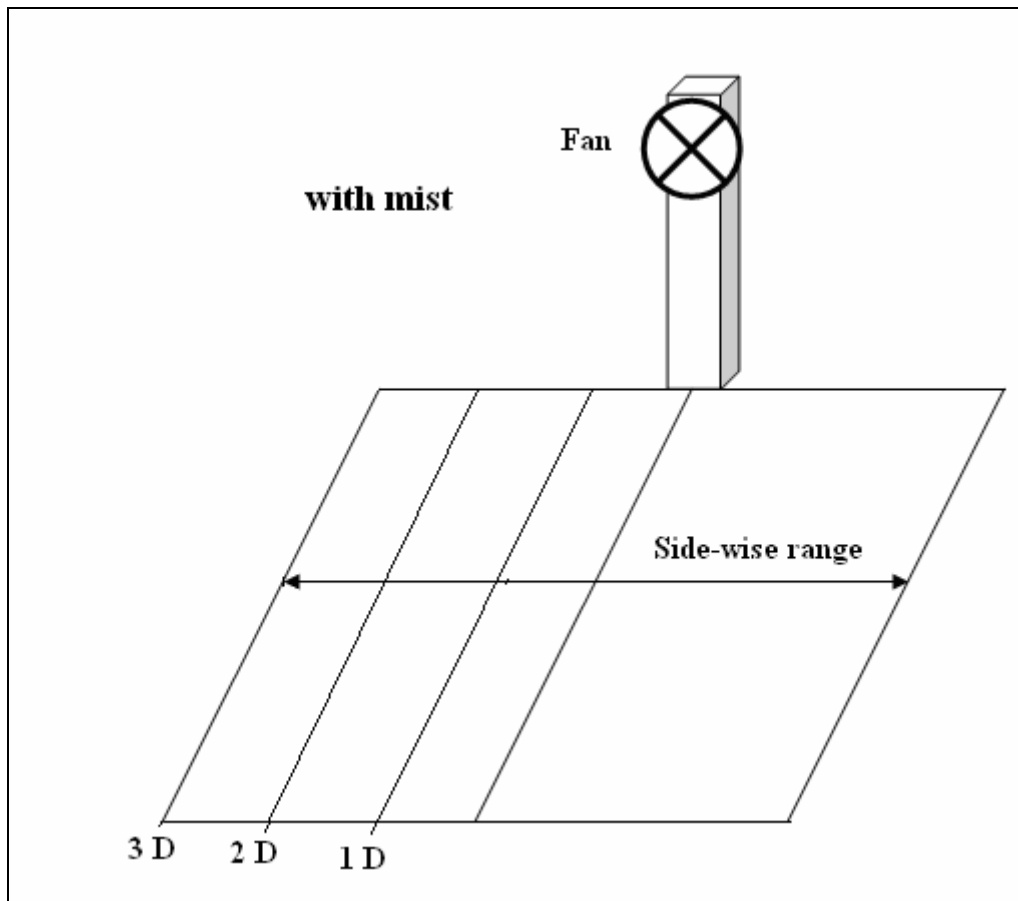


Figure 6.48 Temperature measurements in the side-wise of 20-inch Fan

The temperatures were measured along the 11th diameter (11D_S) front wise location where the minimum temperature value was registered before.

Table 6.28 Temperature measurements in the side-wise of 20-inch Fan (D_S) (with mist)

20-inch Fan (side-wise)								
Distance in diameter (D _S)	Temperature (°C)							
	1-D side-wise	2-D side-wise	3-D side-wise	4-D side-wise	5-D side-wise	6-D side-wise	7-D side-wise	8-D side-wise
11	32.5	33	33.8	34.7	35.6	36.8	38	40

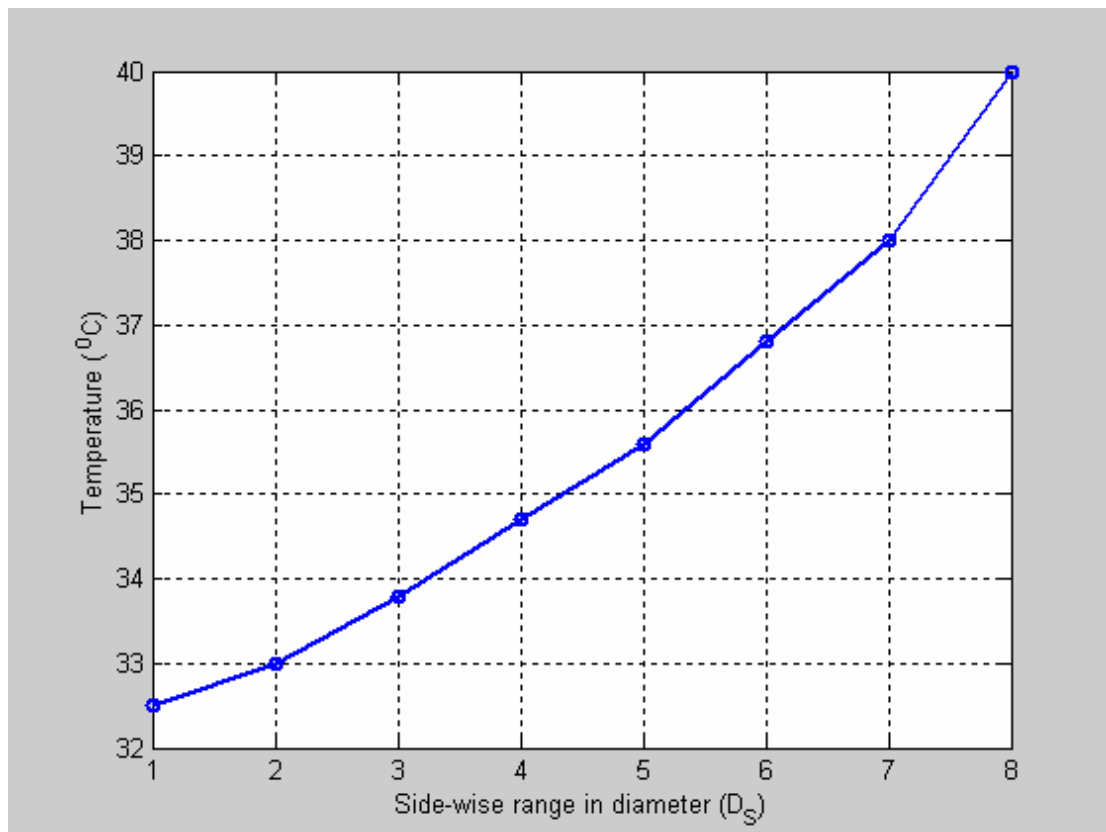


Figure 6.49 Temperature measurements in the side-wise of 20-inch Fan (D_S) (with mist)

6.2.3 24-inch Fan (with mist)

6.2.3.1 1-Diameter in Height

The 24-inch fan is leveled for its first to fifth diameters consequently as the same as it has been done for the 20-inch fan shown in figure 6.39.

The temperature is measured for each diameter converge area for the first diameter in height and tabulated in table 6.29

Table 6.29 Temperature measurements of 24-inch fan (D_m) for 1-diameter in height ($h = 1D$) (with mist)

Range in diameter (D_m)	Temperature ($^{\circ}C$)
1	37.5
2	36.7
3	35.8
4	34.9
5	34.3
6	33.5
7	32
8	33.5
9	36
10	40

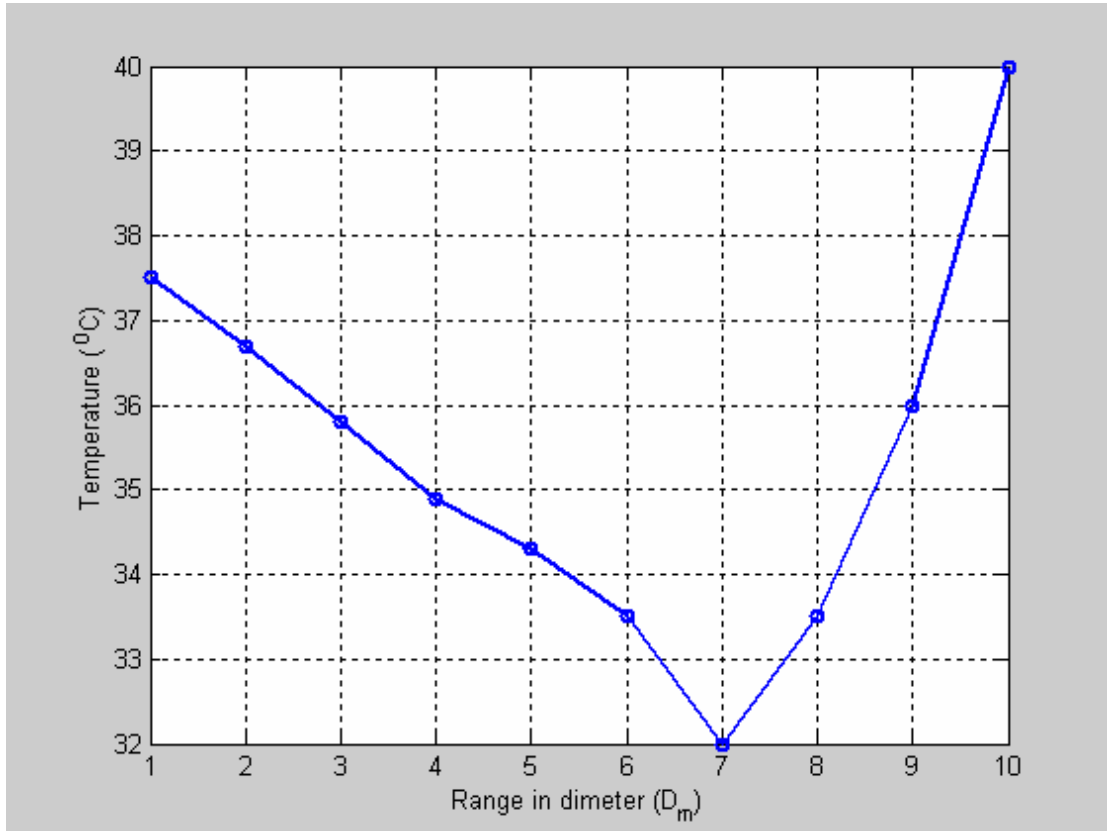


Figure 6.50 Temperature measurements of 24-inch fan (D_m) for 1-diameter in height ($h = 1D$) (with mist)

6.2.3.2 2-Diameter in Height

The 24-inch fan is leveled for its second diameter in height. The temperature is measured for each diameter converge area and tabulated in table 6.30

Table 6.30 Temperature measurements of 24-inch fan (D_m) for 2-diameter in height ($h = 2D$) (with mist)

Range in diameter (D_m)	Temperature ($^{\circ}C$)
1	37
2	36.5
3	35.7
4	35
5	34.1
6	33.6
7	32.7
8	32
9	32.5
10	34.5
11	37
12	40

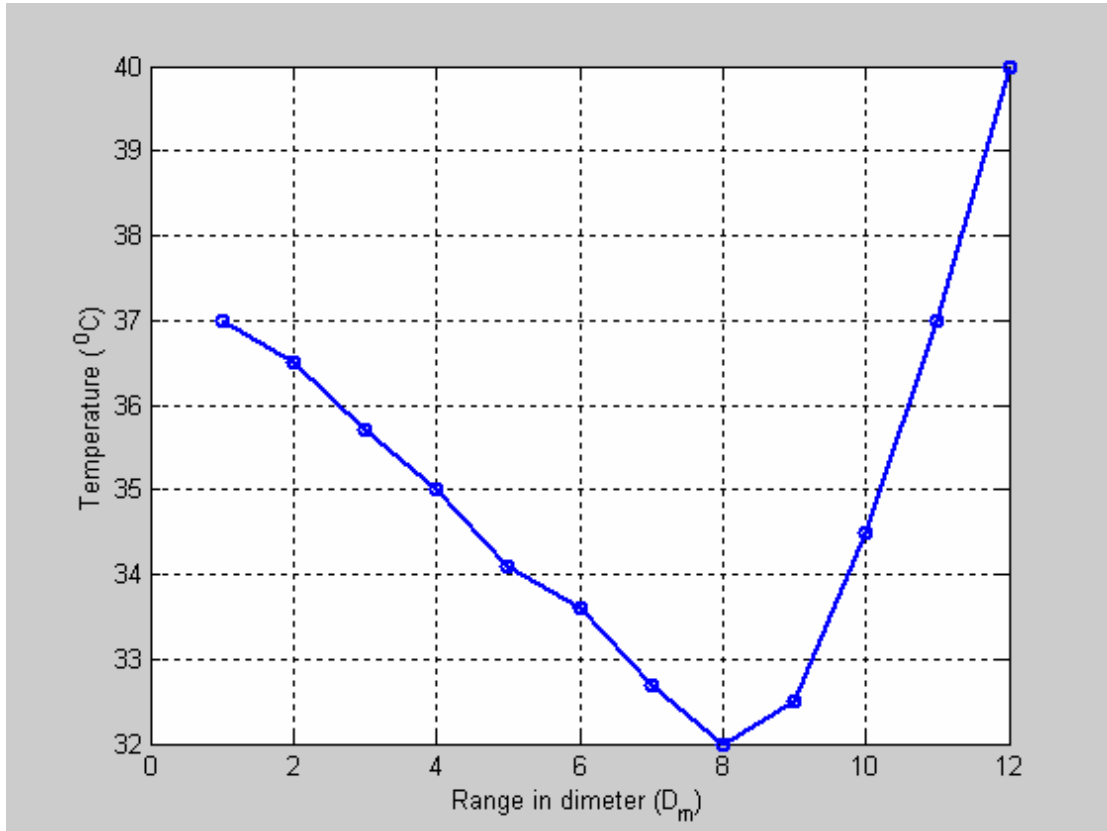


Figure 6.51 Temperature measurements of 24-inch fan (D_m) for 2-diameter in height ($h = 2D$) (with mist)

6.2.3.3 3-Diameter in Height

The 24-inch fan is leveled for its third diameter in height. The temperature is measured for each diameter converge area and tabulated in table 6.31

Table 6.31 Temperature measurements of 24-inch fan (D_m) for 3-diameter in height
($h = 3D$) (with mist)

Range in diameter (D_m)	Temperature ($^{\circ}C$)
1	37.9
2	37
3	36.2
4	35.5
5	34.6
6	34.0
7	33.2
8	32.8
9	32
10	32.5
11	33.9
12	35.8
13	38
14	40

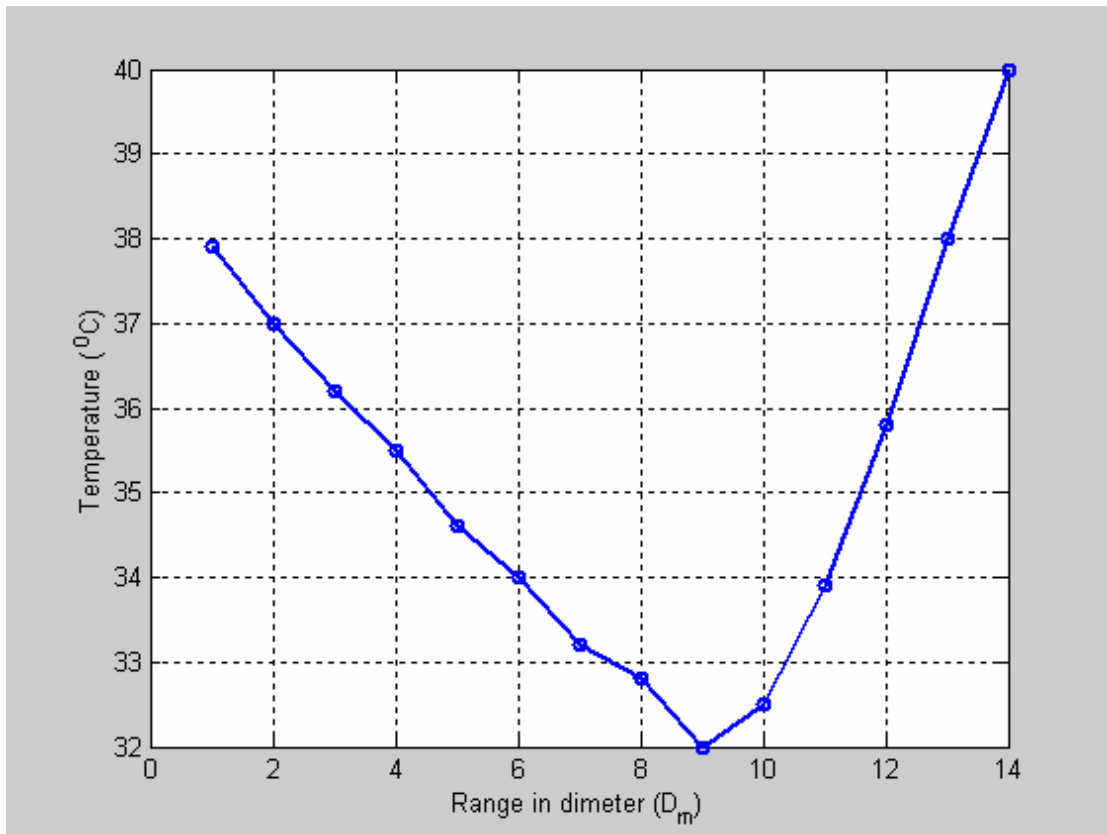


Figure 6.52 Temperature measurements of 24-inch fan (D_m) for 3-diameter in height ($h = 3D$) (with mist)

6.2.3.4 4-Diameter in Height

The 24-inch fan is leveled for its fourth diameter in height. The temperature is measured for each diameter converge area and tabulated in table 6.32

Table 6.32 Temperature measurements of 24-inch fan (D_m) for 4-diameter in height
($h = 4D$) (with mist)

Range in diameter (D_m)	Temperature ($^{\circ}C$)
1	38.9
2	37.6
3	36.8
4	36
5	35.2
6	34.6
7	33.8
8	33.1
9	32.6
10	31.8
11	32.5
12	33.5
13	35
14	36.3
15	38.2
16	40

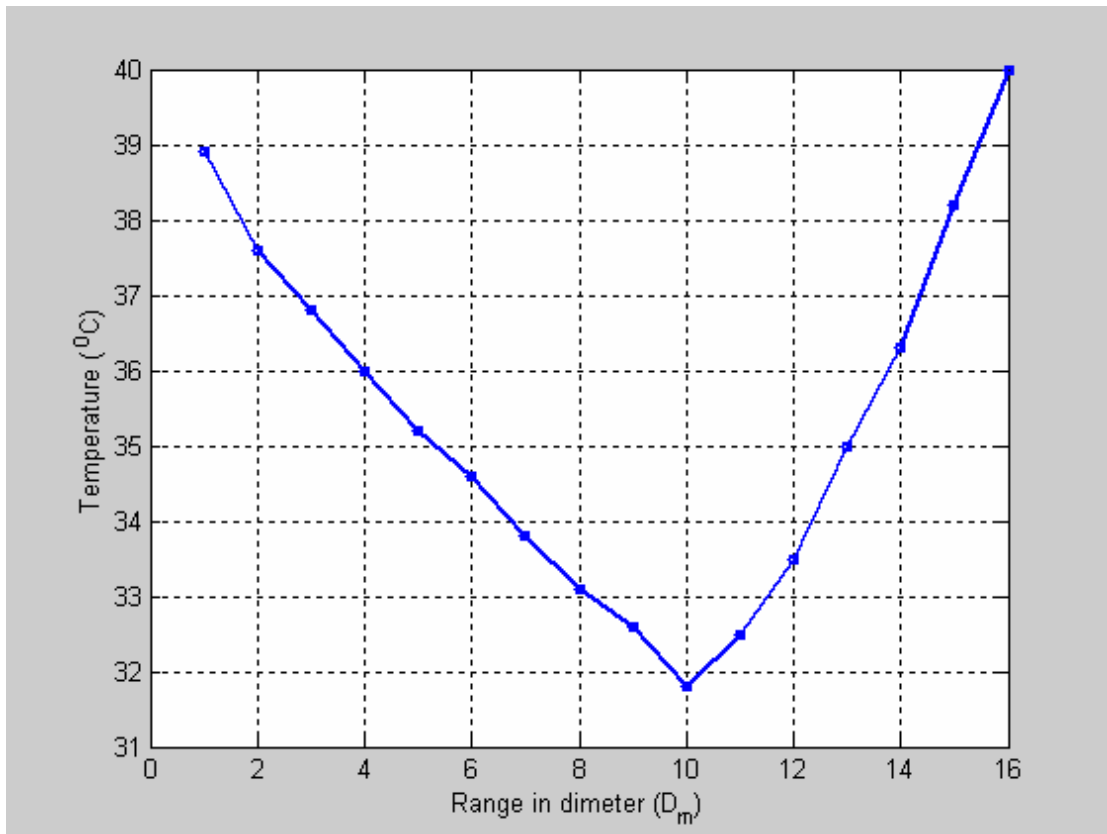


Figure 6.53 Temperature measurements of 24-inch fan (D_m) for 4-diameter in height ($h = 4D$) (with mist)

6.2.3.5 5-Diameter in Height

The 24-inch fan is leveled for its fifth diameter in height. The temperature is measured for each diameter converge area and tabulated in table 6.33

Table 6.33 Temperature measurements of 24-inch fan (D_m) for 5-diameter in height
($h = 5D$) (with mist)

Range in diameter (D_m)	Temperature ($^{\circ}C$)
1	39.9
2	38.4
3	37.3
4	36.5
5	35.7
6	35.1
7	34.5
8	33.5
9	32.1
10	32.8
11	34.2
12	36.2
13	38.2
14	40

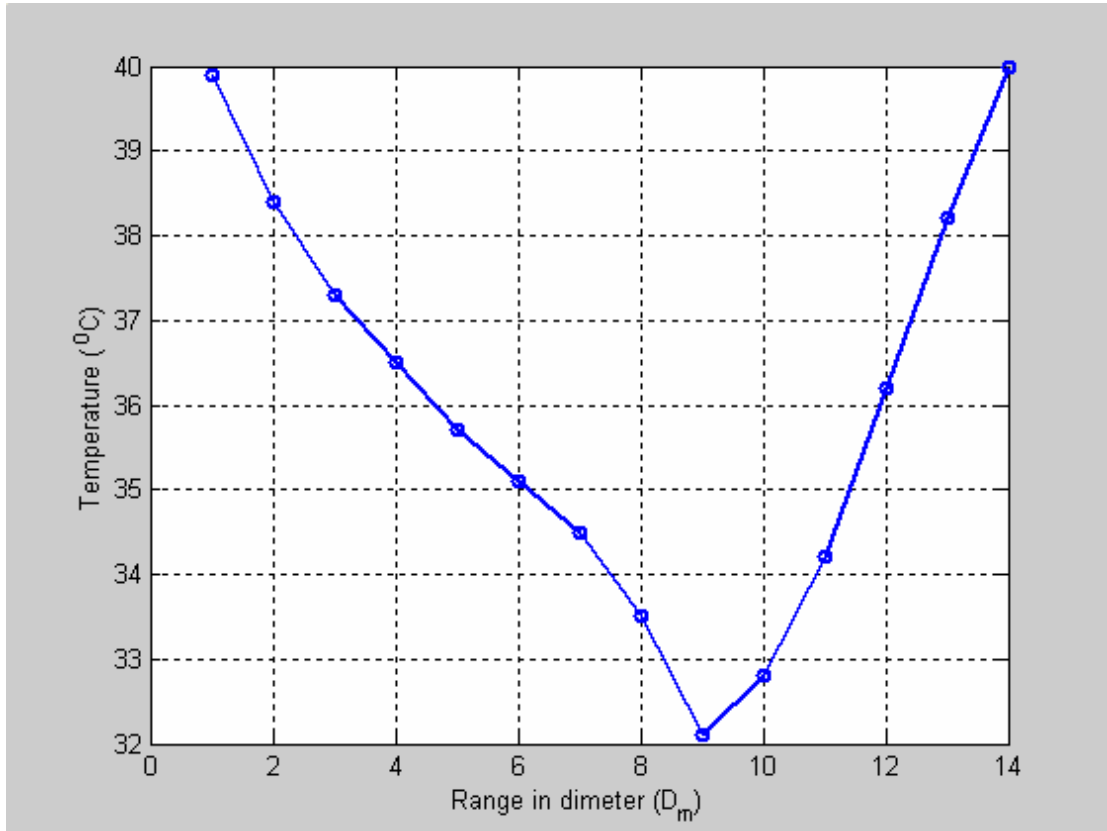


Figure 6.54 Temperature measurements of 24-inch fan (D_m) for 5-diameter in height ($h = 5D$) (with mist)

The temperature measurements of 24-inch fan for all heights are plotted in figure 6.55 showing fan maximum temperature range occurs at the 4th diameter height.

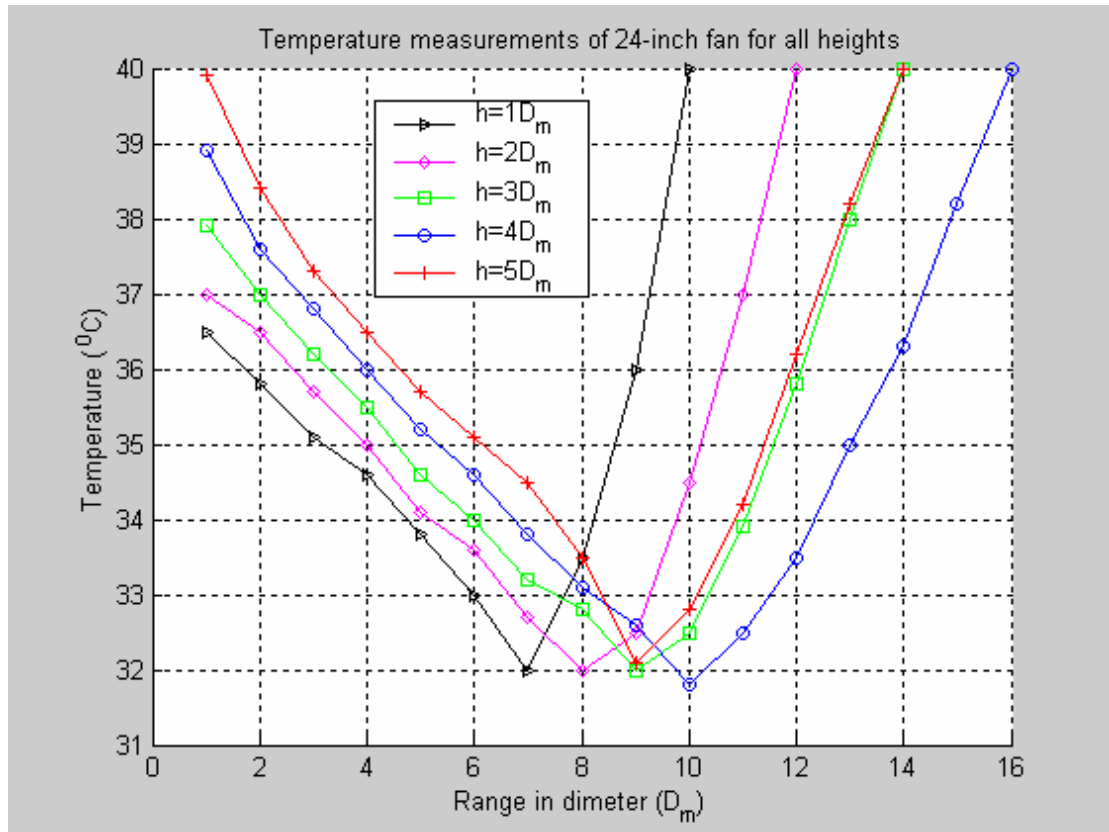


Figure 6.55 Temperature measurements of 24-inch fan (D_m) for all heights (with mist)

6.2.3.6 Angle Effect of 24-inch Fan (with mist)

As done in the first stage, the angle effect of the 24-inch fan is also investigated in the second stage with mist using equations (6.4), (6.5) and (6.6); measuring the temperature as shown in figure 6.46.

Table 6.34 Temperature measurements of 24-inch fan (D_m) for angle case (with mist)

24-inch Fan (angle case)			
Range in diameter (D_m)	Temperature ($^{\circ}\text{C}$)		
	θ_0	θ_1	θ_2
1	39.9	38.9	37.8
2	38.4	37.4	36.1
3	37.3	36.3	35.4
4	36.5	35.5	34.8
5	35.7	34.7	33.9
6	35.1	34.1	33
7	34.5	33	32
8	33.5	32	33.1
9	32.1	33.3	35.1
10	32.8	34.6	40
11	34.2	36.9	
12	36.2	40	
13	38.2		
14	40		

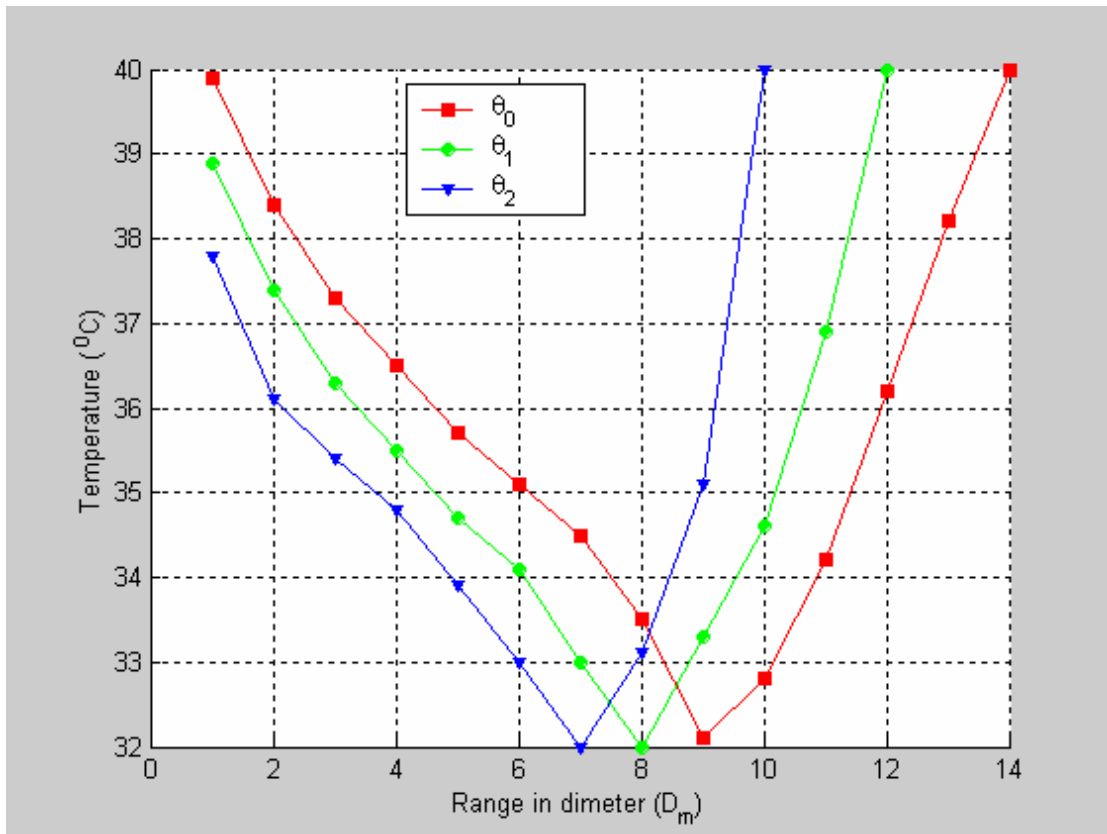


Figure 6.56 Temperature measurements of 24-inch fan (D_m) for angle case (with mist)

6.2.3.7 Side-wise Investigation of 24-inch Fan (with mist)

As shown in figure 6.55, the maximum covered range of the 24-inch fan is 16 diameters front-wise ($16D_m$) in the fourth diameter in height. The side-wise maximum range is investigated as shown in figure 6.48.

The temperatures were measured along the 10th diameter ($10D_m$) front wise location where the minimum temperature value was registered before.

Table 6.35 Temperature measurements in the side-wise of 24-inch Fan (D_m) (with mist)

24-inch Fan (side-wise)							
Distance in diameter (D_m)	Temperature ($^{\circ}C$)						
	1-D side-wise	2-D side-wise	3-D side-wise	4-D side-wise	5-D side-wise	6-D side-wise	7-D side-wise
10	31.8	32.5	33.3	34.5	36	38	40

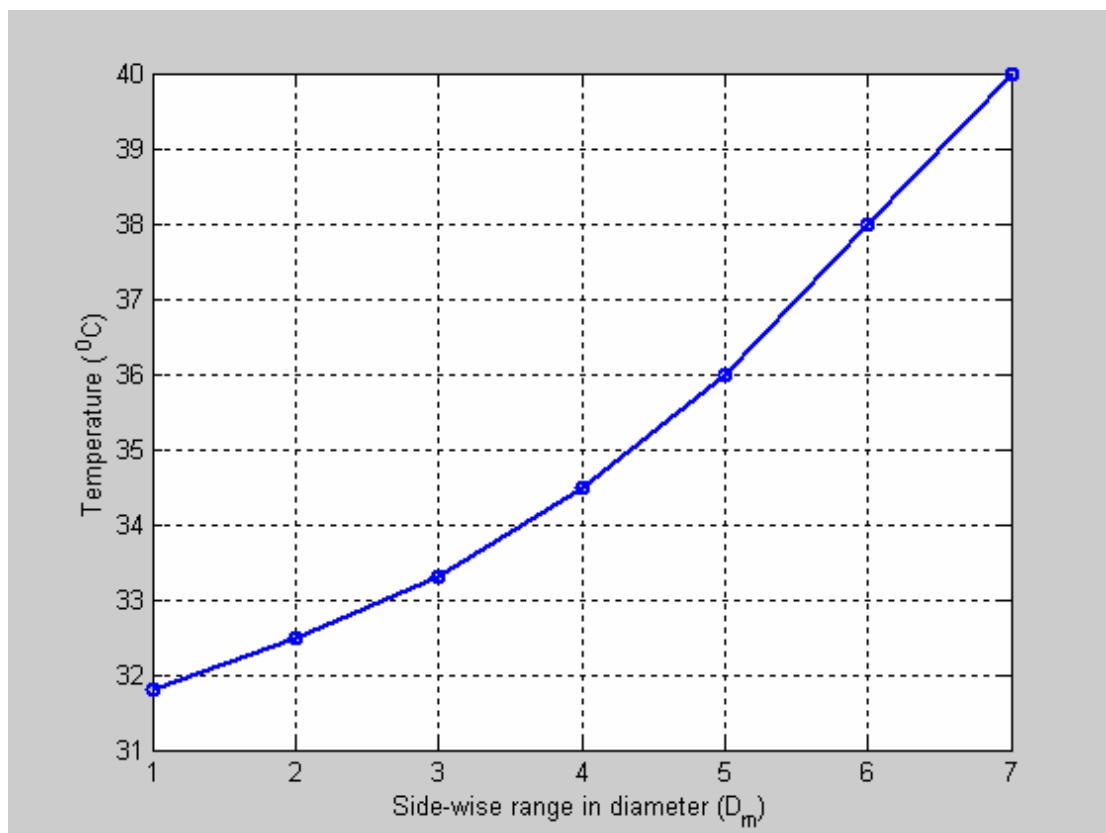


Figure 6.57 Temperature measurements in the side-wise of 24-inch Fan (D_m) (with mist)

6.2.4 30-inch Fan (with mist)

6.2.4.1 1-Diameter in Height

The 30-inch fan is leveled for its first to fifth diameters consequently as the same as it has been done for the 20-inch fan shown in figure 6.39.

The temperature is measured for each diameter converge area for the first diameter in height and tabulated in table 6.36

Table 6.36 Temperature measurements of 30-inch fan (D_L) for 1-diameter in height ($h = 1D$) (with mist)

Range in diameter (D_L)	Temperature ($^{\circ}C$)
1	36.3
2	35.5
3	35
4	34.3
5	33.1
6	31.9
7	33.3
8	40

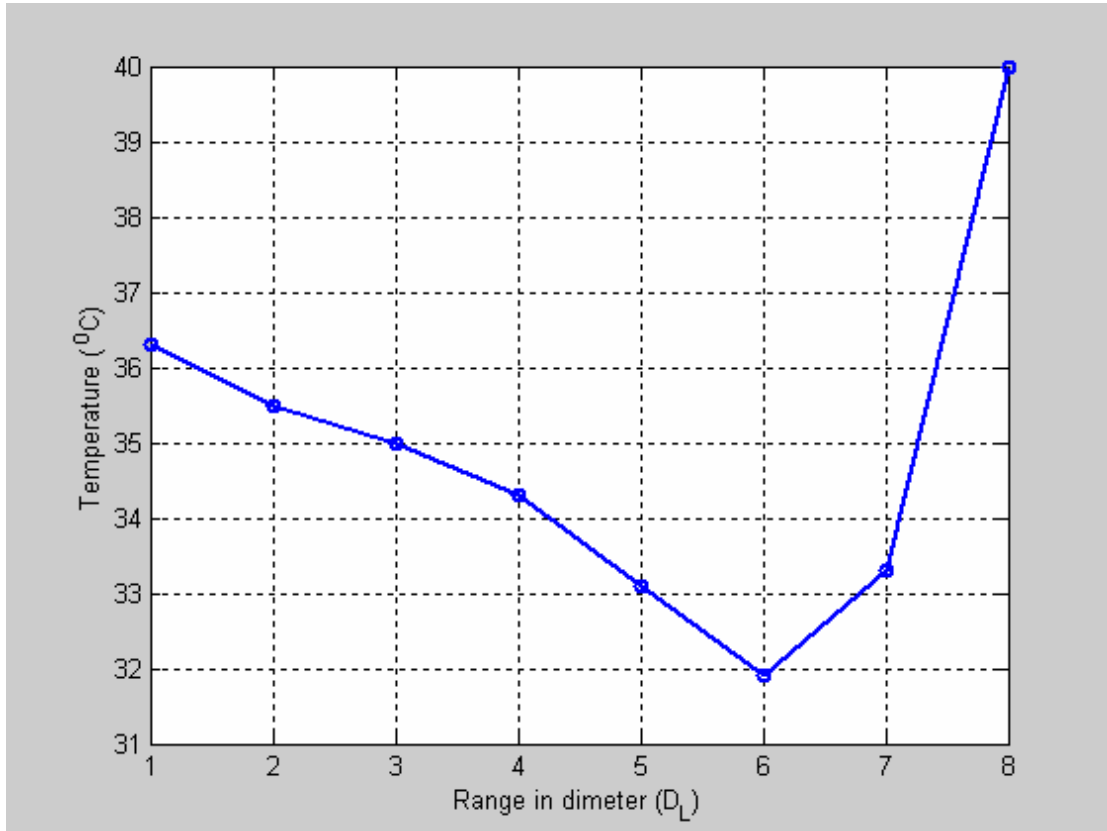


Figure 6.58 Temperature measurements of 30-inch fan (D_L) for 1-diameter in height ($h = 1D$) (with mist)

6.2.4.2 2-Diameter in Height

The 30-inch fan is leveled for its second diameter in height. The temperature is measured for each diameter converge area and tabulated in table 6.37

Table 6.37 Temperature measurements of 30-inch fan (D_L) for 2-diameter in height
($h = 2D$) (with mist)

Range in diameter (D_L)	Temperature ($^{\circ}\text{C}$)
1	37.1
2	36.3
3	35.7
4	35
5	34
6	33.1
7	31.7
8	32.8
9	35.6
10	40

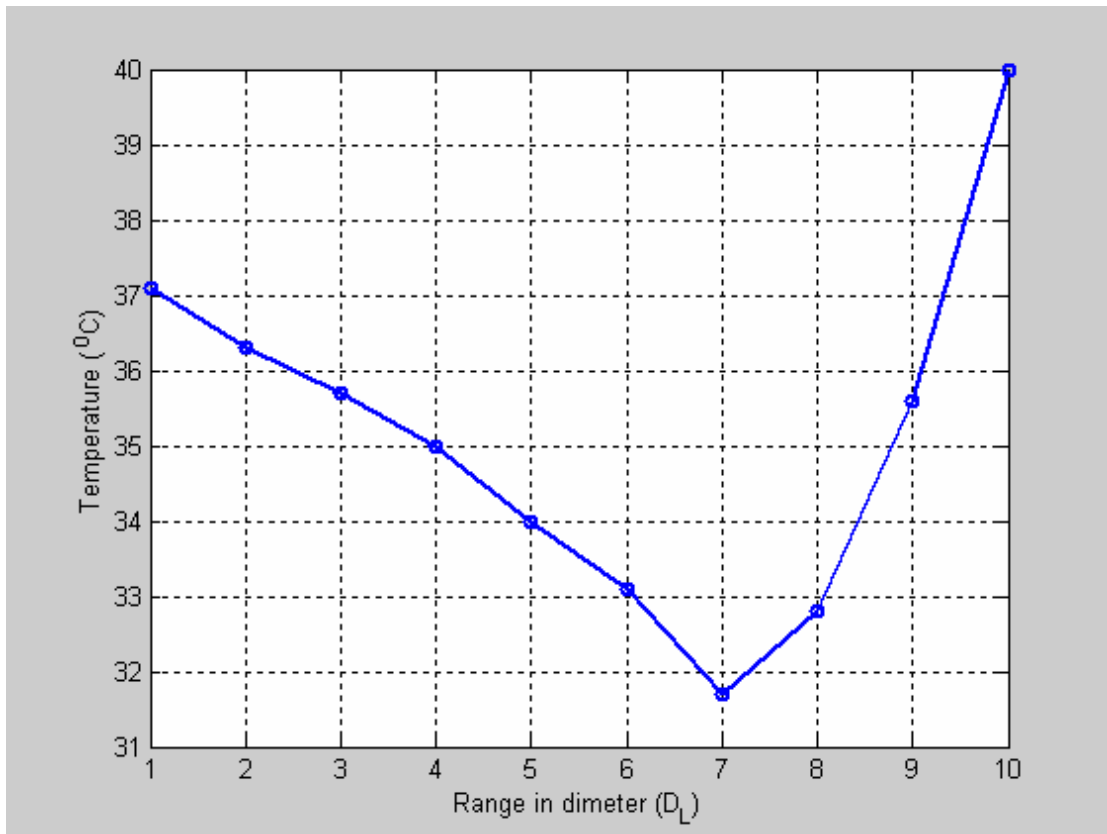


Figure 6.59 Temperature measurements of 30-inch fan (D_L) for 2-diameter in height ($h = 2D$) (with mist)

6.2.4.3 3-Diameter in Height

The 30-inch fan is leveled for its third diameter in height. The temperature is measured for each diameter converge area and tabulated in table 6.38

Table 6.38 Temperature measurements of 30-inch fan (D_L) for 3-diameter in height ($h = 3D$) (with mist)

Range in diameter (D_L)	Temperature ($^{\circ}\text{C}$)
1	38
2	37
3	36.2
4	35.5
5	34.5
6	33.7
7	32.5
8	31.7
9	32.7
10	34.8
11	37.4
12	40

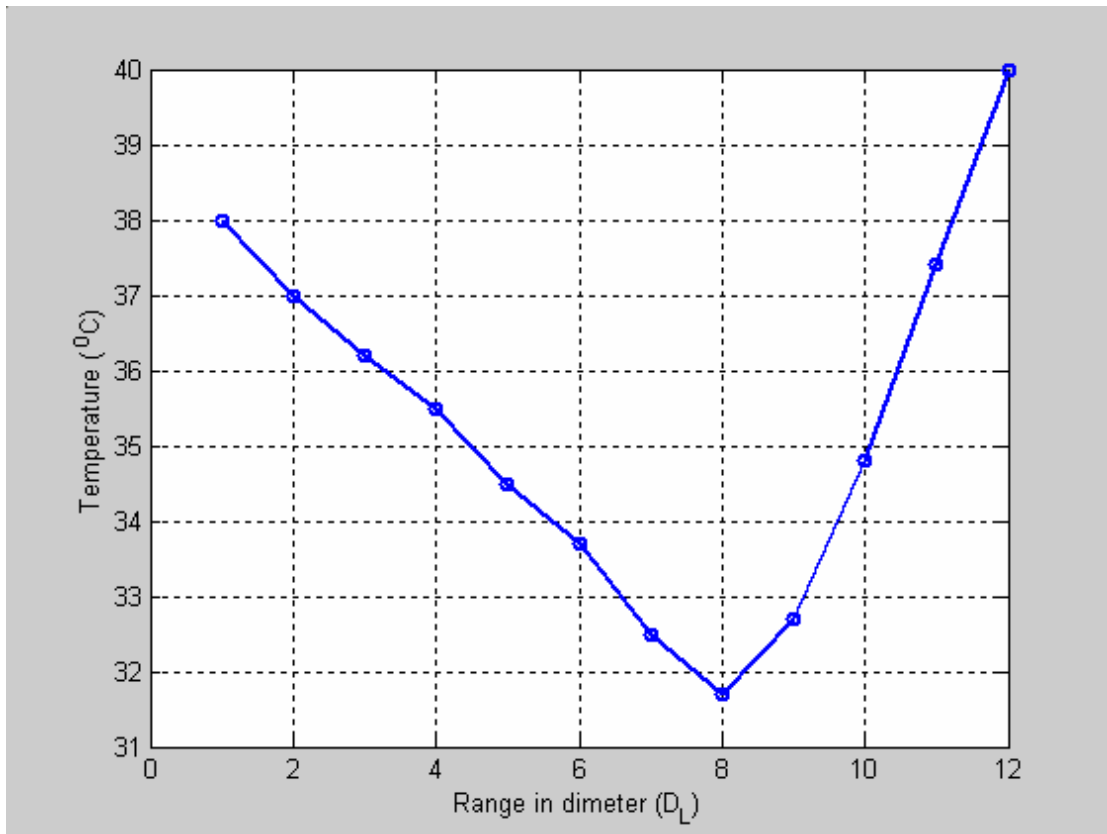


Figure 6.60 Temperature measurements of 30-inch fan (D_L) for 3-diameter in height ($h = 3D$) (with mist)

6.2.4.4 4-Diameter in Height

The 30-inch fan is leveled for its fourth diameter in height. The temperature is measured for each diameter converge area and tabulated in table 6.39

Table 6.39 Temperature measurements of 30-inch fan (D_L) for 4-diameter in height
($h = 4D$) (with mist)

Range in diameter (D_L)	Temperature ($^{\circ}\text{C}$)
1	38.9
2	37.6
3	36.8
4	36.1
5	35.1
6	34.2
7	32.9
8	32.3
9	31.7
10	32.4
11	33.5
12	35.2
13	37.6
14	40

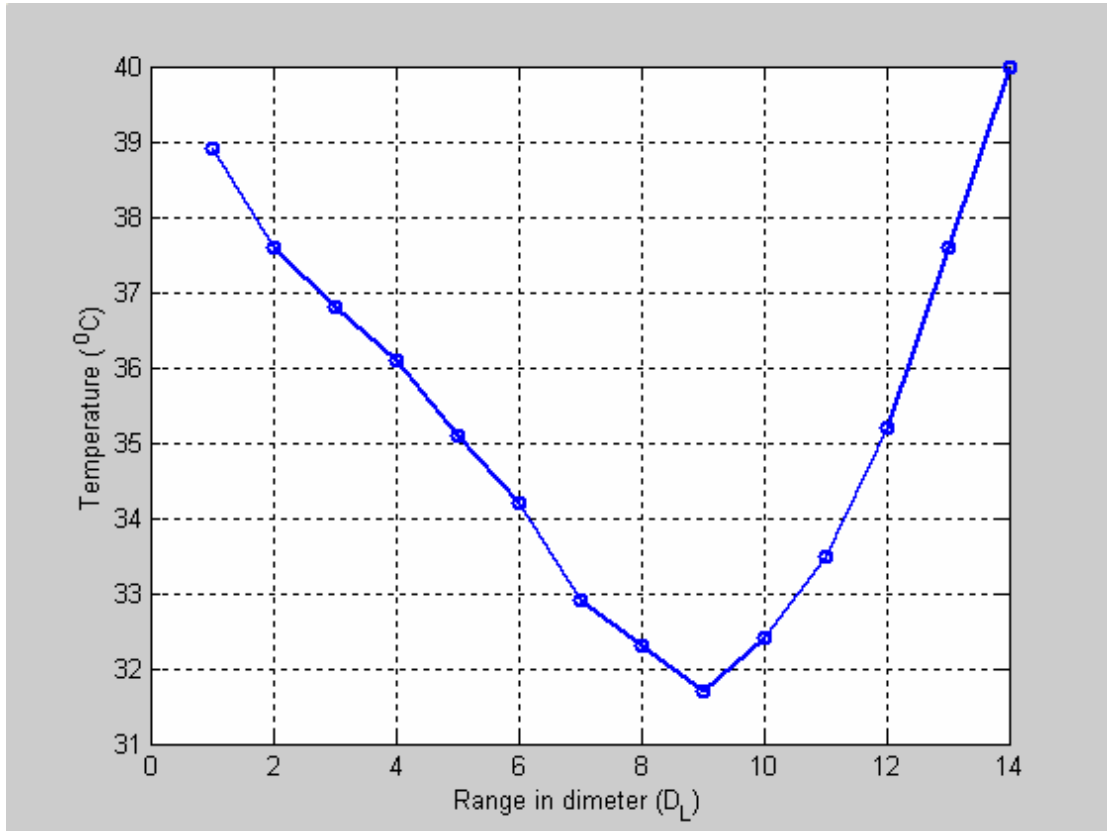


Figure 6.61 Temperature measurements of 30-inch fan (D_L) for 4-diameter in height ($h = 4D$) (with mist)

6.2.4.5 5-Diameter in Height

The 30-inch fan is leveled for its fifth diameter in height. The temperature is measured for each diameter converge area and tabulated in table 6.40

Table 6.40 Temperature measurements of 30-inch fan (D_L) for 5-diameter in height
($h = 5D$) (with mist)

Range in diameter (D_L)	Temperature ($^{\circ}\text{C}$)
1	39.9
2	38.8
3	37.4
4	36.7
5	35.9
6	34.9
7	33.2
8	31.8
9	32.9
10	34.9
11	37.8
12	40

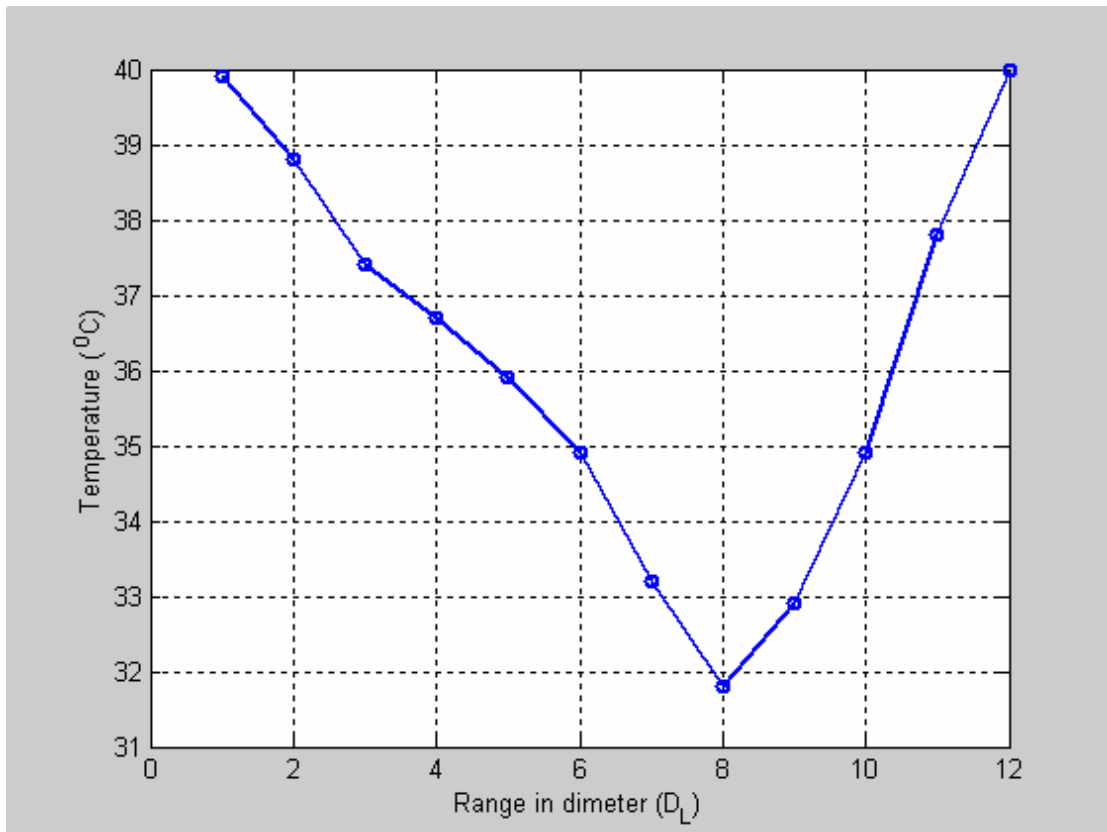


Figure 6.62 Temperature measurements of 30-inch fan (D_L) for 5-diameter in height ($h = 5D$) (with mist)

The temperature measurements of 30-inch fan for all heights are plotted in figure 6.63 showing fan maximum temperature range occurs at the 4th diameter height.

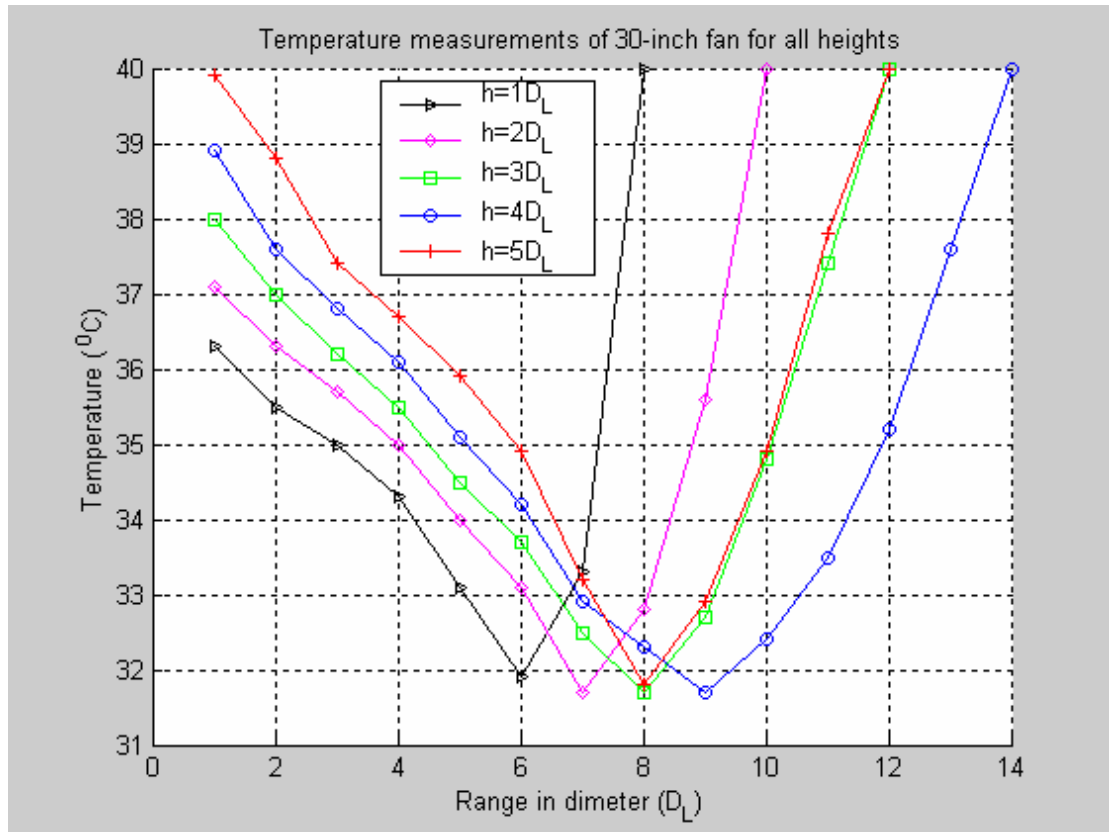


Figure 6.63 Temperature measurements of 30-inch fan (D_L) for all heights (with mist)

6.2.4.6 Angle Effect of 30-inch Fan (with mist)

As done in the first stage, the angle effect of the 24-inch fan is also investigated in the second stage with mist using equations (6.4), (6.5) and (6.6); measuring the temperature as shown in figure 6.44.

Table 6.41 Temperature measurements of 30-inch fan (D_L) for angle case (with mist)

30-inch Fan (angle case)			
Range in diameter (D_L)	Temperature ($^{\circ}C$)		
	θ_0	θ_1	θ_2
1	39.9	38.9	37.9
2	38.8	37.8	36.8
3	37.4	36.4	35.4
4	36.7	35.7	34.7
5	35.9	34.9	33.3
6	34.9	33.9	31.9
7	33.2	31.9	32.8
8	31.8	32.9	34
9	32.9	34.5	36.9
10	34.9	36.8	40
11	37.8	40	
12	40		

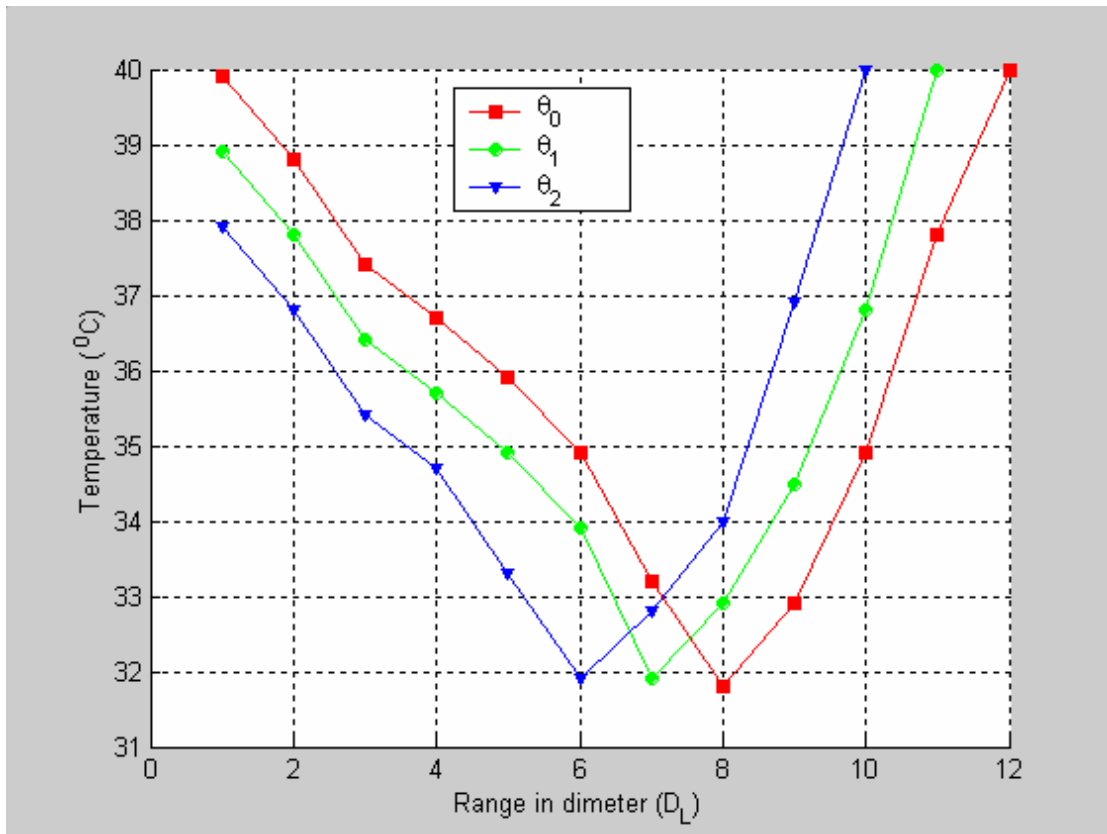


Figure 6.64 Temperature measurements of 30-inch fan (D_L) for angle case (with mist)

6.2.4.7 Side-wise Investigation of 30-inch Fan (with mist)

As shown in figure 6.63, the maximum covered range of the 30-inch fan is 14 diameters front-wise ($14D_L$) in the fourth diameter in height. The side-wise maximum range is investigated as shown in figure 6.48.

The temperatures were measured along the 9th diameter ($9D_L$) front wise location where the minimum temperature value was registered before.

Table 6.42 Temperature measurements in the side-wise of 30-inch Fan (D_L) (with mist)

30-inch Fan (side-wise)						
Distance in diameter (D_L)	Temperature ($^{\circ}C$)					
	1-D side-wise	2-D side-wise	3-D side-wise	4-D side-wise	5-D side-wise	6-D side-wise
9	31.7	32.6	33.9	35.5	37.5	40

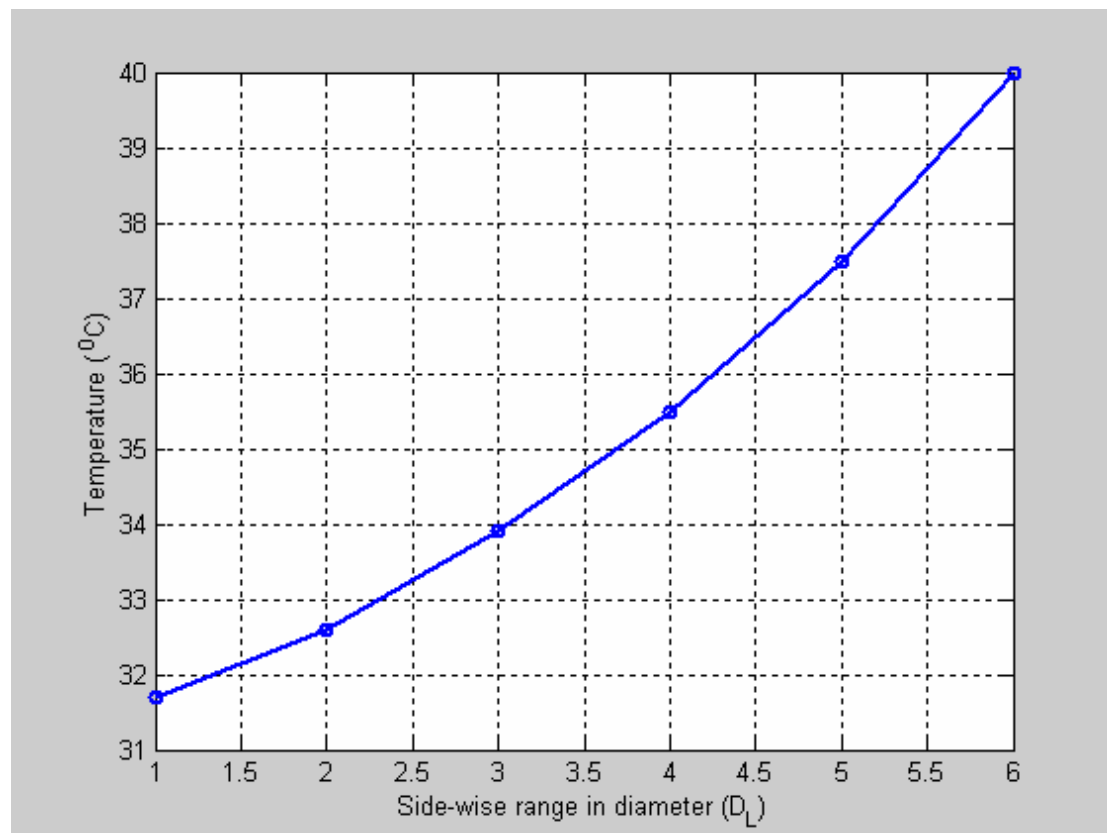


Figure 6.65 Temperature measurements in the side-wise of 30-inch Fan (D_L) (with mist)

CHAPTER 7

NUMERICAL SOLUTION

In this chapter, computational solution is presented based on experimental conditions, such dry bulb temperature, wet bulb temperature, relative humidity, operating pressure droplet velocity and fan airspeed.

All experimental conditions were kept the same for the three fans except the fan airspeed which varies according to different fan diameter. Computational solution is conducted based on mass transfer diffusion equation to calculate the evaporation rate as a first step and based on energy balance equation to calculate the temperature for each fan as a second step.

As mentioned above, the only changing parameter is the fan airspeed which was measured experimentally referred to earlier in chapter 5.

7.1 Thermodynamic Model for an Evaporating Water Droplet

In the thermodynamic modeling of an evaporating liquid-water droplet, use may be made of the transient form of the First Law of Thermodynamics applied to a control volume with a moving boundary. The surface of the control volume coincides with the surface of the droplet, which is assumed spherical, and while evaporation takes place, there are heat-and-mass transfers at the moving surface with thermal-energy storage within the droplet. The heat transfer at the surface may be due to both radiation and forced convection, and the mass transfer with its associated enthalpy-flux occurs as evaporation takes place at the interface. The energy storage within the droplet is by sensible heating as the result of heat conduction. Since the internal

thermal-resistance of the droplet is small compared with the external thermal-resistance, (i.e. The Biot number is small and less than approximately 0.1), the lumped heat-capacity approach to the calculation of the energy storage in the droplet is appropriate. That is, the temperature in the droplet may be assumed to be uniform during the evaporation process. This considerably simplifies the analysis of the overall calculation procedure, since it avoids the need for a conjugate heat-conduction analysis for the internal transient temperature-distribution inside the droplet [36].

7.1.1 Evaporation Model

The bubble modeling of the evaporating droplet is based on the equations of the thermal behavior of a drop in a finite volume (Hinze, 1955; Zung, 1967; Tishkoff 1979; Bellan and Cuffel, 1983; Lefebvre, 1994). The model supposes that drops have a spherical form and that they keep this form during the evaporation process (Fig. 7.1). Furthermore, the radiative heat exchanges are neglected; the steam and air are considered as ideal gases and the concentration at the same temperature.

The drop will be considered as a spherical, characterized by radius r_p , surface concentration C_s and temperature T_p . it is surrounded by a bubble of radius b , concentration C_b and temperature T_b . during this study, the system, constituted by the drop and by surrounding bubble, is considered to be isolated.

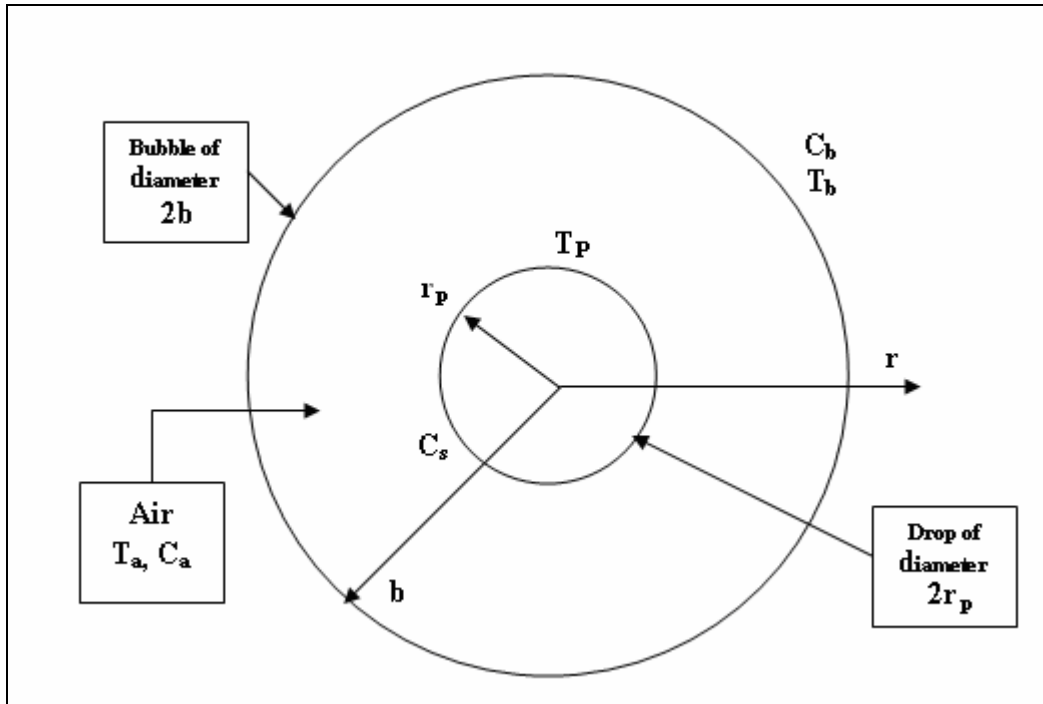


Figure 7.1 Schematic representation of a bubble of water during the evaporation process

7.2 Computational Procedure

Based on mass transfer diffusion equation, the mass transfer from a spherical droplet subjected to a velocity of a drying medium, the Sherwood number correlation as follows:

$$Sh = \frac{k_c D_p}{D_g} = \frac{\text{Convective mass transfer coefficient}}{\text{Diffusive transfer coefficient}} = 2.0 + 0.6 Sc^{1/3} Re^{1/2} \dots \dots \dots (7.1)$$

Where:

The Reynolds's number correlation as follows:

$$Re = \left(\frac{D_p v \rho_a}{\mu_a} \right)^{1/2} = \frac{\text{Inertial forces}}{\text{Viscous forces}} \dots \dots \dots (7.2)$$

The Schmidt number correlation as follows:

$$Sc = \left(\frac{\mu_a}{\rho_a D_g} \right) = \frac{\text{Momentum diffusivity}}{\text{Mass diffusivity}} \dots \dots \dots (7.3)$$

The first step is obtain the Sherwood number, the Reynolds's number and the Schmidt number by evaluating their parameters, the diffusion coefficient (D_g), the density of air (ρ_a), the dynamic viscosity of air (μ_a), water droplet diameter (D_p) and velocity of air and droplet (v).

The diffusion coefficient (D_g), the density of air (ρ_a), and the dynamic viscosity of air (μ_a) all vary according to surrounding temperature.

The dynamic viscosity of air is given by the following empirical relation referred to Ref. [37].

$$\mu_a = (17.1 + 0.067T_a - 0.0004T_a^2) \times 10^{-6} \dots \dots \dots (7.4)$$

Where:

T_a is air temperature in Celsius [$^{\circ}\text{C}$]; viscosity in Pascal x seconds [Pa.s].

Error: $<0.1 \times 10^{-6}$ Pa.s; validity range: 0-54 $^{\circ}\text{C}$.

The diffusion coefficient is given by the following empirical relation referred to Ref. [38].

$$D_g = 21.2 \times 10^{-6} (1 + 0.0071 T_a) \dots\dots\dots(7.5)$$

Where:

T_a is air temperature in Celsius [$^{\circ}\text{C}$]; diffusion coefficient in [m^2/s].

Error: $<0.1 \times 10^{-6}$ m^2/s ; validity range: 0-55 $^{\circ}\text{C}$.

The density of humid air varies according to the air temperature and pressure, and it is given by the following empirical relation referred to Ref. [39].

$$\rho_a = 1.2929 \times \frac{273.15}{T_a + 273.15} \times \frac{B - 0.3783 P_v}{1.013 \times 10^5} \dots\dots\dots(7.6)$$

Where:

Temperature T_a in Celsius [$^{\circ}\text{C}$]; barometric pressure B in [Pa]; partial vapor pressure p_v in [Pa]; ρ_a : density [kg/m^3].

The partial vapor pressure is given by following empirical relation referred to Ref. [40].

$$P_v = \left(\frac{RH}{100}\right) \times P_{sat,d} \dots\dots\dots(7.7)$$

Where:

RH is the relative humidity; $P_{sat,d}$ is the saturated vapor pressure at dry bulb temperature in [Pa].

The saturated vapor pressure at dry bulb temperature is given by following empirical relation referred to Ref. [41].

$$P_{sat,d} = 610.7 \times 10^{7.5T_a / (237.3 + T_a)} \dots\dots\dots(7.8)$$

Where:

Saturated vapor pressure at dry bulb temperature $P_{sat,d}$ in [Pa]; T_a is the dry bulb temperature in Celsius [$^{\circ}C$] validity range roughly 0-80 $^{\circ}C$.

Based on the initial dry bulb temperature of air, initial water droplet temperature and relative humidity, the specific humidity is found from the psychometric chart (figure 7.2) or by equations.

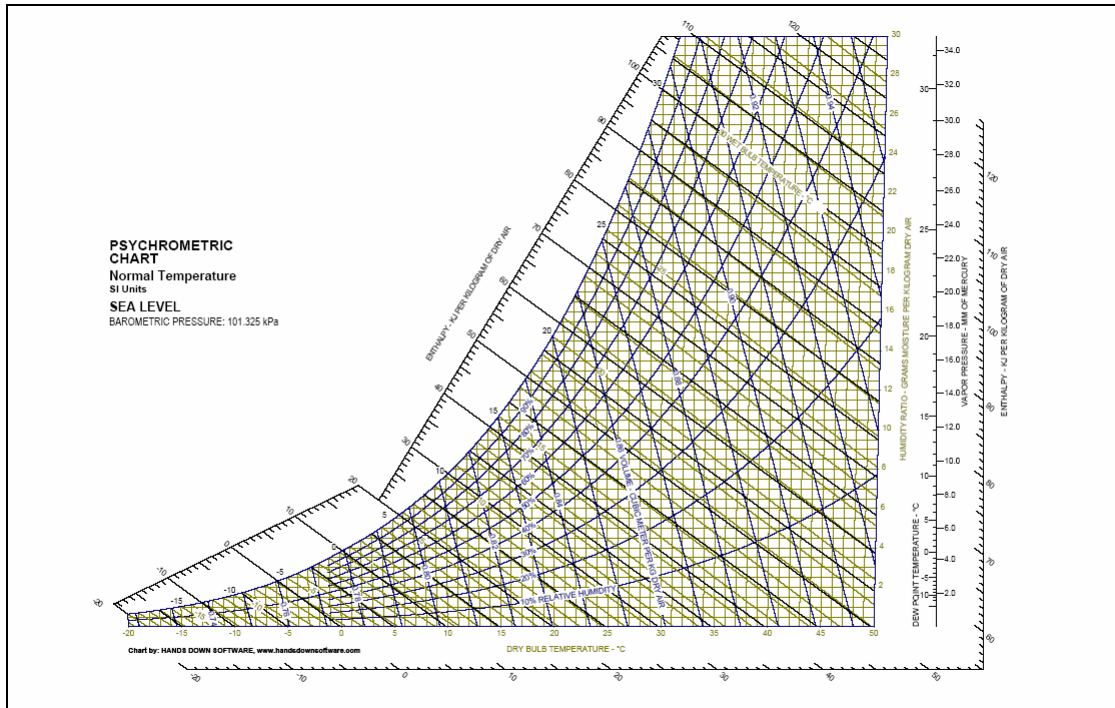


Figure 7.2 Psychrometric chart

Then, the vapor concentration at the droplet surface (C_s) in $[\text{kg}/\text{m}^3]$; vapor concentration in the bulk gas (C_g) in $[\text{kg}/\text{m}^3]$ are defined as:

$$C_s = \frac{P_{sat}(T_p)}{RT_p} \dots\dots\dots(7.9)$$

$$C_g = X_i \frac{B}{RT_a} \dots\dots\dots(7.10)$$

Where:

$P_{sat}(T_p)$ is the saturated pressure at water droplet temperature T_p in [Pa]; T_p is the water droplet temperature in Celsius [$^{\circ}\text{C}$]; R is the perfect gas constant in $[\text{J}/\text{K}\cdot\text{mol}]$; B is the barometric pressure in [Pa]; T_a is the air temperature in Celsius [$^{\circ}\text{C}$];

X_i is the mole fraction, which is defined as follows:

$$X_i = \frac{\text{Number of moles of water vapor}}{\text{Total number of moles}} \dots\dots\dots(7.11)$$

Where:

$$\text{Number of moles of water vapor} = \frac{\text{mass of water vapor}}{\text{molecular weight of } H_2O} \dots\dots\dots(7.12)$$

$$\text{Total number of moles} = (\text{Number of moles of water vapor} + \text{Number of moles of air}) \dots\dots\dots (7.13)$$

$$\text{Number of moles of air} = \frac{\text{mass of air}}{\text{molecular weight of air}} \dots\dots\dots(7.14)$$

Molecular weight of $H_2O = 18 \text{ g / mole}$.

7.2.1 Molecular Mass of Air:

Dry air is a mixture of gases where the molecular weight can be calculated by adding the weight of each component as shown in table 7.1.

Table 7.1 Molecular weight of air

Components in Dry Air	Volume Ratio compared to Dry Air	Molecular Mass (kg/k.mole)	Molecular Mass in Air (g/mole)
Oxygen	0.2095	32.00	6.704
Nitrogen	0.7809	28.02	21.88
Carbon Dioxide	0.0003	44.01	0.013
Hydrogen	0.0000005	2.02	0
Argon	0.00933	39.94	0.373
Neon	0.000018	20.18	0
Helium	0.000005	4.00	0
Krypton	0.000001	83.8	0
Xenon	0.09 10 ⁻⁶	131.29	0
Total Molecular Mass of Air			28.97

Molecular weight of air = 28.97 g / mole.

$$\text{Specific humidity} = \frac{\text{mass kg } H_2O}{1 \text{ kg dry air}} \dots\dots\dots(7.15)$$

Based on mass transfer equation, the mass transfer rate from the water droplet surface to the bulk air is calculated as follows:

$$\frac{dm}{dt} = -4\pi r_p D_g Sh(c_s - c_g) \cdot \exp\left[\frac{-3r_p D_g t}{(b-r_p)^3}\right] \dots\dots\dots(7.16)$$

Where:

$\frac{dm}{dt}$ is the evaporation rate in [kg/s] referred to ref. [42]; the diffusion coefficient D_g in [m²/s]; r_p is the radius of water droplet in [m]; (C_s) is the vapor concentration at the droplet surface in [kg/m³]; (C_g) is the vapor concentration in the bulk gas in [kg/m³]; b is bubble radius in [m]; t is the time in [s].

Based on energy balance, the droplet temperature can be calculated using equation (6.17).

$$m_e C_{pe} \frac{dT_p}{dt} = 2\pi D_p \lambda_a \left(\frac{Nu}{2}\right) (T_a - T_p) + L_{vap} \cdot \frac{dm}{dt} \dots\dots\dots(7.17)$$

Where:

$\frac{dT_p}{dt}$ is the droplet temperature change with time; the diameter of water droplet D_p in [m]; T_a is the air temperature in [Celsius]; T_p is the droplet temperature in [Celsius]; m_e is the mass of water in [kg]; C_{pe} is the specific heat of water [J/kg K]; $\frac{dm}{dt}$ is the evaporation rate in [kg/s]; λ_a is the thermal conductivity of air [W/m.k]; L_{vap} is the latent heat of water in [J/kg] and it is given by the following empirical relation referred to ref. [43].

$$L_{\text{vap}} = 2.5 \times 10^6 - 2350 T_a \dots\dots\dots(7.18)$$

The validity range of equation (6.18) is roughly 0-100°C of the air temperature.

Nu is the Nusselt number and it is given by the correlation as follows [44]:

$$Nu = \frac{h_c D_P}{\lambda_a} = \frac{\text{Convective heat transfer coefficient}}{\text{Conductive heat transfer coefficient}} = 2.0 + 0.6 Re^{1/2} Pr^{1/3} \dots\dots\dots(7.19)$$

Where:

Re represents the Reynolds's number; and Pr represents the Prandtl number and it is given by the correlation as follows:

$$Pr = \left(\frac{c_p \mu_a}{\lambda_a} \right) = \frac{\text{Momentum diffusivity}}{\text{Thermal diffusivity}} \dots\dots\dots(7.20)$$

The air temperature can be calculated using equation (7.21).

$$m_a C_{pa} \frac{dT_a}{dt} = -2\pi D_p \lambda_a \left(\frac{Nu}{2} \right) (T_a - T_p) \dots\dots\dots(7.21)$$

Where:

$\frac{dT_a}{dt}$ is the air temperature change with time; the diameter of water droplet D_p in [m]; T_a is the air temperature in [Celsius]; T_p is the droplet temperature in [Celsius]; m_a is the mass of air in [kg]; C_{pa} is the specific heat of air [J/kg K]; λ_a is the thermal conductivity of air [W/m.k].

To investigate the dynamic motion of the evaporating droplet while flying and to determine where it settles, the equations of motion are as follows:

- In the x-direction:

$$\ddot{X} = \frac{Drag}{mass} \dots\dots\dots(7.22)$$

- In the y-direction:

$$\ddot{Y} = \frac{Drag}{mass} - g \dots\dots\dots(7.23)$$

Where:

\ddot{X} is the acceleration of the droplet in the x-direction; \ddot{Y} is the acceleration of the droplet in the y-direction; g represents the gravity; and the drag force is given by the following relation according to ref. [45].

$$Drag = 6\pi r_p \mu_a V \dots\dots\dots(7.24)$$

Where:

r_p is the radius of water droplet in [m]; μ_a is the dynamic viscosity of air in [Pa.s]; and V represents the droplet velocity in [m/s].

The previous two equations are integrated by the fourth Runge-Kutta method in the code including all relations for heat-and-mass transfer, the temperature-vapor concentration relationships and the momentum equation to get the positions of droplet (X, Y) along the x-direction and y-direction respectively.

7.2.2 Calculation Sequence:

The determination of the history of the temperature and diameter of the evaporating droplet and air temperature is effected using equations (7.16), (7.17) and (7.21).

Initially, the droplet size and temperature and the external conditions, together with all the relevant thermal properties are specified. Also included in the program are the correlations for heat-and-mass transfer, the temperature-vapor concentrations relationships, and the momentum equation as derived above. The sequence in the calculation is as follows.

After selecting a suitable time step, the change in mass of the droplet is determined using equation (7.16). The change in the droplet temperature is then evaluated using equation (7.17). After that, the change in the air temperature is then evaluated using equation (7.21). The velocity after the time step is calculated with the momentum equations (7.22) and (7.23).

At the end of the time interval, the new diameter and surface vapor concentration, as well as the heat-and-mass transfer parameters and properties are the used in the following time step, and the whole calculation repeated until the droplet diameter reaches a specified lower limit or the droplet hits the ground. The output from the program, which was written in MATLAB, may include the histories of the temperature, diameter, velocity and distance traveled by the droplet.

In the present work, environmental conditions appropriate to the experiments were chosen as shown in table 7.2.

Table 7.2 Fixed parameters values in the computational solution

Factor	Value
Relative humidity	50 %
Air temperature	40 °C
Droplet temperature	25 °C
Water droplet diameter	200 x 10 ⁻⁶ m
Injected droplet velocity from nozzle	28 m/s
Pressure	101325 Pa
Pump operating pressure	50 bar

7.2.3 Computational Procedure Flow Chart:

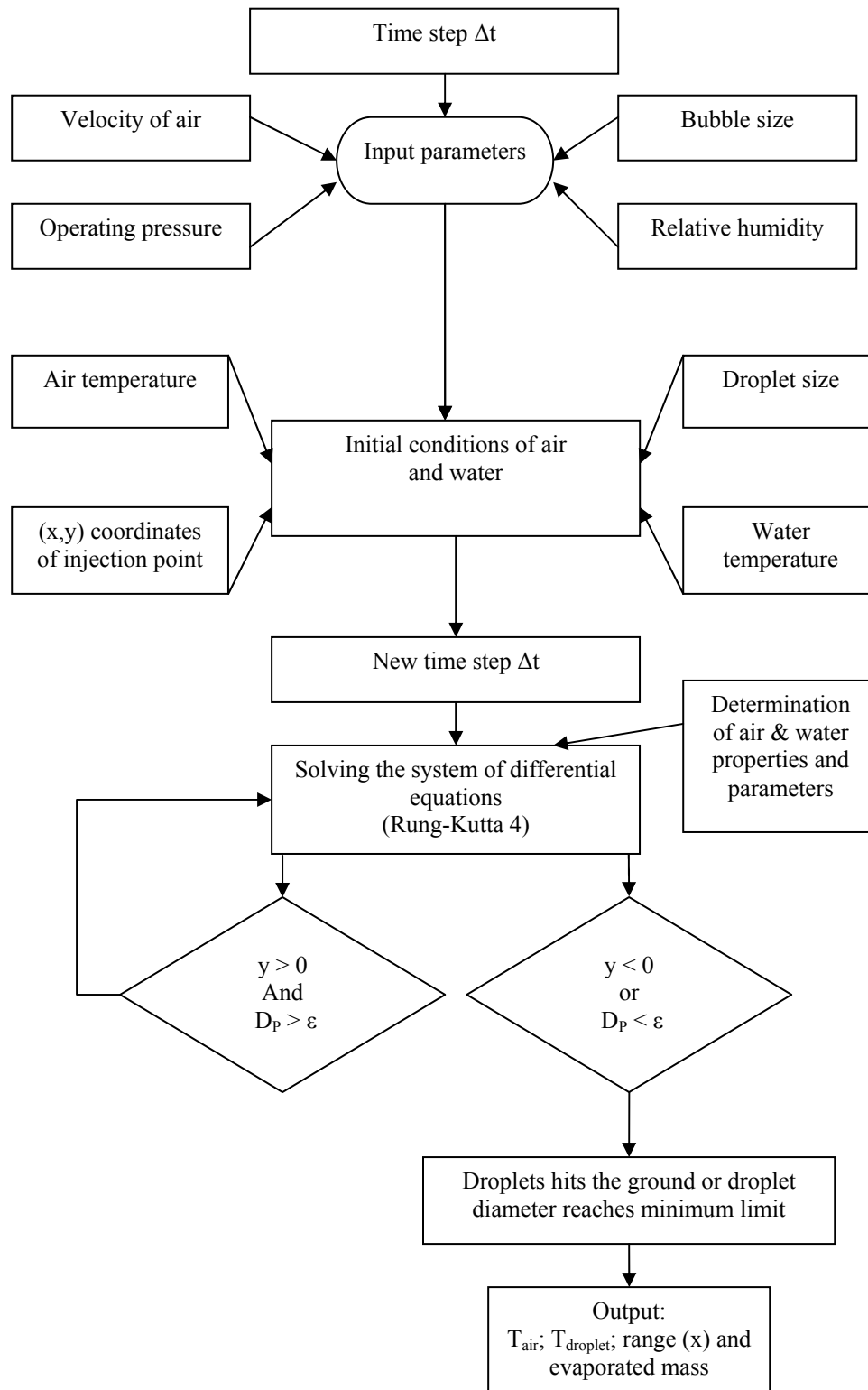


Figure 7.3 Computational Procedure Flow Chart

7.3 20-inch Fan

In the experimental measurements of 20-inch fan, it was observed that the fan maximum range of temperature occurs at a height level of the 4th diameter ($h = 4D_s$). The fan airspeed is about 4.74 m/s and the other experimental conditions are kept the same as shown in table 7.2. To simulate it in the computational solution, the program is run for such height ($h = 4D_s$, $h = 2$ m) and the droplet velocity is equal to the Injected droplet velocity from nozzle plus the fan airspeed ($V = 28 + 4.74 = 32.74$ m/s).

Figure 7.4 shows the water droplet evaporation versus time for this fan. The figure demonstrates the behavior of the evaporation process and it is observed that the droplet hits the ground before it evaporates completely.

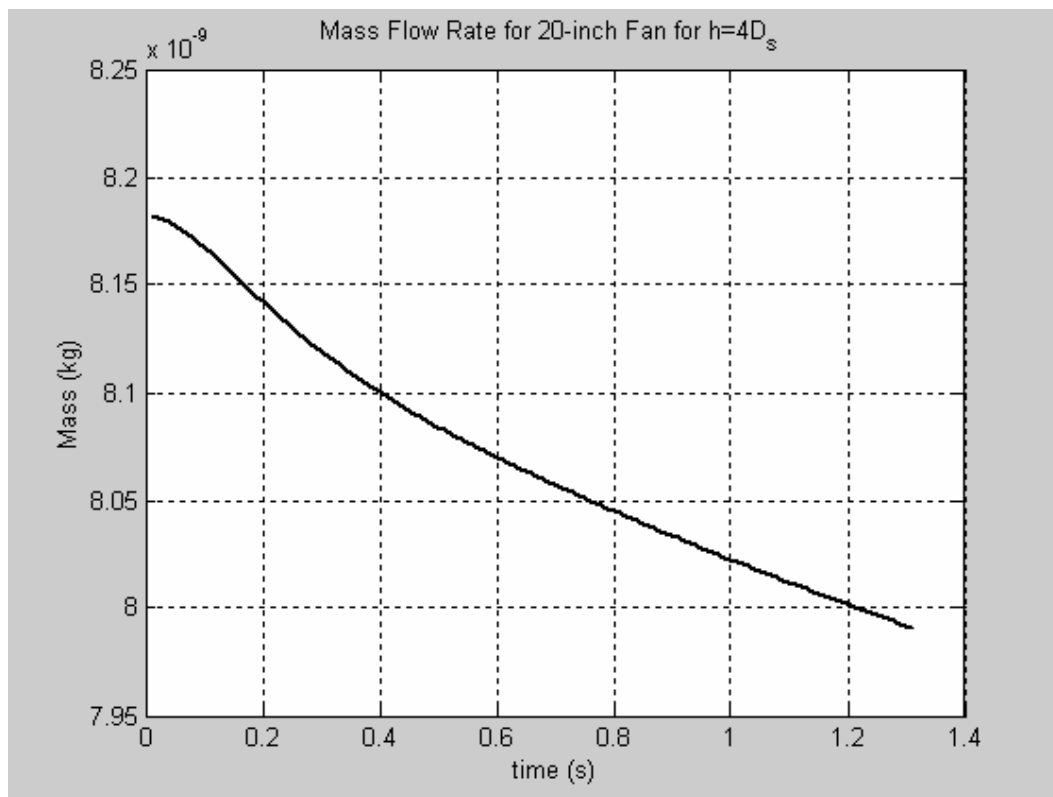


Figure 7.4 The rate of evaporation of droplet mass for 20-inch fan (D_s) for 4-diameter in height ($h = 4D_s$)

Figure 7.5 shows the droplet temperature versus time for this fan. The figure demonstrates the behavior of the droplet temperature which starts from the initial value ($T_p = 25\text{ }^{\circ}\text{C}$) and keeps dropping to final value of terminal droplet temperature of about $32.4\text{ }^{\circ}\text{C}$, which is very close to thermodynamic wet bulb temperature ($T_{\text{wet}} = 31.5$). This temperature is achieved rapidly, indicating that the energy storage within the droplet is more effective in the early stages of evaporation process.

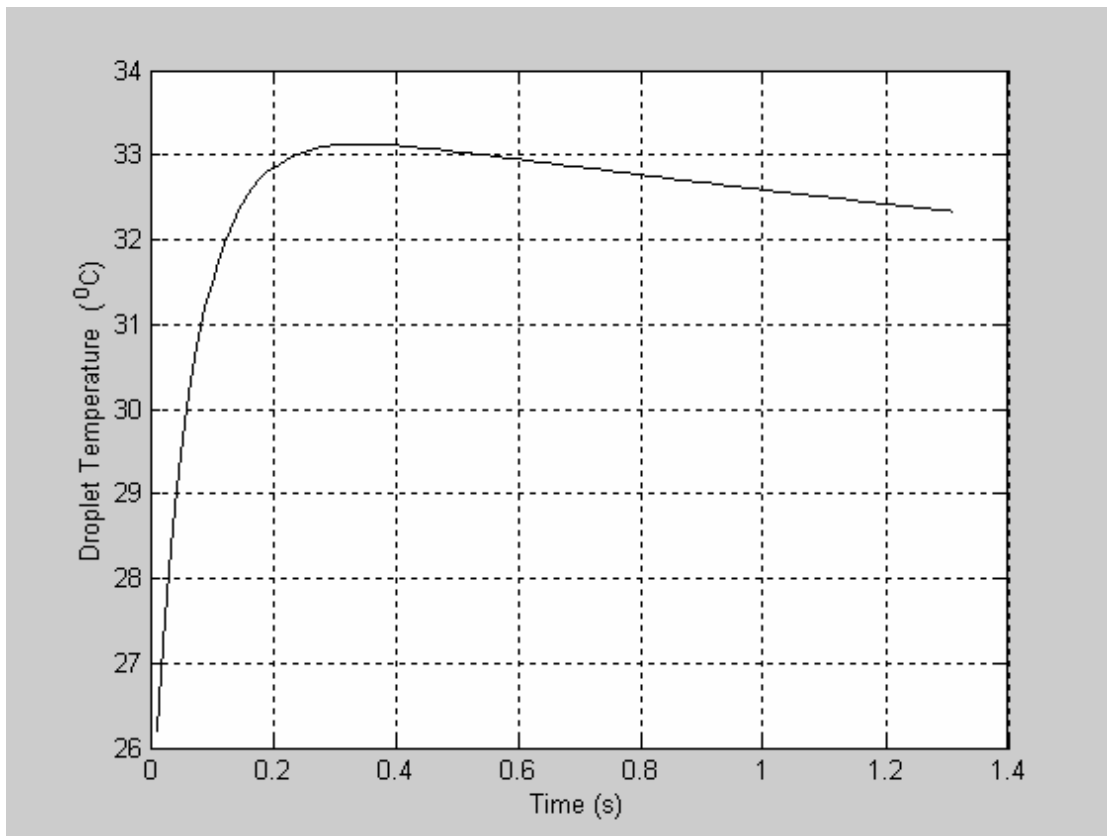


Figure 7.5 Droplet temperature versus time for 20-inch fan (D_s) for 4-diameter in height ($h = 4D_s$)

Figure 7.6 shows the air temperature versus time for this fan. The figure demonstrates the behavior of the air temperature which starts from the initial value ($T_a = 40\text{ }^{\circ}\text{C}$) and keeps dropping to final value of about $34.4\text{ }^{\circ}\text{C}$. The air temperature would drop more and more to get closer to the wet bulb temperature ($T_{\text{wet}} = 31.5$) if the droplet evaporated completely before it hits the ground, which didn't happen in this case as discussed in figure 7.4.

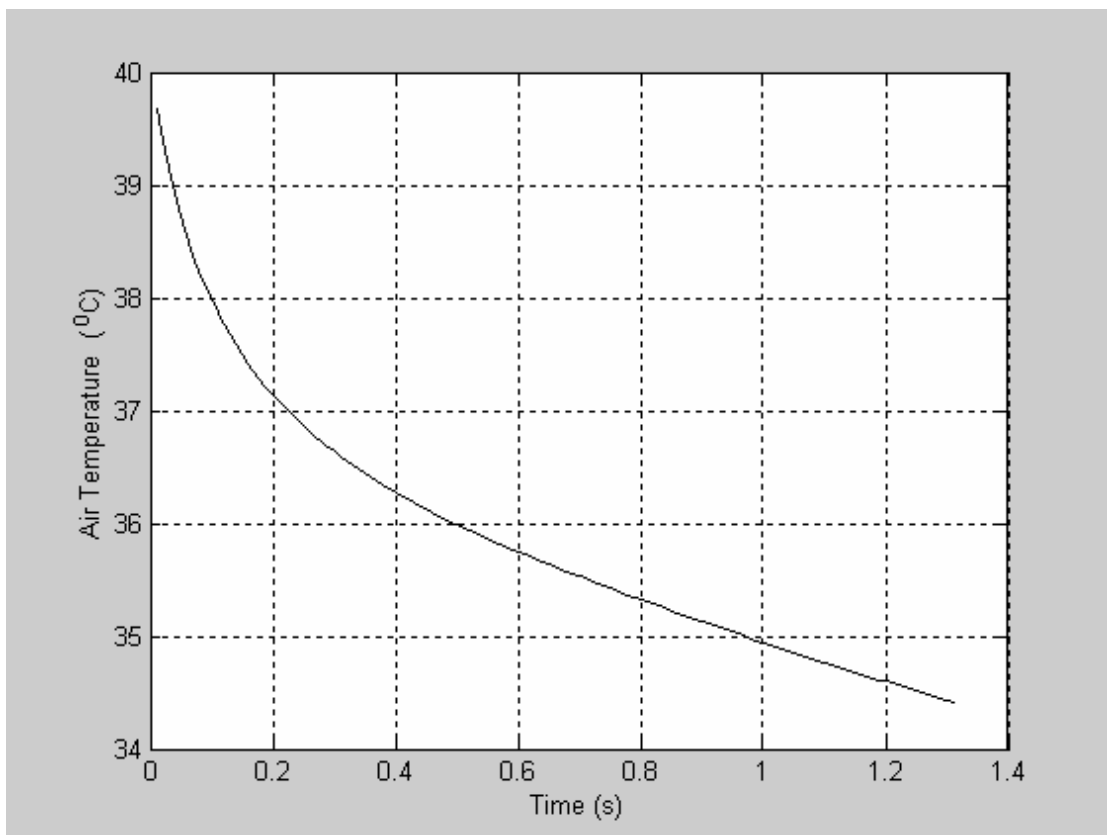


Figure 7.6 Air temperature versus time for 20-inch fan (D_S) for 4-diameter in height ($h = 4D_S$)

Figure 7.7 shows the droplet injection height (same as fan height) versus the horizontal range for this fan. The figure indicates the maximum horizontal range of the droplet of about 5.81 m, which is equivalent to about 11.6 D_S as demonstrated in figure 7.8.

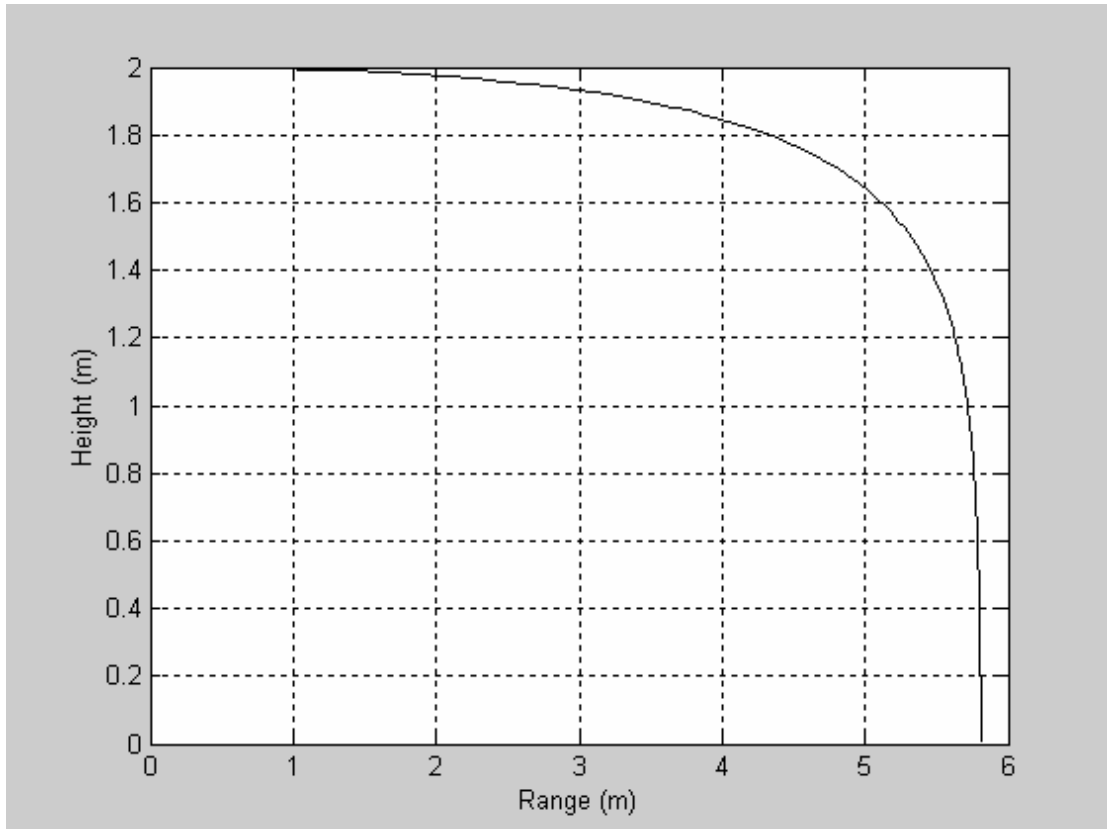


Figure 7.7 Droplet injection height versus the horizontal range for 20-inch fan (D_S) for 4-diameter in height ($h = 4D_S$)

Figure 7.8 shows the droplet injection height in diameter (same as fan height) versus the horizontal range in diameter for this fan. The figure indicates the maximum horizontal range of the droplet of about $11.6 D_s$.

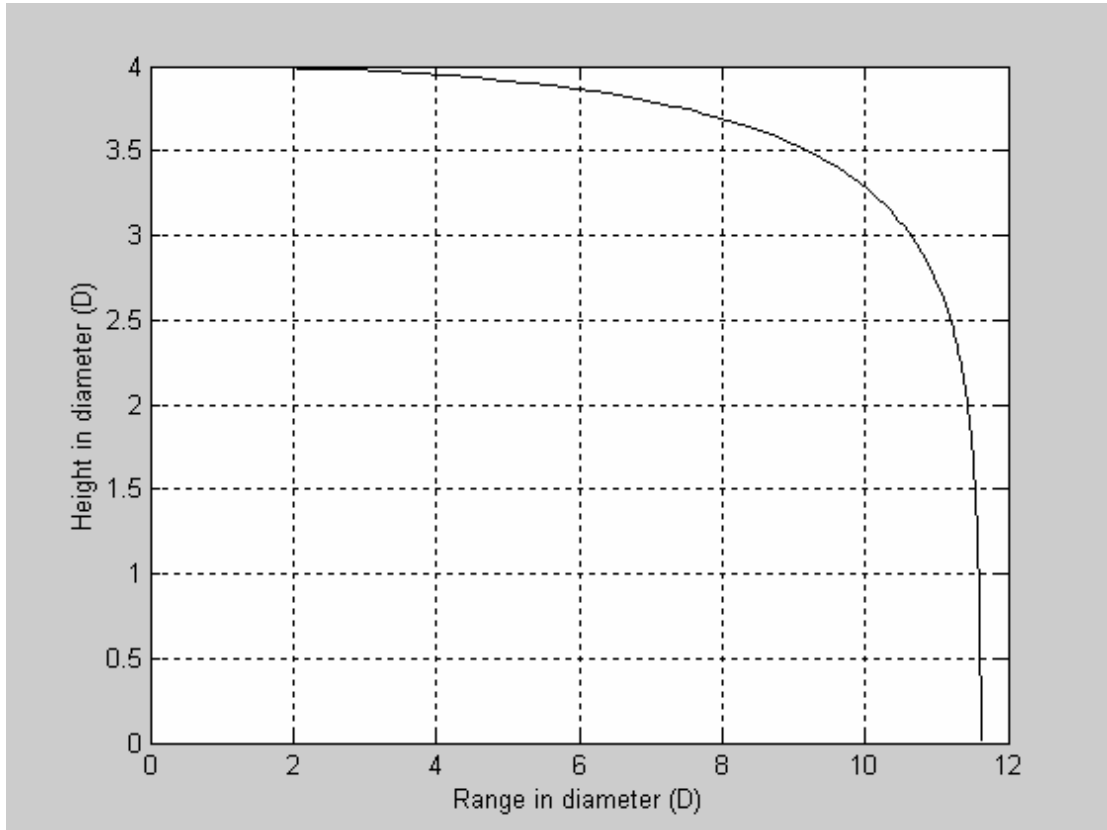


Figure 7.8 Droplet injection height in diameter versus the horizontal range in diameter for 20-inch fan (D_s) for 4-diameter in height ($h = 4D_s$)

Figure 7.9 shows the droplet temperature and air temperature versus the horizontal range for this fan. The figure indicates the history of air temperature along the range, and it shows the minimum air temperature occurs at the distance of 5.81 m, where the droplets hits the ground of about of 34.4 °C. In addition, it demonstrates the history of droplet temperature along the horizontal range, and it shows the terminal droplet temperature of about 32.4 °C.

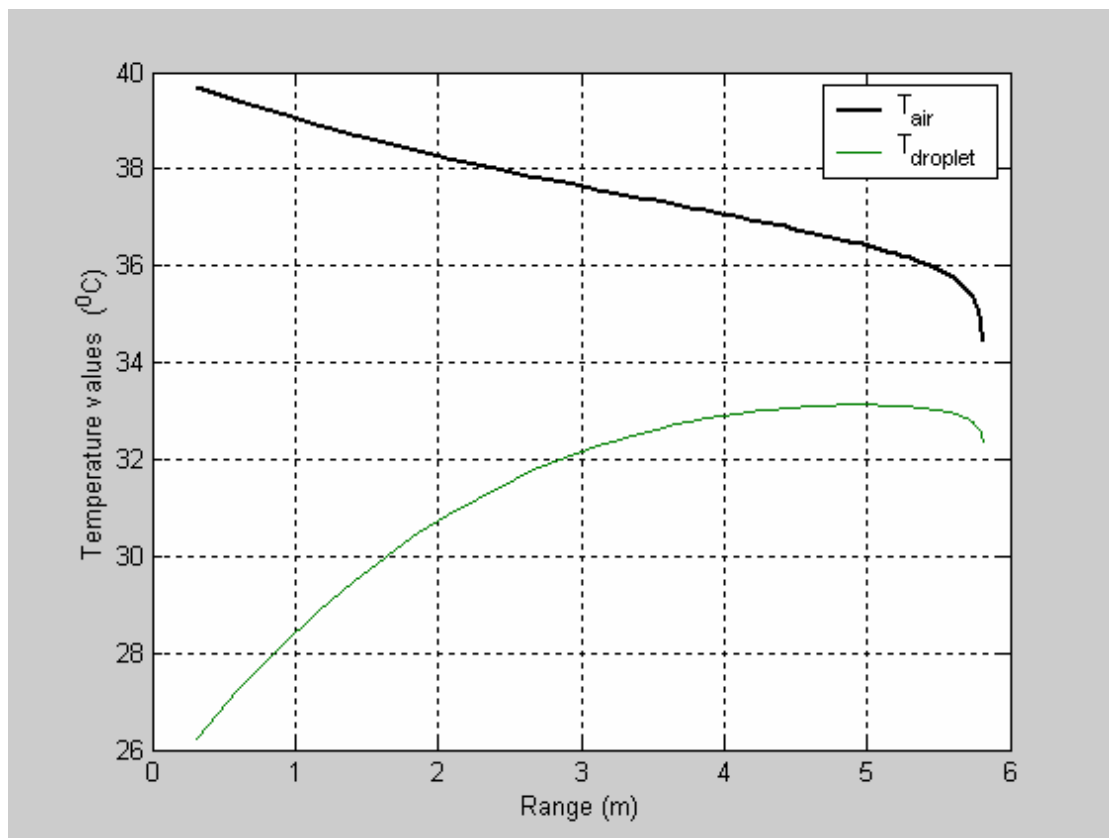


Figure 7.9 Droplet and air temperatures versus the horizontal range for 20-inch fan (D_s) for 4-diameter in height ($h = 4D_s$)

Figure 7.10 expresses the same observations as figure 7.9, but in terms of diameter for horizontal range. Such that, the figure indicates the history of air temperature along the range in diameter, and it shows the minimum air temperature occurs at the distance of $11.6 D_s$, where the droplets hits the ground of about of $34.4 ^\circ\text{C}$. In addition, it demonstrates the history of droplet temperature along the horizontal range, and it shows the terminal droplet temperature of about $32.4 ^\circ\text{C}$.

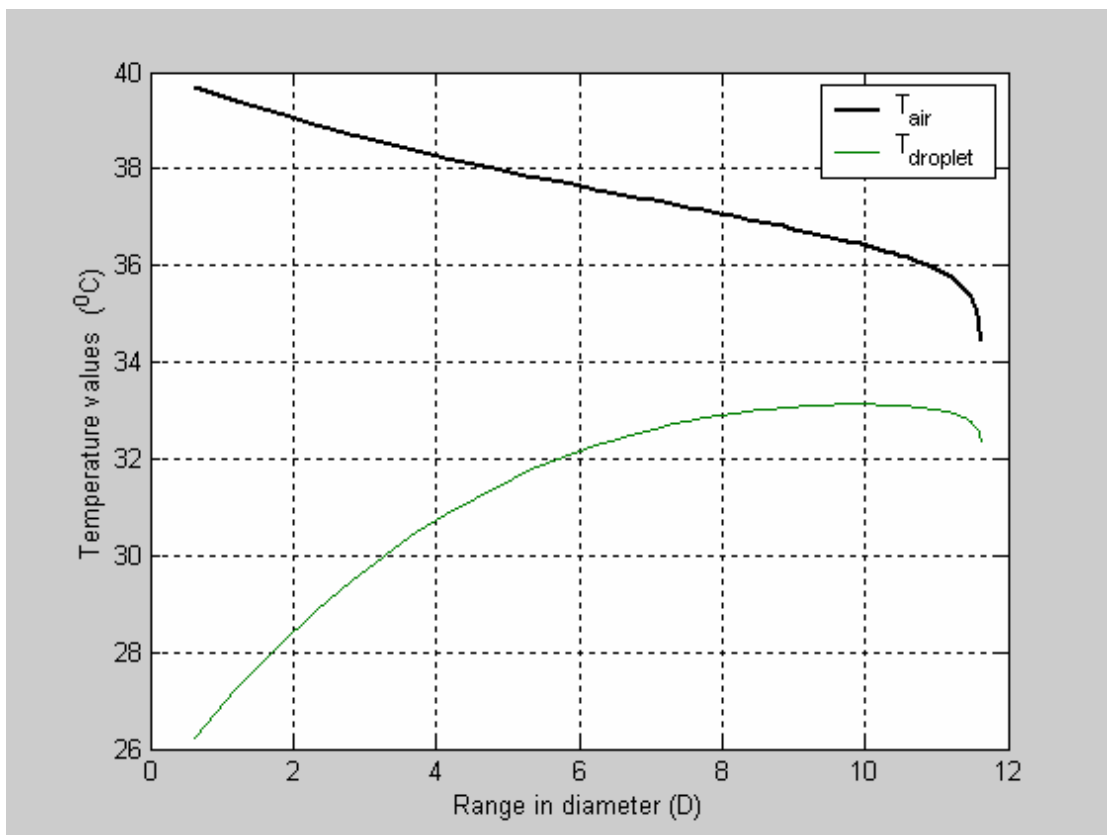


Figure 7.10 Droplet and air temperatures versus the horizontal range in diameter for 20-inch fan (D_s) for 4-diameter in height ($h = 4D_s$)

7.3.1 Angle Effect of 20-inch Fan (computational)

The experimental angle effect case of 20-inch fan is simulated here computationally. In this configuration, the fan is angled for two positions ($\theta_1 = 26.56^\circ$, $\theta_2 = 45^\circ$) as shown in figure 7.11.

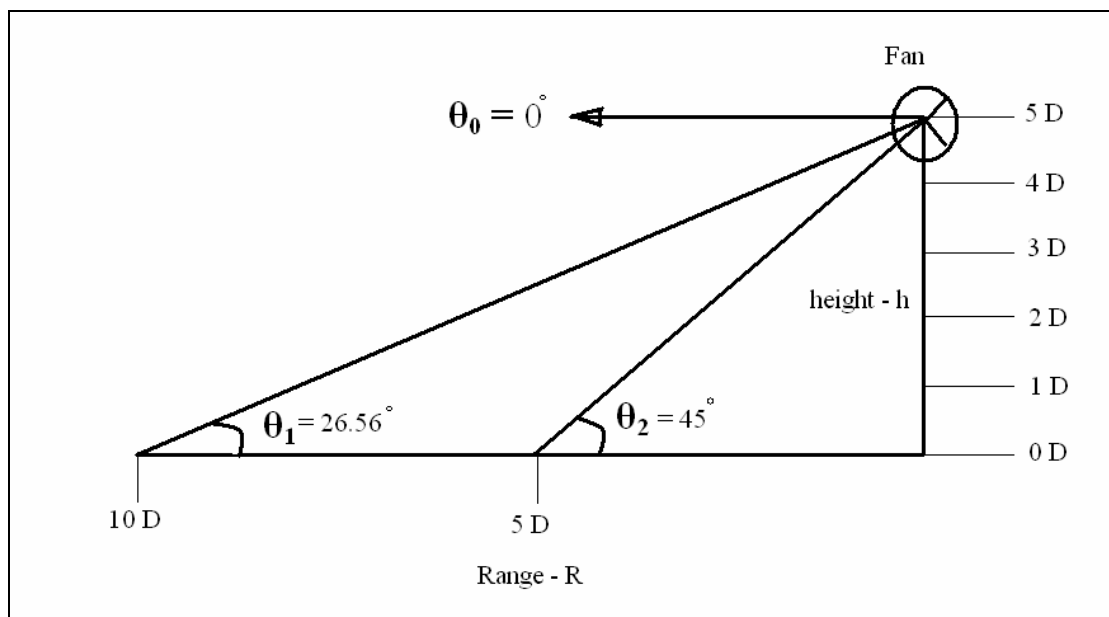


Figure 7.11 Configuration of angle effect case study (computational)

In this case, the program is run for the same condition as the normal case except the velocity which is dropped by a value of $(\cos \theta)$ due the fan deflection, such that $V_1 = 32.74 \cos (\theta_1)$ & $V_2 = 32.74 \cos (\theta_2)$.

7.3.1.1 $\theta_1 = 26.56^\circ$

Figure 7.12 indicates the history of air temperature and droplet temperature versus time for the first angle ($\theta_1 = 26.56^\circ$). It demonstrates the behavior of the air temperature which starts from the initial value ($T_a = 40^\circ\text{C}$) and keeps dropping to final value of about 34.4°C , the same as in the default case ($\theta_0 = 0^\circ$). The figure also demonstrates the behavior of the droplet temperature which starts from the initial value ($T_p = 25^\circ\text{C}$) and keeps dropping to final value of terminal droplet temperature of about 32.4°C , which is very close to thermodynamic wet bulb temperature ($T_{\text{wet}} = 31.5$), the same as in the default case ($\theta_0 = 0^\circ$) too.

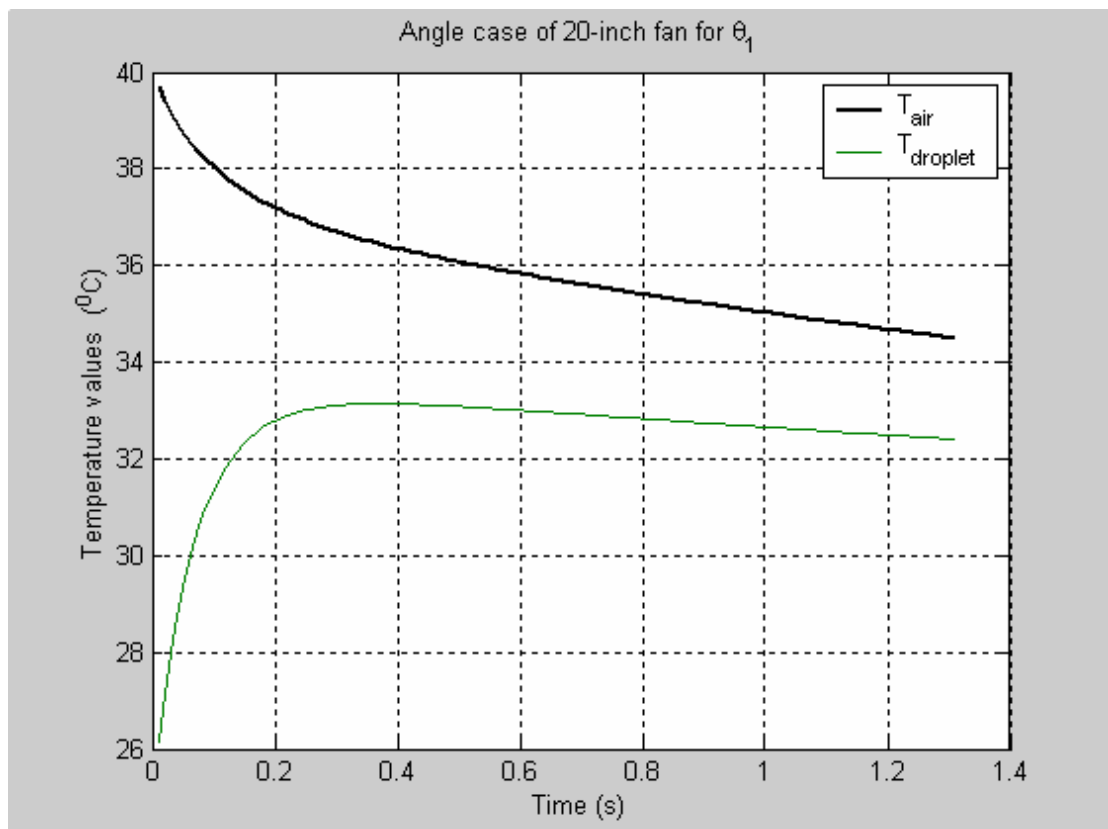


Figure 7.12 Droplet and air temperatures versus time of angle case ($\theta_1 = 26.56^\circ$) for 20-inch fan (D_S)

Figure 7.13 shows the maximum horizontal range of the droplet of about 5.1 m for the first angle ($\theta_1 = 26.56^\circ$), which is equivalent to about 10.4 D_s as demonstrated in figure 7.14.

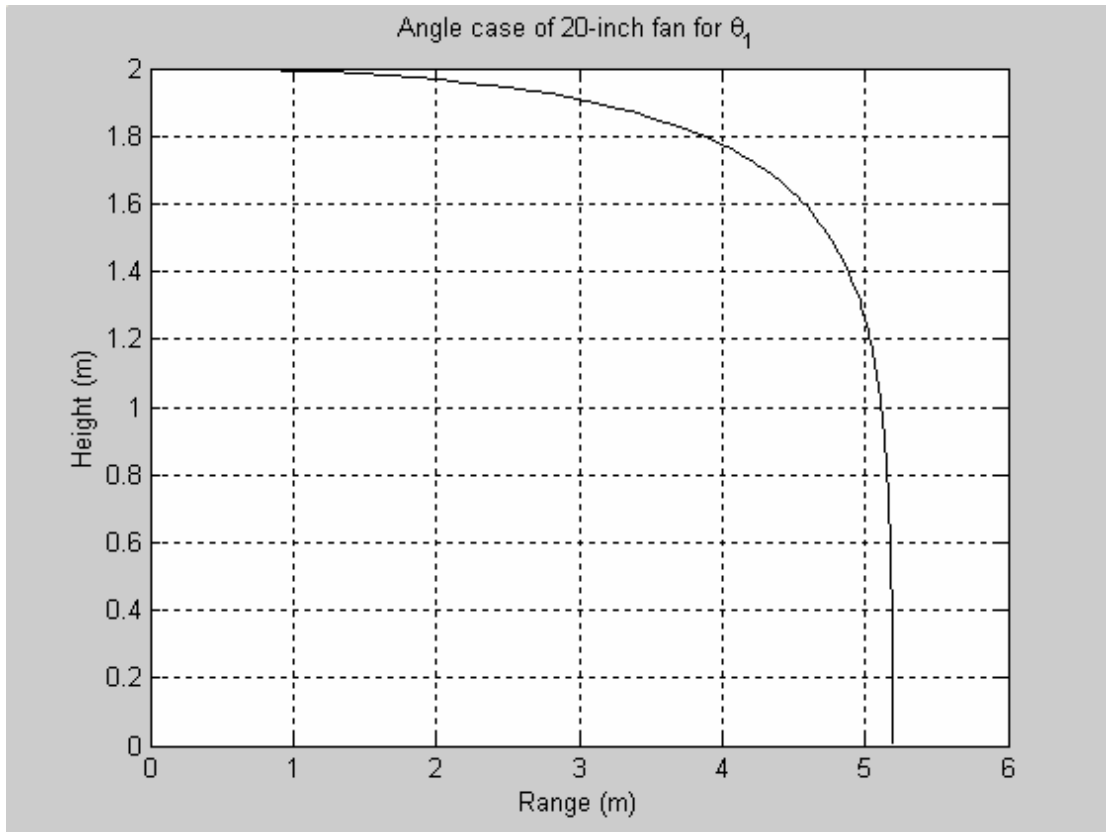


Figure 7.13 Droplet injection height versus the horizontal range of angle case ($\theta_1 = 26.56^\circ$) for 20-inch fan (D_s)

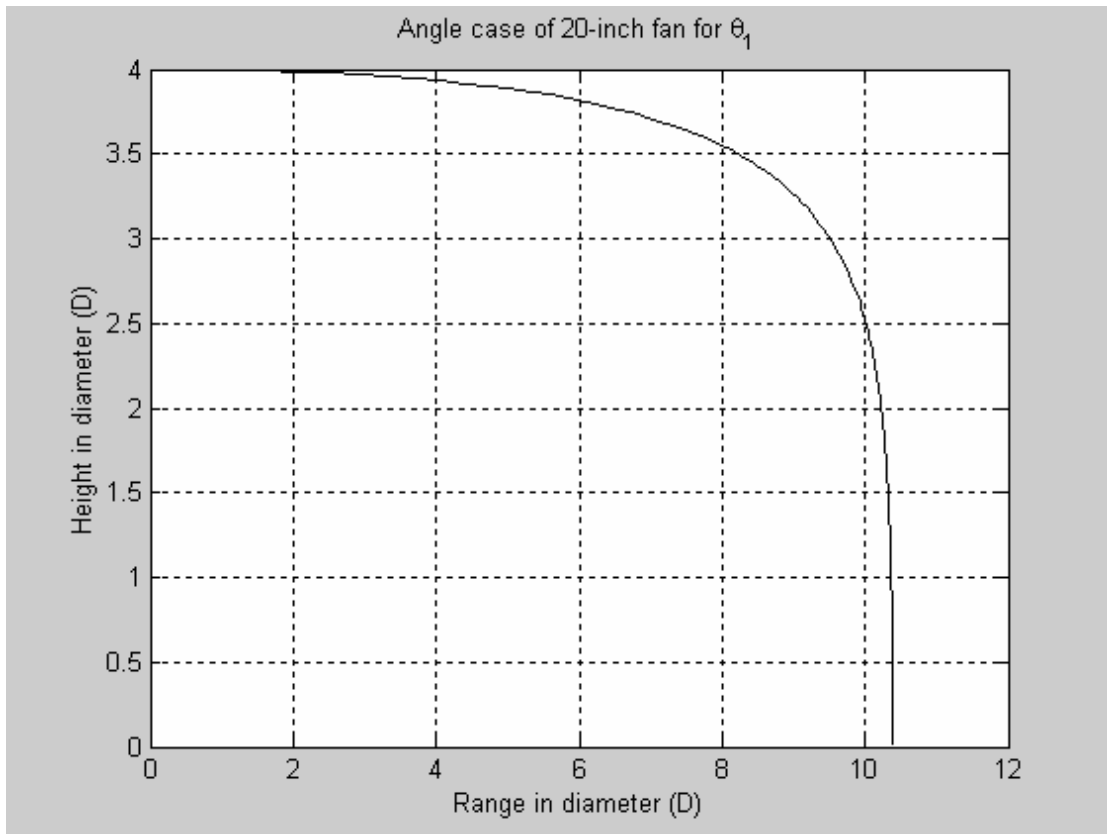


Figure 7.14 Droplet injection height in diameter versus the horizontal range in diameter of angle case ($\theta_1 = 26.56^\circ$) for 20-inch fan (D_s)

Figure 7.15 shows the droplet temperature and air temperature versus the horizontal range for the first angle ($\theta_1 = 26.56^\circ$). The figure indicates the history of air temperature along the range, and it shows the minimum air temperature occurs at the distance of 5.1 m, where the droplets hits the ground of about of 34.4°C . In addition, it demonstrates the history of droplet temperature along the horizontal range, and it shows the terminal droplet temperature of about 32.4°C .

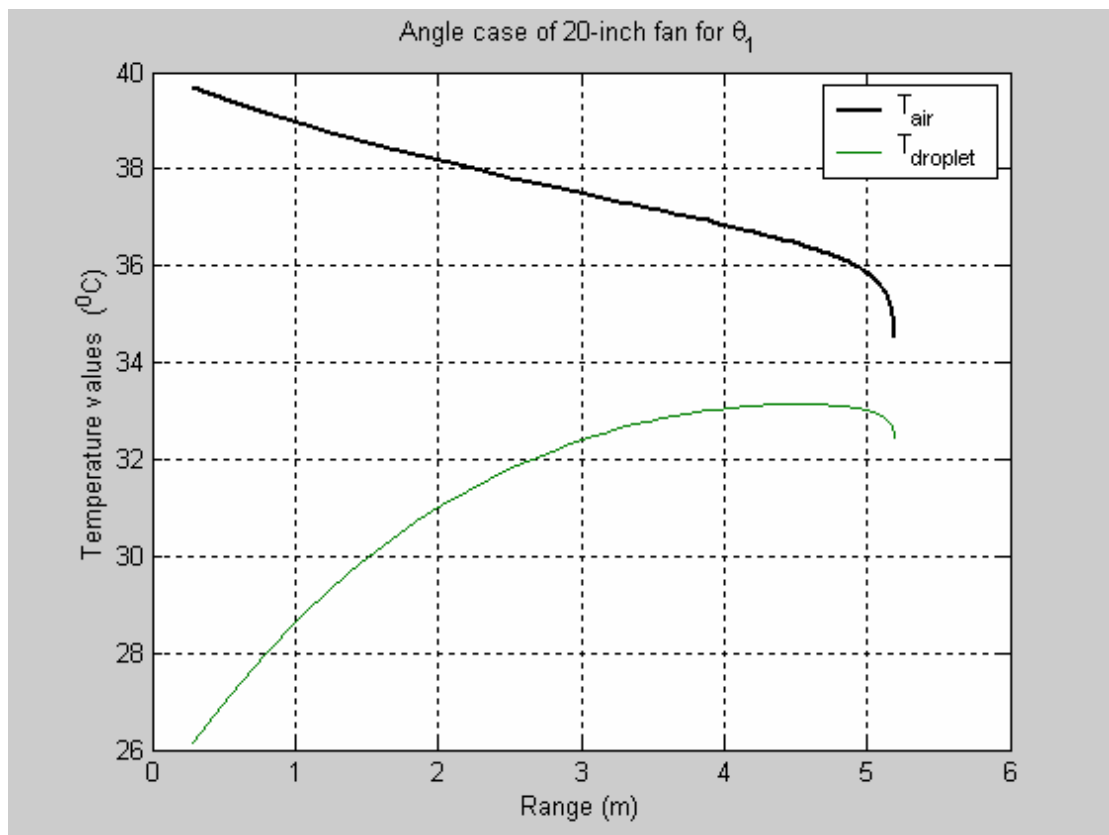


Figure 7.15 Droplet and air temperatures versus the horizontal range of angle case ($\theta_1 = 26.56^\circ$) for 20-inch fan (D_s)

Figure 7.16 expresses the same observations as figure 7.15, but in terms of diameter for horizontal range for the first angle ($\theta_1 = 26.56^\circ$). Such that, the figure indicates the history of air temperature along the range in diameter, and it shows the minimum air temperature occurs at the distance of $10.4 D_S$, where the droplets hits the ground of about of 34.4°C . In addition, it demonstrates the history of droplet temperature along the horizontal range, and it shows the terminal droplet temperature of about 32.4°C .

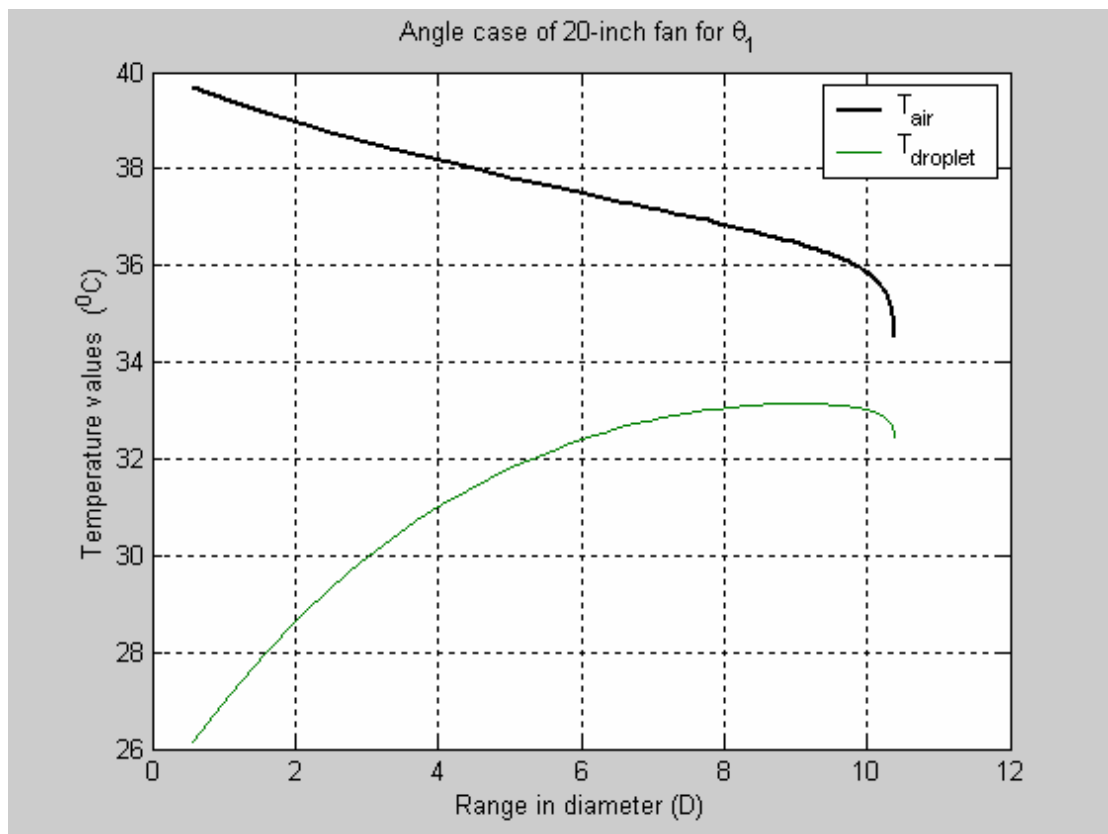


Figure 7.16 Droplet and air temperatures versus the horizontal range in diameter of angle case ($\theta_1 = 26.56^\circ$) for 20-inch fan (D_S)

7.3.1.2 $\theta_2 = 45^\circ$

Figure 7.17 indicates the history of air temperature and droplet temperature versus time for the second angle ($\theta_2 = 45^\circ$). It demonstrates the behavior of the air temperature which starts from the initial value ($T_a = 40^\circ\text{C}$) and keeps dropping to final value of about 34.4°C , the same as in the default case ($\theta_0 = 0^\circ$). The figure also demonstrates the behavior of the droplet temperature which starts from the initial value ($T_p = 25^\circ\text{C}$) and keeps dropping to final value of terminal droplet temperature of about 32.4°C , which is very close to thermodynamic wet bulb temperature ($T_{\text{wet}} = 31.5$), the same as in the default case ($\theta_0 = 0^\circ$) too.

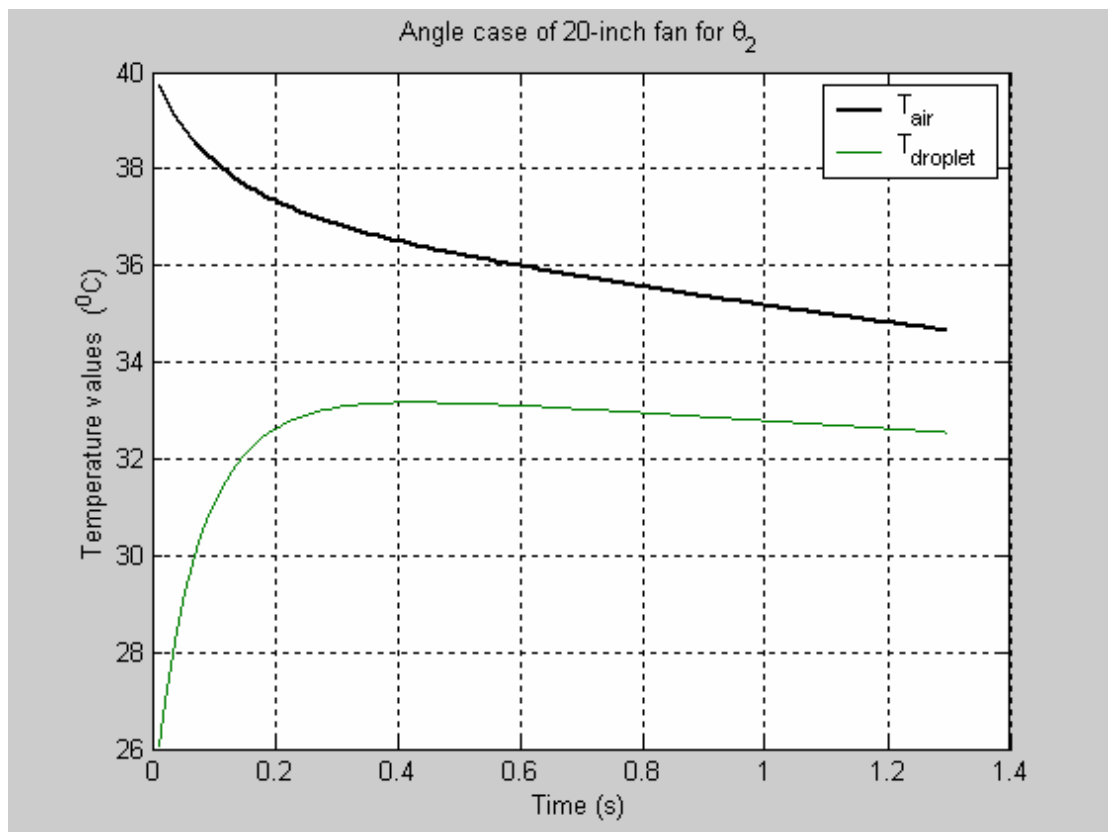


Figure 7.17 Droplet and air temperatures versus time of angle case ($\theta_2 = 45^\circ$) for 20-inch fan (D_S)

Figure 7.18 shows the maximum horizontal range of the droplet of about 4.1 m for the second angle ($\theta_2 = 45^\circ$), which is equivalent to about 8.2 D_s as demonstrated in figure 7.19.

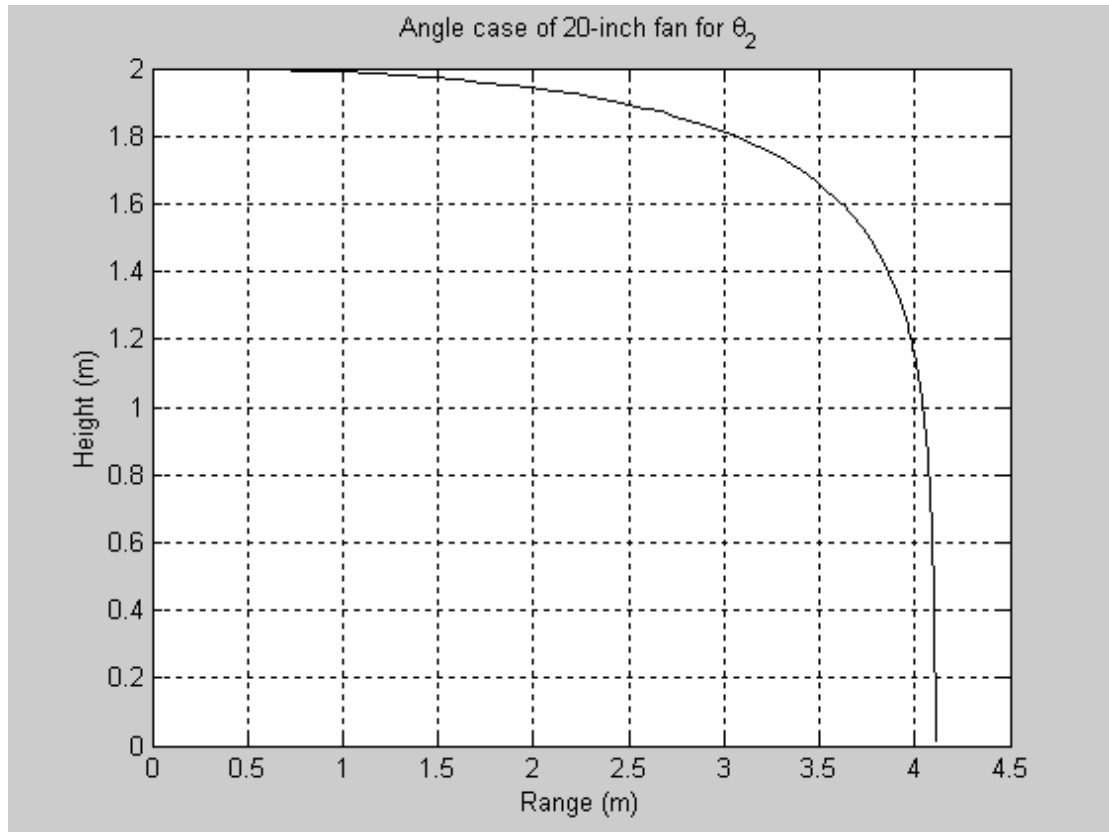


Figure 7.18 Droplet injection height versus the horizontal range of angle case ($\theta_2 = 45^\circ$) for 20-inch fan (D_s)

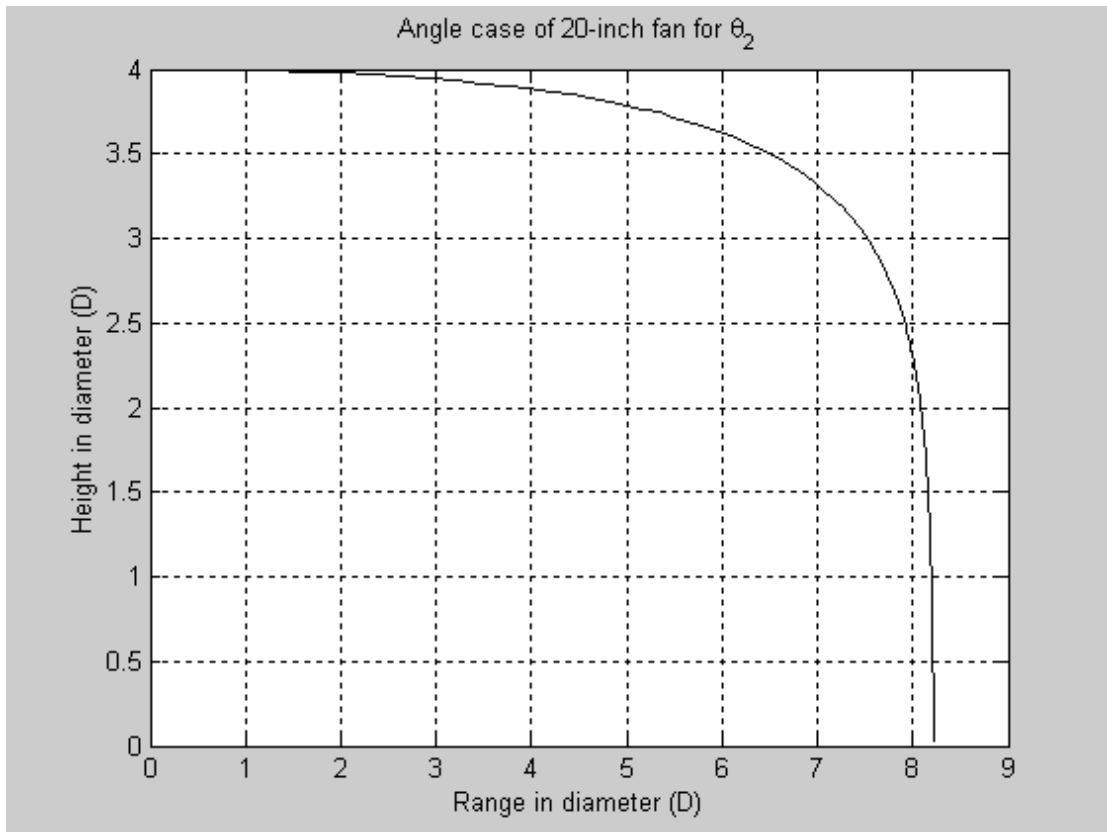


Figure 7.19 Droplet injection height in diameter versus the horizontal range in diameter of angle case ($\theta_2 = 45^\circ$) for 20-inch fan (D_S)

Figure 7.20 shows the droplet temperature and air temperature versus the horizontal range for the second angle ($\theta_2 = 45^\circ$). The figure indicates the history of air temperature along the range, and it shows the minimum air temperature occurs at the distance of 4.1 m, where the droplets hit the ground of about 34.4°C . In addition, it demonstrates the history of droplet temperature along the horizontal range, and it shows the terminal droplet temperature of about 32.4°C .

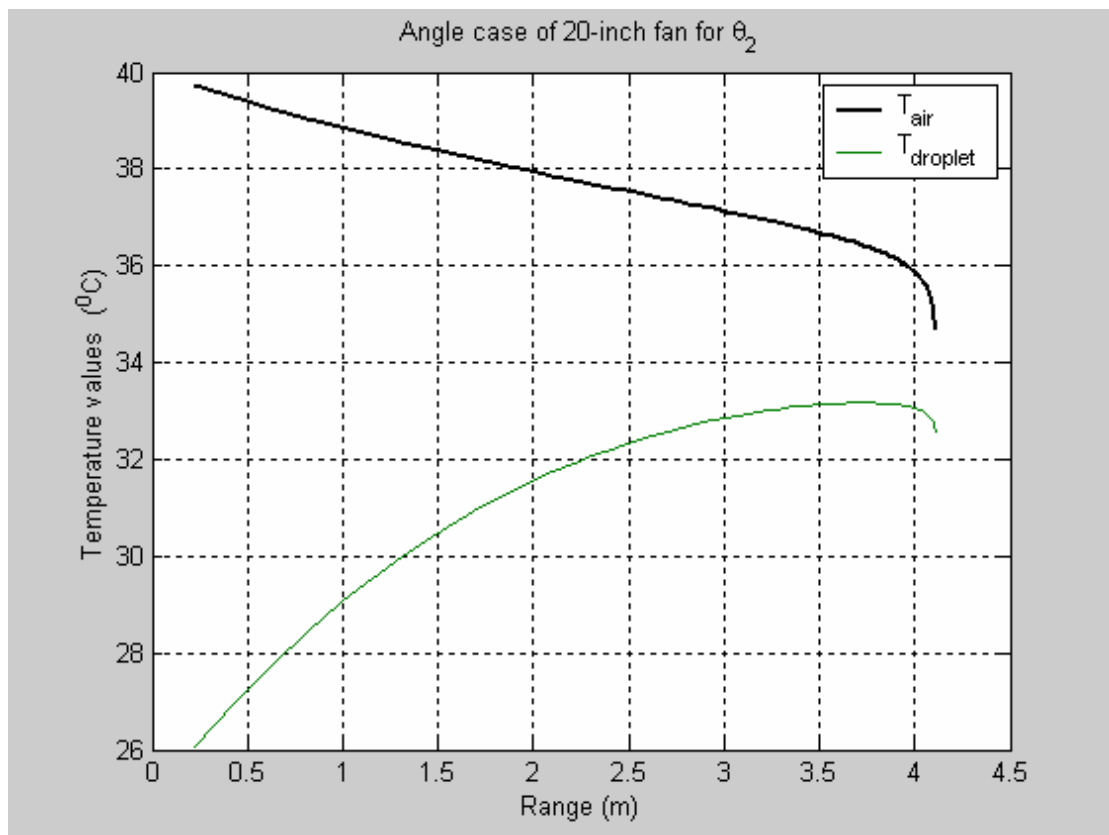


Figure 7.20 Droplet and air temperatures versus the horizontal range of angle case ($\theta_2 = 45^\circ$) for 20-inch fan (D_s)

Figure 7.21 expresses the same observations as figure 7.20, but in terms of diameter for horizontal range for the second angle ($\theta_2 = 45^\circ$). Such that, the figure indicates the history of air temperature along the range in diameter, and it shows the minimum air temperature occurs at the distance of $8.2 D_s$, where the droplets hits the ground of about of 34.4°C . In addition, it demonstrates the history of droplet temperature along the horizontal range, and it shows the terminal droplet temperature of about 32.4°C .

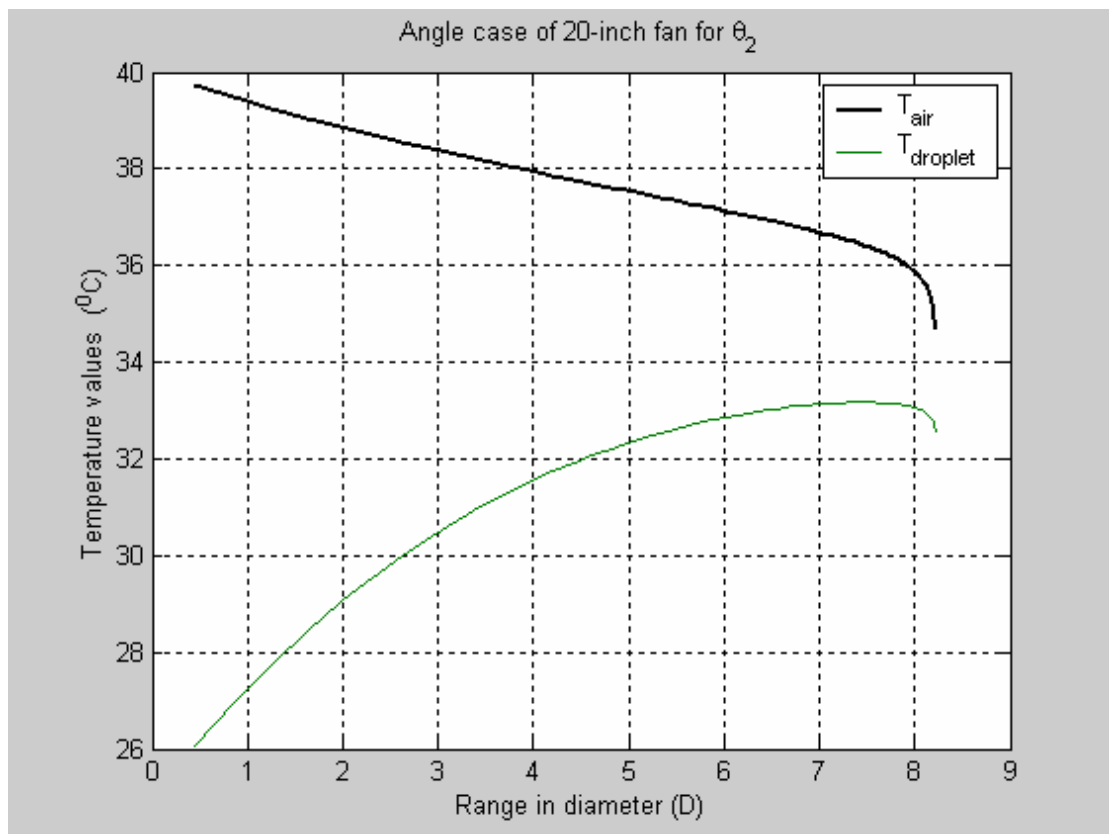


Figure 7.21 Droplet and air temperatures versus the horizontal range in diameter of angle case ($\theta_2 = 45^\circ$) for 20-inch fan (D_s)

Figure 7.22 shows the maximum horizontal range of the droplet in the angle case for different angles of the 20-inch fan angle of about 5.81 m for the default zero angle ($\theta_0 = 0^\circ$), 5.2 m for the first angle ($\theta_1 = 26.56^\circ$), and 4.1 m for the second angle ($\theta_2 = 45^\circ$), which is equivalent to about $11.6 D_S$, $10.4 D_S$ and $8.2 D_S$ respectively as demonstrated in figure 7.23.

It is observed that the maximum horizontal range is shifted backward in the first and second angle compared to the default case. For ($\theta_1 = 26.56^\circ$), the horizontal range is shifted by about $0.7D_S$ backward compared to the default zero angle ($\theta_0 = 0^\circ$); and for ($\theta_2 = 45^\circ$), the horizontal range is shifted by about $1D_S$ backward compared to the first angle ($\theta_1 = 26.56^\circ$).

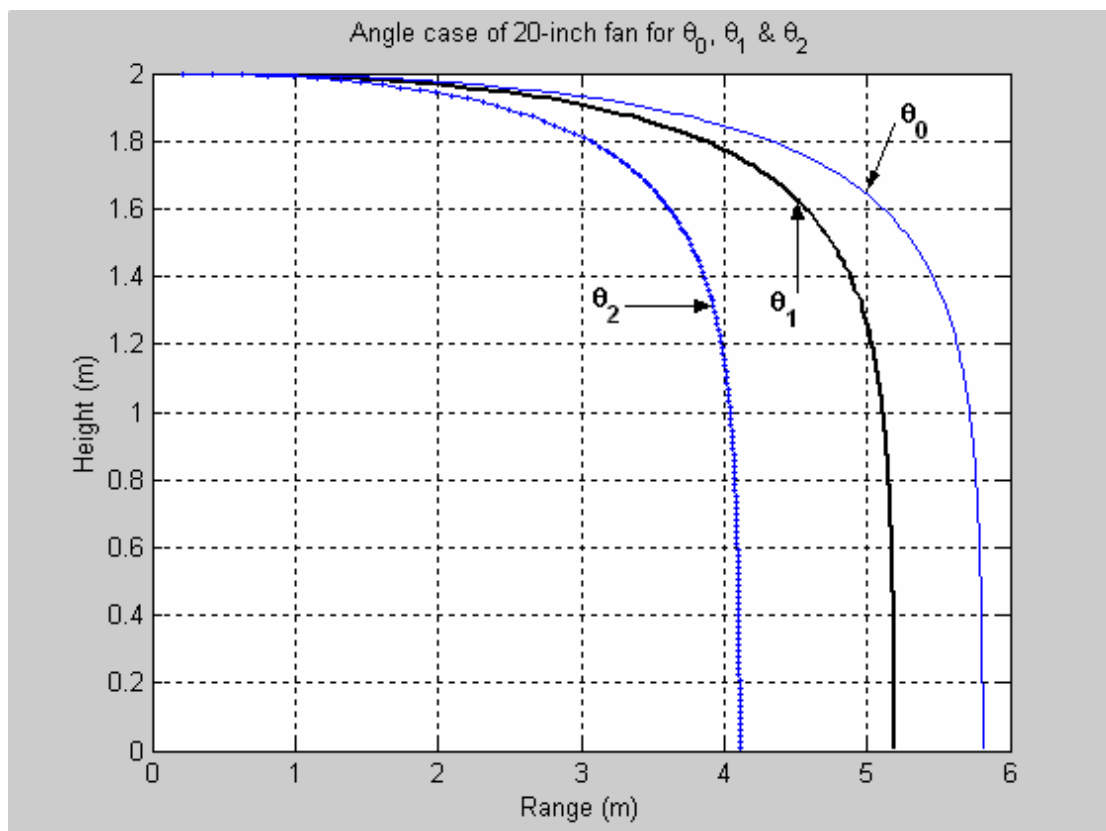


Figure 7.22 Droplet trajectories for different angles of 20-inch fan (D_S)

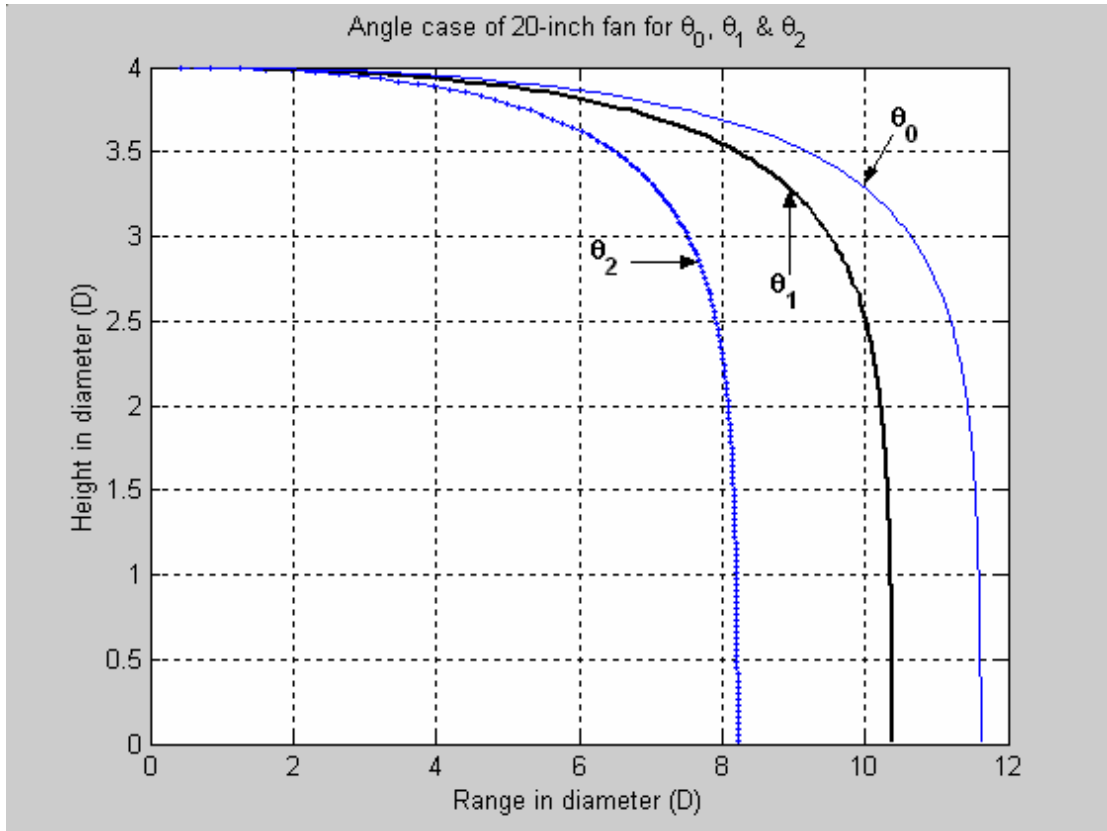


Figure 7.23 Droplet trajectories for different angles of 20-inch fan (D_s) in terms of fan diameter

7.3.2 Side-wise Investigation of 20-inch Fan (computational)

The experimental side-wise study of 20-inch fan is simulated here computationally. In the side-wise study, we are looking for specifying the maximum range of side-wise effect of the fan as shown in figure 7.24.

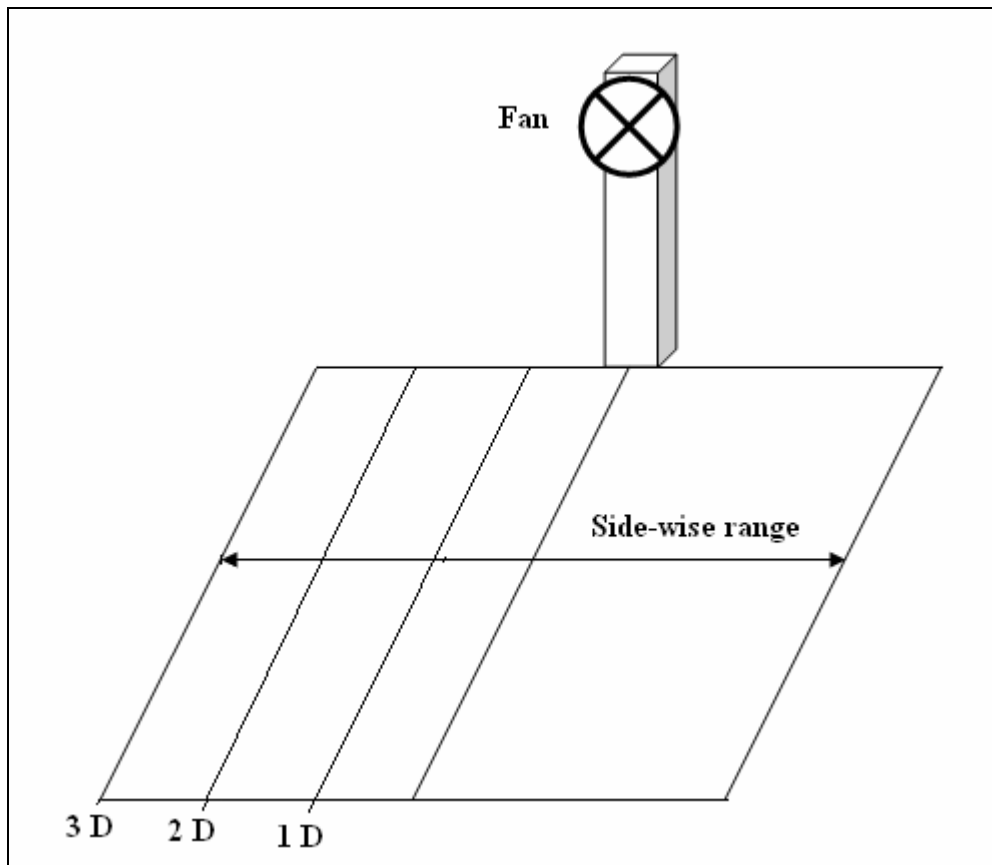


Figure 7.24 Side-wise Investigation of 20-inch Fan (computational)

In this side-wise study, the program is run for the same condition as the normal case except the velocity of the fan, which is dropped by a value of $(\cos \alpha)$. Such that the droplet velocity is $V = 28 + 4.74 \cos (\alpha)$, where $(45^\circ > \alpha > 0^\circ)$.

Figure 7.25 shows the maximum side-wise range of droplet reaches about 4 m, which is equivalent to about 8 D_s side-wise as shown in figure 7.26. The maximum horizontal rang at this location is about 4 m too, which is equivalent to about 8 D_s .

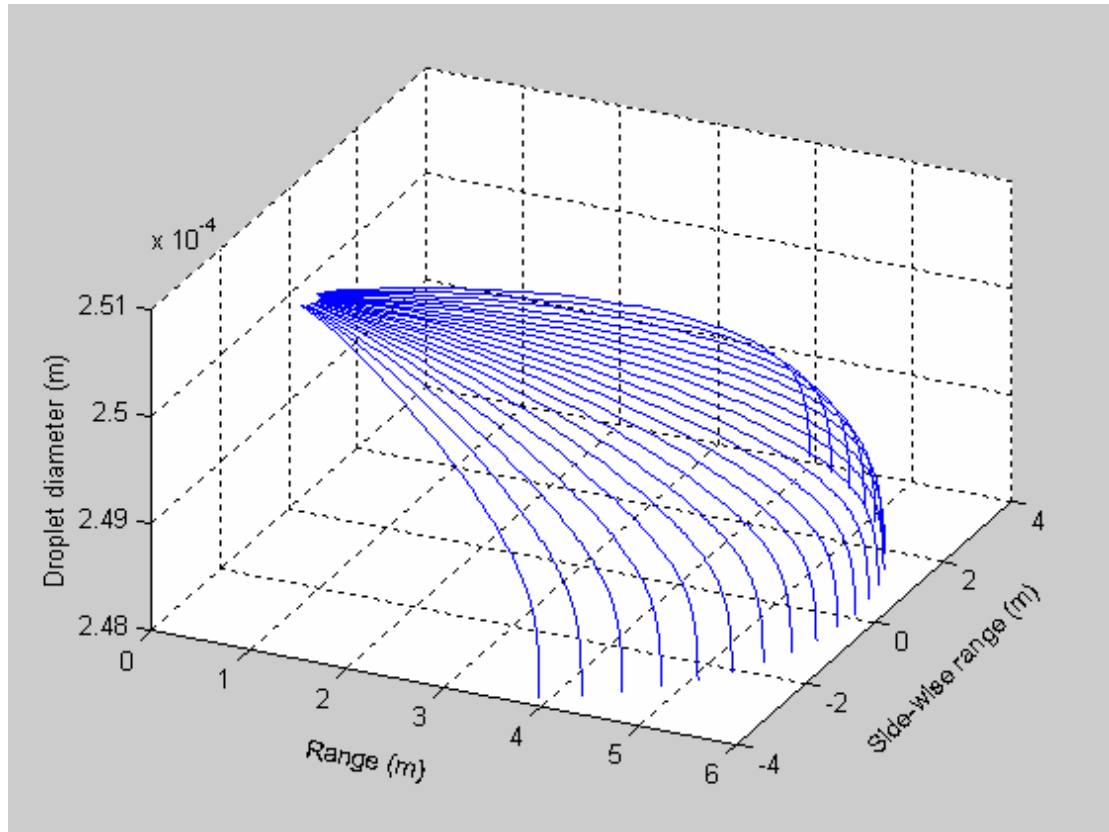


Figure 7.25 Droplet maximum side-wise range for 20-inch fan (D_s) for 4-diameter in height ($h = 4D_s$)

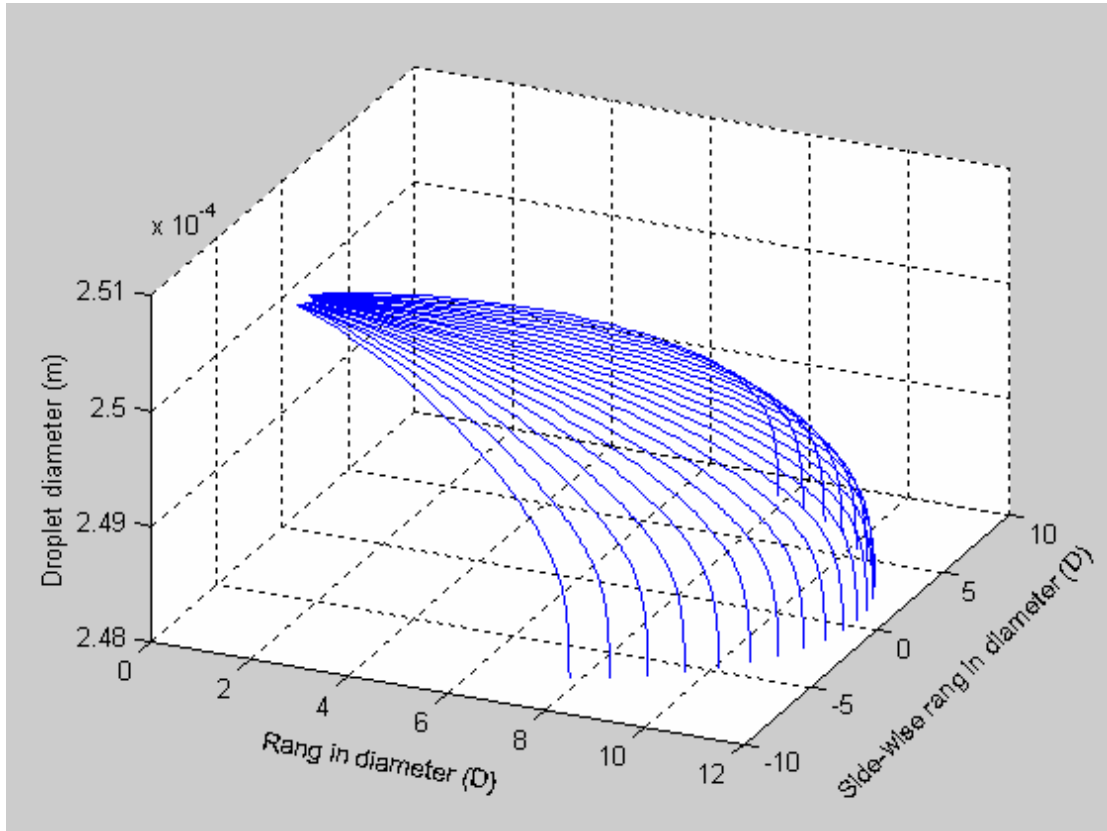


Figure 7.26 Droplet maximum side-wise range in diameter for 20-inch fan (D_S) for 4-diameter in height ($h = 4D_S$)

7.4 24-inch Fan

In the experimental measurements of 24-inch fan, it was observed that the fan maximum range of temperature occurs at a height level of the 4th diameter ($h = 4D_m$). The fan airspeed is about 6.36 m/s and the other experimental conditions are kept the same as shown in table 7.2. To simulate it in the computational solution, the program is run for such height ($h = 4D_m$, $h = 2.4$ m) and the droplet velocity is equal to the Injected droplet velocity from nozzle plus the fan airspeed ($V = 28 + 6.36 = 34.36$ m/s).

Figure 7.27 shows the water droplet evaporation versus time for this fan. The figure demonstrates the behavior of the evaporation process, and it is observed that the droplet hits the ground before it evaporates completely.

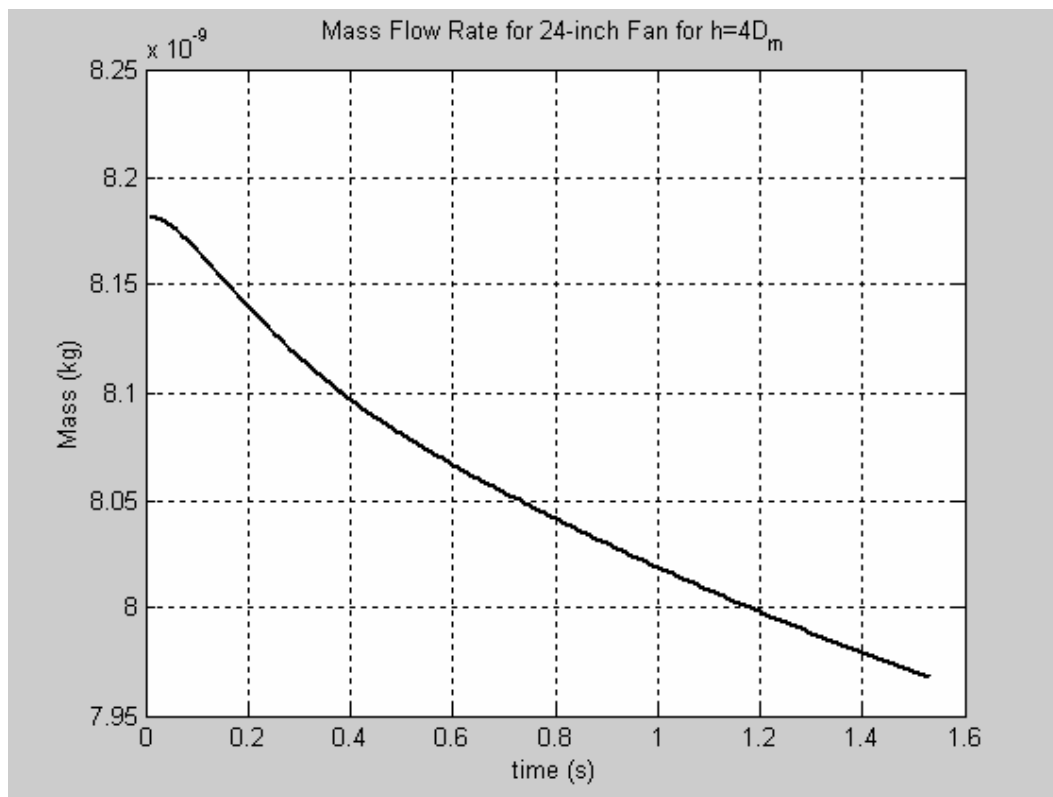


Figure 7.27 The rate of evaporation of droplet mass for 24-inch fan (D_m) for 4-diameter in height ($h = 4D_m$)

Figure 7.28 shows the droplet temperature versus time for this fan. The figure demonstrates the behavior of the droplet temperature which starts from the initial value ($T_p = 25\text{ }^{\circ}\text{C}$) and keeps dropping to final value of terminal droplet temperature of about $32.4\text{ }^{\circ}\text{C}$, which is very close to thermodynamic wet bulb temperature ($T_{\text{wet}} = 31.5$). This temperature is achieved rapidly, indicating that the energy storage within the droplet is more effective in the early stages of evaporation process.

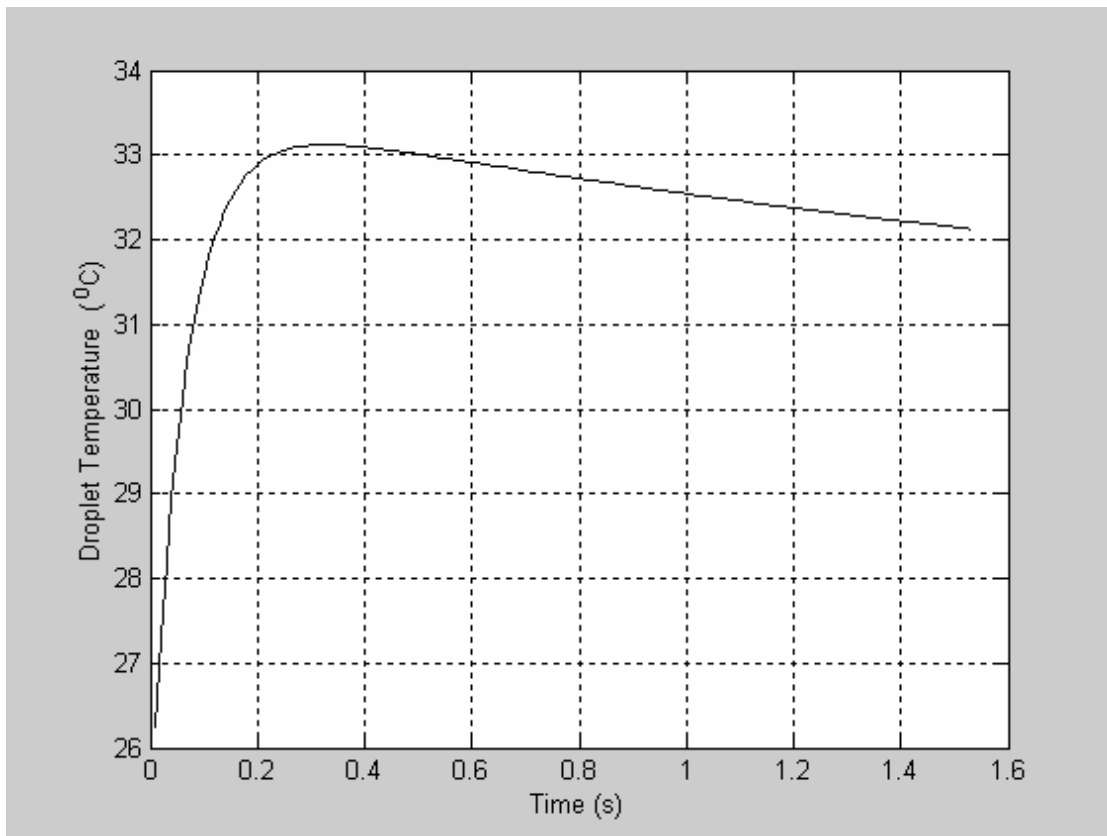


Figure 7.28 Droplet temperature versus time for 24-inch fan (D_m) for 4-diameter in height ($h = 4D_m$)

Figure 7.29 shows the air temperature versus time for this fan. The figure demonstrates the behavior of the air temperature which starts from the initial value ($T_a = 40\text{ }^{\circ}\text{C}$) and keeps dropping to final value of about $34.4\text{ }^{\circ}\text{C}$. The air temperature would drop more and more to get closer to the wet bulb temperature ($T_{\text{wet}} = 31.5$) if the droplet evaporated completely before it hits the ground, which didn't happen in this case as discussed in figure 7.27.

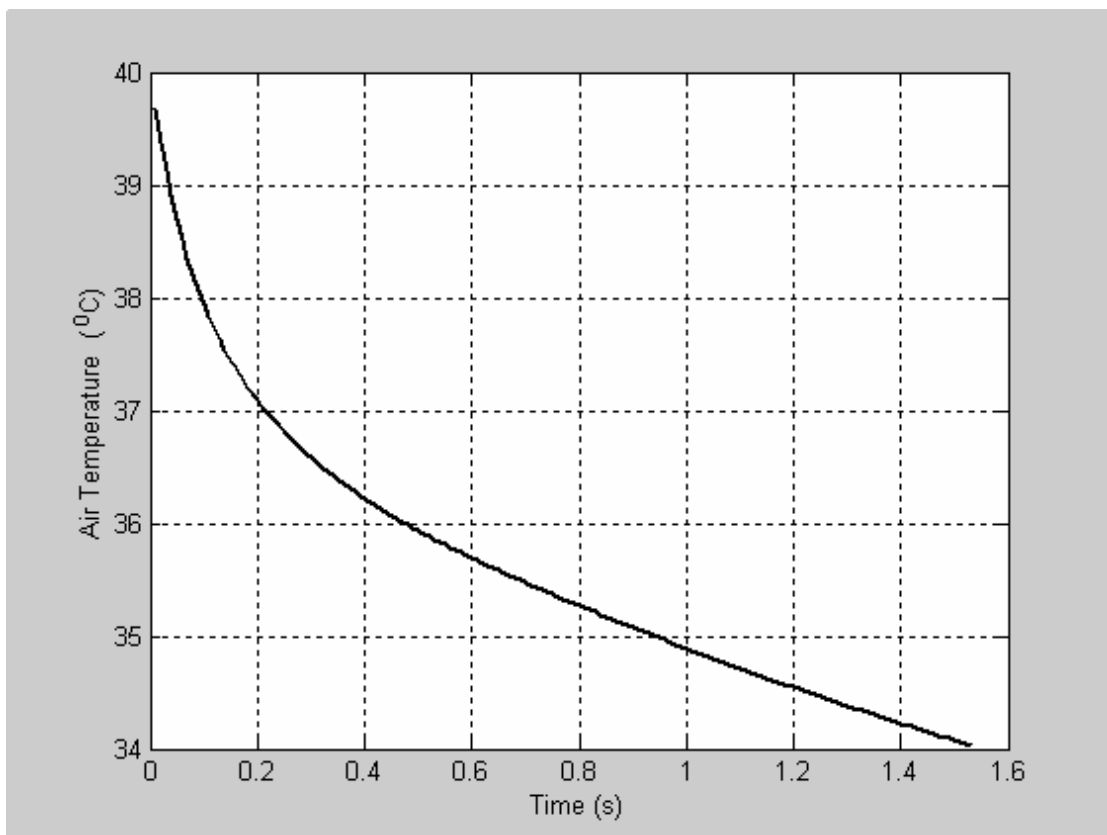


Figure 7.29 Air temperature versus time for 24-inch fan (D_m) for 4-diameter in height ($h = 4D_m$)

Figure 7.30 shows the droplet injection height (same as fan height) versus the horizontal range for this fan. The figure indicates the maximum horizontal range of the droplet of about 6.2 m, which is equivalent to about 10.3 D_m as demonstrated in figure 7.31.

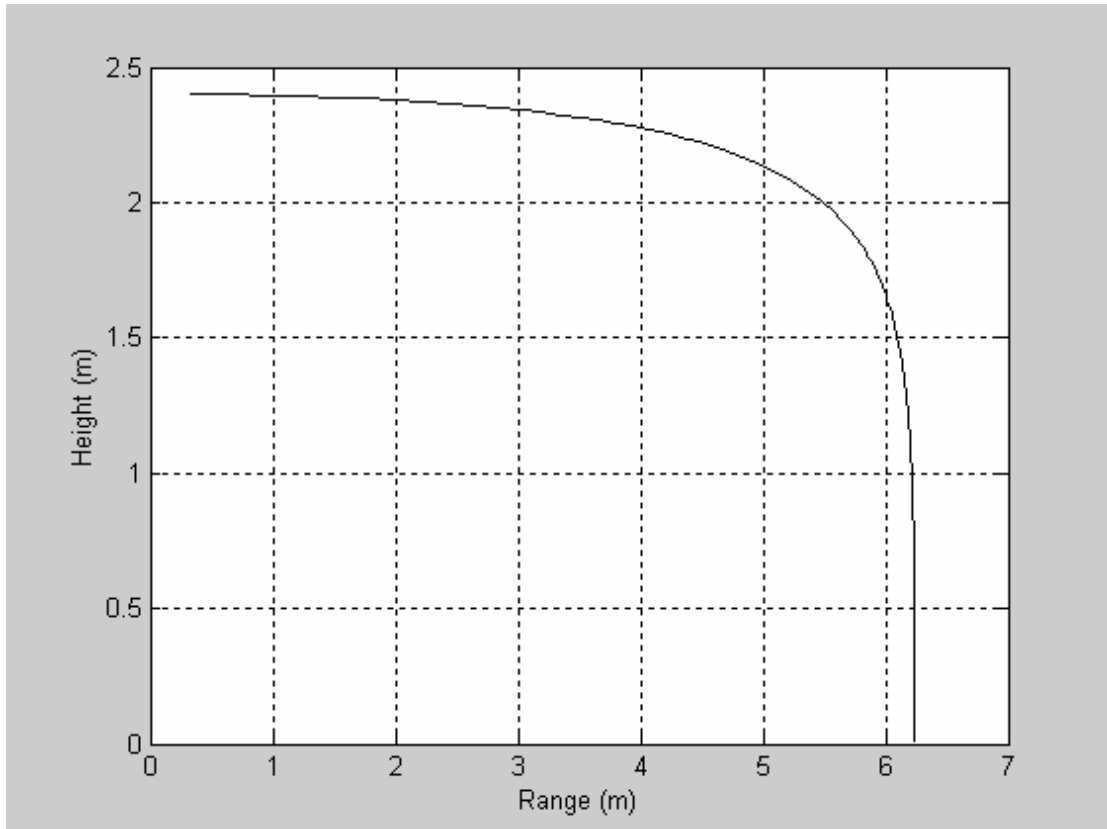


Figure 7.30 Droplet injection height versus the horizontal range for 24-inch fan (D_m) for 4-diameter in height ($h = 4D_m$)

Figure 7.31 shows the droplet injection height in diameter (same as fan height) versus the horizontal range in diameter for this fan. The figure indicates the maximum horizontal range of the droplet of about $10.4 D_m$.

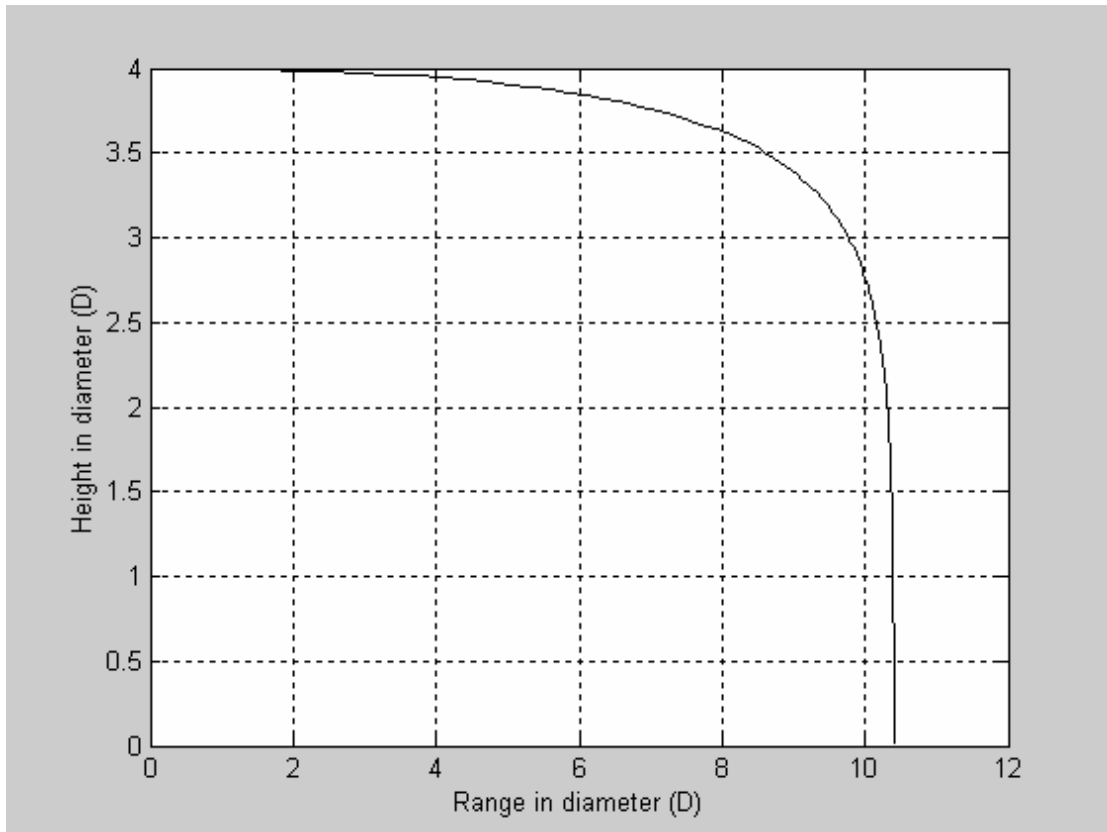


Figure 7.31 Droplet injection height in diameter versus the horizontal range in diameter for 24-inch fan (D_m) for 4-diameter in height ($h = 4D_m$)

Figure 7.32 shows the droplet temperature and air temperature versus the horizontal range for this fan. The figure indicates the history of air temperature along the range, and it shows the minimum air temperature occurs at the distance of 6.2 m, where the droplets hits the ground of about 34.1 °C. In addition, it demonstrates the history of droplet temperature along the horizontal range, and it shows the terminal droplet temperature of about 32.2 °C.

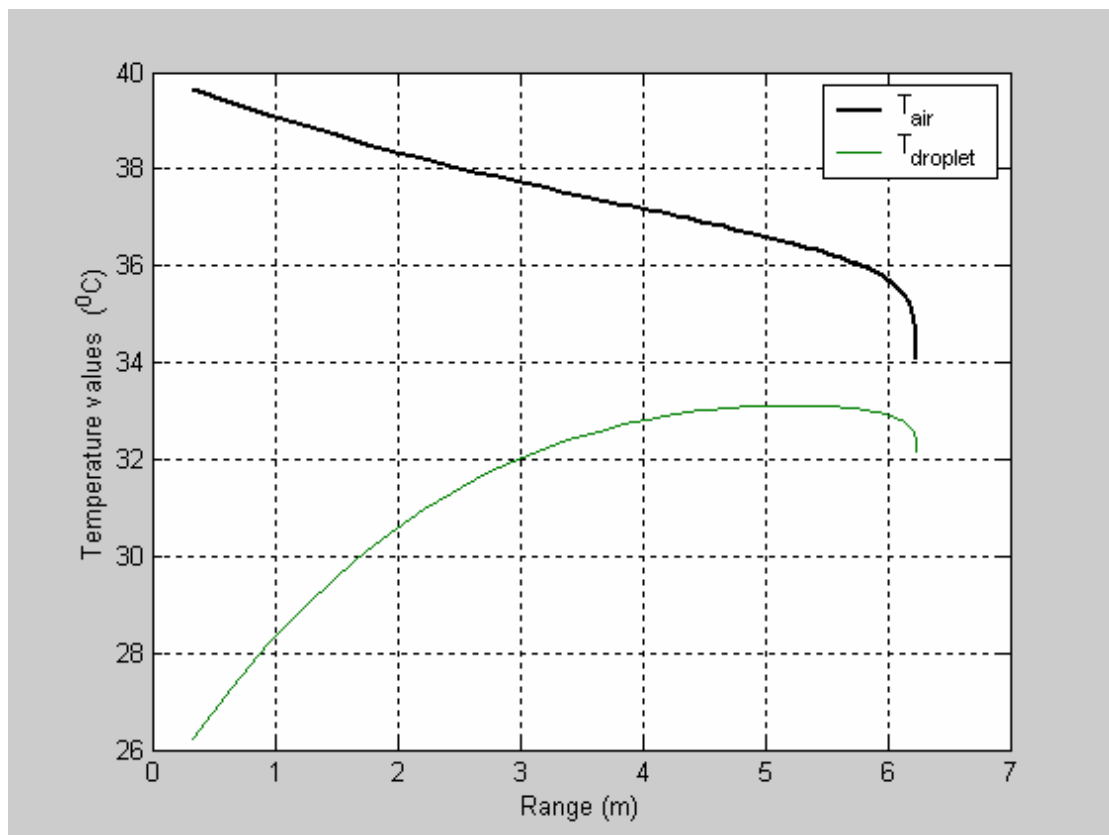


Figure 7.32 Droplet and air temperatures versus the horizontal range for 24-inch fan (D_m) for 4-diameter in height ($h = 4D_m$)

Figure 7.33 expresses the same observations as figure 7.32, but in terms of diameter for horizontal range. Such that, the figure indicates the history of air temperature along the range in diameter, and it shows the minimum air temperature occurs at the distance of $10.4 D_m$, where the droplets hits the ground of about of $34.1 ^\circ\text{C}$. In addition, it demonstrates the history of droplet temperature along the horizontal range, and it shows the terminal droplet temperature of about $32.2 ^\circ\text{C}$.

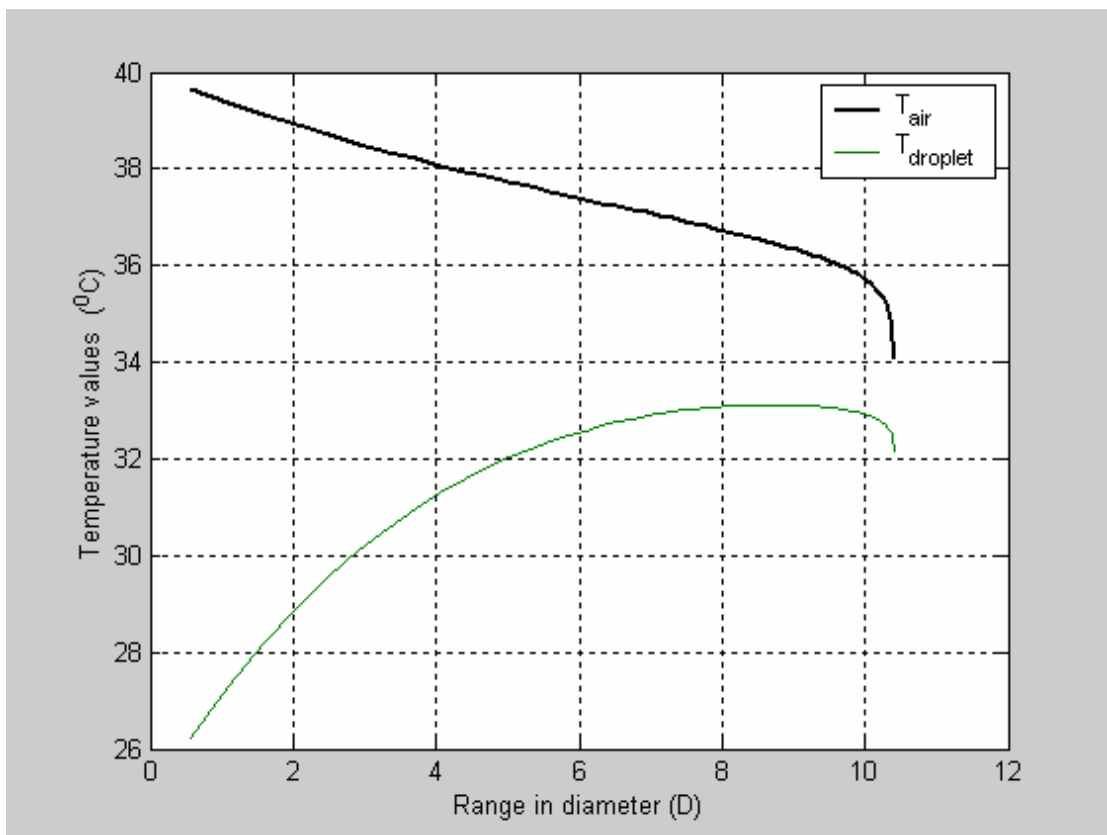


Figure 7.33 Droplet and air temperatures versus the horizontal range in diameter for 24-inch fan (D_m) for 4-diameter in height ($h = 4D_m$)

7.4.1 Angle Effect of 24-inch Fan (computational)

The experimental angle effect case of 24-inch fan is simulated here computationally. In this configuration, the fan is angled for two positions ($\theta_1 = 26.56^\circ$, $\theta_2 = 45^\circ$) as shown in figure 7.11.

In this case, the program is run for the same condition as the normal case except the velocity which is dropped by a value of $(\cos \theta)$ due the fan deflection, such that $V_1 = 34.36 \cos (\theta_1)$ & $V_2 = 34.36 \cos (\theta_2)$.

7.4.1.1 $\theta_1 = 26.56^\circ$

Figure 7.34 indicates the history of air temperature and droplet temperature versus time for the first angle ($\theta_1 = 26.56^\circ$). It demonstrates the behavior of the air temperature which starts from the initial value ($T_a = 40^\circ\text{C}$) and keeps dropping to final value of about 34.1°C , the same as in the default case ($\theta_0 = 0^\circ$). The figure also demonstrates the behavior of the droplet temperature which starts from the initial value ($T_p = 25^\circ\text{C}$) and keeps dropping to final value of terminal droplet temperature of about 32.2°C , which is very close to thermodynamic wet bulb temperature ($T_{\text{wet}} = 31.5$), the same as in the default case ($\theta_0 = 0^\circ$) too.

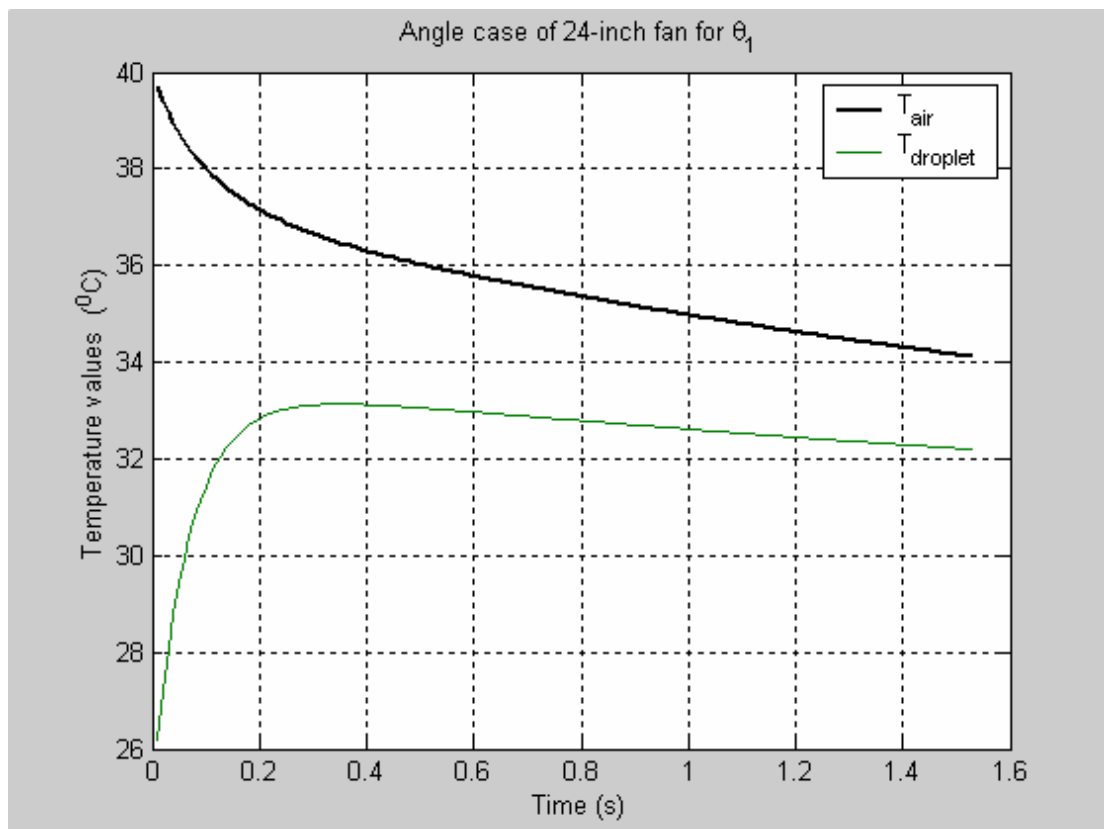


Figure 7.34 Droplet and air temperatures versus time of angle case ($\theta_1 = 26.56^\circ$) for 24-inch fan (D_m)

Figure 7.35 shows the maximum horizontal range of the droplet of about 5.6 m for the first angle ($\theta_1 = 26.56^\circ$), which is equivalent to about $9.3 D_m$ as demonstrated in figure 7.36.

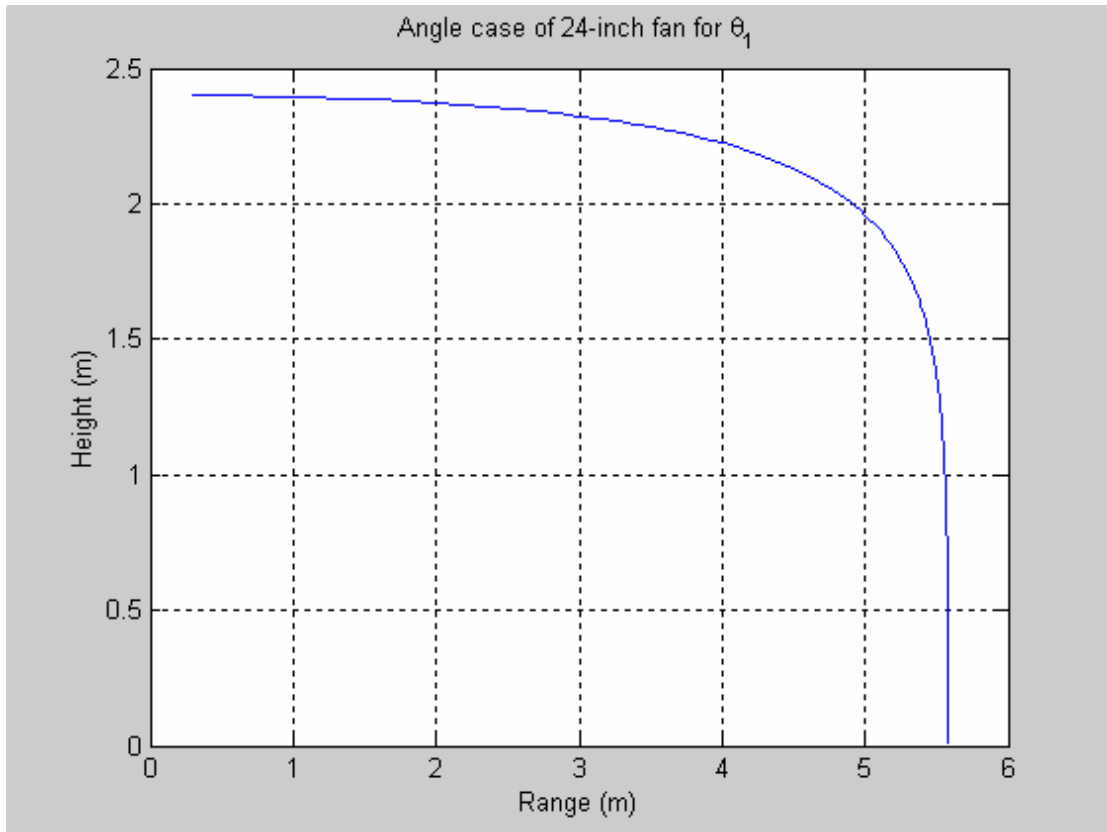


Figure 7.35 Droplet injection height versus the horizontal range of angle case ($\theta_1 = 26.56^\circ$) for 24-inch fan (D_m)

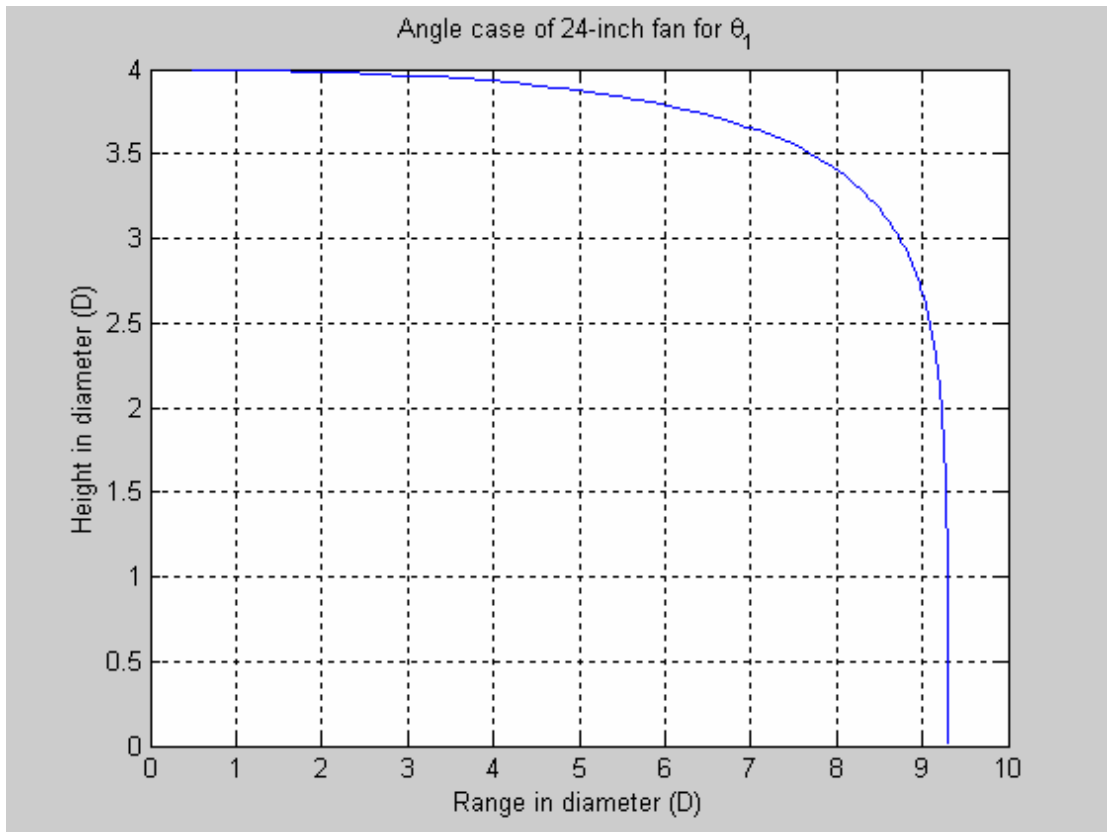


Figure 7.36 Droplet injection height in diameter versus the horizontal range in diameter of angle case ($\theta_1 = 26.56^\circ$) for 24-inch fan (D_m)

Figure 7.37 shows the droplet temperature and air temperature versus the horizontal range for the first angle ($\theta_1 = 26.56^\circ$). The figure indicates the history of air temperature along the range, and it shows the minimum air temperature occurs at the distance of 5.6 m, where the droplets hits the ground of about of 34.1°C . In addition, it demonstrates the history of droplet temperature along the horizontal range, and it shows the terminal droplet temperature of about 32.2°C .

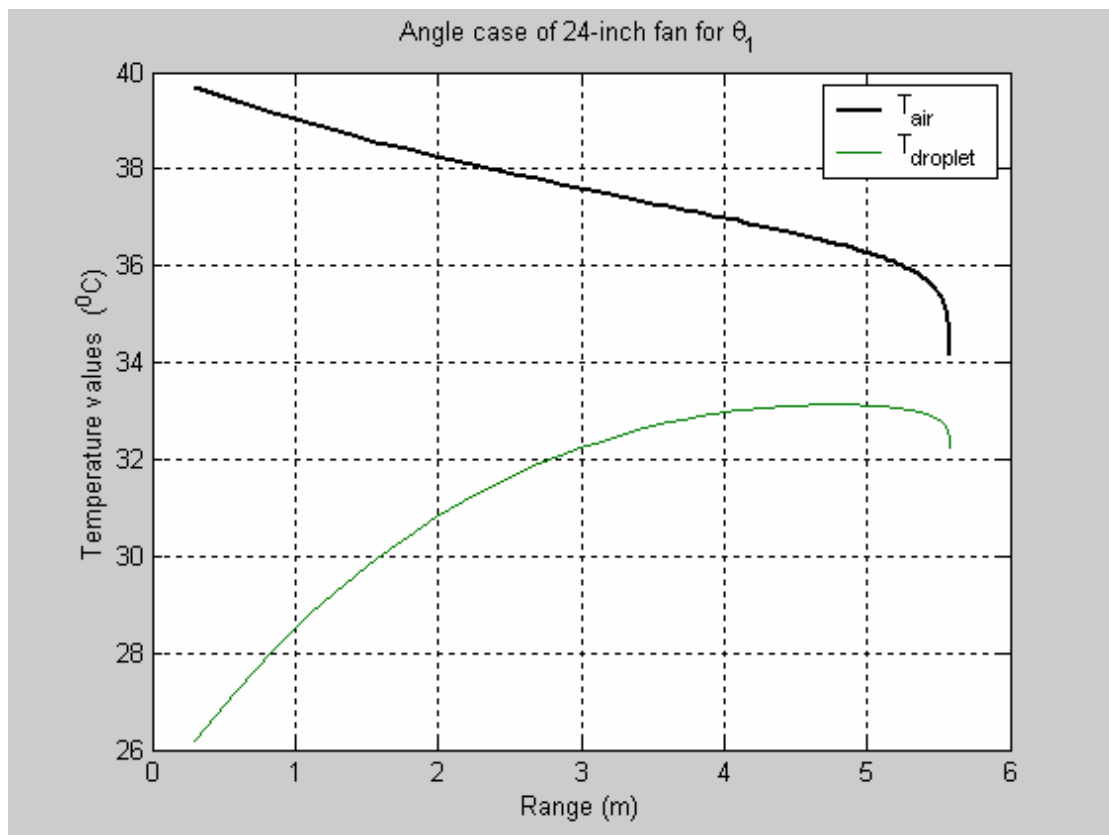


Figure 7.37 Droplet and air temperatures versus the horizontal range of angle case ($\theta_1 = 26.56^\circ$) for 24-inch fan (D_m)

Figure 7.38 expresses the same observations as figure 7.37, but in terms of diameter for horizontal range for the first angle ($\theta_1 = 26.56^\circ$). Such that, the figure indicates the history of air temperature along the range in diameter, and it shows the minimum air temperature occurs at the distance of $9.3 D_m$, where the droplets hits the ground of about of 34.1°C . In addition, it demonstrates the history of droplet temperature along the horizontal range, and it shows the terminal droplet temperature of about 32.2°C .

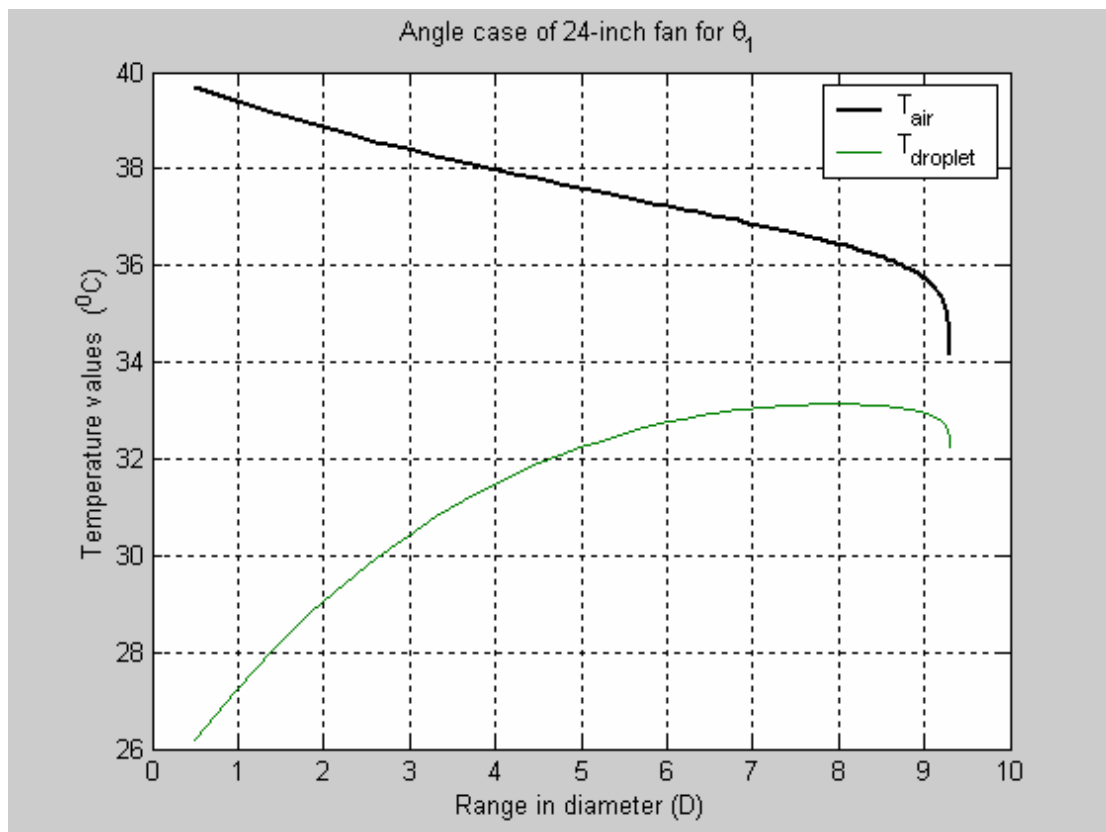


Figure 7.38 Droplet and air temperatures versus the horizontal range in diameter of angle case ($\theta_1 = 26.56^\circ$) for 24-inch fan (D_m)

7.4.1.2 $\theta_2 = 45^\circ$

Figure 7.39 indicates the history of air temperature and droplet temperature versus time for the second angle ($\theta_2 = 45^\circ$). It demonstrates the behavior of the air temperature which starts from the initial value ($T_a = 40^\circ\text{C}$) and keeps dropping to final value of about 34.1°C , the same as in the default case ($\theta_0 = 0^\circ$). The figure also demonstrates the behavior of the droplet temperature which starts from the initial value ($T_p = 25^\circ\text{C}$) and keeps dropping to final value of terminal droplet temperature of about 32.2°C , which is very close to thermodynamic wet bulb temperature ($T_{\text{wet}} = 31.5$), the same as in the default case ($\theta_0 = 0^\circ$) too.

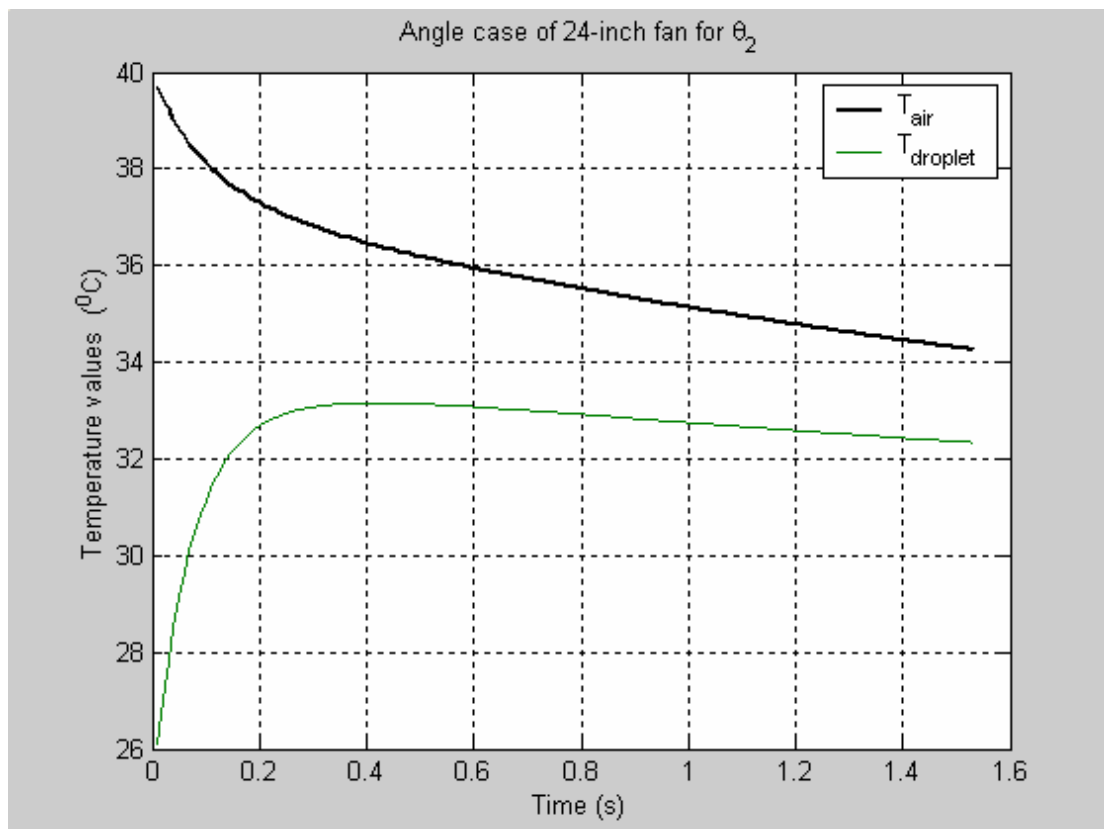


Figure 7.39 Droplet and air temperatures versus time of angle case ($\theta_2 = 45^\circ$) for 24-inch fan (D_m)

Figure 7.40 shows the maximum horizontal range of the droplet of about 4.4 m for the second angle ($\theta_2 = 45^\circ$), which is equivalent to about $7.3 D_m$ as demonstrated in figure 7.41.

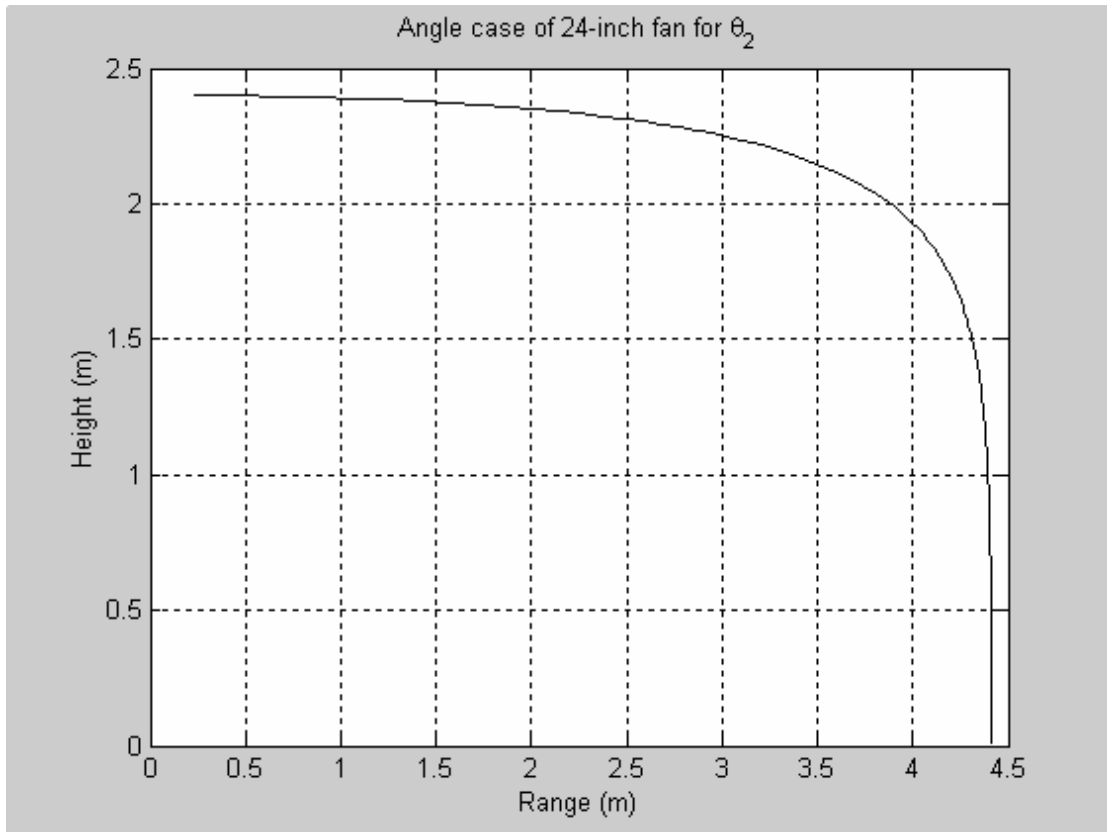


Figure 7.40 Droplet injection height versus the horizontal range of angle case ($\theta_2 = 45^\circ$) for 24-inch fan (D_m)

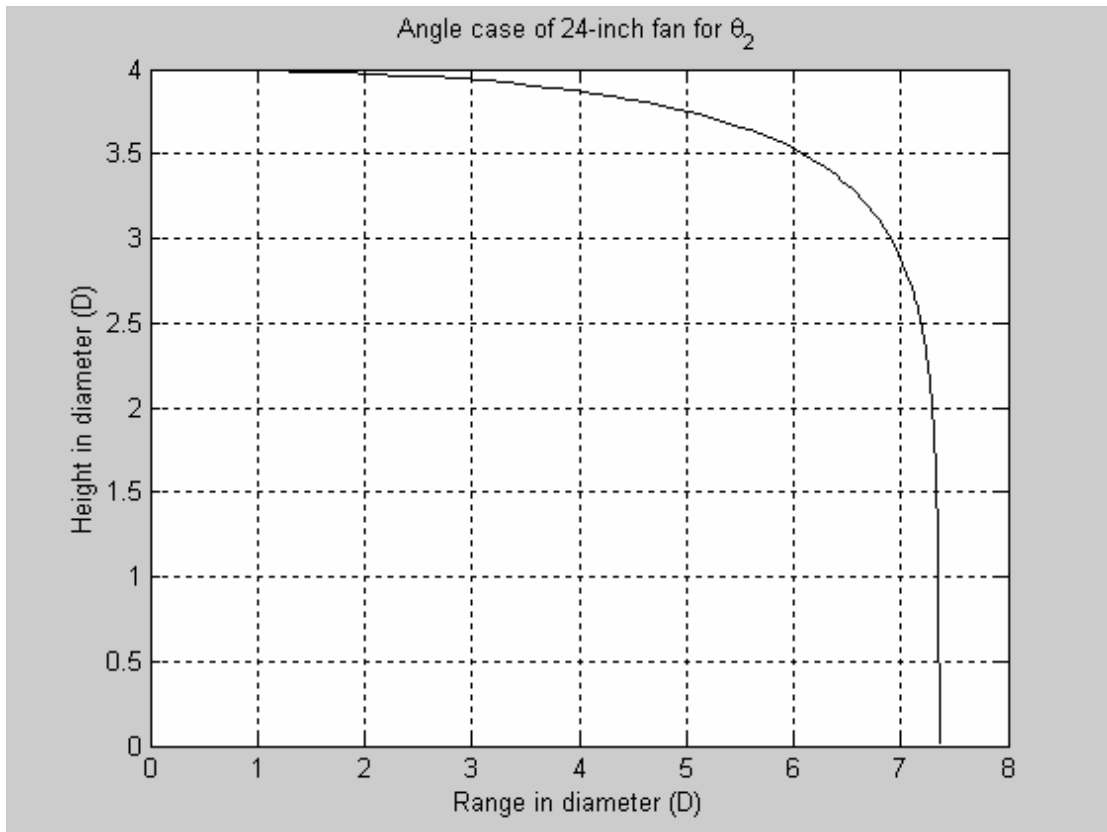


Figure 7.41 Droplet injection height in diameter versus the horizontal range in diameter of angle case ($\theta_2 = 45^\circ$) for 24-inch fan (D_m)

Figure 7.42 shows the droplet temperature and air temperature versus the horizontal range for the second angle ($\theta_2 = 45^\circ$). The figure indicates the history of air temperature along the range, and it shows the minimum air temperature occurs at the distance of 4.4 m, where the droplets hits the ground of about 34.2°C . In addition, it demonstrates the history of droplet temperature along the horizontal range, and it shows the terminal droplet temperature of about 32.3°C .

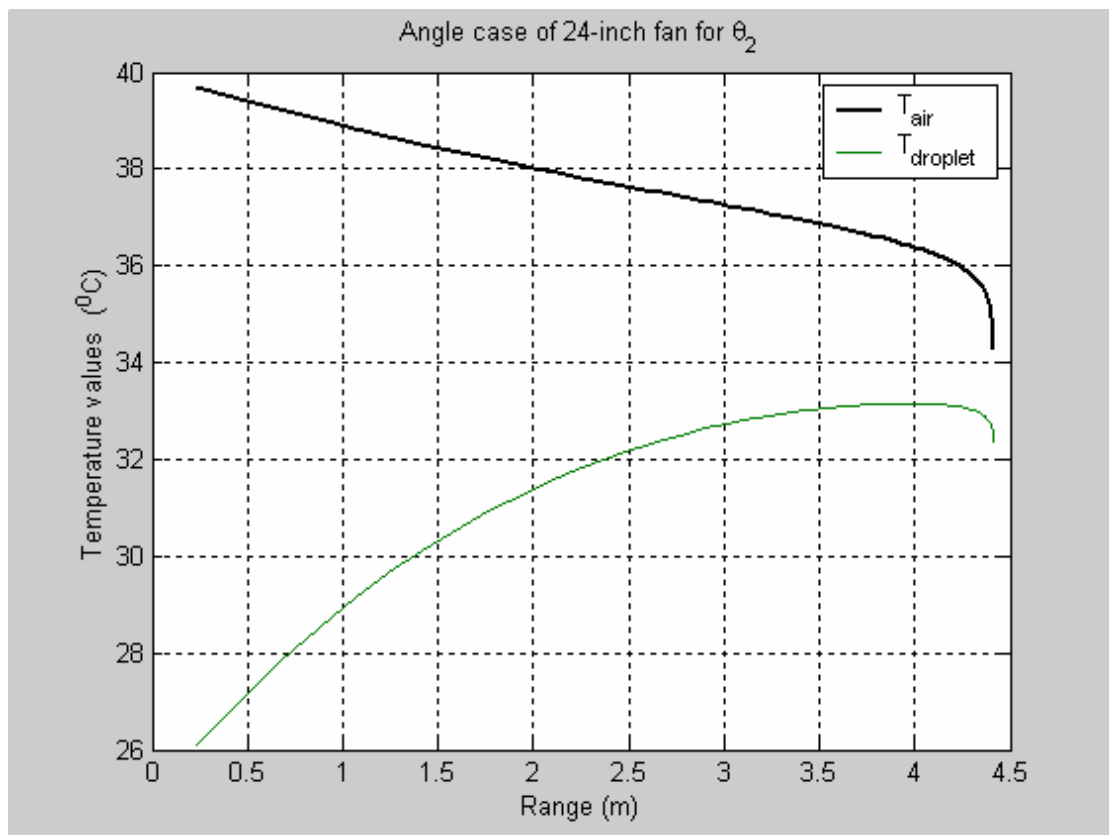


Figure 7.42 Droplet and air temperatures versus the horizontal range of angle case ($\theta_2 = 45^\circ$) for 24-inch fan (D_m)

Figure 7.43 expresses the same observations as figure 7.42, but in terms of diameter for horizontal range for the second angle ($\theta_2 = 45^\circ$). Such that, the figure indicates the history of air temperature along the range in diameter, and it shows the minimum air temperature occurs at the distance of $7.3 D_m$, where the droplets hits the ground of about of 34.2°C . In addition, it demonstrates the history of droplet temperature along the horizontal range, and it shows the terminal droplet temperature of about 32.3°C .

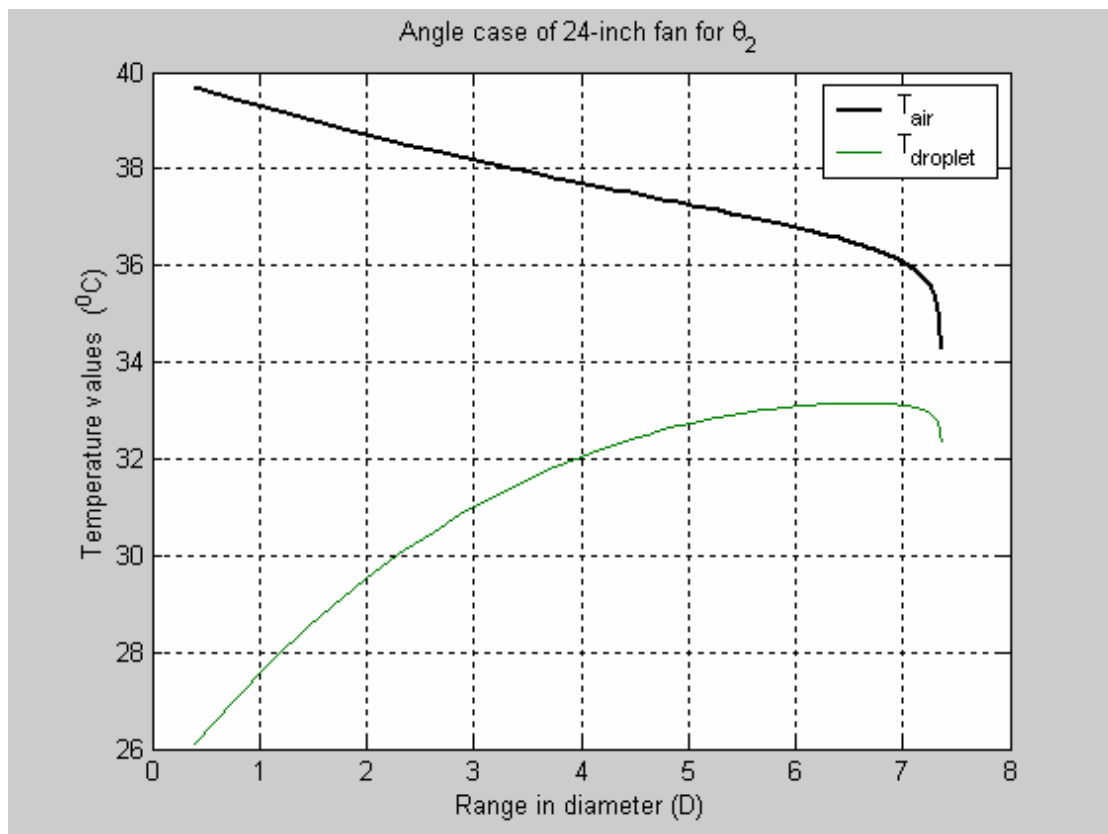


Figure 7.43 Droplet and air temperatures versus the horizontal range in diameter of angle case ($\theta_2 = 45^\circ$) for 24-inch fan (D_m)

Figure 7.44 shows the maximum horizontal range of the droplet in the angle case for different angles of the 24-inch fan angle of about 6.2 m for the default zero angle ($\theta_0 = 0^\circ$), 5.6 m for the first angle ($\theta_1 = 26.56^\circ$), and 4.4 m for the second angle ($\theta_2 = 45^\circ$), which is equivalent to about $10.4 D_m$, $9.3 D_m$ and $7.3 D_m$ respectively as demonstrated in figure 7.45.

It is observed that the maximum horizontal range is shifted backward in the first and second angle compared to the default case. For ($\theta_1 = 26.56^\circ$), the horizontal range is shifted by about $1D_m$ backward compared to the default zero angle ($\theta_0 = 0^\circ$); and for ($\theta_2 = 45^\circ$), the horizontal range is shifted by about $2D_m$ backward compared to the first angle ($\theta_1 = 26.56^\circ$).

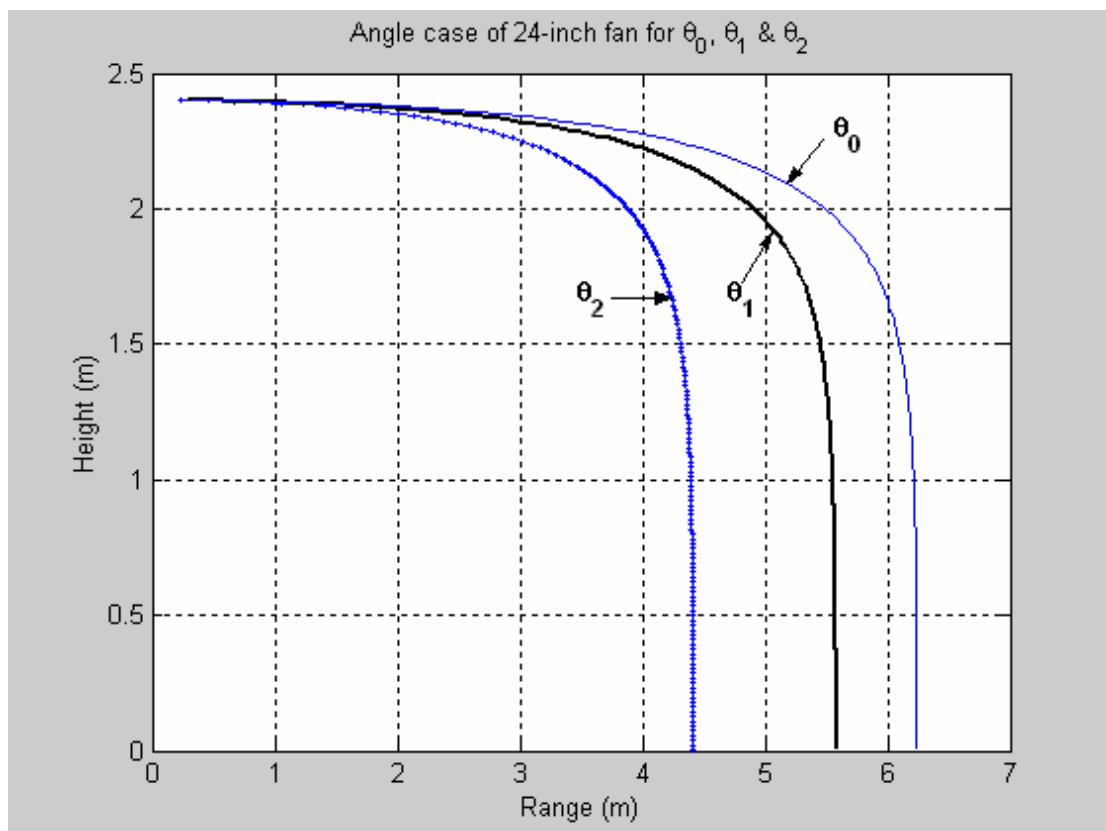


Figure 7.44 Droplet trajectories for different angles of 24-inch fan (D_m)

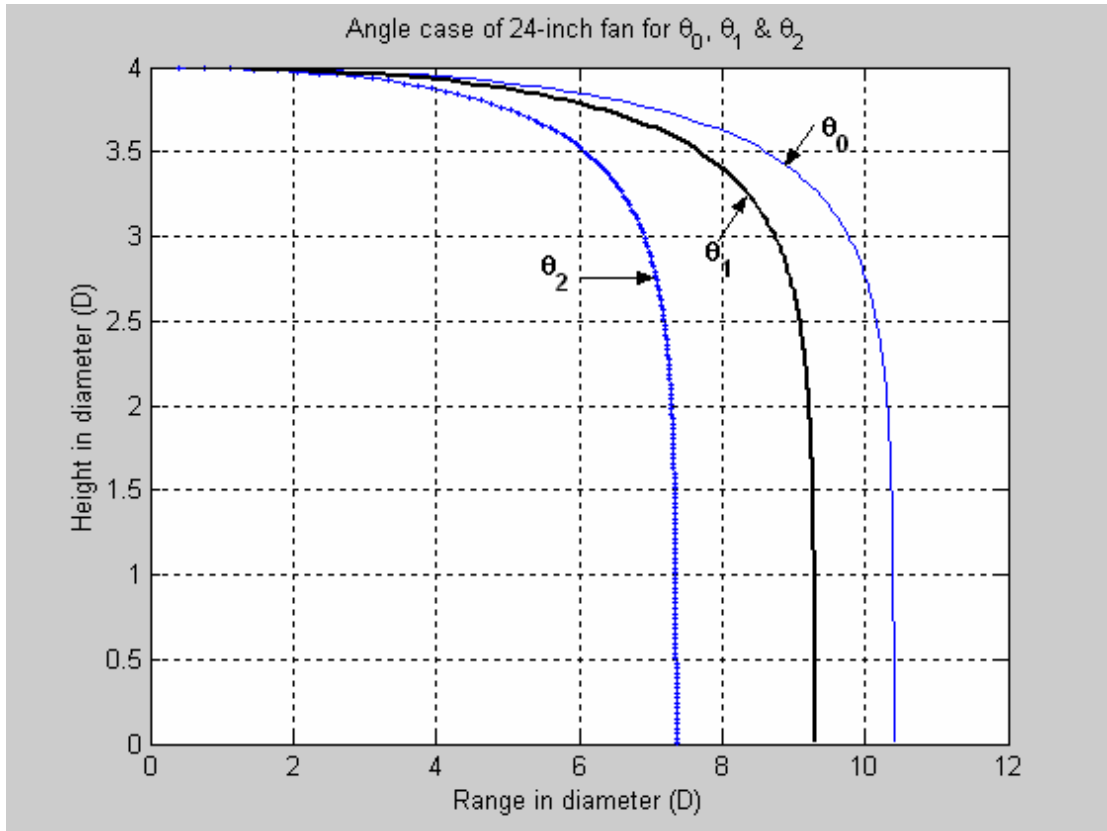


Figure 7.45 Droplet trajectories for different angles of 24-inch fan (D_m) in terms of fan diameter

7.4.2 Side-wise Investigation of 24-inch Fan (computational)

The experimental side-wise study of 24-inch fan is simulated here computationally. In the side-wise study, we are looking for specifying the maximum range of side-wise effect of the fan as shown in figure 7.24.

In this side-wise study, the program is run for the same condition as the normal case except the velocity of the fan, which is dropped by a value of $(\cos \alpha)$. Such that the droplet velocity is $V = 28 + 6.36 \cos (\alpha)$, where $(45^\circ > \alpha > 0^\circ)$.

Figure 7.46 shows the maximum side-wise range of droplet reaches about 4.3 m, which is equivalent to about 7.2 D_m side-wise as shown in figure 7.47. The maximum horizontal rang at this location is about 4.2 m, which is equivalent to about 7 D_m .

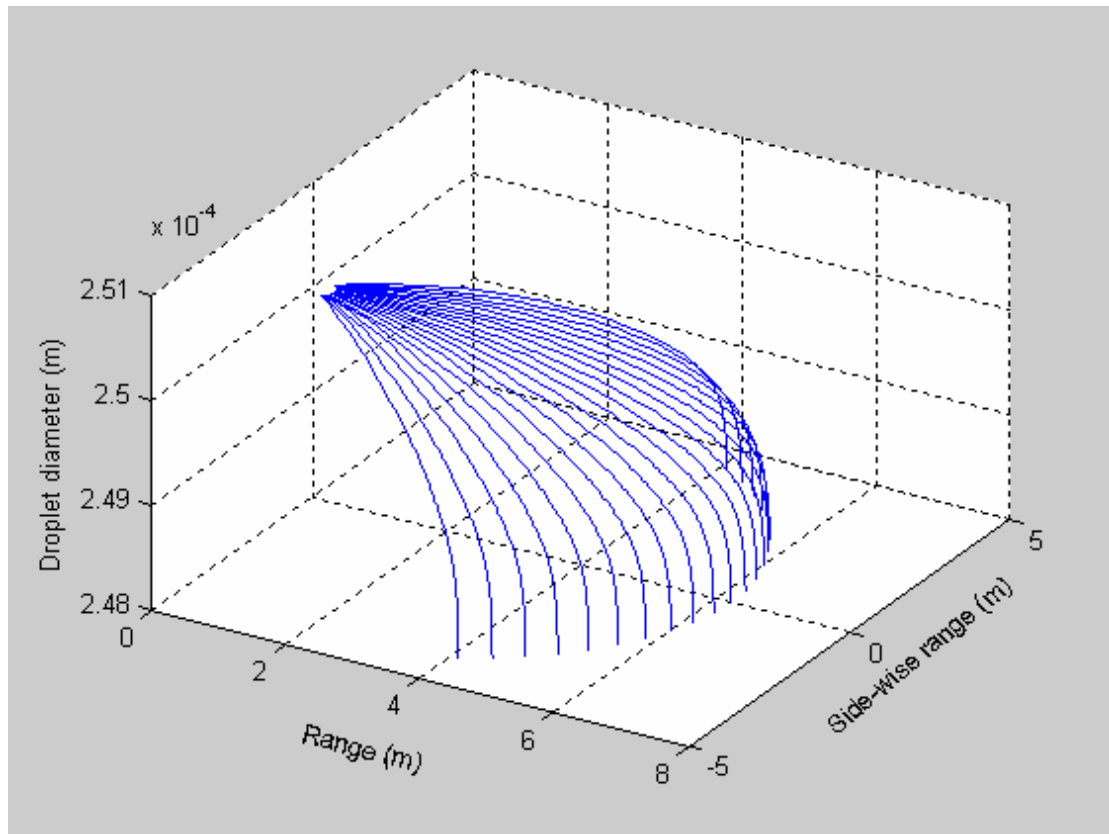


Figure 7.46 Droplet maximum side-wise range for 24-inch fan (D_m) for 4-diameter in height ($h = 4D_m$)

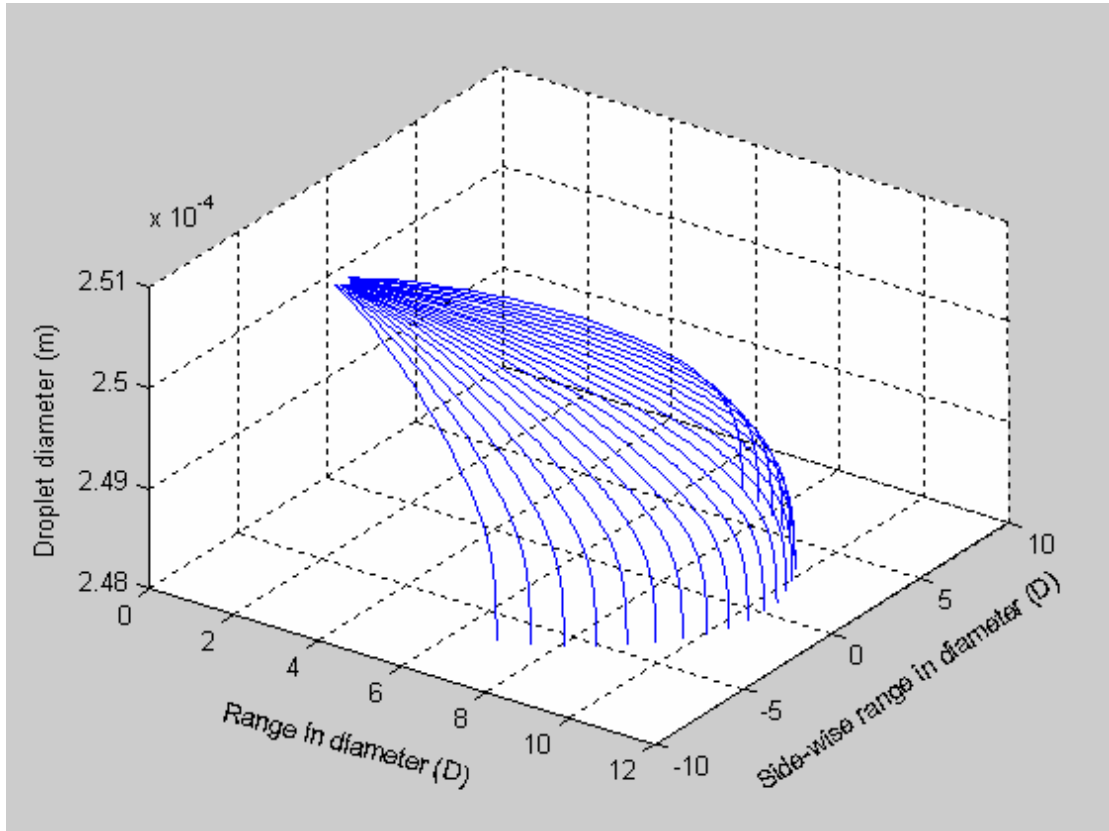


Figure 7.47 Droplet maximum side-wise range in diameter for 24-inch fan (D_m) for 4-diameter in height ($h = 4D_m$)

7.5 30-inch Fan

In the experimental measurements of 30-inch fan, it was observed that the fan maximum range of temperature occurs at a height level of the 4th diameter ($h = 4D_L$). The fan airspeed is about 7.49 m/s and the other experimental conditions are kept the same as shown in table 7.2. To simulate it in the computational solution, the program is run for such height ($h = 4D_m$, $h = 3$ m) and the droplet velocity is equal to the Injected droplet velocity from nozzle plus the fan airspeed ($V = 28 + 7.99 = 35.99$ m/s).

Figure 7.48 shows the water droplet evaporation versus time for this fan. The figure demonstrates the behavior of the evaporation process, and it is observed that the droplet hits the ground before it evaporates completely.

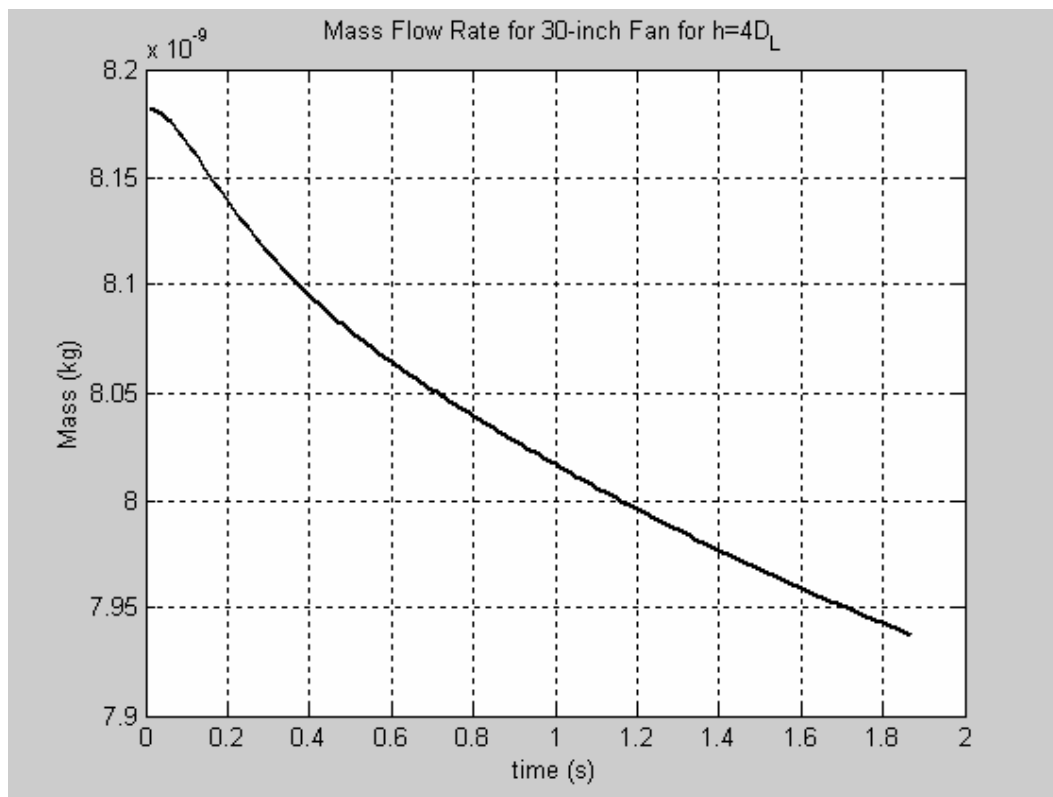


Figure 7.48 The rate of evaporation of droplet mass for 30-inch fan (D_L) for 4-diameter in height ($h = 4D_L$)

Figure 7.49 shows the droplet temperature versus time for this fan. The figure demonstrates the behavior of the droplet temperature which starts from the initial value ($T_p = 25\text{ }^{\circ}\text{C}$) and keeps dropping to final value of terminal droplet temperature of about $31.9\text{ }^{\circ}\text{C}$, which is very close to thermodynamic wet bulb temperature ($T_{\text{wet}} = 31.5$). This temperature is achieved rapidly, indicating that the energy storage within the droplet is more effective in the early stages of evaporation process.

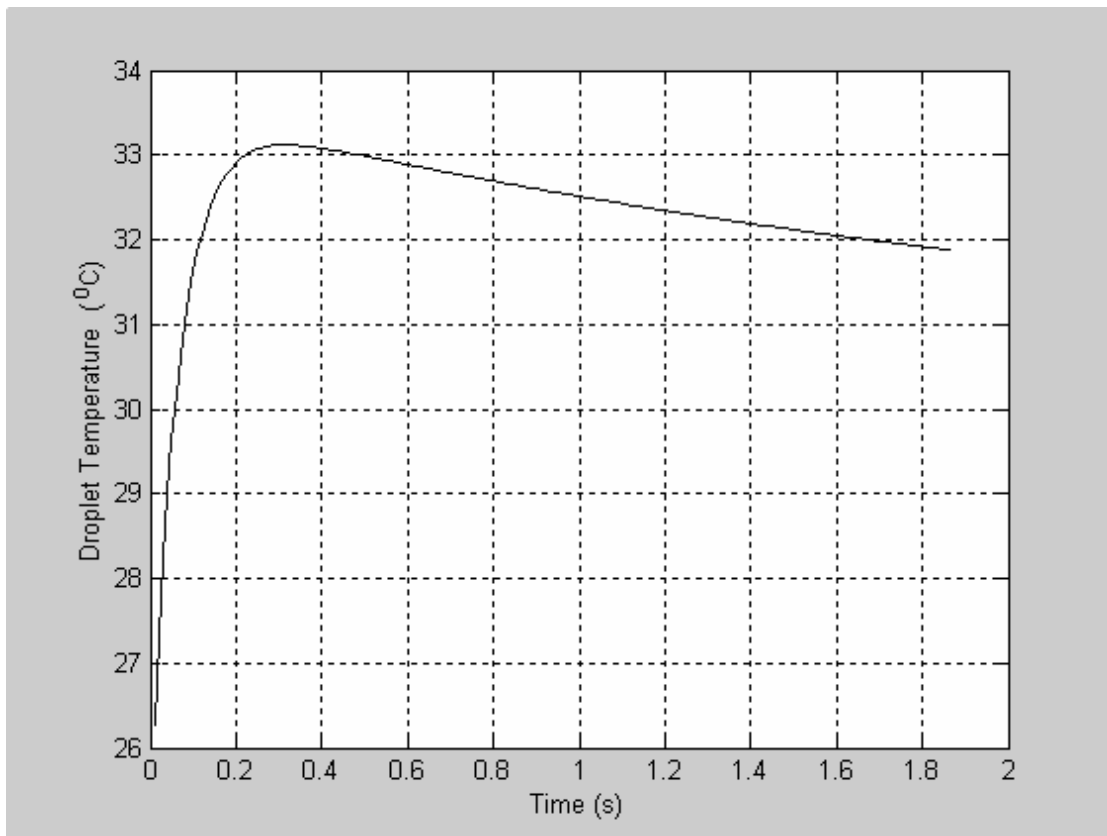


Figure 7.49 Droplet temperature versus time for 30-inch fan (D_L) for 4-diameter in height ($h = 4D_L$)

Figure 7.50 shows the air temperature versus time for this fan. The figure demonstrates the behavior of the air temperature which starts from the initial value ($T_a = 40\text{ }^{\circ}\text{C}$) and keeps dropping to final value of about $33.5\text{ }^{\circ}\text{C}$. The air temperature would drop more and more to get closer to the wet bulb temperature ($T_{\text{wet}} = 31.5$) if the droplet evaporated completely before it hits the ground, which didn't happen in this case as discussed in figure 7.49.

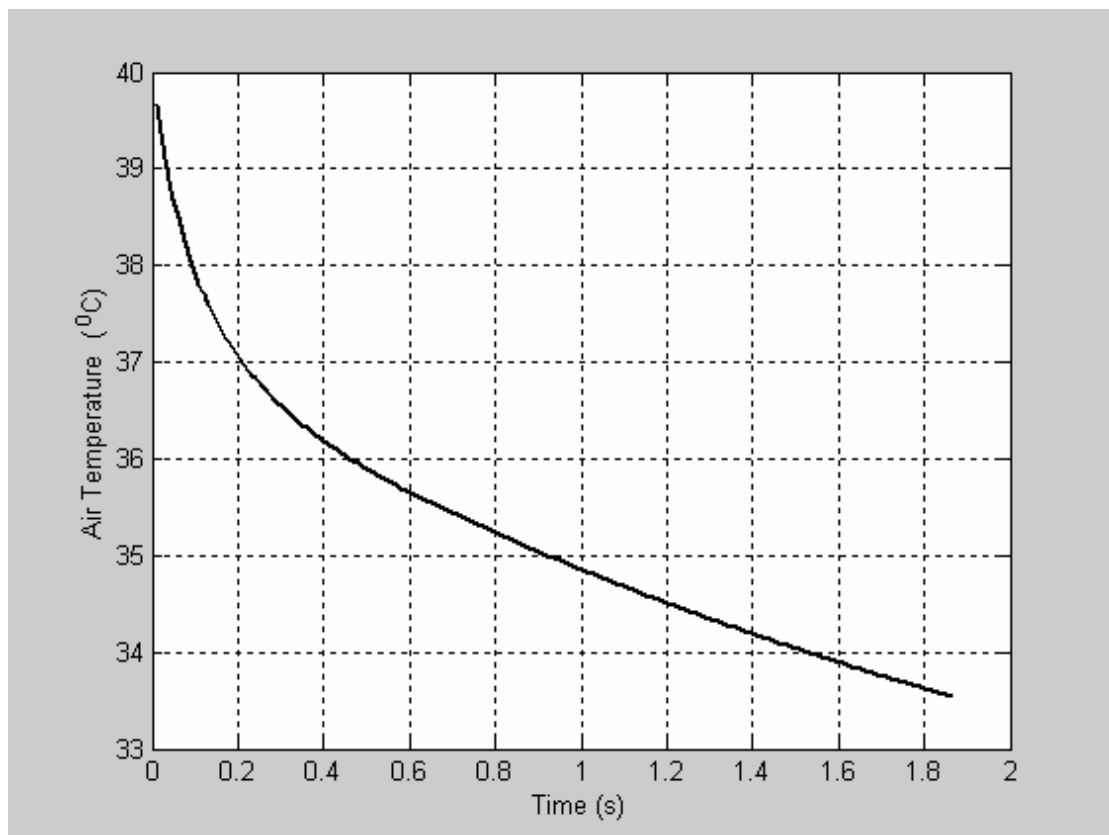


Figure 7.50 Air temperature versus time for 30-inch fan (D_L) for 4-diameter in height ($h = 4D_L$)

Figure 7.51 shows the droplet injection height (same as fan height) versus the horizontal range for this fan. The figure indicates the maximum horizontal range of the droplet of about 6.5 m, which is equivalent to about 8.7 D_L as demonstrated in figure 7.52.

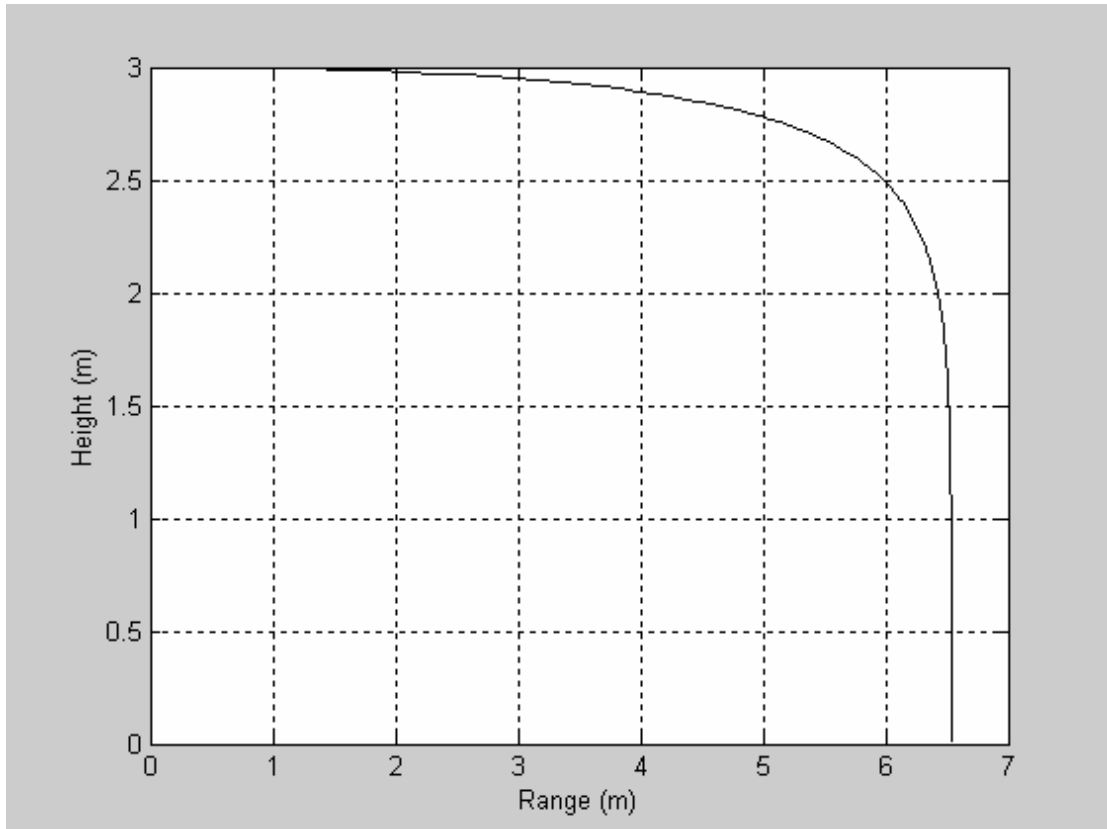


Figure 7.51 Droplet injection height versus the horizontal range for 30-inch fan (D_L) for 4-diameter in height ($h = 4D_L$)

Figure 7.52 shows the droplet injection height in diameter (same as fan height) versus the horizontal range in diameter for this fan. The figure indicates the maximum horizontal range of the droplet of about $8.7 D_L$.

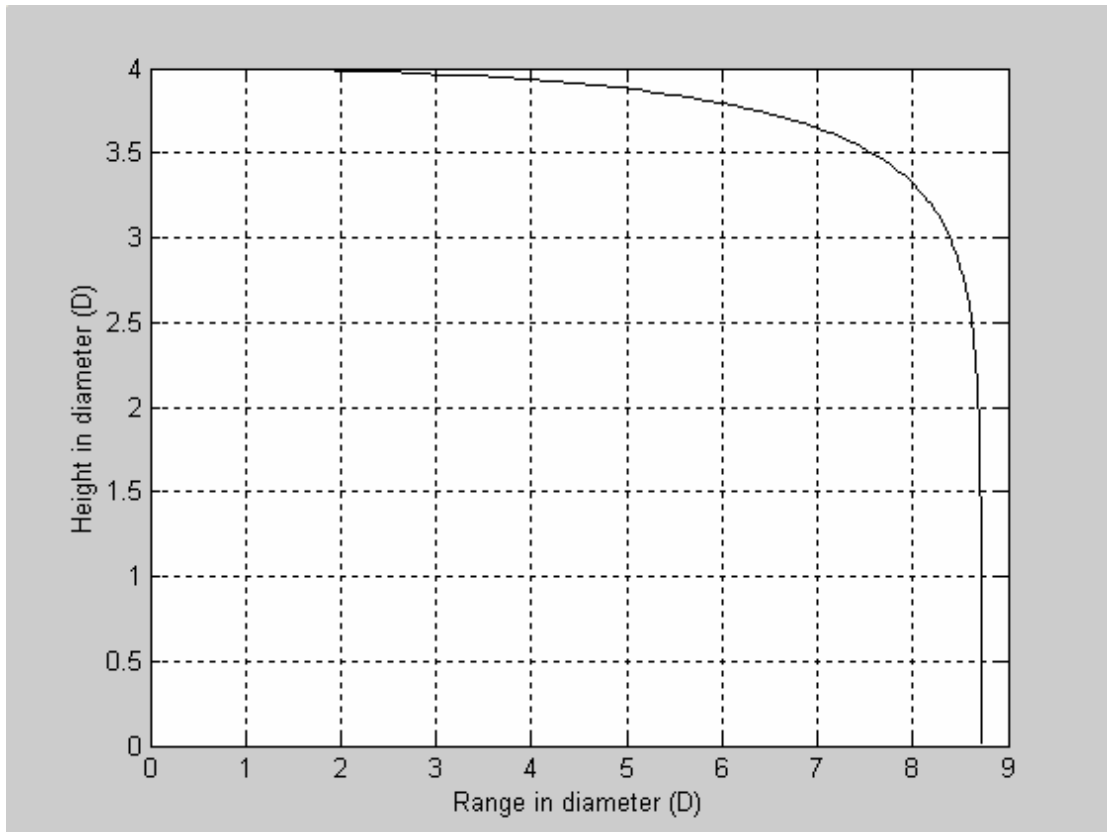


Figure 7.52 Droplet injection height in diameter versus the horizontal range in diameter for 30-inch fan (D_L) for 4-diameter in height ($h = 4D_L$)

Figure 7.53 shows the droplet temperature and air temperature versus the horizontal range for this fan. The figure indicates the history of air temperature along the range, and it shows the minimum air temperature occurs at the distance of 6.5 m, where the droplets hits the ground of about 33.5 °C. In addition, it demonstrates the history of droplet temperature along the horizontal range, and it shows the terminal droplet temperature of about 31.9 °C.

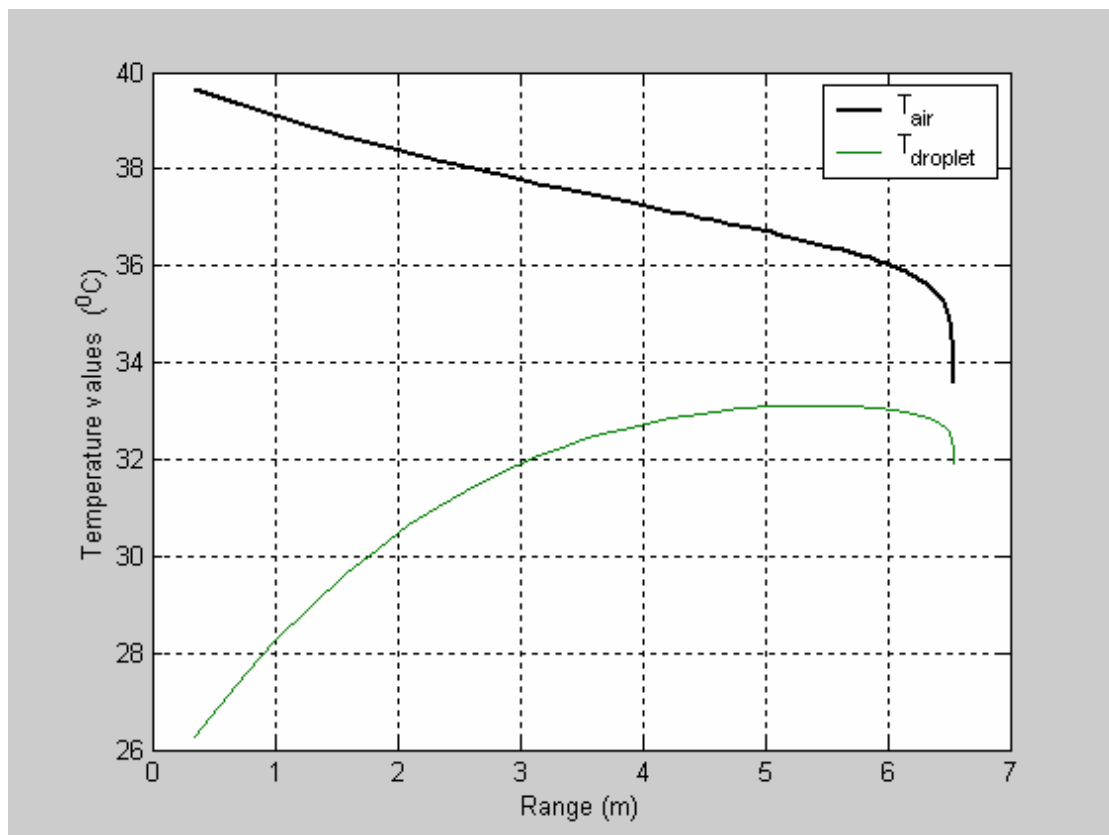


Figure 7.53 Droplet and air temperatures versus the horizontal range for 30-inch fan (D_L) for 4-diameter in height ($h = 4D_L$)

Figure 7.54 expresses the same observations as figure 7.53, but in terms of diameter for horizontal range. Such that, the figure indicates the history of air temperature along the range in diameter, and it shows the minimum air temperature occurs at the distance of $8.7 D_L$, where the droplets hits the ground of about of 33.5°C . In addition, it demonstrates the history of droplet temperature along the horizontal range, and it shows the terminal droplet temperature of about 31.9°C .

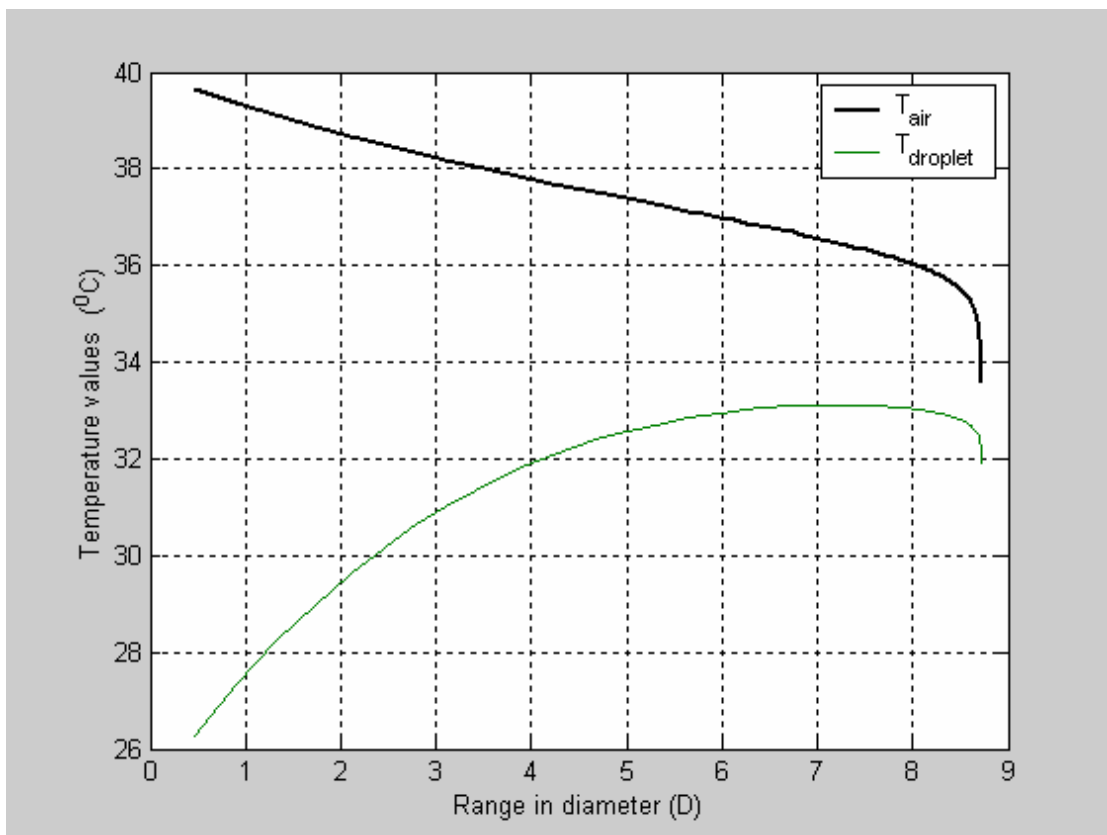


Figure 7.54 Droplet and air temperatures versus the horizontal range in diameter for 30-inch fan (D_L) for 4-diameter in height ($h = 4D_L$)

7.5.1 Angle Effect of 30-inch Fan (computational)

The experimental angle effect case of 30-inch fan is simulated here computationally. In this configuration, the fan is angled for two positions ($\theta_1 = 26.56^\circ$, $\theta_2 = 45^\circ$) as shown in figure 7.11.

In this case, the program is run for the same condition as the normal case except the velocity which is dropped by a value of $(\cos \theta)$ due the fan deflection, such that $V_1 = 35.99 \cos (\theta_1)$ & $V_2 = 35.99 \cos (\theta_2)$.

7.5.1.1 $\theta_1 = 26.56^\circ$

Figure 7.55 indicates the history of air temperature and droplet temperature versus time for the first angle ($\theta_1 = 26.56^\circ$). It demonstrates the behavior of the air temperature which starts from the initial value ($T_a = 40^\circ\text{C}$) and keeps dropping to final value of about 33.5°C , the same as in the default case ($\theta_0 = 0^\circ$). The figure also demonstrates the behavior of the droplet temperature which starts from the initial value ($T_p = 25^\circ\text{C}$) and keeps dropping to final value of terminal droplet temperature of about 31.9°C , which is very close to thermodynamic wet bulb temperature ($T_{\text{wet}} = 31.5$), the same as in the default case ($\theta_0 = 0^\circ$) too.

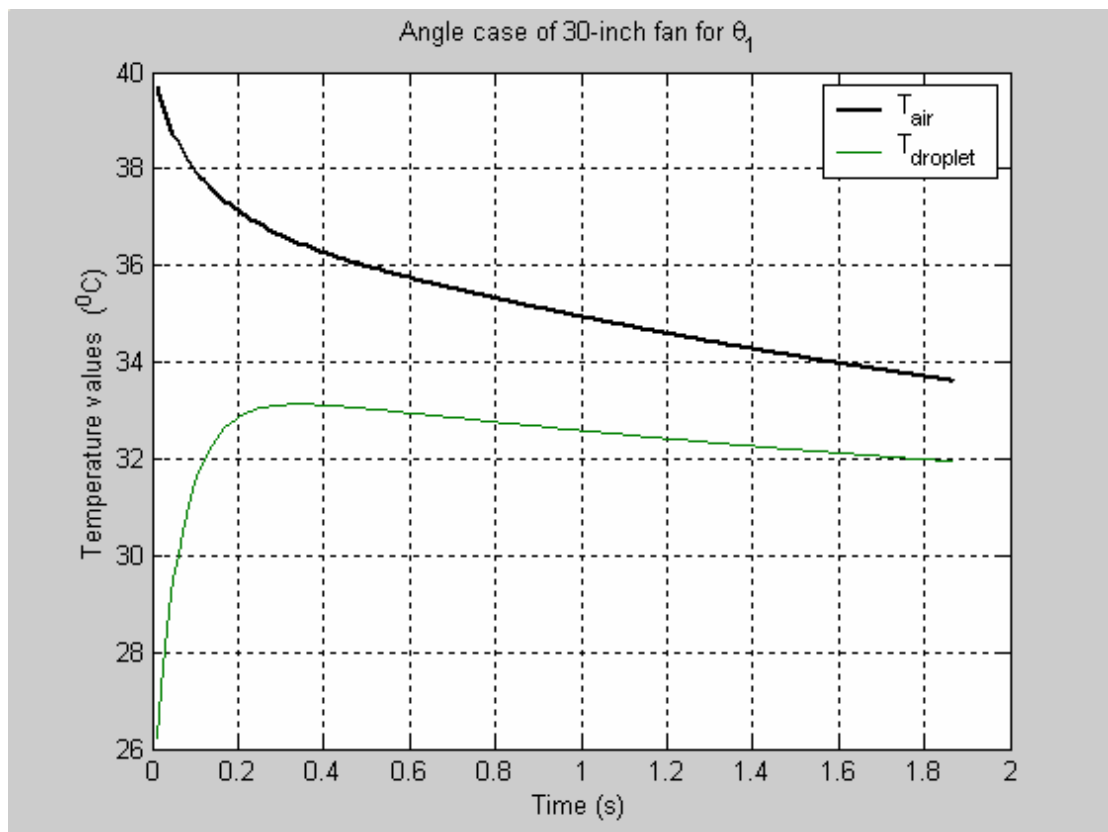


Figure 7.55 Droplet and air temperatures versus time of angle case ($\theta_1 = 26.56^\circ$) for 30-inch fan (D_L)

Figure 7.56 shows the maximum horizontal range of the droplet of about 5.8 m for the first angle ($\theta_1 = 26.56^\circ$), which is equivalent to about 7.8 D_L as demonstrated in figure 7.57.

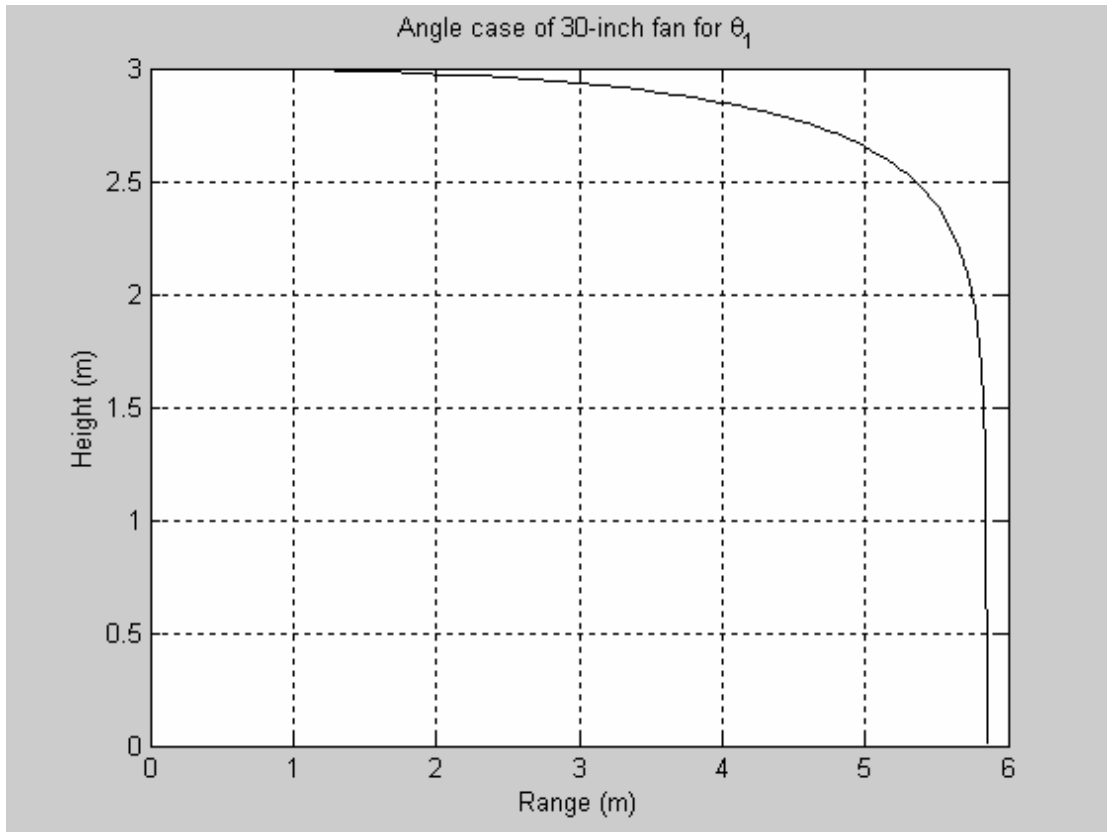


Figure 7.56 Droplet injection height versus the horizontal range of angle case ($\theta_1 = 26.56^\circ$) for 30-inch fan (D_L)

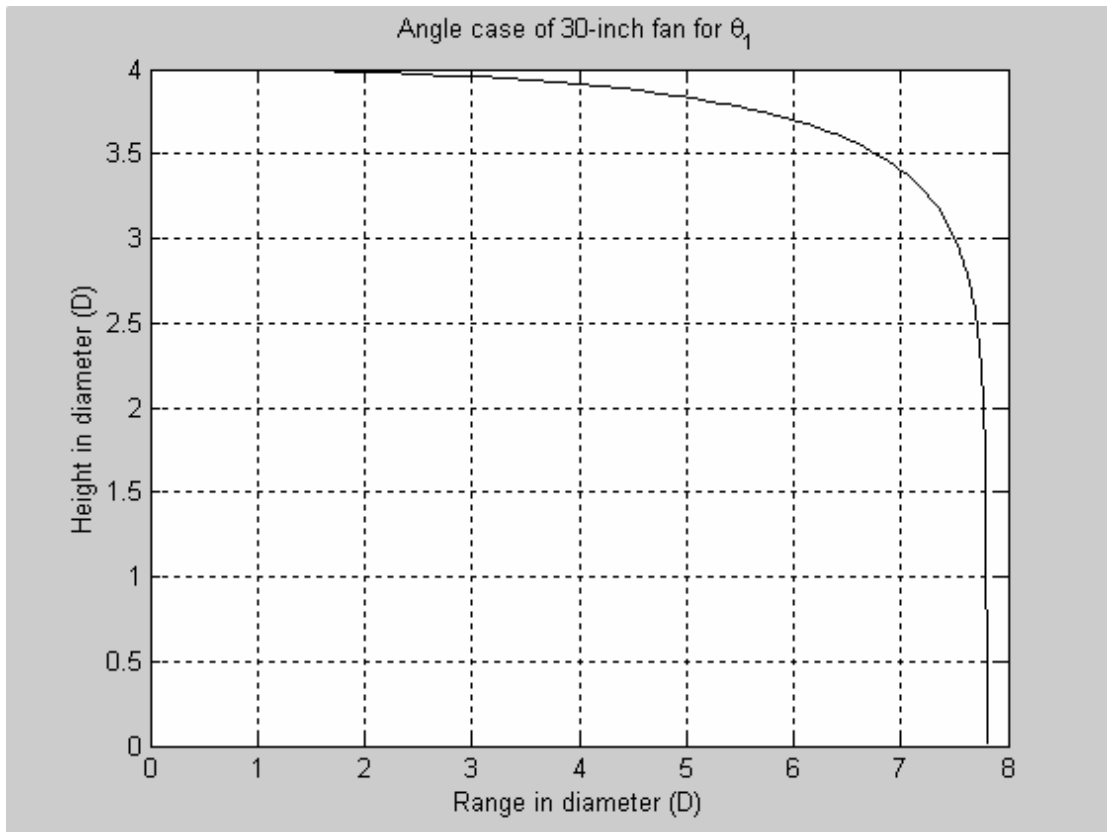


Figure 7.57 Droplet injection height in diameter versus the horizontal range in diameter of angle case ($\theta_1 = 26.56^\circ$) for 30-inch fan (D_L)

Figure 7.58 shows the droplet temperature and air temperature versus the horizontal range for the first angle ($\theta_1 = 26.56^\circ$). The figure indicates the history of air temperature along the range, and it shows the minimum air temperature occurs at the distance of 5.8 m, where the droplets hits the ground of about of 33.5°C . In addition, it demonstrates the history of droplet temperature along the horizontal range, and it shows the terminal droplet temperature of about 31.9°C .

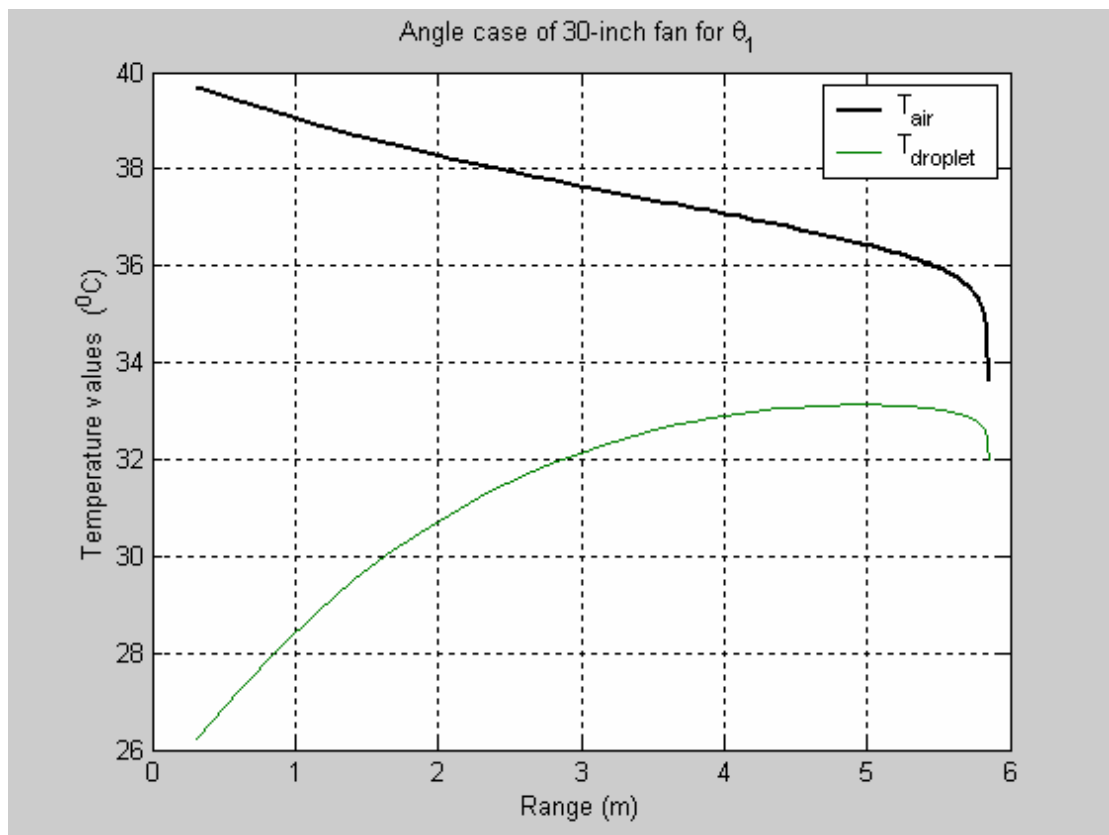


Figure 7.58 Droplet and air temperatures versus the horizontal range of angle case ($\theta_1 = 26.56^\circ$) for 30-inch fan (D_L)

Figure 7.59 expresses the same observations as figure 7.58, but in terms of diameter for horizontal range for the first angle ($\theta_1 = 26.56^\circ$). Such that, the figure indicates the history of air temperature along the range in diameter, and it shows the minimum air temperature occurs at the distance of $7.8 D_L$, where the droplets hits the ground of about of 33.5°C . In addition, it demonstrates the history of droplet temperature along the horizontal range, and it shows the terminal droplet temperature of about 31.9°C .

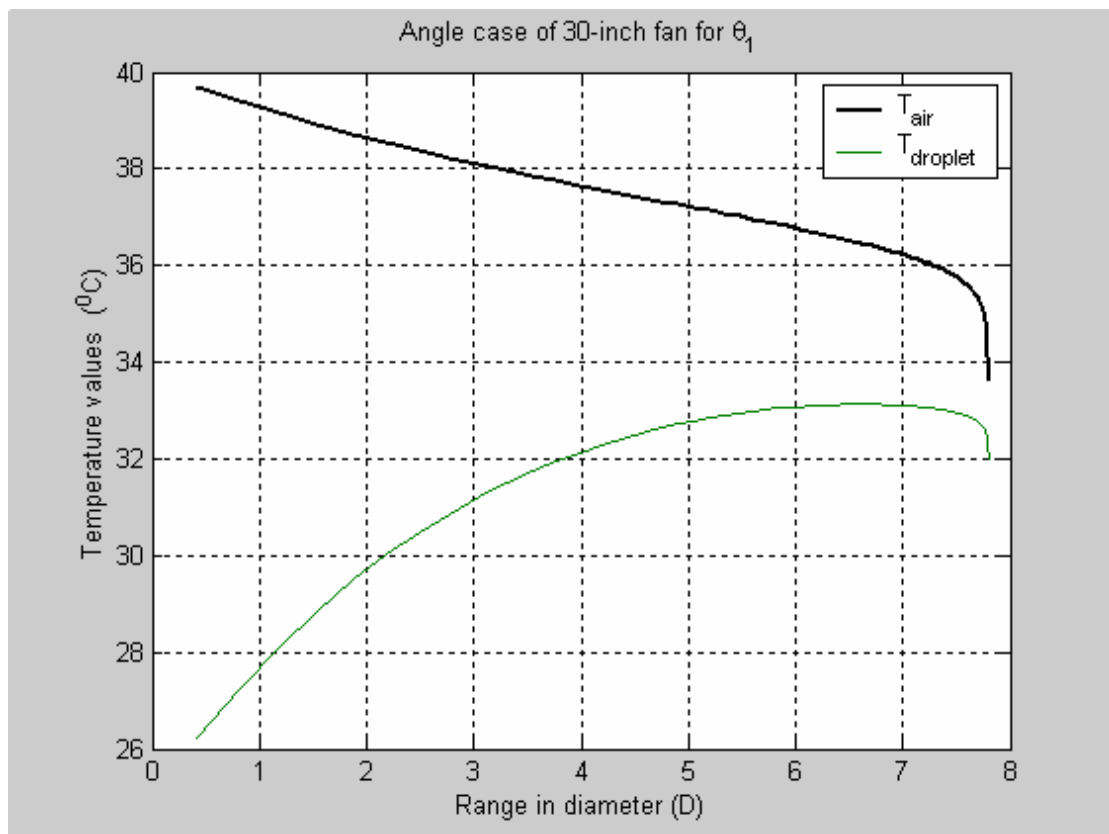


Figure 7.59 Droplet and air temperatures versus the horizontal range in diameter of angle case ($\theta_1 = 26.56^\circ$) for 30-inch fan (D_L)

7.5.1.2 $\theta_2 = 45^\circ$

Figure 7.60 indicates the history of air temperature and droplet temperature versus time for the second angle ($\theta_2 = 45^\circ$). It demonstrates the behavior of the air temperature which starts from the initial value ($T_a = 40^\circ\text{C}$) and keeps dropping to final value of about 33.8°C , almost the same as in the default case ($\theta_0 = 0^\circ$). The figure also demonstrates the behavior of the droplet temperature which starts from the initial value ($T_p = 25^\circ\text{C}$) and keeps dropping to final value of terminal droplet temperature of about 32.1°C , which is very close to thermodynamic wet bulb temperature of about 31.5°C , the same as in the default case ($\theta_0 = 0^\circ$) too.

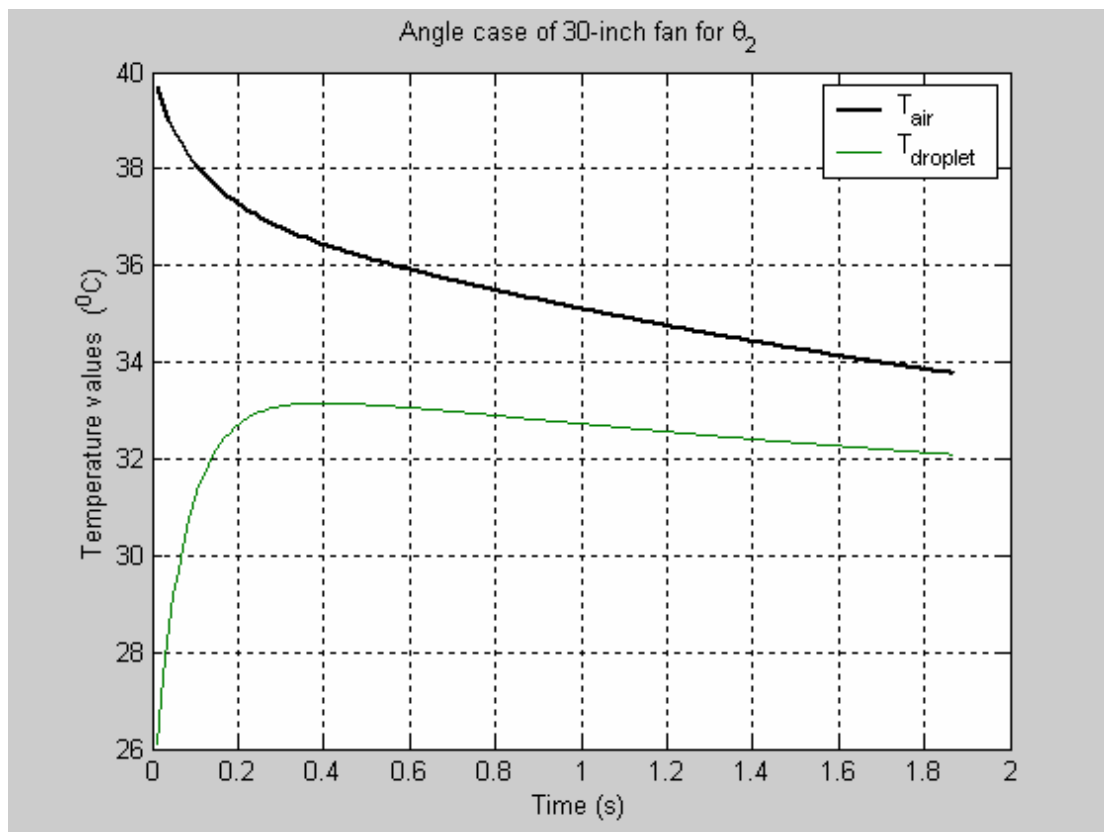


Figure 7.60 Droplet and air temperatures versus time of angle case ($\theta_2 = 45^\circ$) for 30-inch fan (D_L)

Figure 7.61 shows the maximum horizontal range of the droplet of about 4.6 m for the second angle ($\theta_2 = 45^\circ$), which is equivalent to about $6.2 D_L$ as demonstrated in figure 7.62.

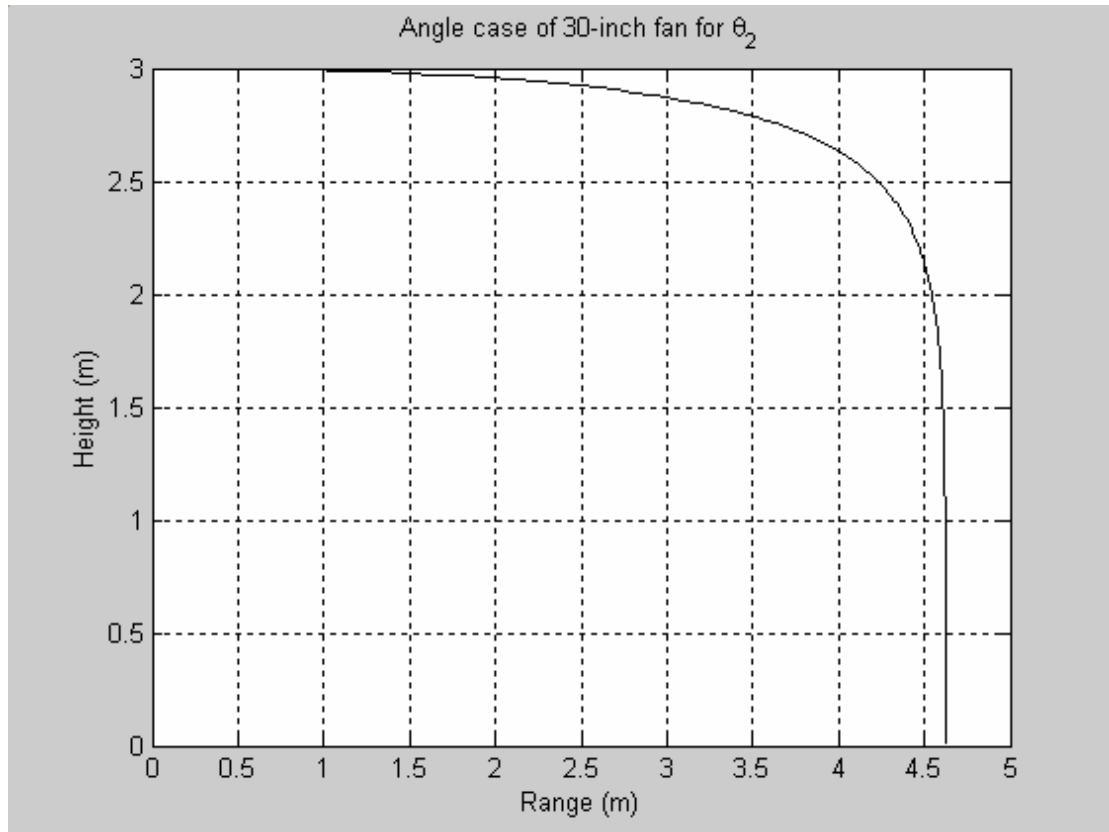


Figure 7.61 Droplet injection height versus the horizontal range of angle case ($\theta_2 = 45^\circ$) for 30-inch fan (D_L)

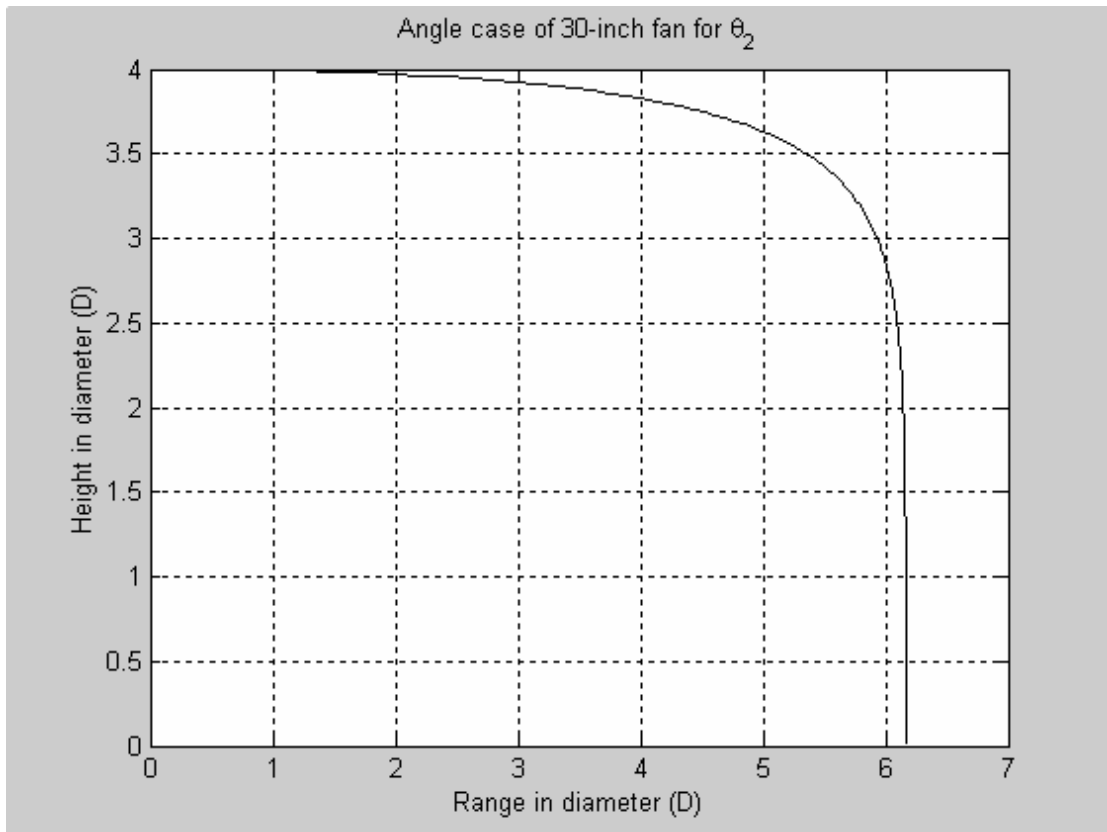


Figure 7.62 Droplet injection height in diameter versus the horizontal range in diameter of angle case ($\theta_2 = 45^\circ$) for 30-inch fan (D_L)

Figure 7.63 shows the droplet temperature and air temperature versus the horizontal range for the second angle ($\theta_2 = 45^\circ$). The figure indicates the history of air temperature along the range, and it shows the minimum air temperature occurs at the distance of 4.6 m, where the droplets hits the ground of about 33.8°C . In addition, it demonstrates the history of droplet temperature along the horizontal range, and it shows the terminal droplet temperature of about 32.1°C .

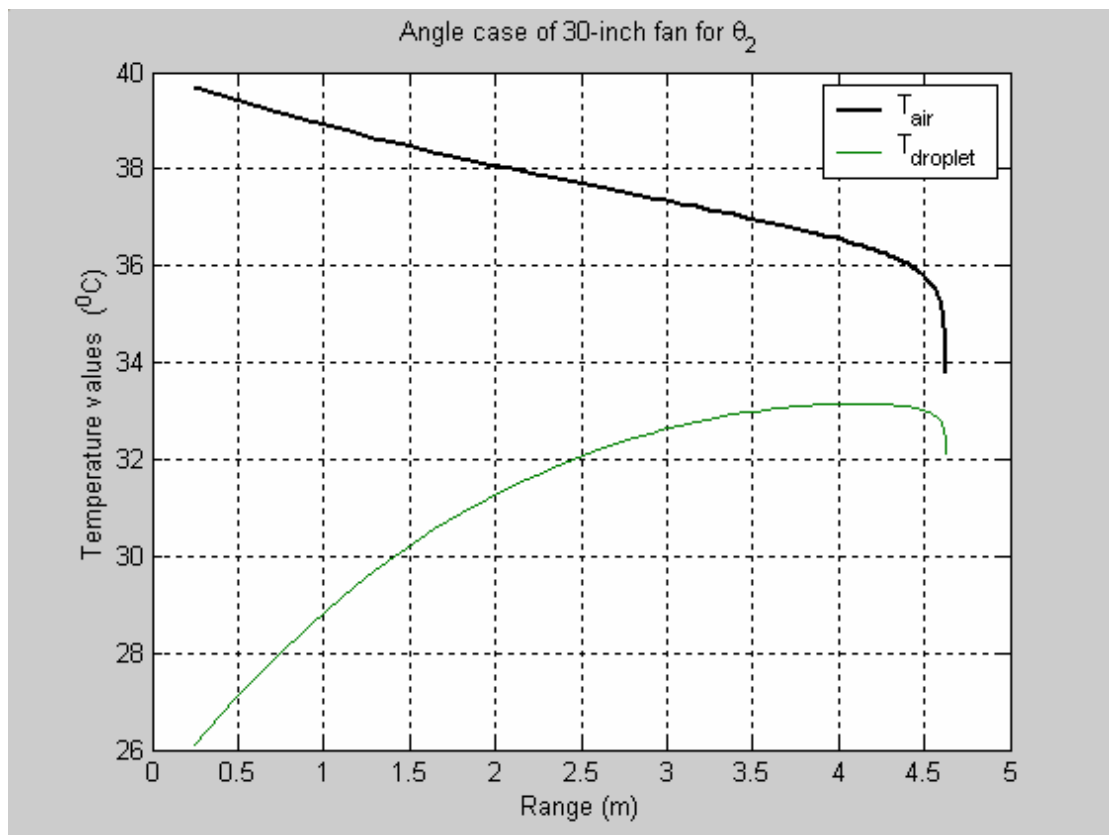


Figure 7.63 Droplet and air temperatures versus the horizontal range of angle case ($\theta_2 = 45^\circ$) for 30-inch fan (D_L)

Figure 7.64 expresses the same observations as figure 7.62, but in terms of diameter for horizontal range for the second angle ($\theta_2 = 45^\circ$). Such that, the figure indicates the history of air temperature along the range in diameter, and it shows the minimum air temperature occurs at the distance of $6.2 D_L$, where the droplets hits the ground of about of 33.8°C . In addition, it demonstrates the history of droplet temperature along the horizontal range, and it shows the terminal droplet temperature of about 32.1°C .

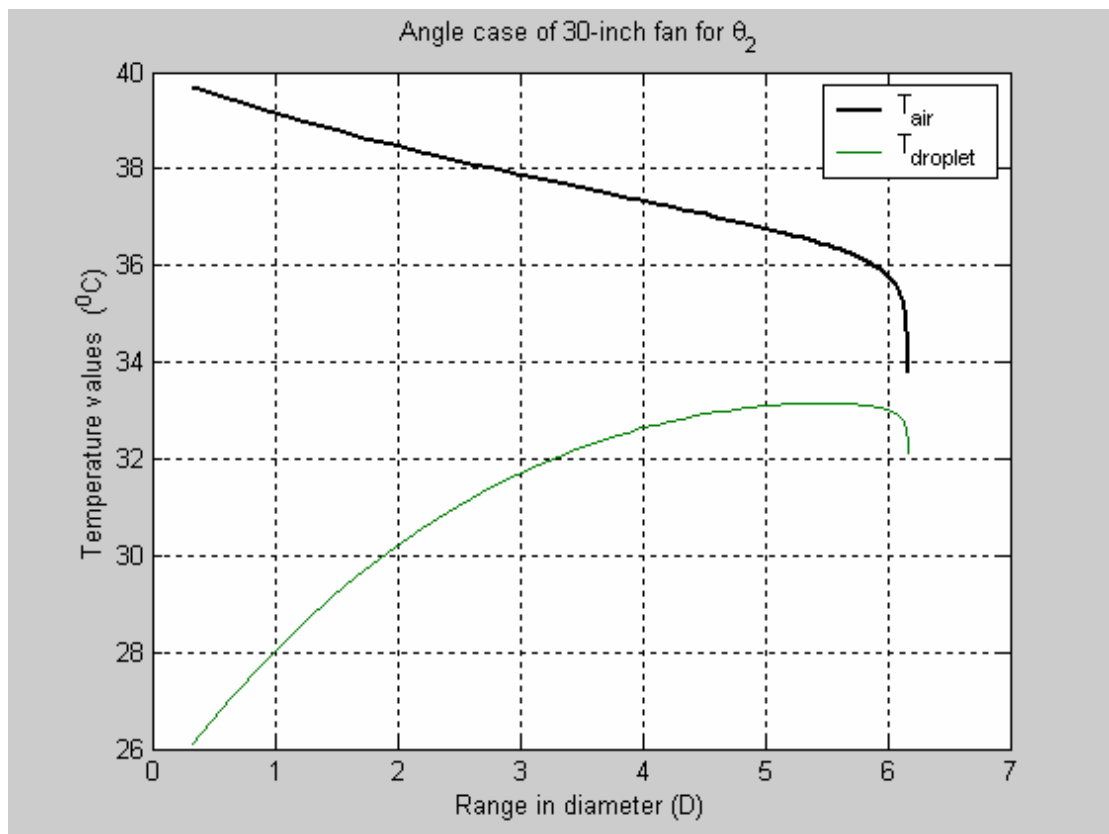


Figure 7.64 Droplet and air temperatures versus the horizontal range in diameter of angle case ($\theta_2 = 45^\circ$) for 30-inch fan (D_L)

Figure 7.65 shows the maximum horizontal range of the droplet in the angle case for different angles of the 30-inch fan angle of about 6.5 m for the default zero angle ($\theta_0 = 0^\circ$), 5.8 m for the first angle ($\theta_1 = 26.56^\circ$), and 4.6 m for the second angle ($\theta_2 = 45^\circ$), which is equivalent to about 8.7 D_L , 7.8 D_L and 6.2 D_L respectively as demonstrated in figure 7.66.

It is observed that the maximum horizontal range is shifted backward in the first and second angle compared to the default case. For ($\theta_1 = 26.56^\circ$), the horizontal range is shifted by about 0.9 D_L backward compared to the default zero angle ($\theta_0 = 0^\circ$); and for ($\theta_2 = 45^\circ$), the horizontal range is shifted by about 1.6 D_L backward compared to the first angle ($\theta_1 = 26.56^\circ$).

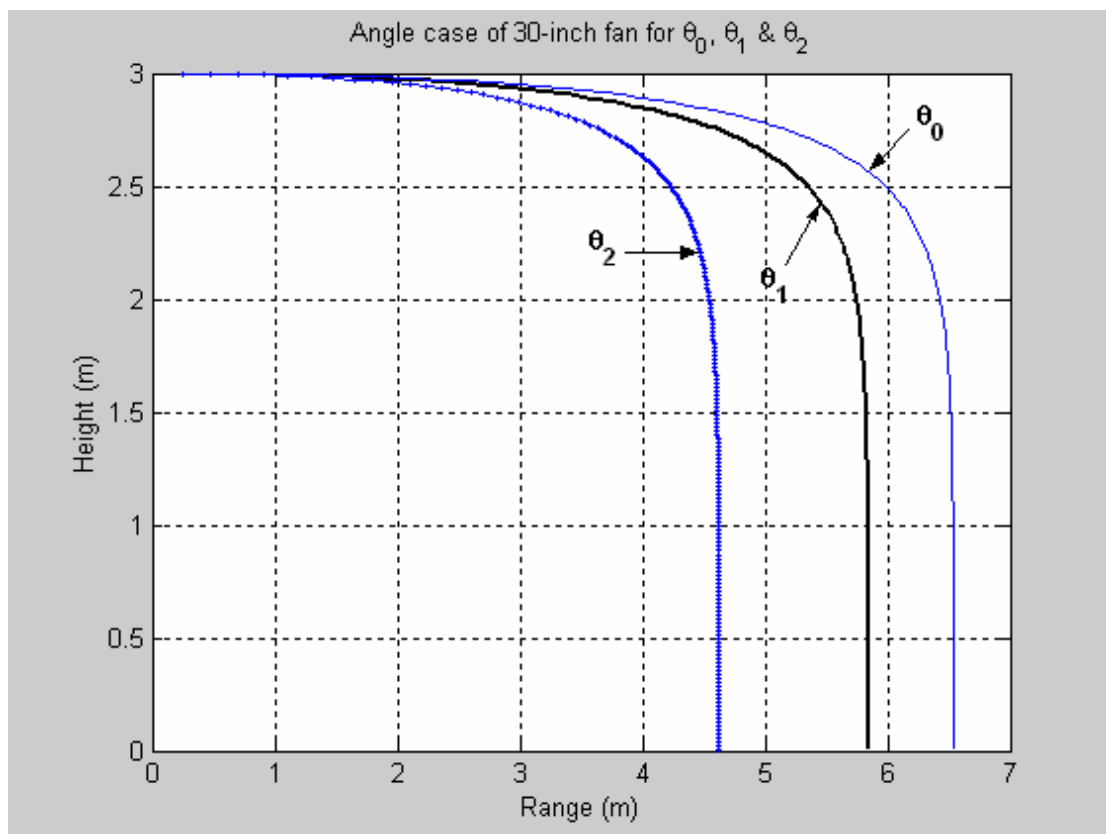


Figure 7.65 Droplet trajectories for different angles of 30-inch fan (D_L)

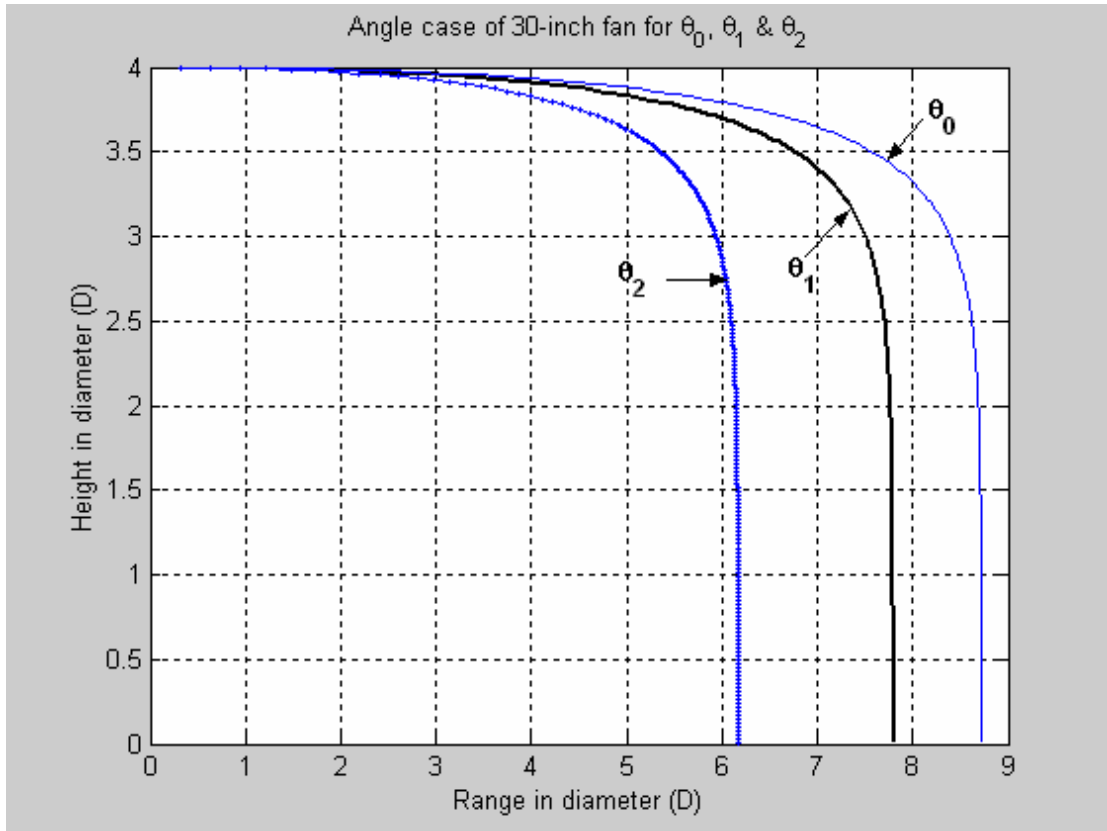


Figure 7.66 Droplet trajectories for different angles of 30-inch fan (D_L) in terms of fan diameter

7.5.2 Side-wise Investigation of 30-inch Fan (computational)

The experimental side-wise study of 30-inch fan is simulated here computationally. In the side-wise study, we are looking for specifying the maximum range of side-wise effect of the fan as shown in figure 7.24.

In this side-wise study, the program is run for the same condition as the normal case except the velocity of the fan, which is dropped by a value of $(\cos \alpha)$. Such that the droplet velocity is $V = 28 + 7.99 \cos (\alpha)$, where $(45^\circ > \alpha > 0^\circ)$.

Figure 7.67 shows the maximum side-wise range of droplet reaches about 4.5 m, which is equivalent to about $6 D_L$ side-wise as shown in figure 7.68. The maximum horizontal rang at this location is about 4.4 m, which is equivalent to about $5.9 D_L$.

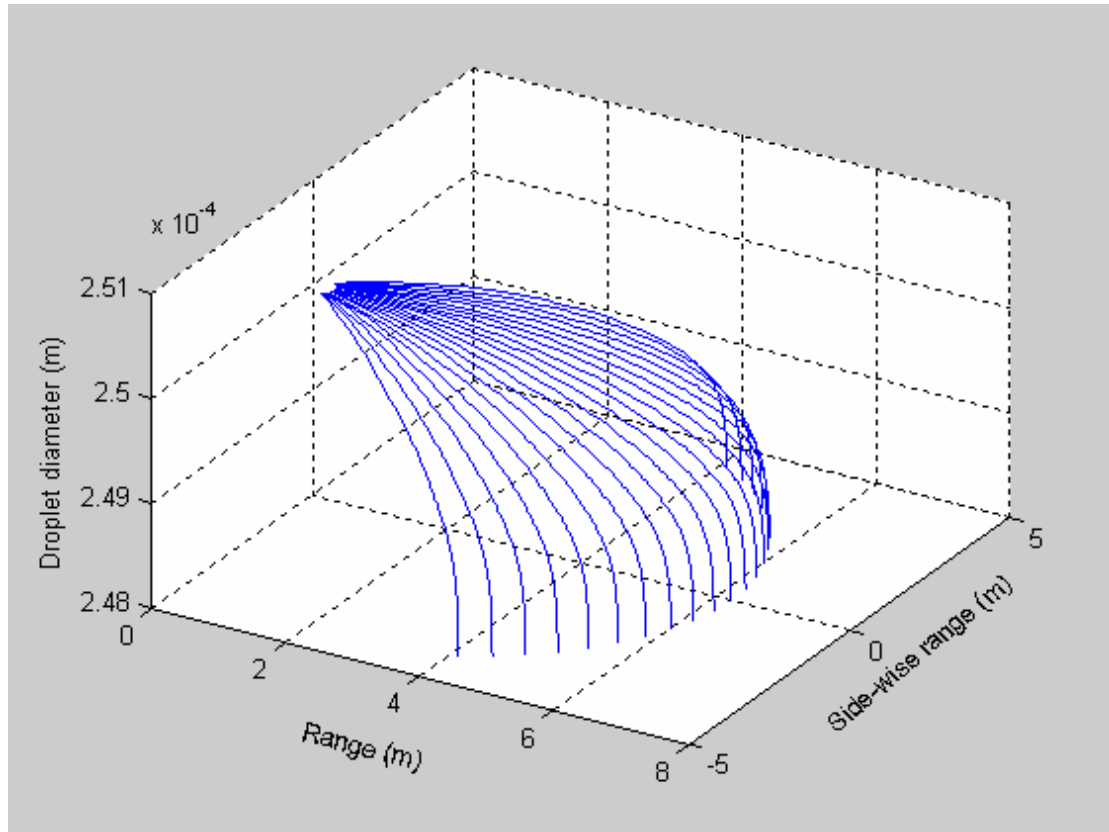


Figure 7.67 Droplet maximum side-wise range for 30-inch fan (D_L) for 4-diameter in height ($h = 4D_L$)

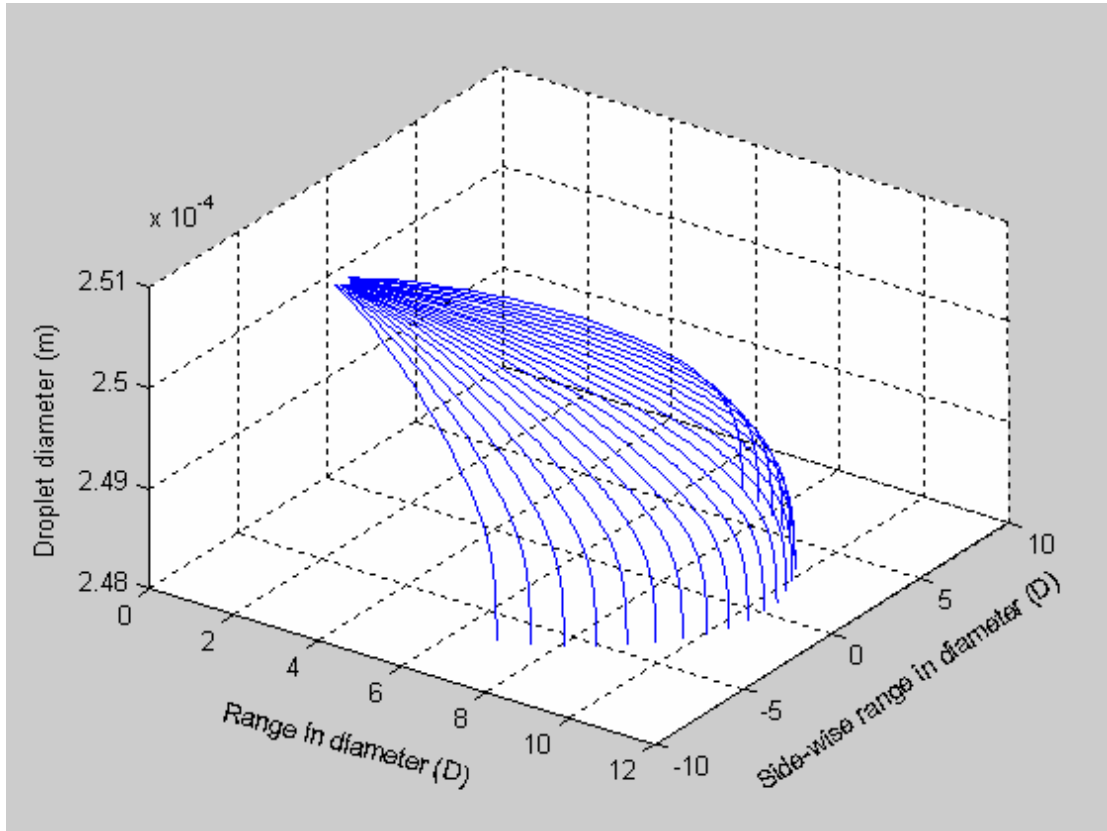


Figure 7.68 Droplet maximum side-wise range in diameter for 30-inch fan (D_L) for 4-diameter in height ($h = 4D_L$)

CHAPTER 8

RESULTS AND DISCUSSION

In this chapter, experimental with mist and computational results are analyzed and compared for the three fans to generate the relationships between the temperature domain and cooling fan diameters from one aspect and the relationship between the temperature domain and cooling fan heights from the other aspect.

8.1 Results of 20-inch Fan (D_S)

By looking generally to the results of 20-inch fan presented for individual cases in previous chapters, a very good agreement is observed between the experimental results and computational results, which gives an indication of well chosen assumptions proposed for the computational solution.

Figure 8.1 shows an agreement on the temperature behavior of the experimental and the computational results of the 20-inch fan, and the following observations are concluded.

- The location of the minimum temperature is almost the same for both experimental and computational. The experimental minimum temperature occurs at the 11th diameter front-wise ($11 D_S$) of about 32.5 °C which is very close to the calculated wet bulb temperature; while the computational minimum temperature occurs exactly at the 11.6th diameter front-wise ($11.6 D_S$) of about 34.4 °C, which shows well agreement between the experimental and the computational.

- There are some experimental temperature values differ from their corresponding computational values for the same diameter, basically that doesn't mean disagreement since the computational indicates the air temperatures around the water droplet in different stages while flying in air till it hits the ground; while the experimental indicates the surrounding air temperatures measured after some time after the steady state is reached. That demonstrates why we get closer air temperature values in the experimental to the wet bulb temperature and not in the computational case.
- The minimum computational temperature is about 34.4°C , which is a little bit different from the expected wet bulb temperature of about 31.5°C . that's indicates that the water droplet hits the ground before it evaporates completely, which was observed in figure 7.4.
- The 20-inch fan maximum range with respect to temperature is reached at the 18^{th} diameter ($18 D_S$) at height of 4 diameter ($h = 4 D_S$) experimentally.

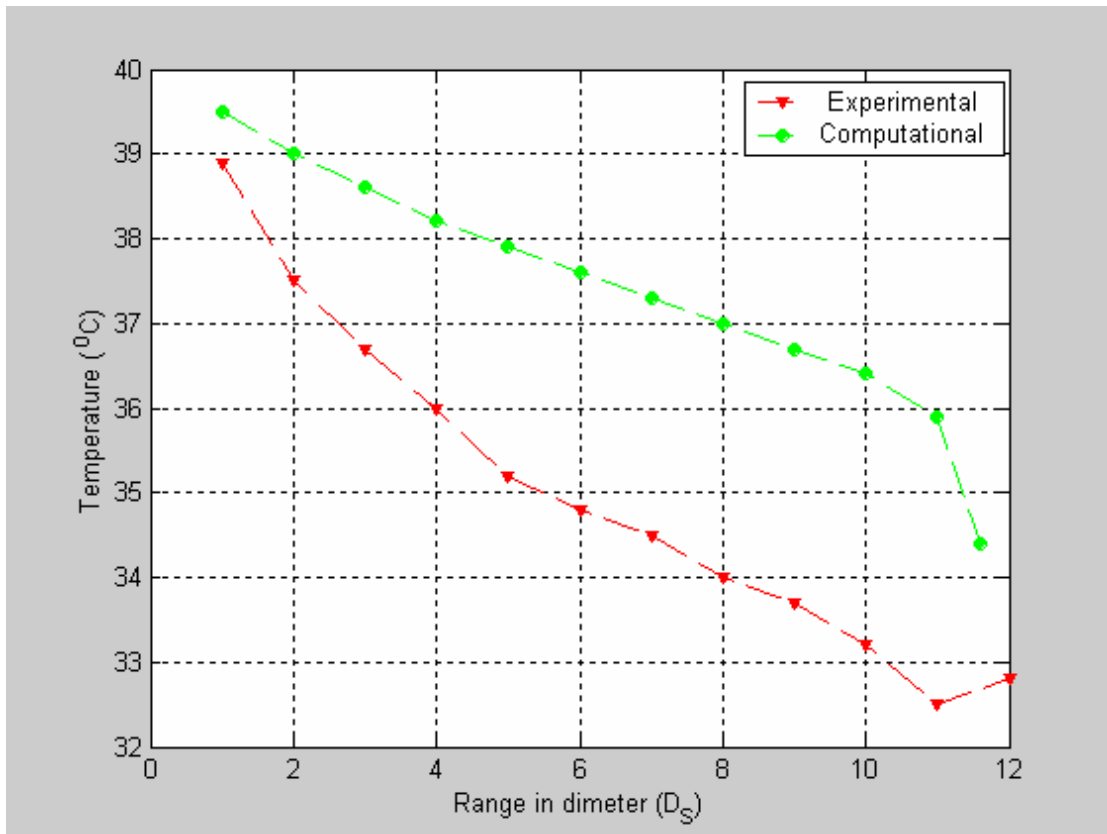


Figure 8.1 Temperature ($^{\circ}C$) VS distance in diameter (D_S), for the small fan (D_S), for 4-diameter in height ($h = 4D_S$)

By looking at figures 6.47 and 7.22 and comparing them, they show a good agreement of the experimental and the computational results for angle effect case investigation of the 20-inch fan, and the following observations are concluded.

- The minimum computational temperature location occurs at of about 5.81 m for the default zero angle ($\theta_0 = 0^\circ$), 5.2 m for the first angle ($\theta_1 = 26.56^\circ$), and 4.1 m for the second angle ($\theta_2 = 45^\circ$), which is equivalent to about 11.6 D_S , 10.4 D_S and 8.2 D_S respectively. In the experimental result, the minimum temperature location occurs at of about 10 D_S m for the default zero angle ($\theta_0 = 0^\circ$), 9 D_S for the first angle ($\theta_1 = 26.56^\circ$), and 8 D_S for the second angle ($\theta_2 = 45^\circ$). That indicates good matching.
- It is observed that the minimum computational temperature location is shifted backward in the first angle by about 1.2 D_S compared to the default case, and it is shifted in the second angle compared to the default case by 3.4 D_S . In the experimental, a similar regime behavior happens such that, the minimum experimental temperature location is shifted backward in the first angle by 1 D_S compared to the default case, and it is shifted in the second angle compared to the default case by 2 D_S . The small difference between the computational and the experimental is maybe due to the wind effect in the location of the experiments.
- The 20-inch fan maximum range with respect to temperature is reached at the 16th diameter (16 D_S) for angle ($\theta_1 = 26.56^\circ$) experimentally.

- The 20-inch fan maximum range with respect to temperature is reached at the 14th diameter (14 D_s) for angle ($\theta_2 = 45^\circ$) experimentally.
- As expected, a little more drop in the temperature values occurs in the area close to the fan when it is angled down motivating the evaporation process in that area, but a shrinking in the temperature range happens as a penalty of that.

By looking at figures 6.49 and 7.25 and comparing them, they show a good agreement of the experimental and the computational results for side-wise case investigation of the 20-inch fan, and the following observations are concluded.

- The maximum side-wise range of droplet reaches about 4 m, which is equivalent to about $8 D_S$ side-wise computationally. While the maximum side-wise range in the experiment reaches about $8 D_S$ side-wise, this indicates identical results of both computational and experimental.

8.2 Results of 24-inch Fan

By looking generally to the results of 24-inch fan presented for individual cases in previous chapters, a very good agreement is observed between the experimental results and computational results, which gives an indication of well chosen assumptions proposed for the computational solution.

Figure 8.2 shows an agreement on the temperature behavior of the experimental and the computational results of the 24-inch fan, and the following observations are concluded.

- The location of the minimum temperature is almost the same for both experimental and computational. The experimental minimum temperature occurs at the 10th diameter front-wise (10 D_m) of about 31.8 °C which is very close to the calculated wet bulb temperature; while the computational minimum temperature occurs exactly at the 10.4th diameter front-wise (10.4 D_m) of about 34 °C, which shows well agreement between the experimental and the computational.
- There are some experimental temperature values differ from their corresponding computational values for the same diameter, basically that doesn't mean disagreement since the computational indicates the air temperatures around the water droplet in different stages while flying in air till it hits the ground; while the experimental indicates the surrounding air temperatures measured after some time after the steady state is reached. That

demonstrates why we get closer air temperature values in the experimental to the wet bulb temperature and not in the computational case.

- The minimum computational temperature is about 34 °C, which is a little bit different from the expected wet bulb temperature of about 31.5 °C. that's indicates that the water droplet hits the ground before it evaporates completely, which was observed in figure 7.26.
- The 24-inch fan maximum range with respect to temperature is reached at the 16th diameter (16 D_m) at height of 4 diameter (h = 4 D_m) experimentally.

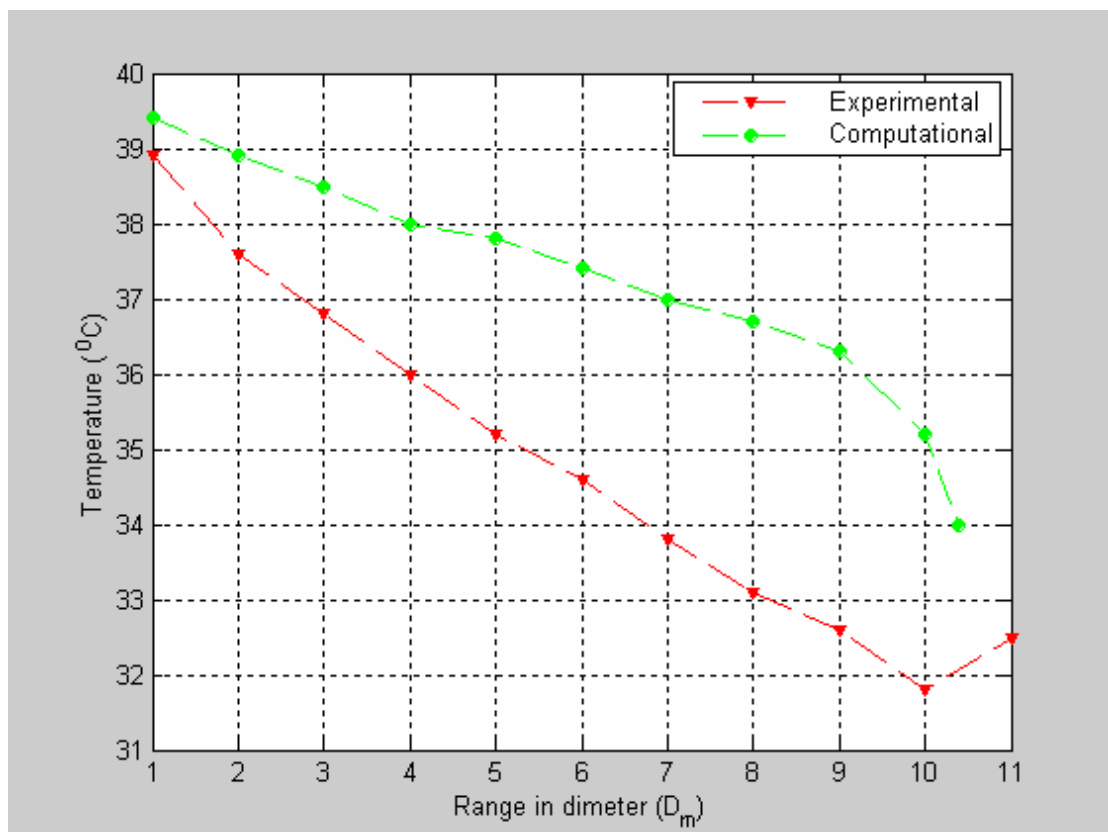


Figure 8.2 Temperature (°c) VS distance in diameter (D_m), for the medium fan (D_m), for 4-diameter in height (h = 4D_m)

By looking at figures 6.56 and 7.44 and comparing them, they show a good agreement of the experimental and the computational results for angle effect case investigation of the 24-inch fan, and the following observations are concluded.

- The minimum computational temperature location occurs at of about 6.2 m for the default zero angle ($\theta_0 = 0^\circ$), 5.6 m for the first angle ($\theta_1 = 26.56^\circ$), and 4.4 m for the second angle ($\theta_2 = 45^\circ$), which is equivalent to about 10.4 D_m , 9.3 D_m and 7.3 D_m respectively. In the experimental result, the minimum temperature location occurs at about 9 D_m m for the default zero angle ($\theta_0 = 0^\circ$), 8 D_m for the first angle ($\theta_1 = 26.56^\circ$), and 7 D_m for the second angle ($\theta_2 = 45^\circ$). That indicates good matching.
- It is observed that the minimum computational temperature location is shifted backward in the first angle by about 1.1 D_m compared to the default case, and it is shifted in the second angle compared to the default case by 3.1 D_m . In the experimental, a similar regime behavior happens such that, the minimum experimental temperature location is shifted backward in the first angle by 1 D_m compared to the default case, and it is shifted in the second angle compared to the default case by 2 D_m . The small difference between the computational and the experimental is maybe due to the wind effect in the location of the experiments.
- The 24-inch fan maximum range with respect to temperature is reached at the 12th diameter (12 D_m) for angle ($\theta_1 = 26.56^\circ$) experimentally.

- The 24-inch fan maximum range with respect to temperature is reached at the 10th diameter (10 D_m) for angle ($\theta_2 = 45^\circ$) experimentally.
- As expected, a little more drop in the temperature values occurs in the area close to the fan when it is angled down motivating the evaporation process in that area, but a shrinking in the temperature range happens as a penalty of that.

By looking at figures 6.57 and 7.46 and comparing them, they show a good agreement of the experimental and the computational results for side-wise case investigation of the 24-inch fan, and the following observations are concluded.

- The maximum side-wise range of droplet reaches about 4.3 m, which is equivalent to about 7.2 D_m side-wise computationally. While the maximum side-wise range in the experiment reaches about 7 D_m side-wise, this indicates almost identical results of both computational and experimental.

8.3 Results of 30-inch Fan

By looking generally to the results of 30-inch fan presented for individual cases in previous chapters, a very good agreement is observed between the experimental results and computational results, which gives an indication of well chosen assumptions proposed for the computational solution.

Figure 8.3 shows an agreement on the temperature behavior of the experimental and the computational results of the 30-inch fan, and the following observations are concluded.

- The location of the minimum temperature is almost the same for both experimental and computational. The experimental minimum temperature occurs at the 9th diameter front-wise (9 D_L) of about 31.7 °C which is very close to the calculated wet bulb temperature; while the computational minimum temperature occurs exactly at the 8.7th diameter front-wise (8.7 D_L) of about 33.9 °C, which shows well agreement between the experimental and the computational.
- There are some experimental temperature values differ from their corresponding computational values for the same diameter, basically that doesn't mean disagreement since the computational indicates the air temperatures around the water droplet in different stages while flying in air till it hits the ground; while the experimental indicates the surrounding air temperatures measured after some time after the steady state is reached. That demonstrates why we get closer air temperature values in the experimental to the wet bulb temperature and not in the computational case.

- The minimum computational temperature is about 33.9 °C, which is a little bit different from the expected wet bulb temperature of about 31.5 °C. that's indicates that the water droplet hits the ground before it evaporates completely, which was observed in figure 7.47.
- The 24-inch fan maximum range with respect to temperature is reached at the 14th diameter (14 D_L) at height of 4 diameter ($h = 4 D_L$) experimentally.

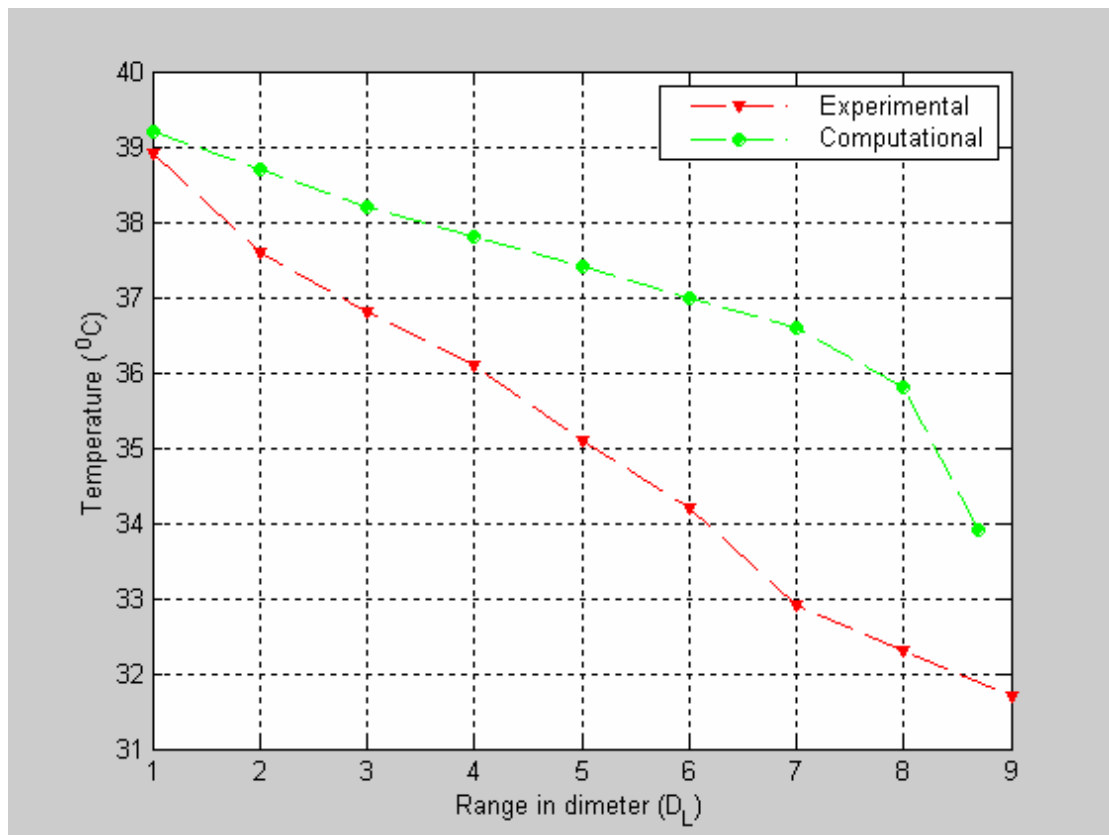


Figure 8.3 Temperature (°c) VS distance in diameter (D_L), for the big fan (D_L), for 4-diameter in height ($h = 4D_L$)

By looking at figures 6.64 and 7.65 and comparing them, they show a good agreement of the experimental and the computational results for angle effect case investigation of the 30-inch fan, and the following observations are concluded.

- The minimum computational temperature location occurs at of about 6.5 m for the default zero angle ($\theta_0 = 0^\circ$), 5.8 m for the first angle ($\theta_1 = 26.56^\circ$), and 4.6 m for the second angle ($\theta_2 = 45^\circ$), which is equivalent to about 8.7 D_L , 7.8 D_L and 6.2 D_L respectively. In the experimental result, the minimum temperature location occurs at about 8 D_L m for the default zero angle ($\theta_0 = 0^\circ$), 7 D_L for the first angle ($\theta_1 = 26.56^\circ$), and 6 D_L for the second angle ($\theta_2 = 45^\circ$). That indicates good matching.
- It is observed that the minimum computational temperature location is shifted backward in the first angle by about 0.9 D_L compared to the default case, and it is shifted in the second angle compared to the default case by 2.1 D_L . In the experimental, a similar regime behavior happens such that, the minimum experimental temperature location is shifted backward in the first angle by 1 D_L compared to the default case, and it is shifted in the second angle compared to the default case by 2 D_L . The small difference between the computational and the experimental is maybe due to the wind effect in the location of the experiments.
- The 30-inch fan maximum range with respect to temperature is reached at the 11th diameter (11 D_L) for angle ($\theta_1 = 26.56^\circ$) experimentally.

- The 30-inch fan maximum range with respect to temperature is reached at the 10th diameter (10 D_L) for angle ($\theta_2 = 45^\circ$) experimentally.
- As expected, a little more drop in the temperature values occurs in the area close to the fan when it is angled down motivating the evaporation process in that area, but a shrinking in the temperature range happens as a penalty of that.

By looking at figures 6.65 and 7.66 and comparing them, they show a good agreement of the experimental and the computational results for side-wise case investigation of the 30-inch fan, and the following observations are concluded.

- The maximum side-wise range of droplet reaches about 4.5 m, which is equivalent to about $6 D_L$ side-wise computationally. While the maximum side-wise range in the experiment reaches about $6 D_L$ side-wise, this indicates identical results of both computational and experimental.

8.4 Relationships and Concluded Remarks of the Three Fans

By looking to the results of three fans previously, the following is concluded:

- The maximum temperature range occurs at the 4th diameter level for each fan, which was investigated experimentally.
- In the lower levels, the evaporation rate is enhanced in a better manner compared to the upper levels, which indicates more evaporation since the temperature in the lower levels is closer to the calculated wet bulb temperature. However, the evaporation process might take place and get completed in the upper levels and get cooled there before the water droplets get close to the ground level where it is considered as the reference of temperature measurements.
- The experimental values and the computational values agreed well in all cases which reflects wise selected assumptions of the computational solution.
- The measured temperatures values are lower than the computed ones; that indicates not complete evaporation of water droplets when flying before it hits the ground in the computational solution. However, the measured values indicates that the evaporation process continues to take a place even when the water droplets on the ground.

- The maximum range of each fan occurs at the 4th diameter level ($h = 4D$) and it is determined by measuring the airspeed for its maximum range; and the temperature range is determined by measuring the temperature for its maximum range as shown in tables 8.1 and 8.2.

Table 8.1 Fan maximum range with respect to airspeed of the three fans

Fan type	Fan Max. range WRT airspeed (D)	Fan Max. range WRT airspeed (inch)	Fan Max. range WRT airspeed (m)
20-inch Fan (D_S)	16 D_S	320	8
24-inch Fan (D_m)	14 D_m	336	8.4
30-inch Fan (D_L)	12 D_L	360	9

Table 8.2 Fan maximum range with respect to temperature of the three fans

Fan type	Fan Max. range WRT temperature (D)	Fan Max. range WRT temperature (inch)	Fan Max. range WRT temperature (m)
20-inch Fan (D_S)	18 D_S	360	9
24-inch Fan (D_m)	16 D_m	384	9.6
30-inch Fan (D_L)	14 D_L	420	10.5

- The empirical relationship of fan maximum range with respect to fan airspeed (for fan airspeed $v \neq 0$) in normalized diameter is generated from data in figure 8.4 and formulated by equation 8.1.

$$\text{Fan Max. Range}_{\text{for airspeed} \neq 0} = 0.017(D_{\text{length}})^2 - 1.2D_{\text{length}} + 34 \dots\dots\dots(8.1)$$

The unit of fan maximum range with respect to fan airspeed (for fan airspeed $v \neq 0$) is the number of diameter, and D_{length} represents the fan diameter length in inches.

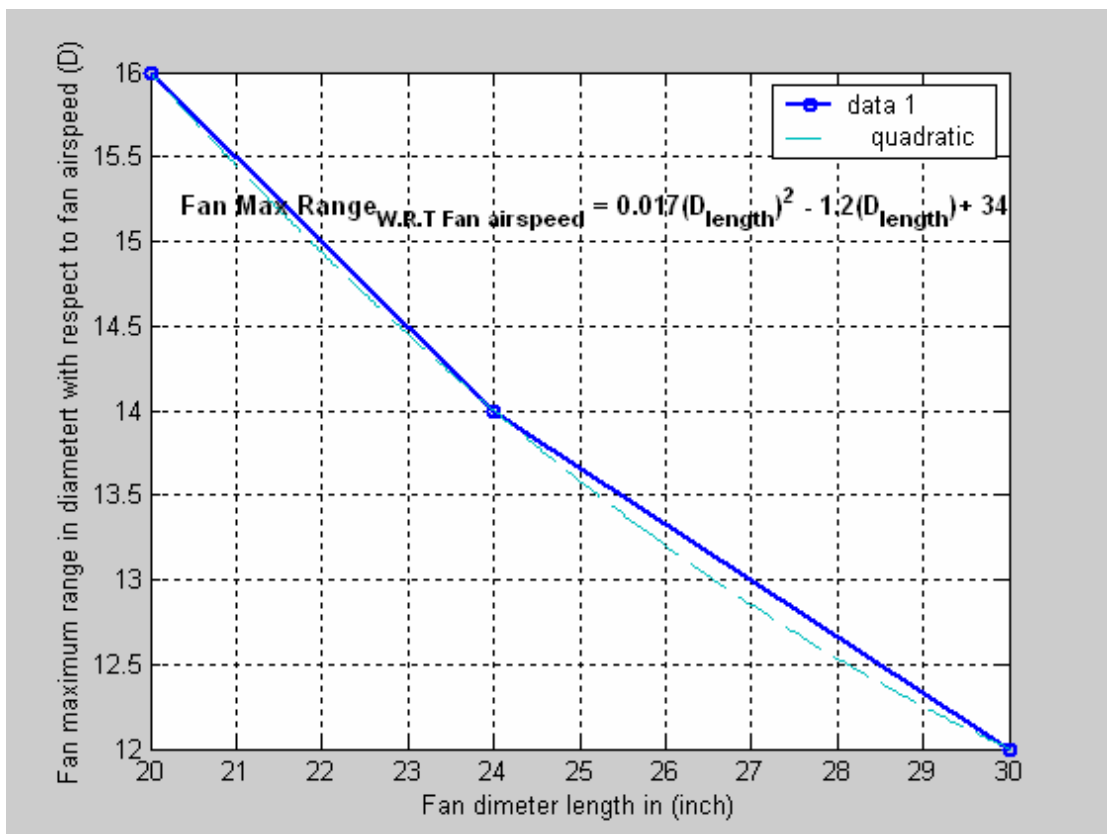


Figure 8.4 Fan maximum range with respect to fan airspeed (for fan airspeed $v \neq 0$) as a function of fan diameter

- The empirical relationship of fan maximum range with respect to temperature of a fan (for $\Delta T \neq 0$) in normalized diameter is generated from data in figure 8.5 and formulated by equation 8.2.

$$\text{Fan Max. Range}_{\text{for } \Delta T \neq 0} = 0.017 (D_{\text{length}})^2 - 1.2 D_{\text{length}} + 36 \dots\dots\dots (8.2)$$

Where:

The unit of fan maximum range with respect to temperature (for $\Delta T \neq 0$) is the number of diameter, and D_{length} represents the fan diameter length in inches.

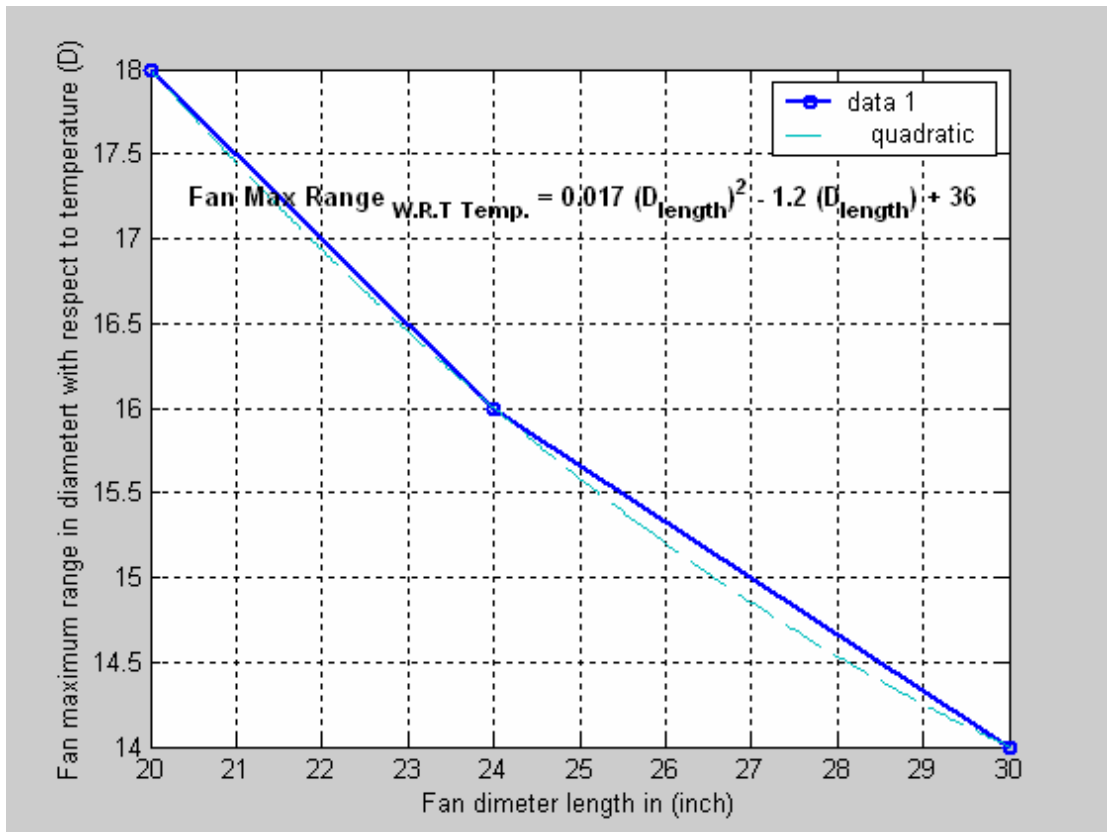


Figure 8.5 Fan maximum range with respect to temperature (for $\Delta T \neq 0$) as a function of fan diameter

- The empirical relationship of fan maximum range with respect to fan airspeed (for fan airspeed $v \neq 0$) in inches is generated from data in figure 8.6 and formulated by equation 8.3.

$$\text{Fan Max. Range}_{\text{for airspeed} \neq 0} \text{ (inches)} = -1.8 (D_{\text{length}})^2 \times 10^{-15} + 4 D_{\text{length}} + 2.4 \times 10^2 \dots\dots(8.3)$$

Where:

The unit of fan maximum range with respect to fan airspeed (for fan airspeed $v \neq 0$) is inch, and D_{length} represents the fan diameter length in inches.

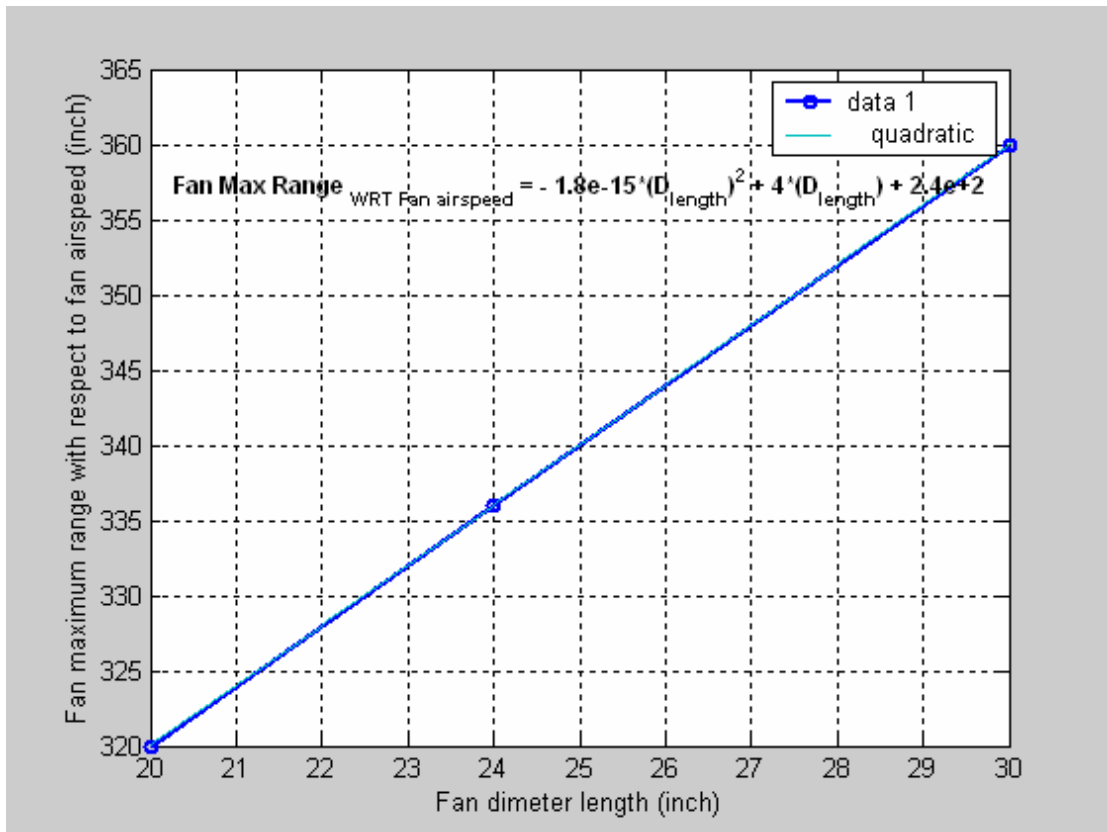


Figure 8.6 Fan maximum range with respect to fan airspeed (for fan airspeed $v \neq 0$) in inches

- The empirical relationship of fan maximum range with respect to temperature of a fan (for $\Delta T \neq 0$) in inches is generated from data in figure 8.7 and formulated by equation 8.4.

$$\text{Fan Max. Range}_{\text{for } \Delta T \neq 0} \text{ (inches)} = -5.5(D_{\text{length}})^2 \times 10^{-16} + 6 D_{\text{length}} + 2.4 \times 10^2 \dots\dots\dots(8.4)$$

Where:

The unit of fan maximum range with respect to temperature (for $\Delta T \neq 0$) is inch, and

D_{length} represents the fan diameter length in inches.

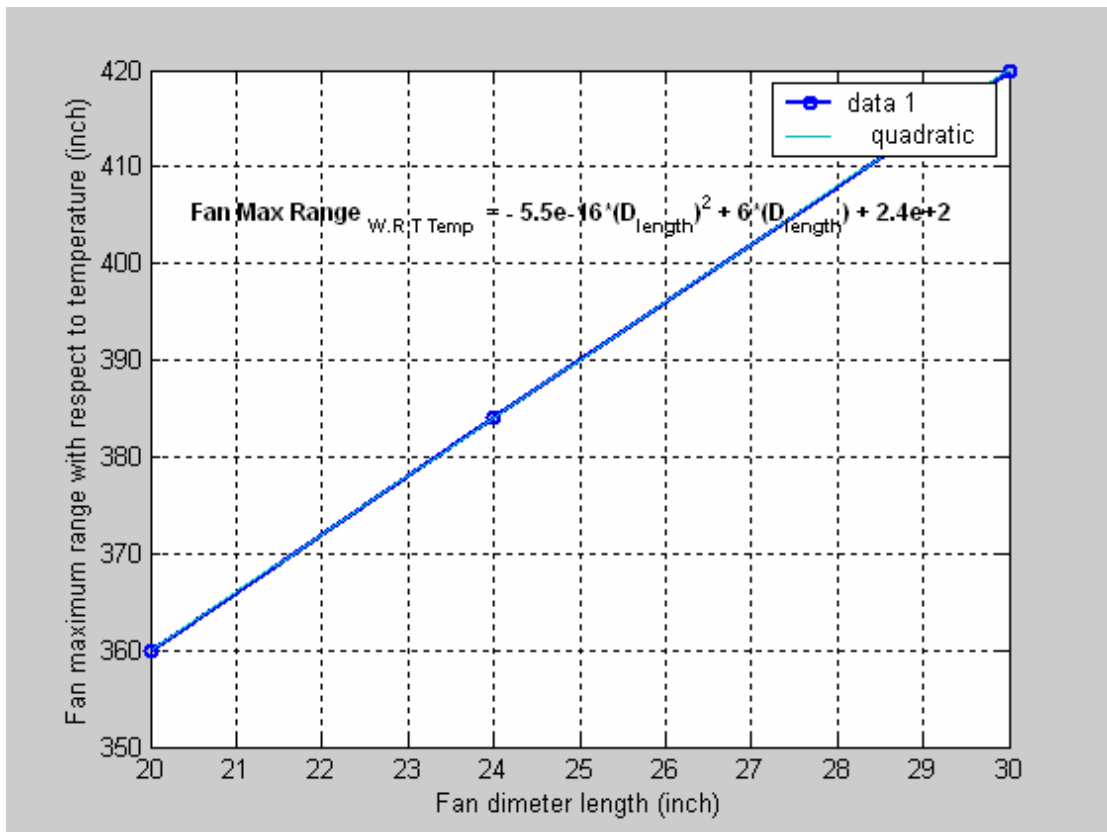


Figure 8.7 Fan maximum range with respect to temperature (for $\Delta T \neq 0$) in inches

- The mean airspeed profile of a fan range area for maximum range (at the 4th diameter level) for the same aerodynamic and power design characteristics of a fan (except the length of fan diameter) is generated from data in figure 8.8 and formulated in equation 8.5.

Mean airspeed profile of fan range area = $-0.0059 D^3 + 0.06 D^2 + 0.15 D - 0.39$

.....(8.5)

Where:

The unit of airspeed is (m/s), and D represents the fan diameter location number in the fan range area.

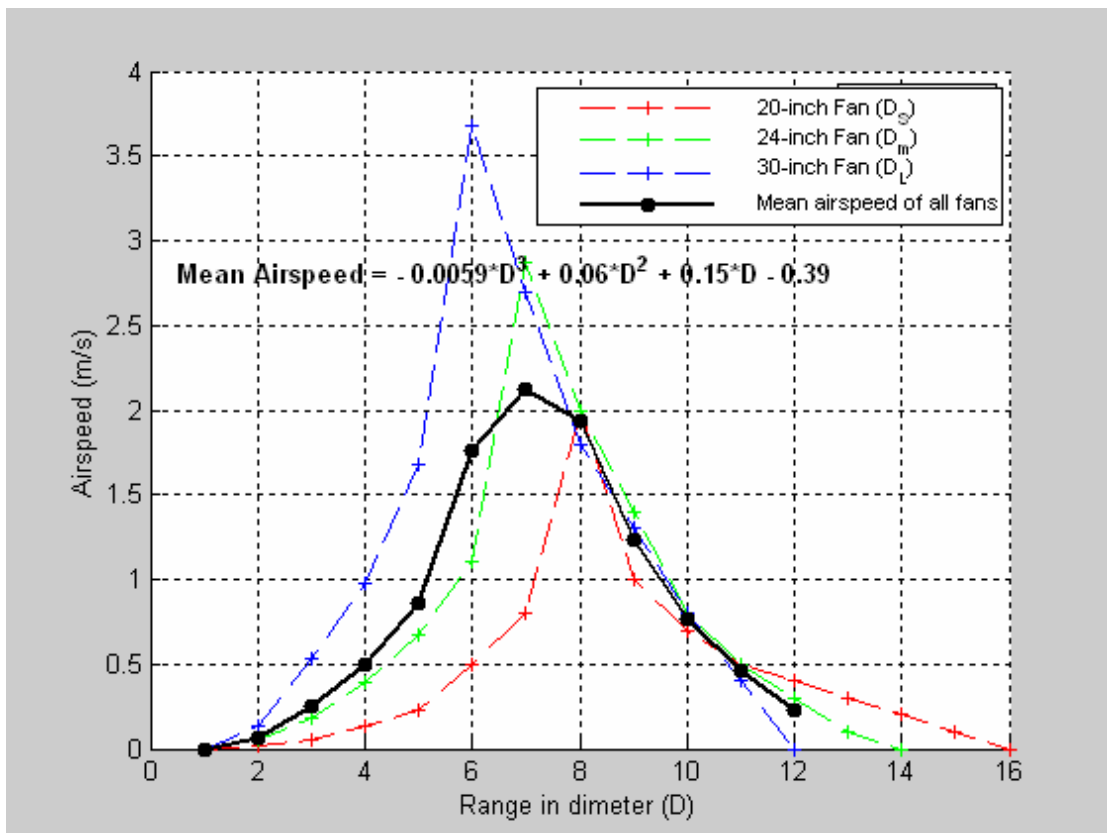


Figure 8.8 Mean airspeed profile of a fan range area

- The mean temperature profile of a mist fan range area for maximum range (at the 4th diameter level) for the applied experimental conditions (e.g. relative humidity = 50, temperature = 40 °C and droplet diameter = 200 μm) is generated from data in figure 8.9 and formulated in equation 8.6.

$$\text{Mean tempertaure profile of mist fan range area} = 0.0098 D^3 - 0.12 D^2 - 0.48 D + 39 \dots\dots\dots(8.6)$$

Where:

The unit of temperature is Celsius, and D represents the fan diameter location number in the fan range area.

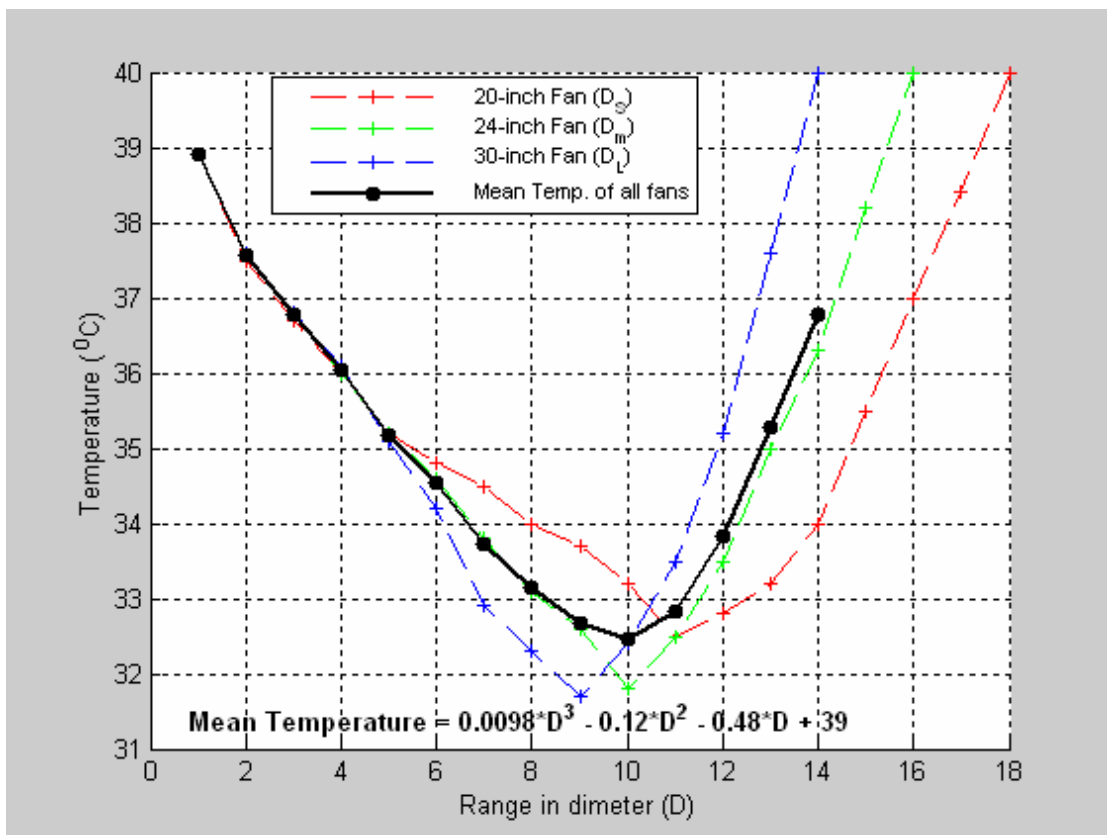


Figure 8.9 Mean temperature profile of a mist fan range area

- The fan maximum side-wise range with respect to fan airspeed was studied for the three fans separately in figures 6.12, 6.20, 6.28, and tables 6.7, 6.4, 6.21. The empirical relationship of fan maximum side-wise range with respect to fan airspeed (for fan airspeed $v \neq 0$) in normalized diameter for the same aerodynamic and power design characteristics of a fan (except the length of fan diameter), is generated from data in figure 8.10 and formulated in equation 8.7.

Table 8.3 Fan maximum side-wise range with respect to airspeed of the three fans

Fan type	Fan Max. side-wise range WRT airspeed (D)	Fan Max. side-wise range WRT airspeed (inch)	Fan Max. side-wise range WRT airspeed (m)
20-inch Fan (D_S)	3 D_S	60	1.5
24-inch Fan (D_m)	3 D_m	72	1.8
30-inch Fan (D_L)	3 D_L	90	2.25

$$Fan\ Max.\ Side - wise\ Range_{for\ airspeed \neq 0} = -4.1(D_{length}) \times 10^{-7} + 3 \dots\dots\dots(8.7)$$

Where:

The unit of fan maximum range with respect to fan airspeed (for fan airspeed $v \neq 0$) is the number of diameter, and D_{length} represents the fan diameter length in inches.

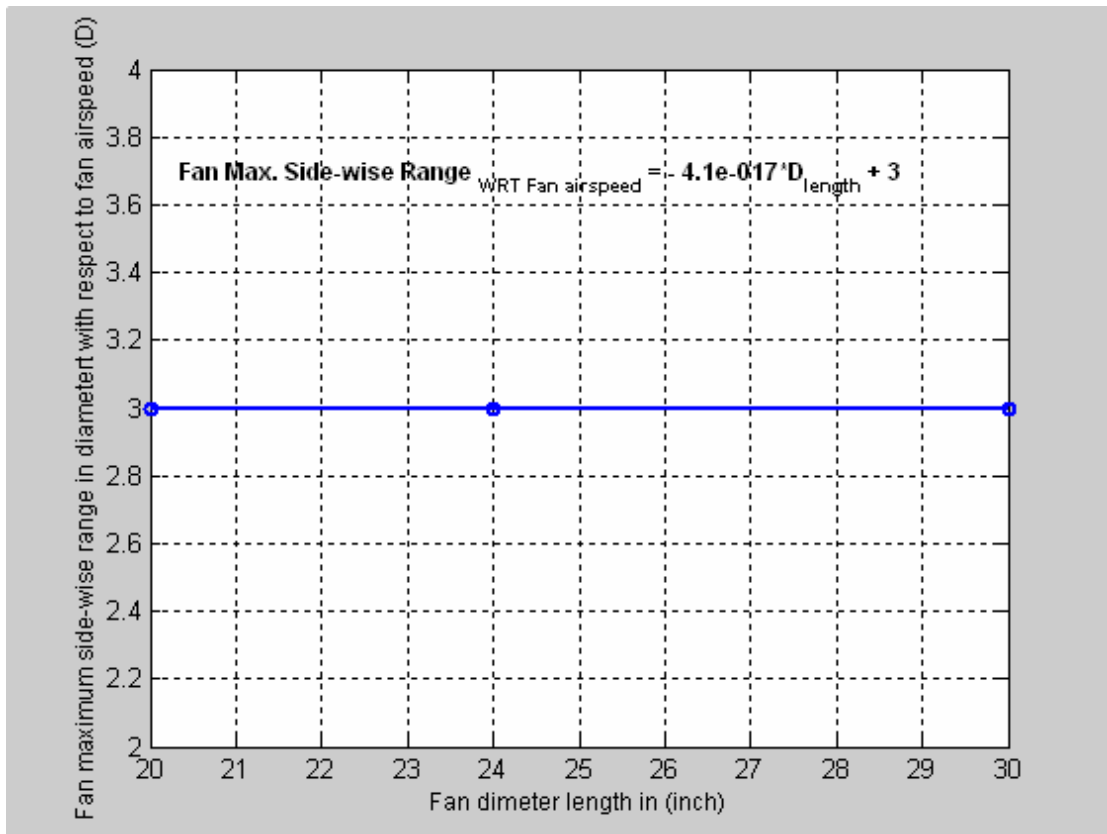


Figure 8.11 Fan maximum side-wise range with respect to fan airspeed (for fan airspeed $v \neq 0$) as a function of fan diameter

- The fan maximum side-wise range with respect to temperature was studied for the three fans separately in figures 6.49, 6.57, 6.65, and tables 6.28, 6.35, 6.42. The empirical relationship of fan maximum side-wise range with respect to temperature of a fan (for $\Delta T \neq 0$) in normalized diameter is generated from data in figure 8.12 and formulated by equation 8.8.

Table 8.4 Fan maximum side-wise range with respect to temperature of the three fans

Fan type	Fan Max. side-wise range WRT temperature (D)	Fan Max. side-wise range WRT temperature (inch)	Fan Max. side-wise range WRT temperature (m)
20-inch Fan (D_S)	8 D_S	160	4
24-inch Fan (D_m)	7 D_m	168	4.2
30-inch Fan (D_L)	6 D_L	180	4.5

$$Fan\ Max.\ Side - wise\ Range_{for\ \Delta T \neq 0} = 0.0083(D_{length})^2 - 0.62D_{length} + 17 \dots\dots\dots(8.8)$$

Where:

The unit of fan maximum side-wise range with respect to temperature (for $\Delta T \neq 0$) is the number of diameter, and D_{length} represents the fan diameter length in inches.

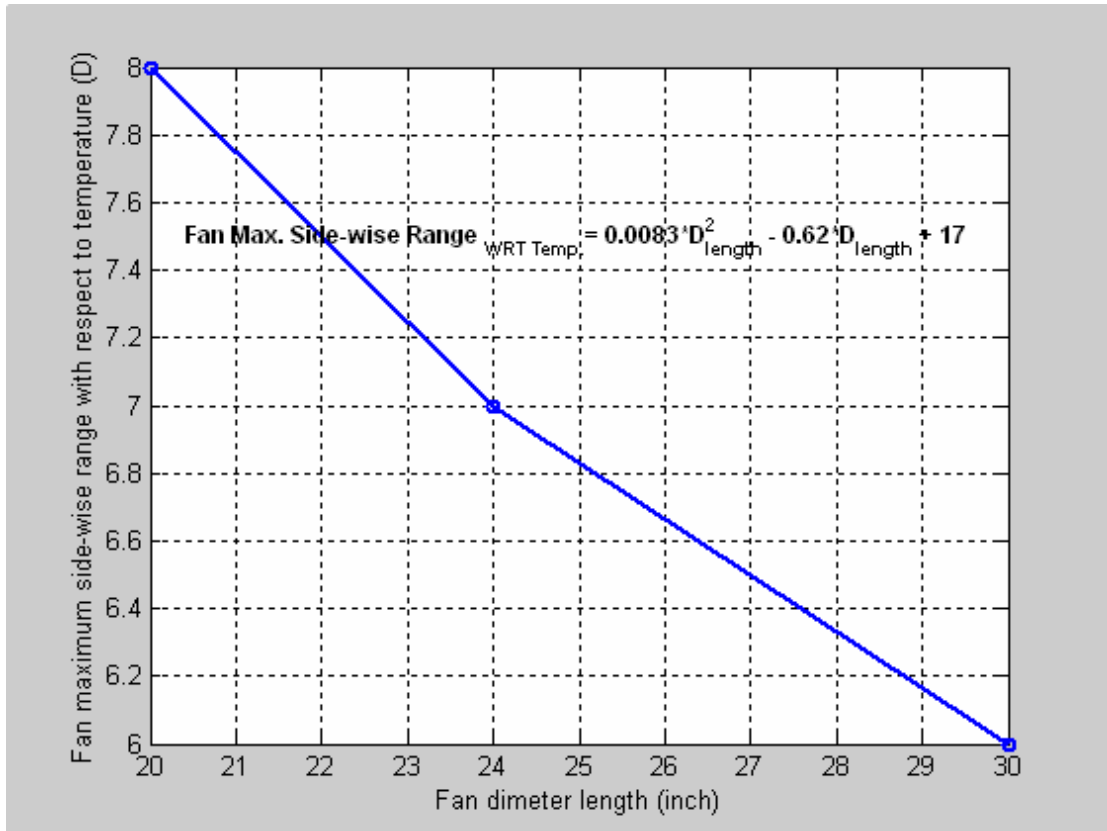


Figure 8.12 Fan maximum side-wise range with respect to temperature (for $\Delta T \neq 0$) as a function of fan diameter

- The empirical relationship of fan maximum side-wise range with respect to fan airspeed (for fan airspeed $v \neq 0$) in inches is generated from data in figure 8.13 and formulated by equation 8.9.

$$Fan\ Max.\ Side_wise\ Range_{for\ airspeed \neq 0\ (inches)} = 3 D_{length} + 2.5 \times 10^{-14} \dots\dots\dots(8.9)$$

Where:

The unit of fan maximum side-wise range with respect to fan airspeed (for fan airspeed $v \neq 0$) is inch, and D_{length} represents the fan diameter length in inches.

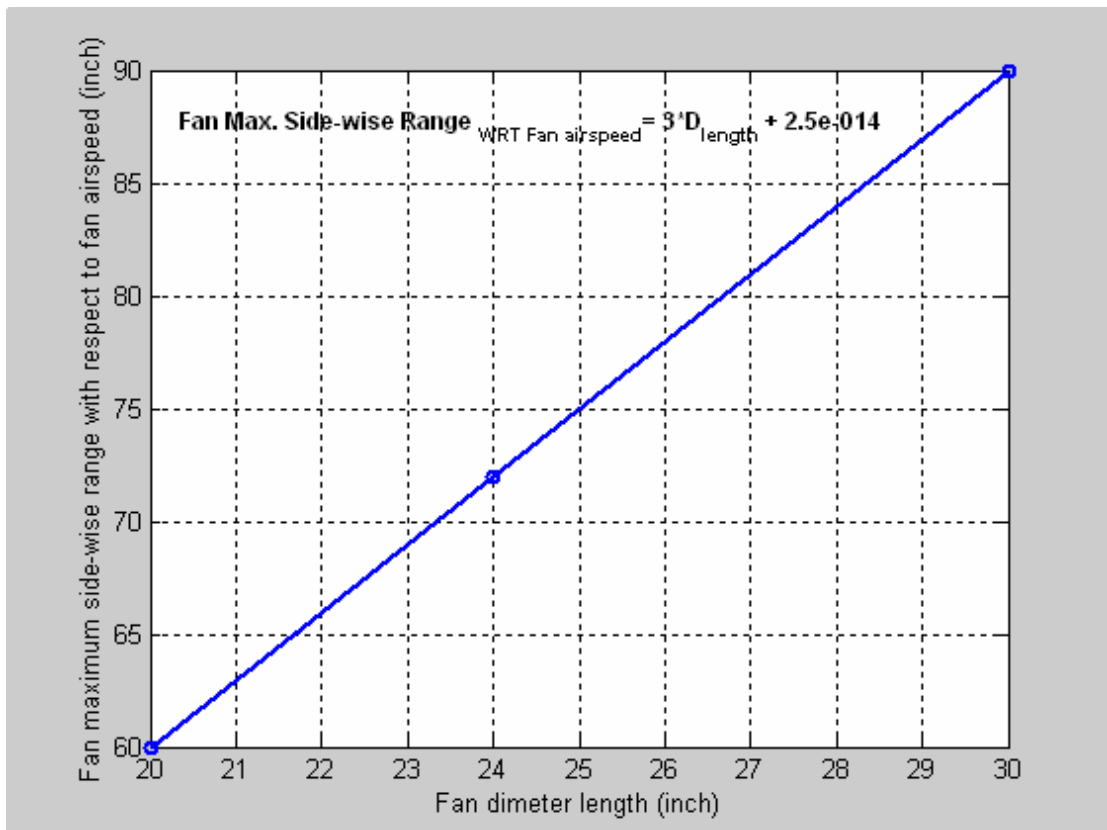


Figure 8.13 Fan maximum side-wise range with respect to fan airspeed (for fan airspeed $v \neq 0$) in inches

- The empirical relationship of fan maximum side-wise range with respect to temperature of a fan (for $\Delta T \neq 0$) in inches is generated from data in figure 8.14 and formulated by equation 8.10.

$$\text{Fan Max. Side_wise Range}_{\text{for } \Delta T \neq 0} \text{ (inches)} = 2D_{\text{length}} + 1.2 \times 10^2 \dots\dots\dots(8.10)$$

Where:

The unit of fan maximum side-wise range with respect to temperature (for $\Delta T \neq 0$) is inch, and D_{length} represents the fan diameter length in inches.

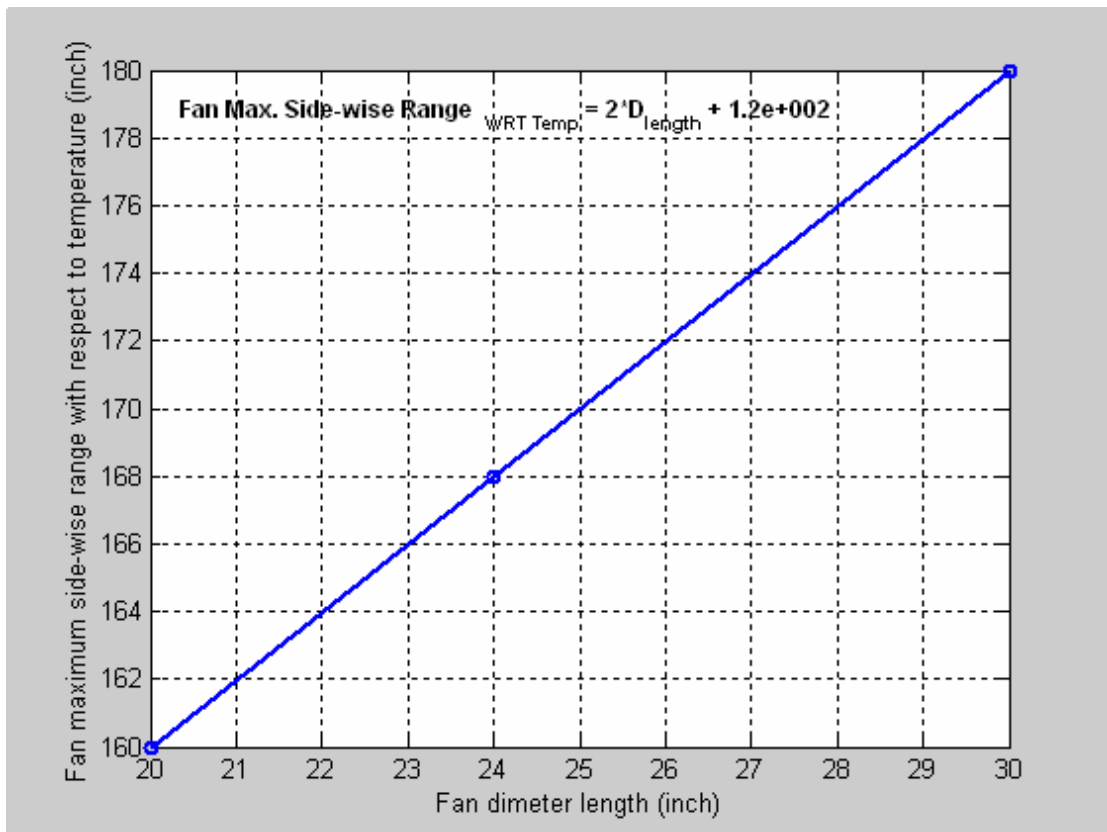


Figure 8.14 Fan maximum side-wise range with respect to temperature (for $\Delta T \neq 0$) in inches

8.5 Heat Absorbed by Water Droplets

To calculate the amount of heat absorbed by water droplets and the cooled air volume for each fan, we consider the control volume in figure 8.15.

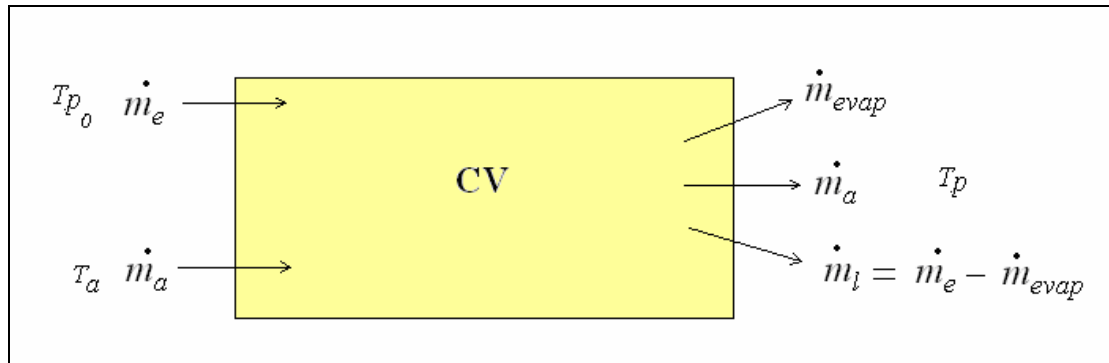


Figure 8.15 A control volume of conserved mass and energy

From conservation of mass and energy principle:

$$\sum \dot{m}_{in} h_{in} - \sum \dot{m}_{out} h_{out} = 0$$

$$\dot{m}_e h_{T_{p0}} + \dot{m}_a h_{T_a} = \dot{m}_a h_{T_p} + \dot{m}_l h_{lT_p} + \dot{m}_{evap} h_{evapoT_p}$$

But, by substituting $\dot{m}_e = \dot{m}_l + \dot{m}_{evap}$

$$\dot{Q}_p = \dot{m}_a (h_{T_a} - h_{T_p}) = \dot{m}_l (h_{T_p} - h_{T_{p0}}) + \dot{m}_{evap} (h_{evapoT_p} - h_{T_{p0}})$$

$$\dot{Q}_p = \dot{m}_a c_{pa} (T_a - T_p) = \dot{m}_l c_{pe} (T_p - T_{p0}) + \dot{m}_{evap} L \dots\dots\dots(8.11)$$

For a single water droplet, the total absorbed heat can be calculated by using equation 8.11.

Where \dot{Q}_p is the total absorbed heat of droplet when falling down, \dot{m}_a is the air mass flow rate, c_{pa} is the specific heat of air, T_a is the air temperature, T_p is the thermal equilibrium temperature of droplet, T_{p0} is the initial droplet temperature, \dot{m}_l is the liquid mass of droplet per time, c_{pe} is the specific heat of water, \dot{m}_{evap} is the vaporized mass of droplet when flying through air per time, L is the latent heat of water and h is the enthalpy.

It is interesting to calculate the total cooling effect of water injected from nozzle. The water vapor produced from the evaporation of droplets would be heated to the air temperature from the equilibrium temperature of the droplet. For a nozzle with certain water mass injected, the total absorbed heat, \dot{Q}_{total} , could be written as:

$$\dot{Q}_{total} = N \dot{Q}_p \dots\dots\dots(8.12)$$

Where \dot{Q}_{total} is the total absorbed heat of all droplets when falling down, N is the droplet number in the injected amount of water.

In our case, there are six nozzles. Each nozzle has a mass flow rate of 8.8×10^{-4} (kg/s). For six nozzles, the total amount of injected water equals 5.28×10^{-3} (kg/s).

The total number of droplets per one second (N) = $\frac{5.28 \times 10^{-3}}{\text{mass of one droplet}}$

$N = 1260.5 \times 10^3$ (per second).

To calculate the total absorbed heat of one droplet \dot{Q}_p according to equation 8.11:

$$\begin{aligned}\dot{Q}_p &= (3.96 \times 10^{-9}) (4187) (31.9-25) + (2.4 \times 10^{-10}) (2412.7 \times 10^3) \\ &= 6.934 \times 10^{-4} \text{ (J/s)}\end{aligned}$$

To calculate the total absorbed heat of all droplets Q_{total} according to equation 8.12:

$$\begin{aligned}Q_{total} &= N \cdot \dot{Q}_p \\ &= (1260.5 \times 10^3) (6.934 \times 10^{-4}) \\ &= 874 \text{ (J)}\end{aligned}$$

To calculate the total absorbed heat of all droplets for different fans is as follows:

8.5.1 Heat Absorbed by Water Droplets of 20-inch Fan

The steady state of this fan is reached after approximately 15 minutes experimentally.

$$N = 1260.5 \times 10^3 \left(\frac{1}{s}\right) * \left(\frac{60s}{1\text{min}}\right) = 75.63 \times 10^6 \text{ (1/min)}$$

$$N \text{ (for 15 minutes)} = 15 \times 75.63 \times 10^6 = 11.345 \times 10^8$$

$$\begin{aligned} Q_{total-steady\ state\ 20-inch\ fan} &= (11.345 \times 10^8) (6.934 \times 10^{-4}) \\ &= 7.8669 \times 10^5 \text{ (J)} \end{aligned}$$

This amount of heat is absorbed from air volume calculated from equation 8.11 as follows:

$$m_a = \frac{Q_{total}}{c_{pa} (T_a - T_p)}$$

$$V_a = \frac{Q_{total}}{\rho_a c_{pa} (T_a - T_p)} \dots\dots\dots(8.13)$$

Where V_a is the air volume, ρ_a is the air density.

$$\begin{aligned} V_a &= \frac{7.8669 \times 10^5}{(1.2)(1005)(40 - 31.9)} \\ &= 80.5 \text{ m}^3 \end{aligned}$$

To compare the calculated volume of air (V_a) that's absorbed this amount of heat to the sub-volume of air in the location of experiment ($V_{sub-air}$), the two volumes are close to each other as follows:

The dimensions of affected volume of air in the place of the experiment is about 9 meters front-wise of the fan, 4 meters side-wise and 2 meters high which represents the height of the fan. By assuming symmetrical triangle shape for the air volume as shown in figure 8.16, then it is calculated as follows:

$$V_{sub-air} = (2) \times (1/2) \times (9) \times (4) \times (2) = 72 \text{ m}^3$$

By comparing the two volumes, it is just a matter of 10.5 % difference, which can be acceptable.

$$diff. = \frac{|80.5 - 72|}{80.5} \times 100 = 10.5\%$$

Eventually, it could be concluded that 7.8669×10^5 (J) of heat was absorbed from the affected fan range air sub-volume for the 20-inch Fan.

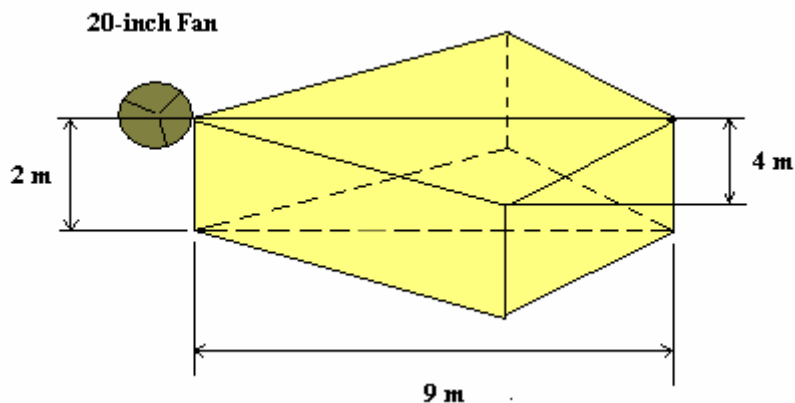


Figure 8.16 Volume of cooled air in fan covered range area of 20-inch fan (D_s)

8.5.2 Heat Absorbed by Water Droplets of 24-inch Fan

The steady state of this fan is reached after approximately 19 minutes experimentally.

$$N = 1260.5 \times 10^3 \left(\frac{1}{s}\right) * \left(\frac{60s}{1\text{min}}\right) = 75.63 \times 10^6 \text{ (1/min)}$$

$$N \text{ (for 19 minutes)} = 19 \times 75.63 \times 10^6 = 14.37 \times 10^8$$

$$\begin{aligned} Q_{\text{total-steady state}_{24\text{-inch fan}}} &= (14.37 \times 10^8) (6.934 \times 10^{-4}) \\ &= 9.9647 \times 10^5 \text{ (J)} \end{aligned}$$

This amount of heat is absorbed from air volume calculated from equation 8.13 as follows:

$$\begin{aligned} V_a &= \frac{9.9647 \times 10^5}{(1.2)(1005)(40 - 31.9)} \\ &= 102 \text{ m}^3 \end{aligned}$$

To compare the calculated volume of air (V_a) that's absorbed this amount of heat to the sub-volume of air in the location of experiment ($V_{\text{sub-air}}$), the two volumes are close to each other as follows:

The dimensions of affected volume of air in the place of the experiment is about 9.6 meters front-wise of the fan, 4.2 meters side-wise and 2.4 meters high which represents the height of the fan. By assuming symmetrical triangle shape for the air volume as shown in figure 8.17, then it is calculated as follows:

$$V_{\text{sub-air}} = (2) \times (1/2) \times (9.6) \times (4.2) \times (2.4) = 96.8 \text{ m}^3$$

By comparing the two volumes, it is just a matter of 5.1 % difference, which can be acceptable.

$$diff. = \frac{|102 - 96.8|}{102} \times 100 = 5.1\%$$

Eventually, it could be concluded that 9.9647×10^5 (J) of heat was absorbed from the affected fan range air sub-volume for the 24-inch Fan.

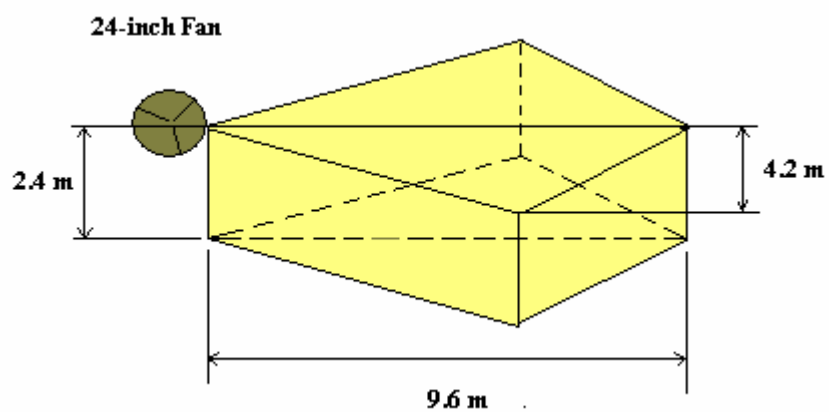


Figure 8.17 Volume of cooled air in fan covered range area of 24-inch fan (D_m)

8.5.3 Heat Absorbed by Water Droplets of 30-inch Fan

The steady state of this fan is reached after approximately 24 minutes experimentally.

$$N = 1260.5 \times 10^3 \left(\frac{1}{s}\right) * \left(\frac{60s}{1\text{min}}\right) = 75.63 \times 10^6 \text{ (1/min)}$$

$$N \text{ (for 24 minutes)} = 24 \times 75.63 \times 10^6 = 14.37 \times 10^8$$

$$\begin{aligned} Q_{\text{total-steady state}_{30\text{-inch fan}}} &= (18.151 \times 10^8) (6.934 \times 10^{-4}) \\ &= 1.2587 \times 10^6 \text{ (J)} \end{aligned}$$

This amount of heat is absorbed from air volume calculated from equation 8.13 as follows:

$$\begin{aligned} V_a &= \frac{1.2587 \times 10^6}{(1.2)(1005)(40 - 31.9)} \\ &= 128.9 \text{ m}^3 \end{aligned}$$

To compare the calculated volume of air (V_a) that's absorbed this amount of heat to the sub-volume of air in the location of experiment ($V_{\text{sub-air}}$), the two volumes are close to each other as follows:

The dimensions of affected volume of air in the place of the experiment is about 10.5 meters front-wise of the fan, 4.5 meters side-wise and 3 meters high which represents the height of the fan. By assuming symmetrical triangle shape for the air volume as shown in figure 8.18, then it is calculated as follows:

$$V_{\text{sub-air}} = (2) \times (1/2) \times (10.5) \times (4.5) \times (3) = 141.7 \text{ m}^3$$

By comparing the two volumes, it is just a matter of 9.9 % difference, which can be acceptable.

$$diff. = \frac{|128.9 - 141.7|}{128.9} \times 100 = 9.9\%$$

Eventually, it could be concluded that 1.2587×10^6 (J) of heat was absorbed from the affected fan range air sub-volume for the 30-inch Fan.

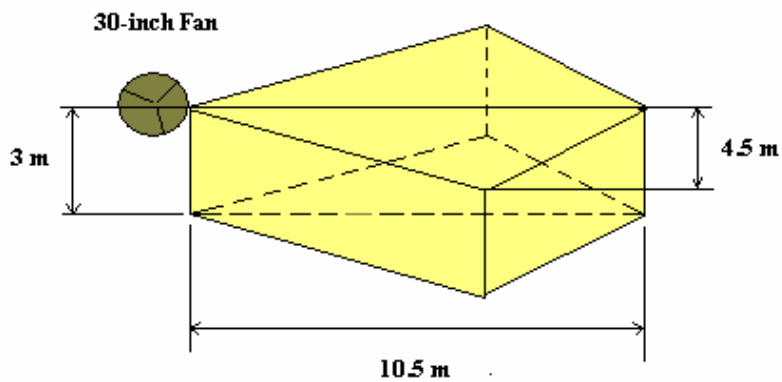


Figure 8.18 Volume of cooled air in fan covered range area of 30-inch fan (D_L)

8.6 Effect of Operating Parameters of Evaporation Rate and Drying Time Performance

In this section, a detailed discussion is presented to study and compare the effects of operating parameters playing role in evaporation rate process and drying performance. These parameters are air humidity, operating pressure, airspeed and air temperature.

8.6.1 Effect of Air Humidity

In figures 8.19 and 8.20, the relative humidity is increased gradually and plotted versus the evaporation rate and drying time respectively, fixing all the other operating parameters.

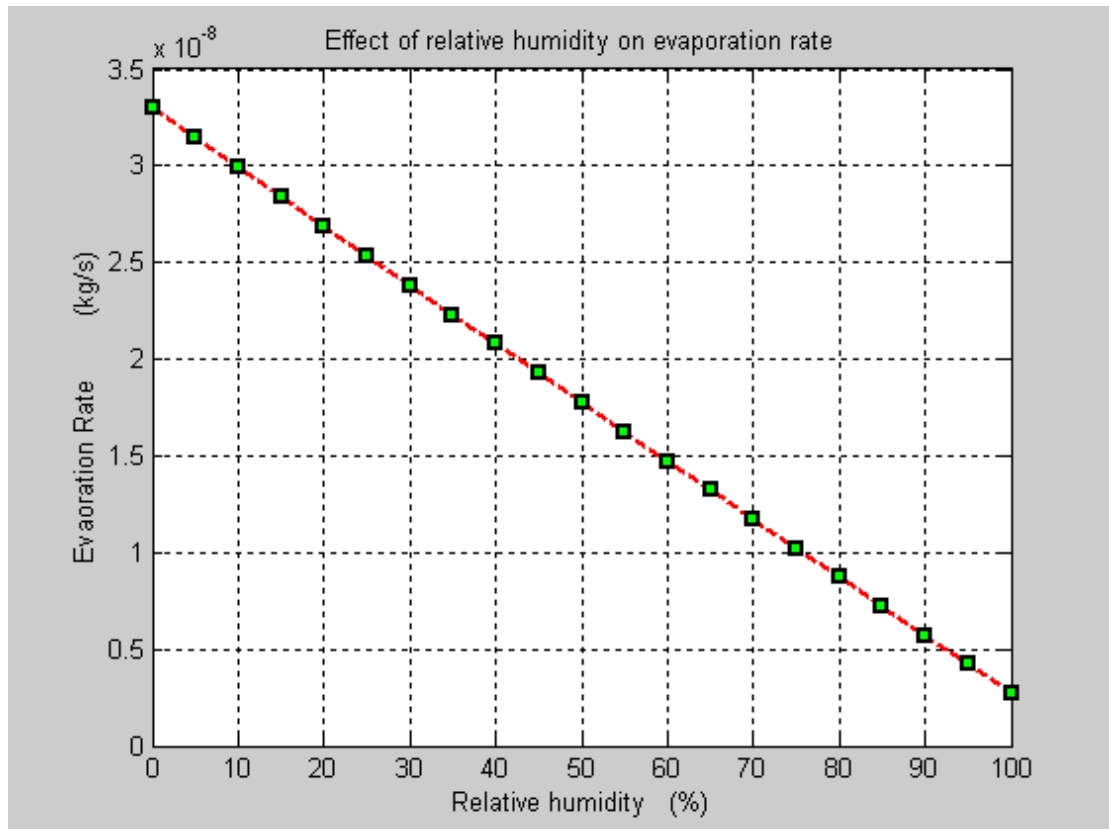


Figure 8.19 Effect of relative humidity on evaporation performance

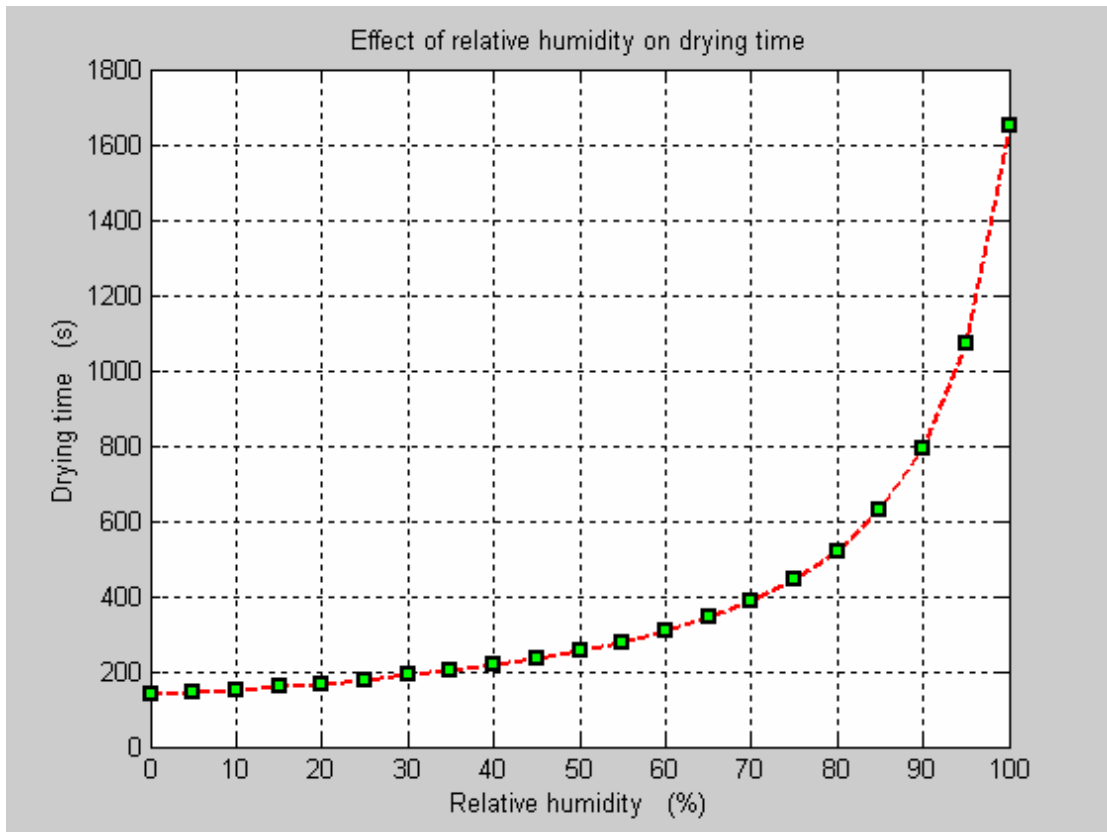


Figure 8.20 Effect of relative humidity on drying performance

It is observed from previous figures that there is a reduction in the evaporation rate due to the increase of relative humidity; and there is an increase in the drying time due to the increase of relative humidity. The reduction in mass transfer driving potential is responsible for this reduction.

8.6.2 Effect of Operating Pressure

In figures 8.21 and 8.22, the operating pressure is decreased gradually and plotted versus the evaporation rate and drying time respectively, fixing all the other operating parameters.

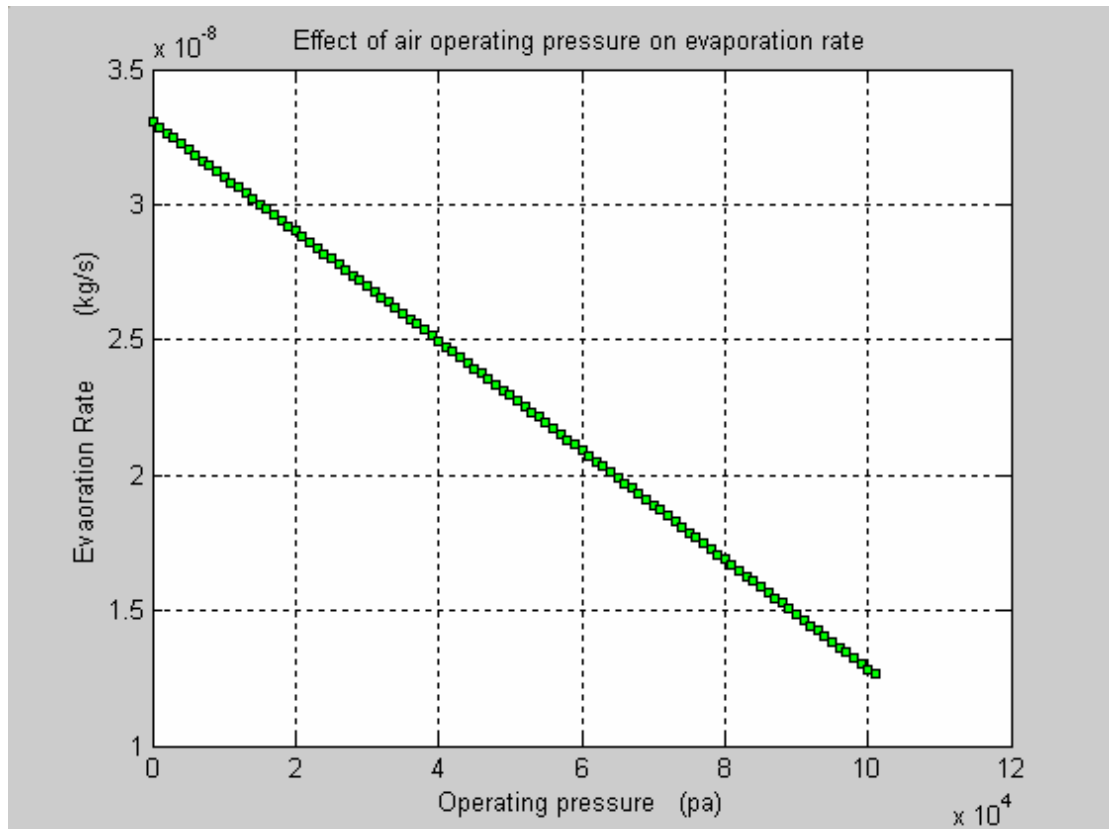


Figure 8.21 Effect of operating pressure on evaporation performance

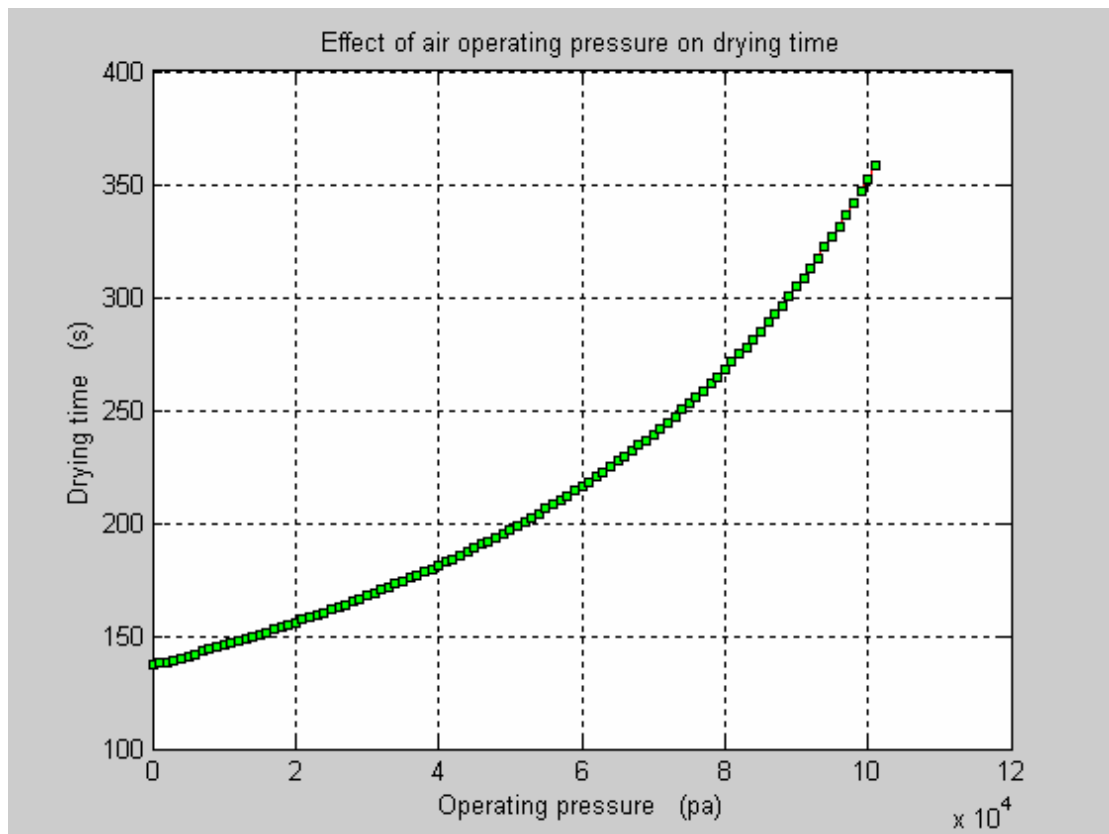


Figure 8.22 Effect of operating pressure on drying performance

It is observed from previous figures that there is an increase in the evaporation rate due to the decrease of operating pressure; and there is a decrease in the drying time due to the decrease of operating pressure.

8.6.3 Effect of Air Velocity

In figures 8.23 and 8.24, the air velocity is increased gradually and plotted versus the evaporation rate and drying time respectively, fixing all the other operating parameters.

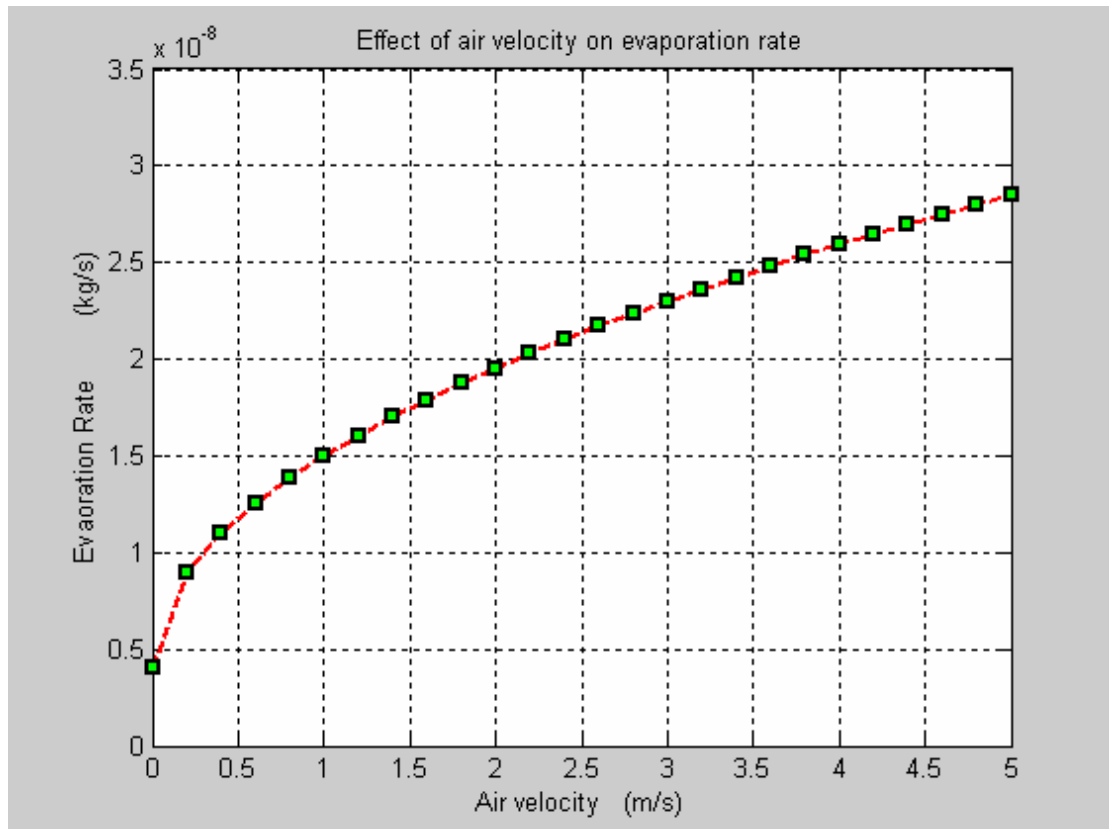


Figure 8.23 Effect of air velocity on evaporation performance

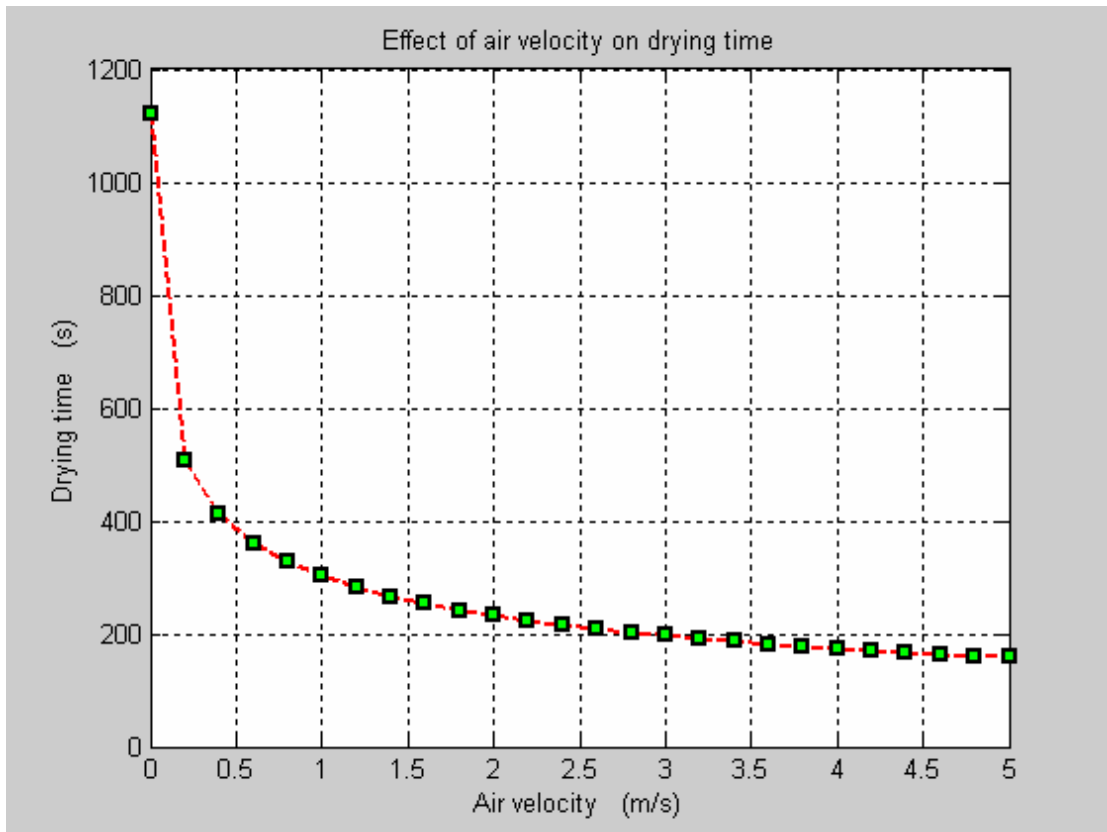


Figure 8.24 Effect of air velocity on drying performance

It is observed from previous figures that there is an increase in the evaporation rate due to the increase of air velocity; and there is a decrease in the drying time due to the increase of air velocity.

8.6.4 Effect of Air Temperature

In figures 8.25 and 8.26, the air temperature is increased gradually and plotted versus the evaporation rate and drying time respectively, fixing all the other operating parameters.

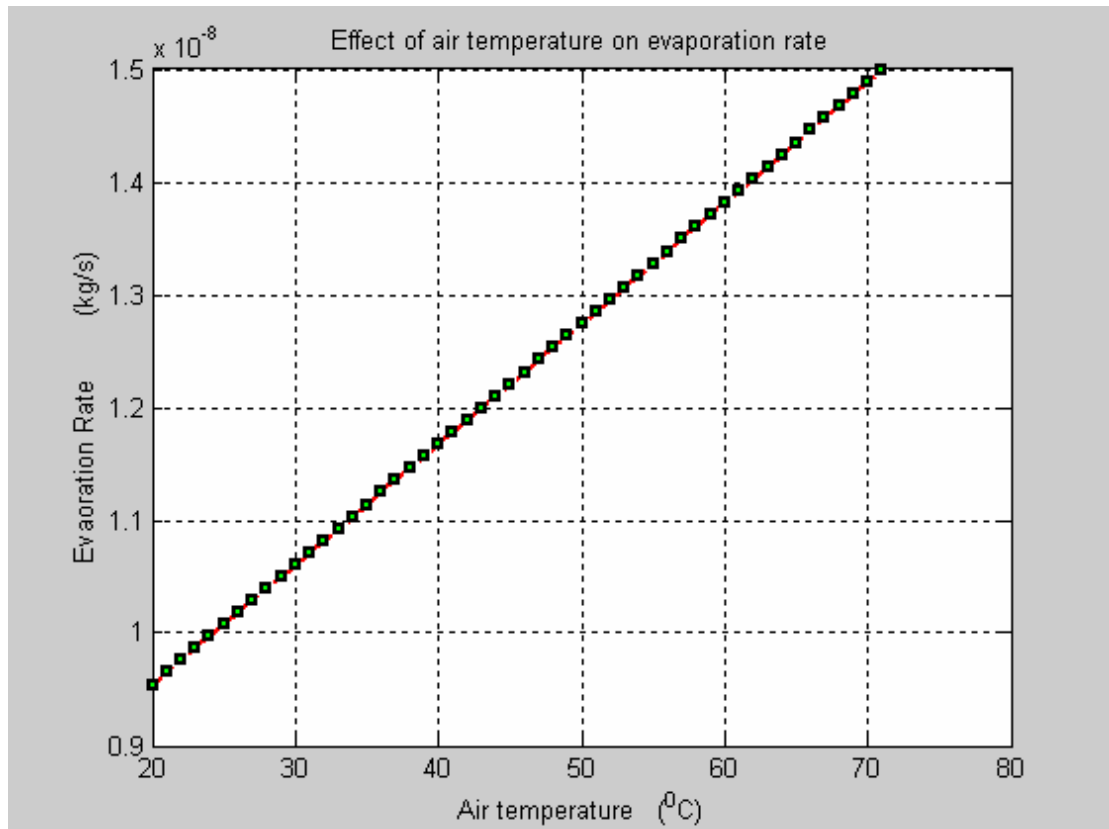


Figure 8.25 Effect of air temperature on evaporation performance

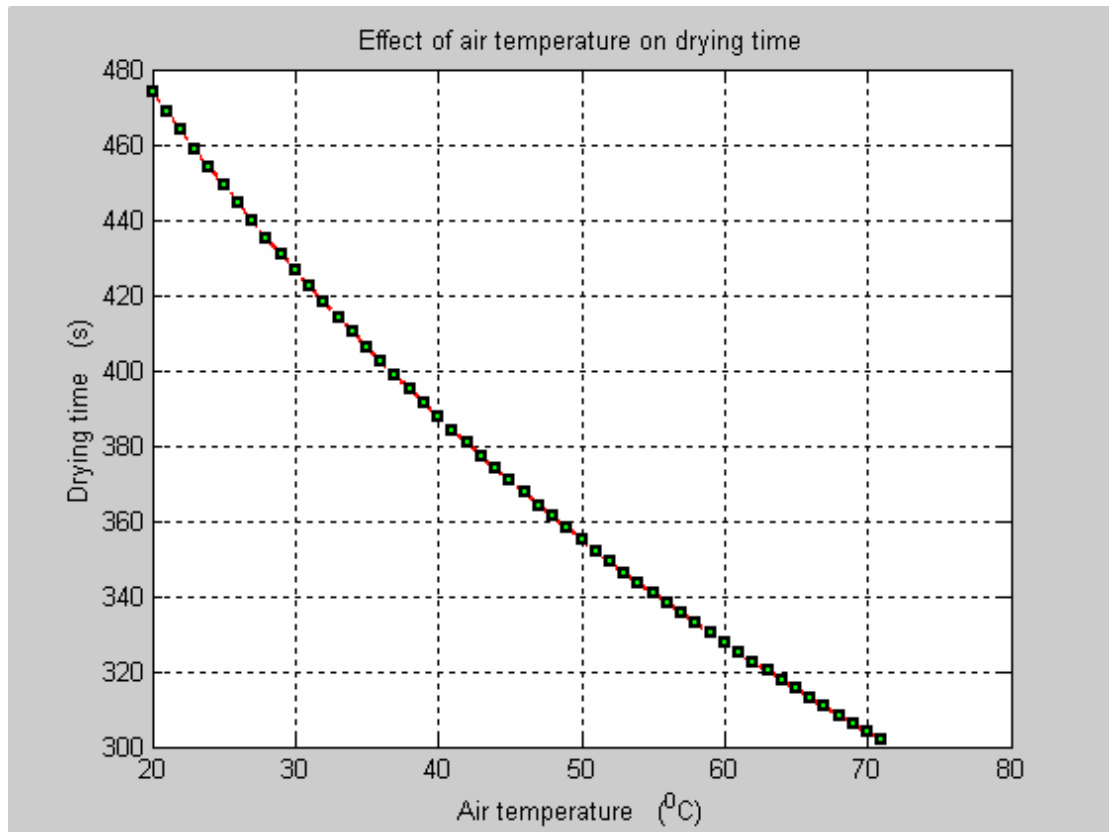


Figure 8.26 Effect of air temperature on drying performance

It is observed from previous figures that there is an increase in the evaporation rate due to the increase of air temperature; and there is a decrease in the drying time due to the increase of air temperature

As a summery from the above computation, the followings are concluded.

- When the relative humidity is increased, the evaporation rate is decreased.
- When the air operating pressure is decreased, the evaporation rate is increased and vice versa.
- When the air velocity is increased, the evaporation rate is increased as well.
- When the air temperature is increased, the evaporation rate is increased.

CHAPTER 9

CONCLUSIONS AND RECOMMENDATIONS

This chapter concludes the work of the thesis by presenting the conclusions, summary and recommendations for future work.

9.1 Conclusions

The contribution of this thesis can be summarized as follows:

- By investigating the relationship between the temperature domain and cooling fan diameters from one aspect, and the relationship between the temperature domain and cooling fan heights from the other aspect with and without mist, and by looking generally to the results of fans presented for individual cases in previous chapters, a good agreement has been observed between the experimental results and computational results, which gives an indication of well chosen assumptions proposed for the computational solution.
- The maximum temperature range occurs at the 4th diameter level ($h = 4D$) for each fan.
- In the lower levels, the evaporation rate is enhanced in a better manner compared to the upper levels which indicates more evaporation since the temperature in the lower levels is close to the calculated wet bulb temperature.
- The experimental values and the computational values agreed well in all cases which reflects wise selected assumptions of the computational solution.

- The measured temperatures values are lower than the computed ones; that indicates not complete evaporation of water droplets when flying before it hits the ground in the computational solution. However, the measured values indicates that the evaporation process continues to take a place even when the water droplets on the ground.
- The maximum range of each fan occurs at the 4th diameter level ($h = 4D$) and it is determined by measuring the airspeed for its maximum range; and the temperature range is determined by measuring the temperature for its maximum range as shown in chapter 8.
- All empirical relationships of fan maximum range with respect to fan airspeed and with respect to temperature including the special case studies are introduced satisfying the main objectives of the study as shown in chapter 8.
- The mean airspeed profile and mean temperature profile of a fan range area for maximum range (at the 4th diameter level) for the same aerodynamic and power design characteristics of a fan (except the length of fan diameter) are formulated as shown in chapter 8.
- The amount of heat absorbed from air for each fan in the location of experiment is demonstrated in chapter 8.

9.2 Summery

In this thesis, an experimental study verified by a computational model has been conducted to understand and investigate the relationship between the temperature domain and cooling fan diameters from one aspect, and the relationship between the temperature domain and cooling fan heights from the other aspect with and without mist. Evaporative cooling by using mist has been an aim of this work to guarantee less energy consumption and this, in turn, will lead to make the solar energy as the energy source of this cooling system. In this manner, it is highly possible to provide thermal comfort to so many active and livable places all over the kingdom of Saudi Arabia without putting any pressure on the government for providing energy.

Experimental part has been basically done in two stages. The first stage has been conducted without mist and the second stage has been done with mist. both stages have been devoted to find empirical relationship that relates the fan coverage area with fan diameter from one aspect and the fan coverage area with fan heights from the other aspect.

In this work, three fans have been selected with the following diameters (20 inch, 24 inch and 30 inch). These fans were selected specifically to have exactly aerodynamic similarities except the length of diameter where we have three different lengths of diameters as stated above.

The fans were leveled to different heights and then operated to take the airspeed measurements and temperature for each diameter of the three fans in front of each one, where it is called coverage area domain. The airspeed and temperature were measured by placing sensitive instruments in the domain.

Also one aspect that has been included in the experiments is the angle effect case study of the fans. For zero angle ($\theta_1 = 0^\circ$) as explained in default case, the airspeed and temperature effect could reach maximum range but for higher levels of fans like the 4th Diameter and the 5th Diameter the area that is directly below the fan could be affected due to less amount of airspeed reaching that area; so because of that the fans were angled down to two angles ($\theta_1 = 26.56^\circ$) and ($\theta_2 = 45^\circ$) to get an idea about the regime in this case.

The experimental results have been verified by a computational study which has been conducted by keeping the same conditions as in the experiments for the three fans, except the fan airspeed which varies according to different fan diameter. The computational study was conducted based on heat and mass transfer diffusion equations to calculate the evaporation rate and the temperature for each fan considering one droplet model.

There were some assumptions made for the model as follows:

- The surface of the control volume coincides with the surface of the droplet.
- The droplet is to be in a spherical shape.
- The heat transfer at the surface is due to convection.
- The mass transfer occurs as evaporation takes place at the interface between the droplet and air.
- The temperature in the droplet is assumed to be uniform during the evaporation process.
- The diameter of the water droplet is considered to be changing with time.

- At the end, there has been a detailed discussion presented to study and compare the effects of operating parameters playing role in evaporation rate process and drying performance. Thesis parameters are air humidity, operating pressure, airspeed and air temperature.

9.3 Recommendations for Future Research Work

Following are the recommendations for possible research that can be carried out in future based on the work presented in this thesis:

- Implementation of more than three fans with different diameter lengths to get more accurate relationships.
- Implementation of different fans aerodynamically similar but with different number of plates and perform the study for such a case.
- Implementation of different fans aerodynamically similar but with different design of plates and perform the study for such a case.
- Implementation of different fans aerodynamically similar but with different plate widths and perform the study for such a case.
- Implementation of different fans aerodynamically similar but with different airfoils of plates and perform the study for such a case.
- Implementation of different fans aerodynamically similar but with different RPM speeds and perform the study for such a case.
- Implementation of different water droplet sizes and perform the study for such a case.
- Implementation of different numbers of nozzles and perform the study for such a case.
- Implementation of different water pump pressures of the mist system since it affects directly the droplet size and perform the study for such a case.
- Reconducting the study in different weather conditions like changing the air humidity, operating pressure, airspeed and air temperature.
- Energy consumption for different fan configuration.

APPENDIX A: Error Analysis on Uncertainty

Calculations

- **Uncertainty in Airspeed Measurement:**

The airspeed was measured for 5 times as follows:

7.85, 7.9, 8.1, 7.96, 8.09 meter per second

The average value of airspeed measurements is:

$$\text{Average} = \frac{7.85 + 7.9 + 8.1 + 7.96 + 8.09}{5}$$

$$= 7.99 \text{ m/s}$$

The **mean deviation from the mean** is the sum of absolute values of the differences between each measurement and the average, divided by the number of measurements:

$$\text{Mean Dev. from Mean} = \frac{0.14 + 0.09 + 0.11 + 0.03 + 0.1}{5}$$

$$= 0.094 \text{ m/s}$$

The mean deviation from the mean gives a reasonable description of the scatter of data around its mean value, which represents the uncertainty in airspeed measurements.

Based on this calculation, the true airspeed measurement is estimated to be ± 0.94 m/s (using mean deviation from the mean):

The uncertainty in measuring airspeed is ± 0.94 m/s.

- **Uncertainty in Temperature Measurement:**

The temperature was measured for 5 times as follows:

36.5, 36.4, 36.6, 36.5, 36.7 $^{\circ}\text{C}$

The average value of temperature measurements is:

$$\begin{aligned} \text{Average} &= \frac{36.5 + 36.4 + 36.6 + 36.5 + 36.7}{5} \\ &= 36.54 \text{ }^{\circ}\text{C} \end{aligned}$$

The **mean deviation from the mean** is the sum of absolute values of the differences between each measurement and the average, divided by the number of measurements:

$$\begin{aligned} \text{Mean Dev. from Mean} &= \frac{0.04 + 0.14 + 0.06 + 0.04 + 0.16}{5} \\ &= 0.088 \text{ }^{\circ}\text{C} \end{aligned}$$

The mean deviation from the mean gives a reasonable description of the scatter of data around its mean value, which represents the uncertainty in temperature measurements.

Based on this calculation, the true temperature measurement is estimated to be ± 0.088 °C (using mean deviation from the mean):

The uncertainty in measuring temperature is ± 0.088 °C.

- **Uncertainty in Fan Maximum Range Measurement:**

The fan maximum range was measured for 5 times as follows:

10.55, 10.59, 10.51, 10.35, 10.3 meter

The average value of fan maximum range measurements is:

$$\begin{aligned} \text{Average} &= \frac{10.55 + 10.59 + 10.51 + 10.35 + 10.3}{5} \\ &= 10.46 \text{ m} \end{aligned}$$

The **mean deviation from the mean** is the sum of absolute values of the differences between each measurement and the average, divided by the number of measurements:

$$\begin{aligned} \text{Mean Dev. from Mean} &= \frac{0.09 + 0.13 + 0.05 + 0.11 + 0.16}{5} \\ &= 0.108 \text{ m} \end{aligned}$$

The mean deviation from the mean gives a reasonable description of the scatter of data around its mean value, which represents the uncertainty in fan maximum range measurements.

Based on this calculation, the true fan maximum range measurement is estimated to be ± 0.108 m (using mean deviation from the mean):

The uncertainty in measuring fan maximum range is ± 0.108 m.

- **Uncertainty in Relative Humidity Measurement:**

The relative humidity was measured for 5 times as follows:

52, 55, 48, 50, 46 %

The average value of relative humidity measurements is:

$$\begin{aligned} \text{Average} &= \frac{52 + 55 + 48 + 50 + 46}{5} \\ &= 50.2 \% \end{aligned}$$

The **mean deviation from the mean** is the sum of absolute values of the differences between each measurement and the average, divided by the number of measurements:

$$\begin{aligned} \text{Mean Dev. from Mean} &= \frac{1.8 + 4.8 + 2.2 + 0.2 + 4.2}{5} \\ &= 2.64 \% \end{aligned}$$

The mean deviation from the mean gives a reasonable description of the scatter of data around its mean value, which represents the uncertainty in fan maximum range measurements.

Based on this calculation, the true relative humidity measurement is estimated to be $\pm 2.64\%$ (using mean deviation from the mean):

The uncertainty in measuring relative humidity is $\pm 2.64\%$.

REFERENCES

- [1] **Santamouris, M.**, "Passive cooling of buildings, progress in solar energy", American Section of ISES. [James](#) and James Science Publisher, London (2005).
- [2] **N. AL-Hemiddi**, (1995). *Passive Cooling Systems Applicable for Buildings in the Hot-Dry Climate of Saudi Arabia* . Doctoral dissertation, University of California, pp.12
- [3] **K. Talib**, (1984). *Shelter in Saudi Arabia*. Academy Editions/St. Martin's Press, pp.39
- [4] **N. AL-Hemiddi**, (1995). *Passive Cooling Systems Applicable for Buildings in the Hot-Dry Climate of Saudi Arabia* . Doctoral dissertation, University of California, pp.13
- [5] <http://www.saudi-arabia-chm.gov.sa/climate.htm>
- [6] **The Saudi Presidency of Metrology and Environment (PME)**, <http://www.pme.gov.sa/en/cc.asp>
- [7] **G. Z. Brown and Mark Dekay**. "SUN, WIND AND LIGHT", JONES WILEY SONS, INC. 2nd Edition, 2000.
- [8] **B. Giovani**, (1994). *Passive and Low Energy Cooling of Buildings*. Van Nostrand and einhold Company, New York, pp. 1
- [9] **N. AL-Hemiddi**, (1995). *Passive Cooling Systems Applicable for Buildings in the Hot-Dry Climate of Saudi Arabia* . Doctoral dissertation, University of California, pp.22
- [10] **H. Fathy**, (1986). *Natural Energy and Vernacular Architecture*. Chicago, The University of Chicago Press, pp. 9

- [11] **M. Bahadori**, 1985. An Improved Design of Wind Towers for Natural Ventilation and Passive Cooling, *Solar Energy*, Vol. 35, No. 2, pp. 119-129
- [12] **Brain, P. and H. Hales**, *A. I. Ch. E. Journal*, 15, 419 (1969)
- [13] **Faeth, G. and D. H. Olson**, The Ignition of Hydrocarbon Fuel Droplets in Air, SAE preprint 680465, Mid-Year Meeting, Detroit, Michigan, 1968
- [14] **H. Barrow and C.W. Pope**. "Droplet evaporation with reference to the effectiveness of water-mist cooling", *Journal of Applied Energy* (2007), **84** (4), pp. 404-412.
- [15] **Gilbert D. Kinzer and Ross Gunn**. "THE EVAPORATION, TEMPERATURE AND THERMAL RELAXATION-TIME OF FREELY FALLING WATERDROPS", *Journal of the Atmospheric Sciences*, **8** (2), pp. 71–83, 1951.
- [16] **S.E. Woo and A.E. Hamielec**. "A Numerical Method of Determining the Rate of Evaporation of Small Water Drops Falling at Terminal Velocity in Air", *Journal of the Atmospheric Sciences*, **28** (8), pp. 1448–1454, 1971
- [17] **M. Pasandideh-Fard, S. D. Aziz, S. Chandra and J. Mostaghimi**. "Cooling effectiveness of a water drop impinging on a hot surface", *International Journal of Heat and Fluid Flow* (2001), **22** (2), pp. 201-210
- [18] **José Rui Camargo, Carlos Daniel Ebinuma and José Luz Silveira**, "Experimental performance of a direct evaporative cooler operating during summer in a Brazilian city ", *International Journal of Refrigeration* (2005), **28** (7), pp. 1124-1132
- [19] **Jiří Smolík, Lucie Džumbová, Jaroslav Schwarz and Markku Kulmala**, "Evaporation of ventilated water droplet: connection between heat and mass transfer ", *Journal of Aerosol Science* (2002), **33** (1), pp.205

- [20] **Clift, Grace, and Weber.** Bubbles, Drops, and Particles, Academic Press, New York, (1978), chapters 3 and 5.
- [21] **Pei, D. C. and W. H. Gauvin,** A. I. Ch. E. Journal, 9, 375 (1963)
- [22] **Borman, G. L., M. N. El Wakil, O. A. Uyehara and P. S. Myer,** Grapas of Reduced Variables for Computing Histories of Vaporizing Fuel Drops, and Drops Histories Under Pressure, NACA, TN-4338, Sept. 1985
- [23] **Savery, W. and G. Borman,** AAIA, Preprint No. 70-6, New York, 1970
- [24] **Noordsu, P. and J. W. Rotte,** Chemical Engineering Science, 22, 1475 (1967)
- [25] **Noordsu, P. and J. W. Rotte,** Chemical Engineering Science, 23, 657 (1968)
- [26] **Skelland, A. H. P. and A. R. H. Cornish,** A. I. Ch. E. Journal, 9, 73 (1963)
- [27] **Y. F. Li, and W. K. Chow,** Study of Water Droplet Behavior in Hot Air Layer in Fire Extinguishment, Journal of Fire Technology (2007).
- [28] **Edna Shaviv, Abraham Yezioro and Isaac G. Capeluto,** "Study of Water Droplet Behavior in Hot Air Layer in Fire Extinguishment", Journal of [Renewable Energy, Volume 24, Issues 3-4](#), Pages 445-452 (2001).
- [29] **Edna Shaviv, Abraham Yezioro and Isaac G. Capeluto,** "Study of Water Droplet Behavior in Hot Air Layer in Fire Extinguishment", Journal of [Renewable Energy, Volume 24, Issues 3-4](#), Pages 445-452 (2001).
- [30] **G. Z. Brown, and Mark Dekay,** Sun, Wind & Light (2000)
- [31] <http://www.americansolar.com/technology/solar-air-cooling.htm>
- [32] http://en.wikipedia.org/wiki/Evaporative_cooling#Evaporative_cooling
- [33] **Santamouris, M.,** "Passive cooling of buildings, progress in solar energy", American Section of ISES. [James](#) and James Science Publisher, London (2005).

- [34] P.O. Fanger. In: *Thermal Comfort Analysis and Application in Environmental Engineering*, McGraw-Hill, New York (1972), p. 244.
- [35] Eileen Fabian Wheeler and A. J. Both, "Evaluating Greenhouse Ventilation Fan Capacity".
- [36] H. Barrow and C.W. Pope. "Droplet evaporation with reference to the effectiveness of water-mist cooling", *Journal of Applied Energy* (2007), **84** (4), pp. 404-412
- [37] Weast, R.C. "Parabolic fit on values", *Handbook of Chemistry and Physics* (1986), CRC Press Inc.; 67th edition; Boca Raton, Florida, USA, page F-42.
- [38] Gates, D. M. "Linear fit on values", *Biophysical ecology* (1980), Springer Verlag; New York, Heidelberg, Berlin; 611 pp.
- [39] Weast, R.C. "Parabolic fit on values", *Handbook of Chemistry and Physics* (1986), CRC Press Inc.; 67th edition; Boca Raton, Florida, USA, page F-8.
- [40] List, R.J. "Calculator for saturated vapor pressure and relation between bulb temperatures and vapor pressures", *Smithsonian Meteorological Tables* (1958), 6th revised ed., 1st reprint; Smithsonian Miscellaneous Collections, Vol. **114**; Smithsonian Institution; City of Washington, USA.
- [41] Monteith, J.L., Unsworth, M.H. *Principles of environmental physics* (1990), Edward Arnold; London, etc.; 290 pp.
- [42] Rafik Belarbi, Cristian Ghiaus and Francis Allard. "Modeling of water spray evaporation: Application to passive cooling of buildings", *Journal of Solar Energy* (2006), **80**, pp. 1540-1552
- [43] Y. F. Li. and W. K. Chow "Study of water droplet behavior in hot air layer in fire extinguishment", *Journal of Fire Technology* (2007), Vol. **44** (4).

- [44] **Mustafa Shaker, Cyrus B. Meher-Homji and Thomas Mee III.** "Inlet Fogging of Gas Turbine Engines – Part A: Fog Droplet Thermodynamics, Heat Transfer and Practical Considerations", *Proceeding of ASME Turbo Expo 2002 Amsterdam*.
- [45] **H. Barrow and C.W. Pope.** "Droplet evaporation with reference to the effectiveness of water-mist cooling", *Journal of Applied Energy* (2007), **84** (4), pp. 404-412.

VITAE

➤ SALMAN AMSARI AL-FIFI

- Born in Faifa, Saudi Arabia. My Nationality is Saudi.
- Address: Kingdom of Saudi Arabia, Dhahran (31261) King Fahd University of Petroleum & Minerals (KFUPM), Aerospace Engineering Department, P. O. Box # 648, E-mail (fifis@kfupm.edu.sa) or (ss_alfaiifi@hotmail.com).
- Received Bachelor of Science Degree with distinction in Aerospace Engineering from King Fahd University of Petroleum & Minerals, Dhahran, Saudi Arabia, in 2004.
- Joined Aerospace Engineering Department, King Fahd University of Petroleum & Minerals, Dhahran, Saudi Arabia, as a Research Assistant in 2004.
- Joined Aerospace Engineering Department, King Fahd University of Petroleum & Minerals, Dhahran, Saudi Arabia, as a Graduate Assistant in 2005.
- Received Master of Science Degree in Aerospace Engineering with emphasis on Aerodynamics, Gas Dynamics and Propulsion as a major from King Fahd University of Petroleum & Minerals, Dhahran , Saudi Arabia, in 2010.